

Photochemical Activation of Nanoparticles with (Bio)macromolecular Structures

zur Erlangung des akademischen Grades eines
DOKTORS DER NATURWISSENSCHAFTEN
(Dr. rer. nat.)

der Fakultät für Chemie und Biowissenschaften
Karlsruher Institut für Technologie (KIT) - Universitätsbereich
genehmigte

DISSERTATION

von
Dipl. Chem. Lukas Degenhard Frank Stolzer
aus
München, Deutschland

Dekan: Prof. Dr. Peter Roesky

Referent: Prof. Dr. Christopher Barner-Kowollik

Korreferent: Priv. Doz. Dr. Ljiljana Fruk

Tag der mündlichen Prüfung: 17.07.2015

DOI: 10.5445/IR/1000049310



Dieses Werk ist lizenziert unter einer Creative Commons Namensnennung –
Weitergabe unter gleichen Bedingungen 3.0 Deutschland Lizenz
(CC BY-SA 3.0 DE): <http://creativecommons.org/licenses/by-sa/3.0/de/>

Hiermit erkläre ich, dass ich die vorliegende Doktorarbeit im Rahmen der Betreuung durch Prof. Dr. Christopher Barner-Kowollik und Priv. Doz. Dr. Ljiljana Fruk selbstständig verfasst und keine anderen als die angegebenen Quellen und Hilfsmittel verwendet habe. Des Weiteren erkläre ich, dass ich mich zurzeit in keinem weiteren laufenden Promotionsverfahren befinde und keine vorausgegangenen Promotionsversuche unternommen habe.

Karlsruhe, den 03.06.2015

Lukas Stolzer

Die vorliegende Arbeit wurde von Oktober 2011 bis Juni 2015 unter Anleitung von Prof. Dr. Christopher Barner-Kowollik und Priv. Doz. Dr. Ljiljana Fruk am Karlsruher Institut für Technologie (KIT) - Universitätsbereich angefertigt.

Für meine Familie und Freunde

Abstract

During the last decades, very significant progress has been made in the synthesis, functionalization and application of engineered nanoparticles (NP) and their application in biomedical fields such as biosensing, bioimaging or drug delivery. However, there is an ongoing search for mild, high yielding, and orthogonal ligation strategies to enable attachment of the functional molecules to the NP surface, which allows for colloidal stability, biocompatibility, or precise targeting.

Research presented in the current thesis describes the use of light-induced modular ligation techniques for the modification of different metallic NPs with functional polymers or biomolecules. In addition, NPs functionalized with photoreactive groups could be used for the spatially resolved encoding *via* direct laser writing (DLW) technique into various patterns. Two classes of metallic NPs were used for the study, silver and gold NPs. To attach photoreactive groups on the NP surface, a novel bifunctional linker was prepared containing benzotriazole as the Ag NP anchoring group and a caged diene (photoenol) for light-induced cycloaddition. After attachment of the bifunctional linker *via* a ligand exchange procedure, Ag NPs were modified with functional polymers such as zwitterionic poly(carboxybetaine methacrylate) (pCBMA) and poly(ethylene glycol) (PEG) *via* light-induced Diels-Alder cycloaddition. The obtained Ag NP core-polymer shell structures were evidenced by X-ray photoelectron spectroscopy (XPS), high-resolution transmission electron microscopy (HRTEM) and energy-dispersive X-ray spectroscopy (EDXS).

In a subsequent study, the photoenol moiety was tethered to Au NPs by esterification of mercaptoundecanol-capped Au NPs. Photoreactive Au NPs were encoded in a spatially resolved fashion using direct laser writing (DLW) into a range of patterns making use of a rapid, light-induced Diels–Alder cycloaddition with surface anchored enes. Subsequent to surface encoding, the particles featured residual caged dienes, which were reactivated for secondary surface encoding.

Finally, light-induced nitrile imine-mediated tetrazole-ene chemistry (NITEC) was employed for the biofunctionalization of Au nanorods (NR). To achieve that, a novel bifunctional poly(ethylene glycol) linker was designed containing a thioctic acid as the Au anchoring group and a tetrazole moiety enabled the formation of

fluorescent pyrazoline compounds. The fluorescent product was utilized to assess the success of the surface functionalization. The NITEC strategy represented an excellent self-reporting system, particularly useful for monitoring of the NP surface modification. In addition, tetrazole-modified Au NRs were functionalized with DNA, which remained fully functional and was further employed in hybridization protocols. The efficient biofunctionalization of Au NRs was evidenced by fluorescence spectroscopy, zeta potential measurements, and gel electrophoresis confirming a successful and previously not reported use of NITEC for modification of NP surface.

Zusammenfassung

Im letzten Jahrzehnt wurden enorme Fortschritte in der Synthese, Funktionalisierung und Verwendung von künstlich hergestellten Nanopartikeln (NP) und deren Verwendung im biomedizinischen Bereich wie beispielsweise die Biosensorik, biologische Bildgebung und der Wirkstoffverabreichung. Allerdings gibt es eine kontinuierliche Suche nach milden, orthogonalen Ligationsstrategien mit hoher Ausbeute, um die Anbindung von funktionellen Molekülen an die Nanopartikeloberfläche zu ermöglichen, was die kolloidale Stabilität, Biokompatibilität und präzise Zielführung erlaubt.

Die in dieser Arbeit präsentierte Forschung beschreibt die Verwendung von Licht-induzierten, modularen Ligationstechniken für die Modifikation von verschiedenen metallischen NPs mit funktionellen Polymeren oder Biopolymeren. Des Weiteren wurden mit photoreaktiven Gruppen funktionalisierte NPs für die orts aufgelöste Kodierung in verschiedene Muster mittels direkten Laserschreibens benutzt. Zwei unterschiedliche Klassen von metallischen NPs wurden für die Untersuchungen verwendet, Silber und Gold NP. Um photoreaktive Gruppen an die Nanopartikeloberfläche anzubinden, wurden neue bifunktionelle Linker mit Benzotriazole als Ag-NP-Verankerungsgruppe und einem Dien (Photoenol) für die Licht-induzierte Cycloaddition synthetisiert. Nach der Anbindung des bifunktionellen Linkers mittels Ligandenaustauschprozess wurden die Ag NP mit funktionalen Polymeren wie Poly(carboxybetainmethacrylat) und Poly(ethylenglycol) mittels Licht-induzierter Diels-Alder Cycloaddition modifiziert. Die erhaltenen Ag NP-Kern-Polymerhülle Struktur wurde mit Röntgenphotoelektronenspektroskopie (XPS), hochauflösender Transmissionselektronenmikroskopie (HRTEM) und energiedispersive Röntgenspektroskopie (EDXS) nachgewiesen.

In den nachfolgenden Untersuchungen wurde die Photoenolgruppe an Au NP durch eine Veresterung an Mercaptoundecanol-bedeckten Au NP angebunden. Die photoreaktiven Au NP wurden in einer orts aufgelösten Weise mittels direktem Laserschreiben (Direct Laser Writing, DLW) in eine Reihe von Mustern kodiert, indem die schnelle, Licht-induzierte Diels-Alder Cycloaddition mit oberflächenverankerten Enen verwendet wurde. Im Anschluss an die Oberflächenkodierung

rung wiesen die Partikel restliche Diene auf, die reaktiviert wurden zur zweiten Oberflächenkodierung.

Im letzten Projekt wurde die Licht-induzierte Nitrilimin-vermittelte Tetrazol-En Chemie (NITEC) für die Biofunktionalisierung von Au Nanostäbchen (NR) genutzt. Zu diesem Zweck wurde ein neuer bifunktionaler Poly(ethylenglycol)-Linker konzipiert, der aus Liponsäure als Au-Verankerungsgruppe und die Tetrazolgruppe zur Bildung der fluoreszierenden Pyrazolinverbindung bestand. Die fluoreszierenden Produkte wurden zur Bestimmung der erfolgreichen Oberflächenfunktionalisierung genutzt. Die NITEC-Strategie stellt ein ausgezeichnetes self-reporting-System dar, das insbesondere für die Kontrolle der NP Oberflächenmodifikation nützlich ist. Tetrazol-modifizierte Au NR wurden mit DNA funktionalisiert, die voll funktionsfähig geblieben ist und zur weiteren Hybridisierung verwendet wurde. Die effiziente Biofunktionalisierung von Au NR wurde mit Fluoreszenzspektroskopie, Zetapotenzialmessungen und Gelelektrophorese nachgewiesen, die die erfolgreiche und bislang nicht berichtete Verwendung von NITEC für die Modifikation der NP-Oberfläche bestätigten.

Publications Arising from the Thesis

1. **Light-induced DNA-protein conjugation**

Bauer, D. M.; Rogge, A.; Stolzer, L.; Barner-Kowollik, C.; Fruk, L. *Chem. Commun.* **2013**, 49, 8626.

2. **Light-induced modification of silver nanoparticles with functional polymers**

Stolzer, L.; Ahmed, I.; Rodriguez-Emmenegger, C.; Trouillet, V.; Bockstaller, P.; Barner-Kowollik, C.; Fruk, L. *Chem. Commun.* **2014**, 50, 4430.

3. **Photo-induced surface encoding of gold nanoparticles**

Stolzer, L.; Quick, A. S.; Abt, D.; Welle, A.; Naumenko, D.; Lazzarino, M.; Wegener, M.; Barner-Kowollik, C.; Fruk, L. *Chem. Commun.* **2015**, 51, 3363.

4. **A self-reporting tetrazole-based linker for the biofunctionalization of gold nanorods**

Stolzer, L.; Vigovskaya, A.; Barner-Kowollik, C.; Fruk, L. *Chem. Eur. J.* **2015**, DOI: 10.1002/chem.201502070.

Abbreviations

APS	= ammonium persulfate
Boc	= <i>tert</i> -butyloxycarbonyl
BTPE	= benzotriazole photoenol
BTTEG	= benzotriazole triethylene glycol
CTAB	= cetyltrimethylammonium bromide
CTAC	= cetyltrimethylammonium chloride
CuAAC	= copper-catalyzed azide-alkyne cycloaddition
DCC	= <i>N,N'</i> -dicyclohexylcarbodiimide
DCM	= dichloromethane
DLW	= direct laser writing
DLS	= dynamic light scattering
DMAP	= 4-(dimethylamino)pyridine
DMF	= <i>N,N</i> -dimethylformamide
DNA	= deoxyribonucleic acid
EDC	= 1-ethyl-3-(3-dimethylaminopropyl)carbodiimide
EDXS	= energy-dispersive X-ray spectroscopy
ESI-MS	= electrospray-ionization mass spectrometry
FAB-MS	= fast atom bombardment mass spectrometry
HOBt	= 1-hydroxybenzotriazole
HPLC	= high performance liquid chromatography
HRTEM	= high-resolution transmission electron microscopy
LSPR	= localized surface plasmon resonance
MALDI-ToF	= matrix assisted laser desorption/ionization time-of-flight
NMR	= nuclear magnetic resonance
NHS	= <i>N</i> -hydroxysuccinimide
NITEC	= nitrile imine mediated tetrazole-ene chemistry
NP	= nanoparticle
NR	= nanorod
pCBMA	= poly(carboxybetaine methacrylate)
PEG	= poly(ethylene glycol)
PVP	= poly(vinylpyrrolidone)

Abbreviations

R_f	= ratio of fronts
RAFT	= reversible addition-fragmentation chain-transfer
SERS	= surface-enhanced Raman scattering
ssDNA	= single stranded deoxyribonucleic acid
sSMCC	= sulfosuccinimidyl-4-(<i>N</i> -maleimidomethyl)cyclohexane-1-carboxylate
TA	= thioctic acid
TEMED	= tetramethylethylenediamine
THF	= tetrahydrofuran
TOAB	= tetra- <i>n</i> -octylammonium bromide
ToF-SIMS	= time-of flight secondary ion mass spectrometry
TZ	= tetrazole
UV	= ultraviolet
Vis	= visible
XPS	= X-ray photoelectron spectroscopy

Contents

Abstract	I
Zusammenfassung	III
Publications Arising from the Thesis.....	V
Abbreviations.....	VI
Contents	1
1 Introduction	3
1.1 Synthesis and Modification of Nanoparticles	4
1.1.1 Synthesis of Gold Nanoparticles	5
1.1.2 Synthesis of Silver Nanoparticles.....	8
1.2 Properties of Metallic Nanoparticles (Gold and Silver).....	10
1.3 Modification of Nanoparticle Surface	13
1.3.1 Methods	14
1.3.2 Polymer Nanocomposites	28
1.3.3 DNA-Nanoparticle Conjugates	30
1.4 Surface Immobilization of Nanoparticles.....	33
1.5 Applications of Nanoparticles	34
2 Research Outline	39
3 Light-Induced (Bio)Functionalization of Gold and Silver Nanoparticles	41
4 Photo-Induced Surface Encoding of Gold Nanoparticles	69
5 Tetrazole Modified Gold Nanorods for Biofunctionalization.....	85
6 Conclusions and Outlook	99
7 Experimental Part.....	104
7.1 Materials and Methods	104
7.2 Syntheses.....	113
Bibliography.....	IX
List of Figures	XXIII
List of Schemes	XXX
List of Tables	XXXV
Curriculum Vitae	XXXVI
Danksagung	XXXVIII

Contents

1 Introduction

Nanoparticles (NPs) are organic or inorganic materials ranging from 1 to 100 nm in size, which exhibit unique optical, electrical and catalytic properties in comparison to the equivalent bulk counterparts.^[1] NPs can be classified in insulating NPs, consisting of polymeric NPs and silica NPs, semiconductor NPs such as CdSe or CdTe, and metal NPs such as Au, Ag or Pt (Figure 1).

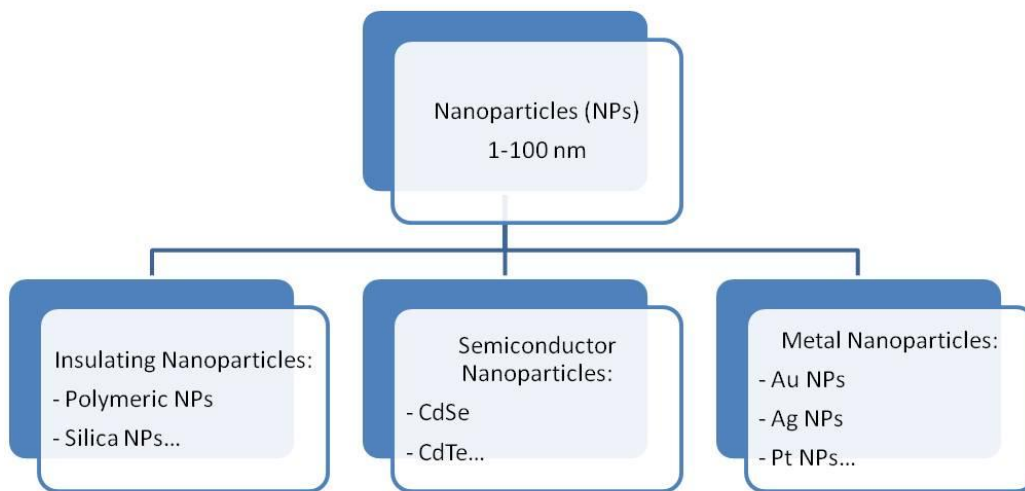


Figure 1. Nanoparticles can be classified in insulating nanoparticles, semiconductor nanoparticles, and metal nanoparticles.

Polymeric NPs are widely explored for drug delivery systems, because they promote the prolonged circulation of drugs or enhance the internalization of drugs into the cancer cells by positively charged NP surfaces.^[2] Especially silica as shell of core-shell NPs with inorganic cores provides better stability and biocompatibility of the hybrids.^[3] Mesoporous silica NPs attract significant attention as well due to their properties of high surface areas, large pore sizes, and high biocompatibility.^[4] The class of semiconductor NPs is dominated by quantum dots, which are fragments of semiconductors in the range of hundreds to thousands atoms. Therefore, quantum dots, such as II-VI (CdS) or III-V (InP) nanocrystals, have tunable band

gaps with specific electronic states.^[5] The unique electrical and optical properties including fluorescence enables quantum dots for imaging, labeling and sensing.^[6] In addition, noble metal NPs have attracted great interests due to their plasmonic properties based on the localized surface plasmon resonance (LSPR).^[7] The large surface area-to-volume ratio led to numerous applications in electronics, sensing and biomedicine. However, to be successfully used for such applications their properties often need to be tuned either by employing various synthetic procedures or allowing for surface modification according to the subsequent requirements. The following sections focus on the synthesis, modification, properties, and applications of Au and Ag NPs.

1.1 Synthesis and Modification of Nanoparticles

The formation of NPs controlled by the reduction, nucleation and growth of salt metals has been investigated for more than a century. However, only in the recent decade, the field of nanotechnology has developed monodisperse NPs based on the enhanced control over the nanomaterials production. In general, nanoparticles are synthesized in various shapes and sizes using different synthesis techniques which are divided into top-down and bottom-up approaches. The top-down approach is a physical method which employs metal bulk and reduces its size to the nanoscale either with lithography or the laser ablation.^[8] The bottom-up technique is based on the chemical reduction of metal salts.^[9] Unfortunately, due to their small size NPs tend to agglomerate, which often results in the loss of their properties. To prevent agglomerations of the NPs during the synthesis, the electrostatic or steric stabilization by the use of ligands is the crucial aspect. Different approaches are available for the synthesis of NPs such as chemical reduction, the polyol method, seed-mediated growth or the photochemical method.^[10] Typically, the chemical reduction method requires three components: a metal salt precursor, a reducing agent and a stabilization agent. The following sections will address some of the synthetic methods to prepare the noble metal NPs, which were used within this thesis.

1.1.1 Synthesis of Gold Nanoparticles

Citrate Reduction

The popular and most widely used procedure for the synthesis of Au NPs in aqueous solution is the citrate reduction method. Already in 1951, Turkevich *et al.* reported the reduction of tetrachloroauric acid in presence of trisodium citrate at boiling temperature to Au NPs.^[11] The NP formation was explained by a nucleation and a growth step, but the detailed mechanism is nowadays still a subject of discussion.^[12] The widely accepted mechanism is based on a fast initial formation of nuclei followed by the coalescence of the nuclei and the growth to bigger particles (Figure 2).

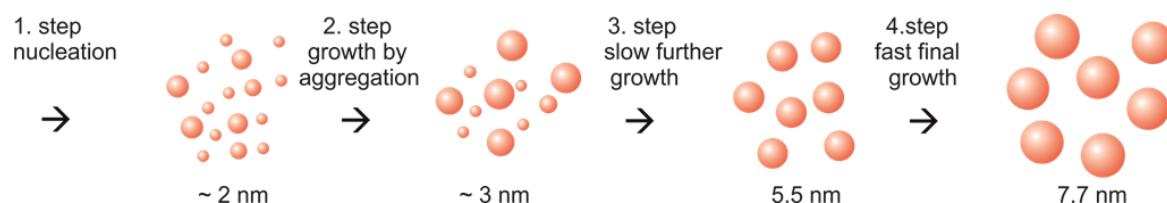


Figure 2. Schematic illustration for the nucleation-growth process for the formation of gold nanoparticles. Adapted with permission from [12a]. Copyright 2010 American Chemical Society.

Even though the detailed mechanism is not completely understood, the citrate method allows for the controlled synthesis of spherical Au NPs in different sizes without using harsh reducing agents.

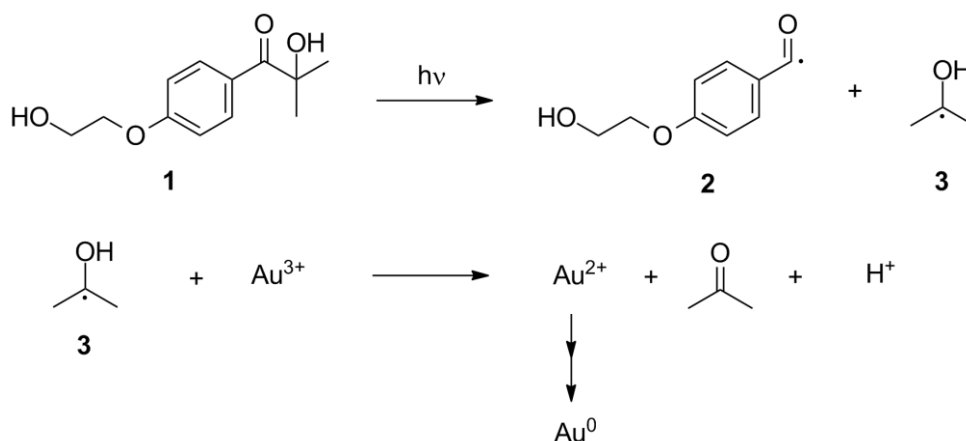
Borohydride Reduction

An alternative well-known method for the preparation of Au NPs is the reduction with sodium borohydride in presence of different thiols as ligands. The use of thiols enables the direct modification of Au NPs with functional groups, which can be employed i.e. for attachment of various biomolecules. In recent years, different procedures for the synthesis of Au NPs were developed, which differ in the type of the thiols, solvents and ratios between ligands and gold salt.^[13] A scientific breakthrough in the synthesis of small Au NPs was a two-phase process to obtain thiolated Au NPs. In the so-called Brust-Schiffrin-method, tetrachloroauric acid was dissolved in aqueous solution, subsequently transferred from aqueous solution to toluene using the surfactant tetraoctylammonium chloride and reduced by sodium borohydride in presence of alkanethiols.^[14] More recently, Oh *et al.* devel-

oped a water-based synthesis for Au NPs which were stabilized with lipoic acid functionalized PEG as bidentate ligands.^[15] The Au NPs in the range of 1.5 nm and 18 nm exhibited a remarkable stability in the presence of high salt concentrations and over a wide range of pH values.

Photochemical Reduction

A comparatively milder synthesis of Au NPs represents the photochemical approach, which is based on the use of light to form radicals for the reduction of gold salts. The photochemical synthesis provides many advantages such as the spatial and temporal control over the reaction; it is very versatile and can be employed in different media including emulsions, polymer films, glasses, and cells.^[16]



Scheme 1. Scheme of photochemical cleavage of 2-hydroxy-1-(4-(2-hydroxyethoxy)phenyl)-2-methylpropan-1-one (Irgacure-2959) **1** to generate ketyl acetone radicals **3** which are capable to reduce Au³⁺ to Au⁰. Adapted with permission from [17]. Copyright 2006 American Chemical Society.

One of the photochemical methods for the facile synthesis of aqueous unprotected Au NPs was demonstrated by McGilvray *et al.* using 2-hydroxy-1-(4-(2-hydroxyethoxy)phenyl)-2-methylpropan-1-one (Irgacure-2959) **1**, which decomposes in a Norrish-type-I-cleavage to ketyl acetone radicals **3** and benzoyl radicals **2** upon 350 nm excitation (Scheme 1).^[17] While benzoyl radicals react to the corresponding benzoic acid, the ketyl radicals **3** are able to reduce Au³⁺ to Au⁰ and form Au NPs in various sizes depending on the irradiation time and illumination intensity.

Other Reduction Methods

Other reducing agents were used for oxygen- or nitrogen based ligands, containing electronegative groups such as amine or carboxylic groups.^[18] For instance, ascorbic acid acted as reducing agent in the growth step of Au NRs^[19] or for the synthesis of 4-(dimethylamino)pyridine-capped Au NPs with approximately 12 nm in size.^[20] Of growing interest are the one-pot synthesis of Au NPs with biomolecules using for example aspartate for the reduction of Au chloride to obtain Au nanoplates^[21] or the method using amino acids L-tyrosine, glycyl-L-tyrosine, and L-arginine for the Au NP synthesis based on KAuBr_4 as metal salt precursor.^[22]

Seed-mediated Growth

An important and challenging task for the synthesis of metallic NP is the control over shape and size, which is crucial to adjust the resulting properties of the NPs. The seed-mediated growth allows for a temporal control of nucleation and growth and therefore, results in nanoparticles of various shapes and sizes. Typically, small size spherical Au NPs are first synthesized as seed crystals, which are added as a nucleation center to a second growth solution consisting of Au salts and a weak reducing agents.^[10] Particularly, the shape control of Au NPs synthesis has attracted much attention due to the shape-dependant properties and widespread applications.

Among various anisotropic Au NPs, triangular nanoprisms and most notably Au nanorods (NR) with different aspect ratios received great interests. The growth to Au NRs can be tuned by different adsorbents including surfactants, polymers, small organic molecules or metal ions.^[23] Jana *et al.* reported the fabrication of Au NR by employing cetyltrimethylammonium bromide (CTAB), silver salts and ascorbic acid.^[19] The silver salts were reduced by the weak reducing agent ascorbic acid and formed a shell onto the gold core.

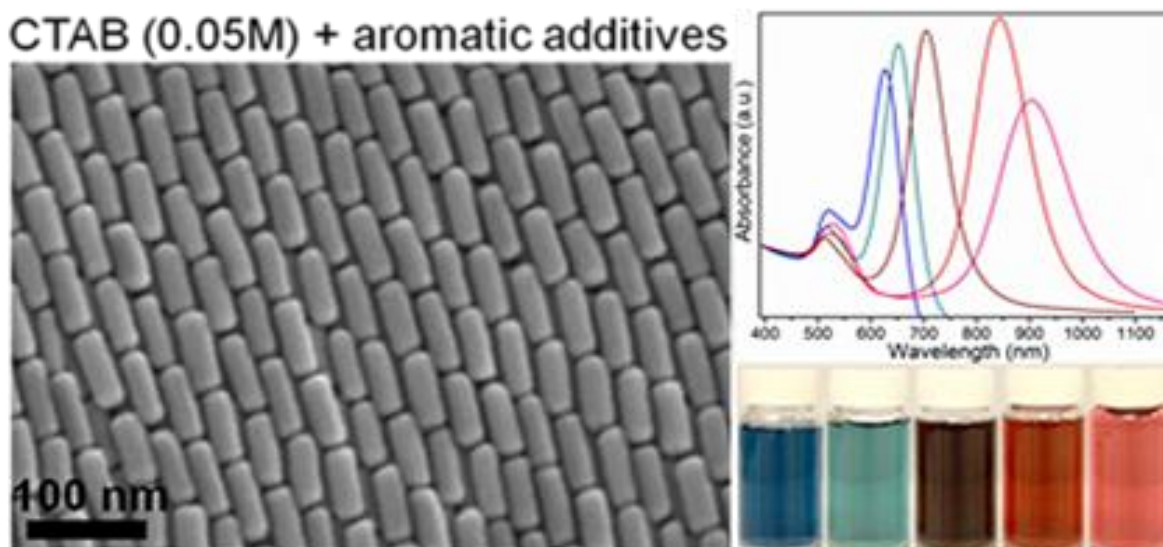


Figure 3. Transmission electron microscopy image of gold nanorods (left) and UV/Vis spectrum of gold nanorods of various sizes prepared using CTAB growth method (right). Reprinted with permission from [24]. Copyright 2012 American Chemical Society.

The broad polydispersity of the Au NRs was narrowed in the last years with different additives. For instance, Ye *et al.* fabricated monodisperse Au NRs with tunable sizes using certain aromatic additives such as salicylate-based sodium salts to reduce the CTAB concentration and to obtain a better control over the monodispersity and spectral tunability (Figure 3).^[24]

1.1.2 Synthesis of Silver Nanoparticles

Chemical Reduction

Citrate and sodium borohydride are most common reducing agents for the preparation of Ag NPs in aqueous solutions. In 1982, Lee and Meisel reported a variation of the Turkevich method and prepared Ag NPs by the reduction of AgNO_3 with citrate in boiling aqueous solution.^[25] In the simple approach of Lee and Meisel, citrate acts as both reducing and stabilizing agents for the formation of Ag NPs. However, the prepared Ag NPs have a broad particle size distribution. In recent years, different attempts have been reported to improve the control over size and shape of citrate-capped Ag NPs. Particularly, the balance of nucleation and growth of NPs determines the resulting properties. Recently, the synthesis of monodisperse, quasi-spherical, citrate-stabilized Ag NPs was performed by pH adjustment,^[26] laser ablation,^[27] or by employing additives such as ascorbic acid

and potassium iodide.^[28] Nowadays, the citrate reduction method enables the reproducible formation of stable, monodisperse Ag NPs with tunable sizes. The stabilization of citrate is based on the affinity of the carboxylic groups to the metal surface. However, the concentration of citrate-stabilized NPs is very low^[29] and the highly negatively charged NPs are prone to agglomeration at high ionic condition,^[30] which restricts their application in biological media.

Therefore, to obtain more stable NPs, the strong reducing agent sodium borohydride has been used for the Ag NP synthesis in combination with stabilization agents. Already in 1979, Creighton *et al.* demonstrated the reduction of AgNO₃ with sodium borohydride to form Ag NPs.^[31] The weak BH₄ anion stabilized only weakly the NP, therefore a wide selection of stabilization agent were established including surfactants such as sodium dodecyl sulfate^[32] or ligands such as thiols or amines.

Additionally to conventional reducing agents, the polyol method utilizes a solvent to reduce the metal salt in presence of polymers. The solvents are high-boiling alcohols such as diethylene glycol, which also enables the stabilization of the NPs. Fievet *et al.* reported, for the first time, a robust route for the synthesis of crystalline and monodispersed NPs using metal powders of Co, Ni, Cu, Ag or a combination thereof in ethylene glycol at elevated temperatures of 160-210°C.^[33] Further, Kim *et al.* stabilized spherical Ag NPs with poly(vinylpyrrolidone) (PVP) in hot ethylene glycol and investigated the effect of temperature and heating rate in the size.^[34] Already in 2002, Komarneni *et al.* employed the microwave-assisted polyol process to synthesize Ag and Pt NPs.^[35] The prepared NPs were stabilized with PVP and the particle size and shape were controlled by adjustment of the molecular weight of PVP and pH. The polyol process has advantages due to the simultaneously use of the solvent also as reducing agent and even sometimes as stabilization agent. Nevertheless, the removal of the high-boiling solvents is still the major issue and new methodologies are still being reported.

1.2 Properties of Metallic Nanoparticles (Gold and Silver)

The properties of metallic NPs are dominated by their small size and the resulting large surface area-to-volume ratio, which provides more surface active sites for example for heterogeneous catalysis. Catalysts play an important role in the conversion of hazardous waste into less harmful products.^[36] For instance, the seminal work of Haruta *et al.* demonstrated the use of Au NPs as active catalyst for the oxidation of CO to CO₂ at low temperatures.^[37] Theoretical calculations of the CO oxidation with small Au clusters revealed two main factors for the better catalytic activity of Au NPs in comparison to Au films: the undercoordination of the Au atom in Au NPs facilitates the adsorption process and the special geometry is well suited for bond breakage of small molecules.^[38]

Other properties of NPs are related to specific sizes and shapes of NPs. The photoluminescence is for example restricted to ultra-small Au and Ag NPs (less than 5 nm).^[39] The phenomenon is attributed to the discrete energy levels for electrons arising from the decreasing size (consisting below hundreds of atoms) and the interband transition between the filled 5d¹⁰ band and 6(sp)¹ conduction band.^[40] The fluorescent property of NPs can be affected by size, shape and environment.^[41]

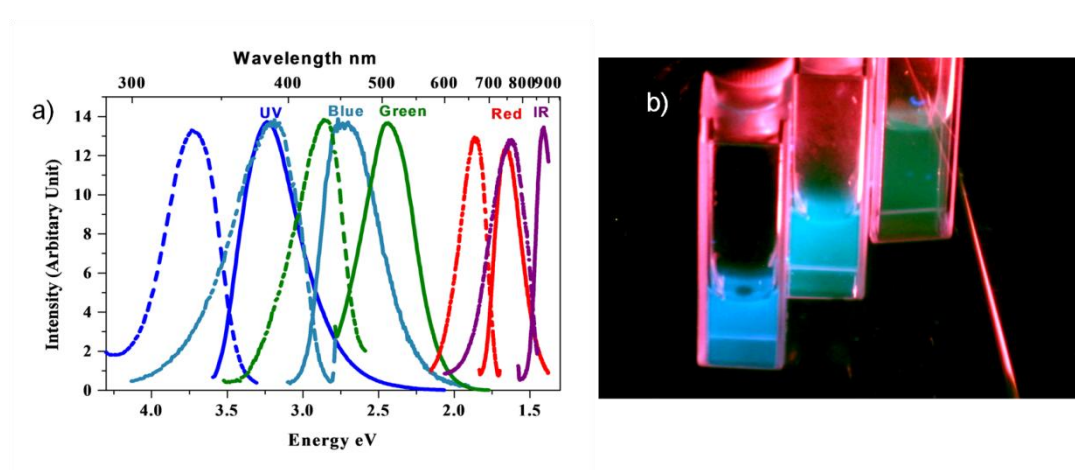


Figure 4. a) Excitation (dashed) and emission (solid) spectra of different Au nanoclusters. The excitation wavelength shifted to the lower wavelength with decreasing size. b) Emission of the three shortest wavelength emitting Au nanocluster upon UV irradiation at 366 nm. Adapted with permission from [42]. Copyrighted by the American Physical Society.

To demonstrate the size dependence of the emission of small Au NPs, Zheng *et al.* synthesized different nanoclusters (between Au₅ and Au₃₁) by the encapsulation with poly(amidoamine) dendrimers.^[42] The decrease in size of the nanoclusters led to lower emission wavelength, tunable from near infrared (Au₃₁) to the UV region (Au₅) (Figure 4). The fluorescent ultra-small Au NPs exhibit attractive features for bioimaging or biosensing.

In general, the noble metallic NPs, Au and Ag NPs, have mainly attracted interest due to their optical properties, which are based on the localized surface plasmon resonance.

Localized Surface Plasmon Resonance (LSPR)

Surface plasmons describe the oscillations of the free electron of a metal, which can interact with incident light when the frequencies are in resonance (Figure 5).

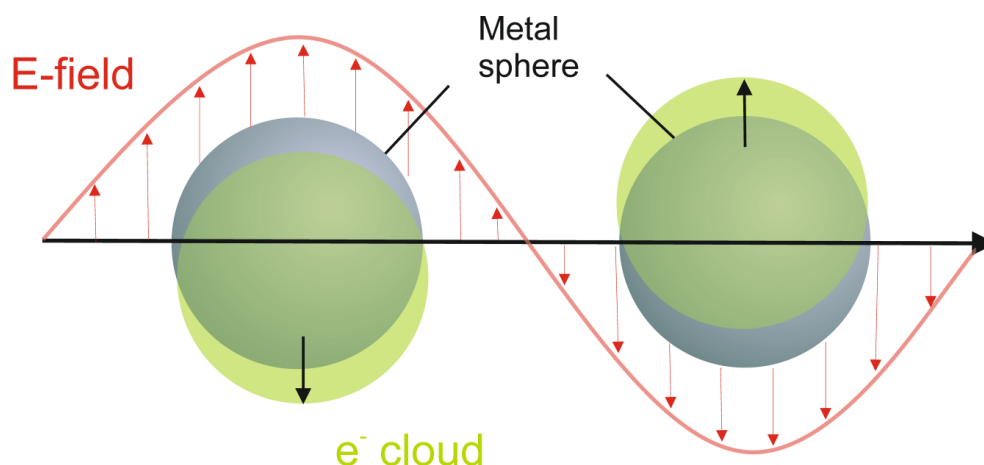


Figure 5. Schematic illustration of the plasmonic oscillation of a sphere showing that the conduction electron charge cloud oscillates in resonance with the incident light. Adapted with permission from [1]. Copyright 2003 American Chemical Society.

The resonance of the surface plasmons with incident light falls within the UV/Vis region and depends on the composition, size, shape and dielectric environment of the NPs. For instance, the LSPR of Au NPs causes absorption of green light approximately at 520 nm leading to the complementary red color of Au NPs in solution. By tuning the size of Au NPs, El-Sayed and co-workers demonstrated the shift of LSPR from 517 nm for 9 nm Au NPs to 575 nm for 99 nm Au NPs.^[43] Chen *et al.* investigated the effect of the shape to the LSPR including

nanospheres, nanocubes, nanobranched, nanorods, and nanobipyramids.^[44] They were able to shift the LSPR from 525 nm to 1150 nm upon the morphology change from small nanospheres to bigger nanobranched. In comparison to Au NPs, Ag NPs are typically yellow due to their absorption around 400 nm. Similar to Au NPs, the shape and size of Ag NPs tunes the resulting optical properties. Mock *et al.* observed a LSPR red-shift of single spherical, pentagonal and triangular Ag NPs.^[45]

The NP environment consisting of the solvent and various surface bound molecules affects the LSPR as well. Solvents without any active functional groups shift the LSPR to the red with increasing refractive index, while complexation processes between the solvent and the NPs neutralize this shift.^[46] The surface chemistry plays a non-negligible role for the optical properties especially for small NPs (<20 nm) with their higher percentage of surface atoms. Adsorbed molecules, which form chemical bonds with the NPs, reduce the conductive electrons, alter the dielectric constant of the surface metal atoms and consequently also the SPR absorption spectrum of NPs.^[47]

In such a way, the interaction of the electromagnetic field of the NPs and (bio)molecules leads to changes in the LSPR. The dependence of the (bio)molecule induced shift in the LSPR peak can be detected and this effect has numerous applications in biosensing. For instance, Ag NPs were employed for the investigation of the biotin-streptavidin system^[48] After covalent attachment of biotin to the Ag NPs by amide bond formation, the incubation of streptavidin resulted in a red-shift of 27 nm. The LSPR shifts regarding different concentrations give information about the mass of the analyte and the binding constant of the system.

Moreover, the LSPR interaction with biomolecules provides a lot of opportunities for therapy using the “water window”, where aqueous tissue absorbs light (~700 nm-1200 nm), to irradiate NPs. The excited conduction band electrons relax to the ground state and release the energy as heat to the surrounding media, the so-called photothermal effect.^[49] Especially Au NPs are suitable due to the good stability in aqueous media and their LSPR, which can be tuned to the near IR region by the preparation of Au NRs. In addition, biomolecules attached to Au NRs can target these nanocomposites to cancer cells. For example, Zhang *et al.* prepared poly(*N*-isopropylacrylamide-*co*-acrylic acid)-capped Au NRs, which can be loaded with the drug doxorubicin in the polymer shell.^[50] *In vivo* experiments in

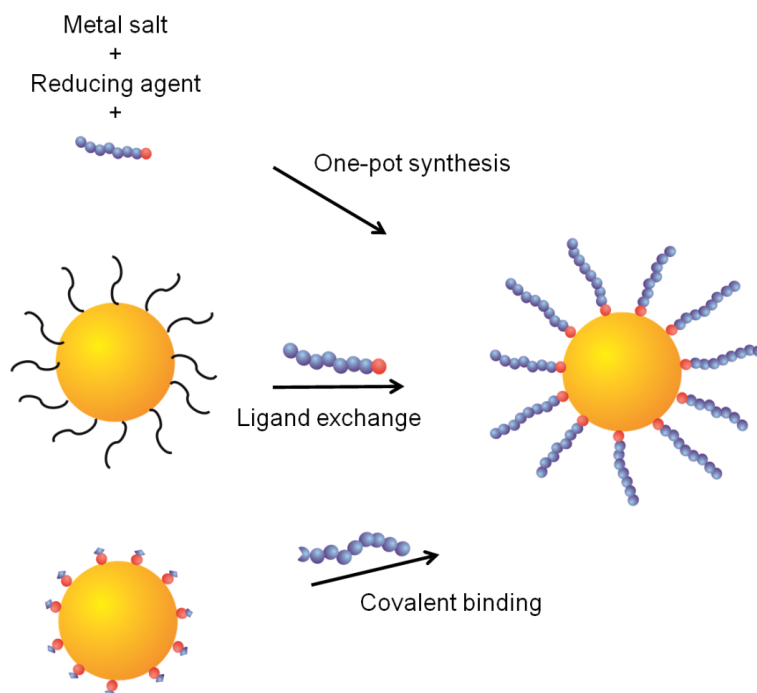
mice with the nanocomposites demonstrated the inhibited tumor growth after NIR laser irradiation due to the photothermal heating of the Au NRs in the irradiated areas and the drug release of doxorubicin, which was caused by the shrinking of the thermoresponsive polymer shell.

Surface-Enhanced Raman Scattering (SERS)

Another nanoscale phenomenon is the surface-enhanced Raman scattering using Raman spectroscopy on metal surfaces. The Raman spectroscopy relates to the inelastic scattering of photons by molecules. The measurement of analytes on rough surfaces leads to an enhancement of the Raman signal due to the interaction of the LSPR with the incident radiation. In addition to the electromagnetic enhancement, a charge-transfer mechanism can occur due to the formation of a chemical bond between the analyte and the surface.^[51] The higher electron density leads then to a higher interaction with the incident photons. In general, metallic nanostructured substrates exhibits higher enhancement factors than planar surfaces due to the higher surface area.^[52] This phenomenon is known as the surface-enhanced Raman scattering (SERS) and there are numerous applications of this method for detection of molecular interactions or detection of single molecules. An important requirement is the presence of suitable surfaces. For the detection of target DNA, Graham and co-workers coupled DNA sequences with SERS active linkers who were able to bind to NPs surfaces and to react with specific functionalized DNA.^[53] After binding of the DNA to Au NPs or Ag NPs, good SERS responses were obtained enabling fast identification and quantification of DNA.

1.3 Modification of Nanoparticle Surface

Noble metallic NPs with their high surface-to-volume ratio have excellent potential for biomedical application due to their unique optical and catalytic properties. To provide colloidal stability, water solubility, and biocompatibility, inorganic NPs need to be functionalized with various small molecules, polymers, and biomolecules by electrostatic adsorption, physisorption or by chemisorption.



Scheme 2. Different strategies to modify NP surface with various (bio)molecules including one-pot synthesis with metal salt and reducing agent, ligand exchange of preformed NPs, and covalent binding to functional NPs.

Different strategies were employed to achieve surface modification such as the one-pot synthesis, ligand exchange and covalent binding (Scheme 2). Next section will focus on the most widely used methodologies.

1.3.1 Methods

Electrostatic adsorption

The colloidal stability of NPs after chemical reduction can be achieved in aqueous solution by ionic ligands. In general, acidic or basic ligands such as citrate, lipoic acid or alkylammoniums lead to negatively or positively charged surfaces and colloidal stability due to Coulomb repulsion.^[54] The charged NPs can interact with oppositely charged biomolecules. For instance, bovine serum albumin (BSA) protein is known to bind electrostatically to negatively charged citrate-capped Au NPs.^[55] Additionally, Shenton *et al.* demonstrated the immobilization of the antibody immunoglobulin G onto citrate-capped Au NPs through noncovalent electrostatic interaction: The effective binding between positively charged amino acids of the side chain and negatively charged citrate groups on the Au NP sur-

face was achieved at high pH above the isoelectric point of citrate.^[56] To immobilize negatively charged DNA to NPs, positive surface charge has to be introduced to NP, for example using spermine, a homo-bifunctional amine molecule. Positively charged spermine-coated Ag NPs were employed to attach fluorescein labeled DNA. In addition, Ag NPs acted after attachment as platform of dye labeled DNA with SERS.^[57] Noncovalent electrostatic adsorption of biomolecules to NPs represents a facile method, to functionalize charged NPs. Nevertheless, the biomolecules-NP conjugates are stabilized by coulomb repulsion which can be diminished by the addition of salts or at higher or lower pH values resulting in agglomerations.^[58]

Chemisorption

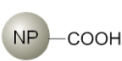

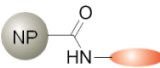
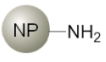

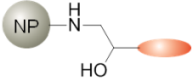
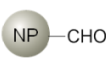
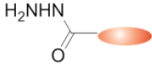
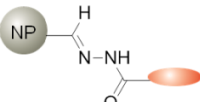
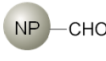

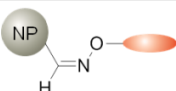
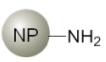
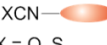
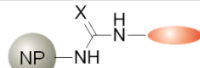
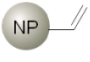

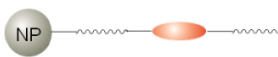
As already mentioned, thiols are strong binding ligands to Au NPs and can be attached directly to Au NPs by the chemical reduction procedures. Another approach for the functionalization of NPs is the replacement of ligands *via* ligand exchange. Different anchoring groups such as thiols,^[59] amines^[60] or catechols^[61] are able to bind strongly to Au NPs or Ag NPs and are able to replace ligands. Murray *et al.* substituted thiol ligands on the Au NP surface to introduce different ω -functionalized thiols to alkanethiolate-stabilized 1.5 nm Au NPs.^[62] The scope of different thiol ligands for replacement was expanded by the use of triphenylphosphine-stabilized Au NPs and ω -functionalized thiols.^[63] Ligand exchange procedures cannot be circumvented when the incorporation of functional groups such as azides or aldehydes are needed, which are not compatible with the use of reducing agents and therefore cannot be added to the NPs in the one pot procedures. There are numerous procedures for ligand exchange. For example, Baranov *et al.* prepared 15 nm Au NPs by the citrate reduction method and replaced the citrate groups with azidoalkylthiol in a water/DMF mixture followed by precipitation and redispersion in organic solvent.^[64] Hiramatsu *et al.* demonstrated the synthesis of monodisperse Au NPs or Ag NPs employing weakly absorbed oleylamine which can be replaced with mercaptoundecanoic acid to afford water soluble NPs.^[60] The replacement of citrate groups on Ag NPs was achieved with different thiols such as 4-mercaptobenzoic acid and 2-naphthalene thiol in ethanoic solution and functionalized Ag NPs were used for SERS measurements.^[65]

Also macromolecules such as polymers or DNA can be attached to NPs surface by the use of the ligand exchange strategy, which will be discussed in later sections.

Covalent Binding

The introduction of functional groups using ligand exchange exhibits some constraints due to the incompatibility or steric hindrance of the anchoring group, in particular when larger molecules such as proteins are present.^[66] To overcome the problems with stabilization or interaction of the functional group with the surface, another approach has been employed based on the use of bifunctional linkers, which can on one hand selectively attach to the NP surface and also contain additional functional groups for further reactions. In Table 1, an overview of different chemical strategies applied to modify NP surface is presented, although not all have been employed for biofunctionalization.^[67]

Table 1. Chemical strategies applied for the covalent modification of NPs. Adapted with permission from [67]. Copyright 2011 American Chemical Society.

Ligand	Substrate	Ligand Attached to Substrate	Reaction
			Amide Bond Formation
			Epoxide Opening
			Imine Formation
			Imine Formation
	 X = O, S		Addition of Amines to Cyanates
			Ring-Closing or Ring-Opening Methathesis

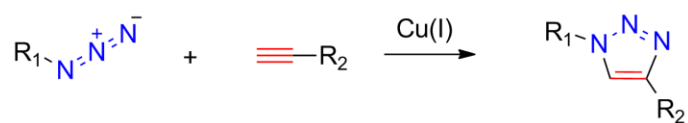
Among various coupling reactions between noble metallic NPs and biomolecules, the amide coupling is the most versatile approach due to the availability of amine and carboxylic acids moieties in biomolecules. Convenient procedures for amide bond formation activate *in situ* the carboxylic acid using reagents such as 1-

ethyl-3-(3-dimethylaminopropyl)carbodiimide (EDC) or *N*-hydroxysuccinimide (NHS) to form *o*-acylisourea or succinimidyl ester intermediates which can couple to primary amines.^[68] For example, Arosio *et al.* reported the successful immobilization of cRGD peptides to Au NPs using the amide bond formation.^[69] The cRGD conjugated Au NPs possess an enhanced affinity for integrin binding and has potential for the use for tumor targeted therapy. Also proteins such as transferrin were attached to mercaptobenzoic acid-stabilized Au NPs using EDC coupling.^[70] The resulting Au NP-transferrin conjugate enables cellular uptake to mammalian cells which was examined with SERS measurements combined with dark-field microscopy. Despite the versatile use of amide coupling, one of the drawbacks of amide coupling using EDC or NHS is the tendency of hydrolysis of the intermediates *o*-acylisourea or succinimidyl ester, although succinimidyl esters formed by NHS-activation are more stable. Therefore, a large excess of activation reagents has to be utilized which can cause an overactivation of the carboxylic acids and a loss of colloidal stability due to the poor solubility of the intermediates.^[68] Prabakaran *et al.* stabilized Au NPs with an amphiphilic copolymer and used the hydrazone ligation to bind doxorubicin covalently to the hydrophobic shell.^[71] Doxorubicin was released by cleavage of the hydrazone linkage at acidic pH. Although the pH-sensitivity of the hydrazone bond may be attractive for drug delivery, the imine formation leads in general to instable NP-bioconjugates.

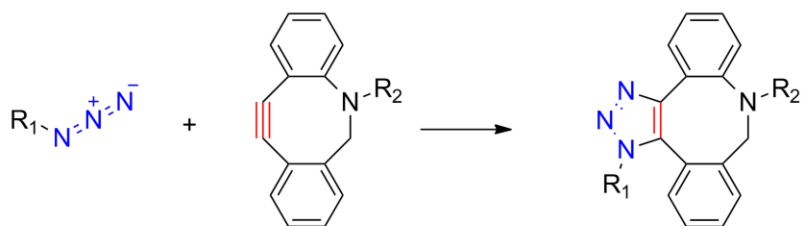
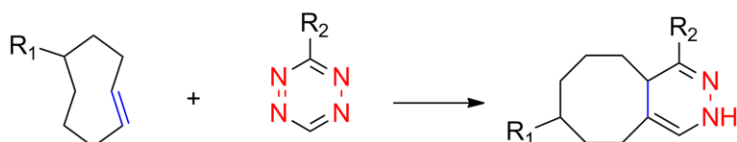
Click Chemistry Procedures

The most widely used amide coupling conjugation has several disadvantages for the biofunctionalization of NPs as outlined above. Therefore, there is a strong demand for effective and bioorthogonal surface chemistries that do not affect the functional groups present in biomolecules including amine, carboxyl, hydroxyl and thiol groups.^[67] A new concept beyond the standard covalent binding strategies was proposed by Sharpless *et al.* in 2001.^[72] The *click* concept is a term for a class of chemical reactions that fulfill different requirements such as efficiency, mild reaction conditions, high selectivity, (bio)orthogonality and are wide in scope. *Click* chemistry has emerged as a powerful strategy in chemistry, biochemistry, polymer chemistry, and in the past decade also in material science.^[73]

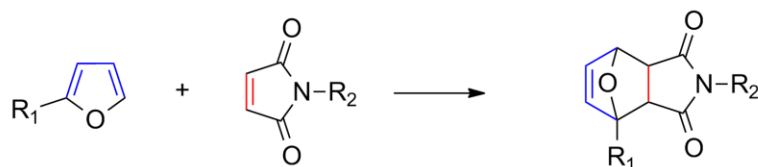
Copper-catalyzed azide-alkyne cycloaddition



Strain-promoted cycloaddition of azides and dibenzocyclooctynes

Inverse electron-demand Diels-Alder reaction of *trans*-cyclooctenes and tetrazines

Diels-Alder reaction of furans and maleimides



Thiol-ene reaction*

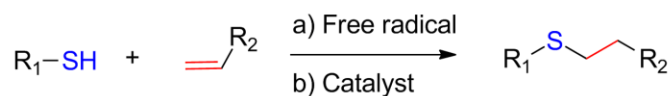
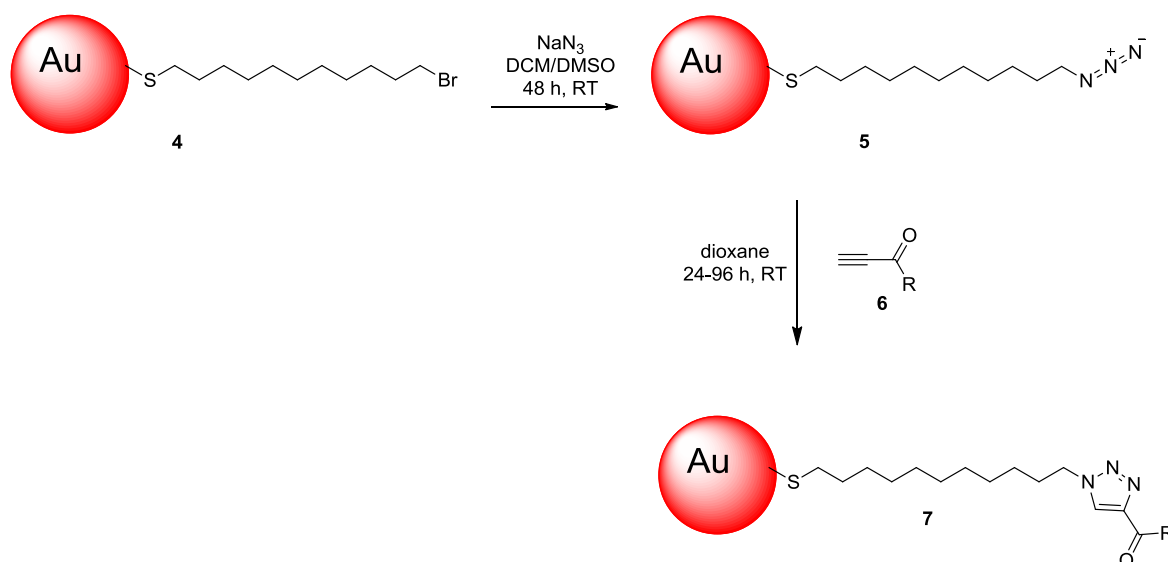


Figure 6. Overview of selected *click* chemistry strategies for the biofunctionalization of nanoparticles. *It should be noted that the radical thiol-ene reactions do not fulfill the *click* criteria for example for polymer-polymer conjugations.^[74]

A variety of cycloadditions including azide-alkyne cycloaddition and Diels-Alder reaction as well as thiol-ene and thiol-yne reactions are examples of *click* reactions (Figure 6).

Some of those reactions have already been successfully used for modification of NP surfaces. Fleming *et al.* used the 1,3-dipolar Huisgen reaction for the first time as a general route for NP functionalization to couple various alkyne functionalized small molecules to azide-coated Au NPs (Scheme 3).^[75]

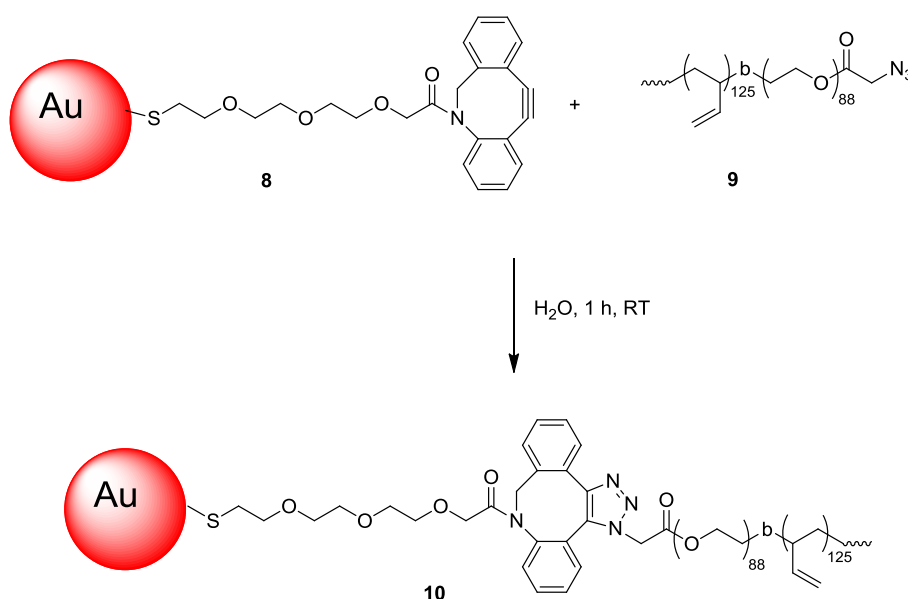


Scheme 3. Bromo-functionalized Au NPs **4** were functionalized with azide moiety using sodium azide. The prepared azide-substituted Au NPs **5** were modified with propyn-1-one derived small molecules **6**. Adapted with permission from [75]. Copyright 2006 American Chemical Society.

The introduction of the azide moiety to the Au NPs was achieved by post-modification technique using sodium azide to convert Br termini of ω -bromo-functionalized thiols **4** to azide. The azide-substituted Au NPs **5** underwent azide-alkyne cycloaddition with propyn-1-one derived small molecules **6** after incubation for 1-4 days. To decrease the reaction time, several copper compounds were added as catalyst, but resulted only in immediate and extensive particle aggregation. In general, the 1,3-dipolar Huisgen reactions on the NPs led to the formation of triazoles, which enabled the binding to heavy metals. The cooperative effect of triazoles in combination with other ligands allowed the binding of specific heavy metal ions resulting in agglomeration of the NPs which can be used for colorimetric sensing. Different triazole modified Ag NPs and Au NPs were employed for the detection of various heavy metal ions as Cd^{2+} ,^[76] Co^{2+} ,^[77] and Pb^{2+} .^[78] Additionally, the 1,3-dipolar Huisgen reactions allows for the functionalization of NPs with polymers^[79] and biomolecules^[80] in reaction times of hours using copper catalysts. Brennan *et al.* attached azide functionalized thiols to Au NPs and performed the

copper-catalyzed Huisgen reaction for the coupling of alkyne-modified lipase to the Au NPs.^[81] Although the copper-catalyzed 1,3-dipolar cycloaddition is widely used due to the high efficiency, high selectivity (no by-products), chemical orthogonality, and compatibility with aqueous media, the toxicity of Cu (I/II) species, however, is considered to be problematic for *in vivo* applications.^[82]

To avoid the use of Cu catalysts, Bertozzi group pioneered the development of copper-free strain-promoted azide-alkyne cycloaddition (SPAAC) using strained cyclooctynes and azides.^[83] To improve the kinetics of the strain-promoted cycloaddition, electron-withdrawing fluorine substituents on the cyclooctyne ring lead to comparable kinetics to the copper-catalyzed Huisgen reaction.^[84] Initially, the copper-free azide-alkyne reaction was used for the dynamic imaging of azide-modified glycans in live cells by means of labeling with cyclooctyne functionalized dyes. Recently, Gobbo *et al.* performed, for the first time, the strain-promoted copper-free azide-alkyne cycloaddition on the Au NP surface.^[85]



Scheme 4. Strain-promoted copper-free azide-alkyne cycloaddition of dibenzocyclooctyne-modified Au NPs **8** and azide-terminated polymersomes containing poly(butadiene)-*b*-poly(ethylene glycol) copolymer **9**. Adapted from [85] with permission from The Royal Society of Chemistry.

Here, they used the non-fluorinated dibenzocyclooctyne group to bind cyclooctyne-modified Au NPs **8** to azide-functionalized polymersomes consisting of the poly(butadiene)-poly(ethylene) block copolymer **9** (Scheme 4). The same group recently employed the strain-promoted azide-alkyne cycloaddition for the

decoration of dibenzocyclooctyne-modified peptides to azide functionalized Au NPs.^[86] However, the SPAAC has been limited to a few examples due to challenges with the solubility and the multistep synthesis of strain-promoted cyclooctynes.

In addition to the cycloaddition between azides and alkynes, the Diels-Alder reaction between dienes and dienophiles has been employed for the functionalization of NPs. One example for the Diels-Alder reaction is the ligation between highly electron-deficient tetrazine and strained dienophiles. The inverse electron demand Diels-Alder reaction was employed to immobilize tetrazine-terminated Au NPs to single wall carbon nanotubes under ambient conditions.^[87] The sidewall of the carbon nanotubes reacted without any pre-treatment with the tetrazine moiety of the Au NPs with the release of nitrogen. Zhu *et al.* prepared maleimide-modified Au NPs which were protected with furan groups.^[88] Thermally reversible Diels-Alder reaction allowed the availability of the maleimide functionality to react with furan-modified Au NPs for the formation of 3D networks of Au NPs. Upon heating at 100°C, the retro-Diels-Alder reactions led to single Au NPs and the precipitated particles could be redissolved. Forward and backward Diels-Alder reaction showed good reversibility with up to 30 cycles.

Besides the use of maleimide functionality in Diels-Alder reaction, the maleimide functionality proved to be very reactive as Michael acceptor in thiol-ene reactions. Although, it should be noted that radical thiol-ene reaction do not fulfill the *click* criteria for polymer-polymer conjugations.^[74] The experimental results were recently confirmed by kinetic modeling for polymer-polymer conjugation and the simulations showed the increased importance of termination by recombination reactions.^[89] Nevertheless, Mattoussi and co-workers prepared Au NPs with a bifunctional PEG linker containing thioctic acid as Au NP anchoring group and a maleimide group for conjugation with a terminal cysteine functionalized peptide sequence.^[90] After successful peptide immobilization onto the Au NPs, the peptide with free amine group was coupled to a NHS-activated carboxylic acid-modified Cy5 dye to determine the number of peptides per Au NP by UV/Vis spectroscopy and the assumption of 100% reaction efficiency. Besides the mentioned reactions referred to as *click* reaction, the thiol-yne reaction and Staudinger ligation meet the criteria of Sharpless, but only limited examples for the functionalization of metallic NPs are found in literature.

Light-Induced Reactions

Light is a powerful tool to provide the energy for chemical reactions based on photosensitive molecules.^[91] Thereby, the photosensitive molecules absorb light and can undergo typical photochemical processes, which can be described by the Jablonski diagram (Figure 7).

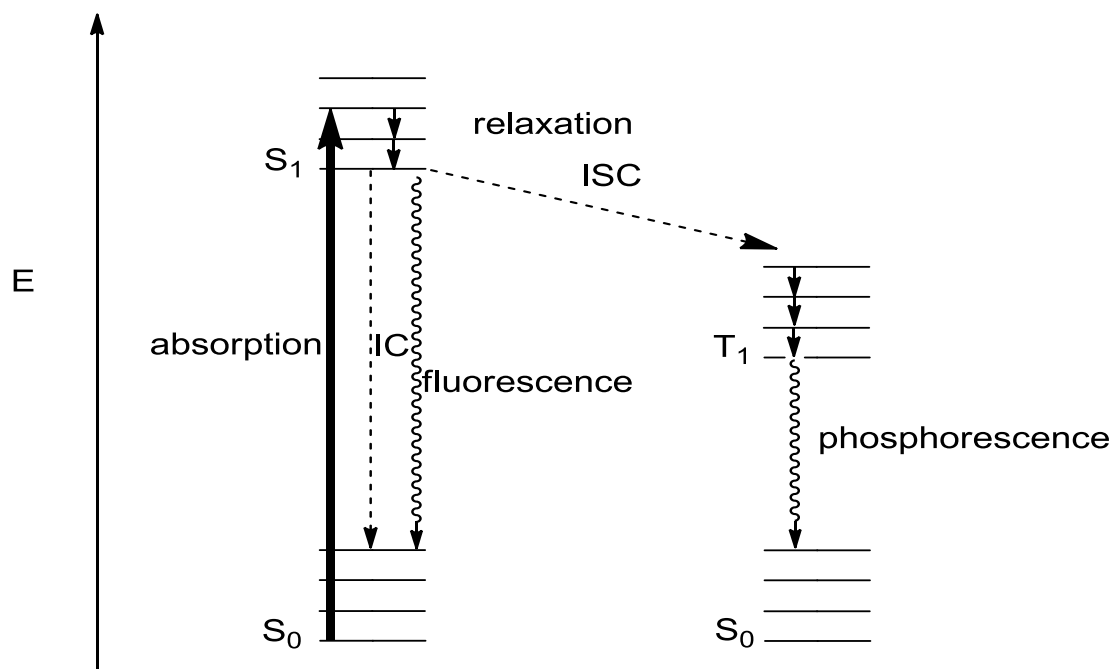
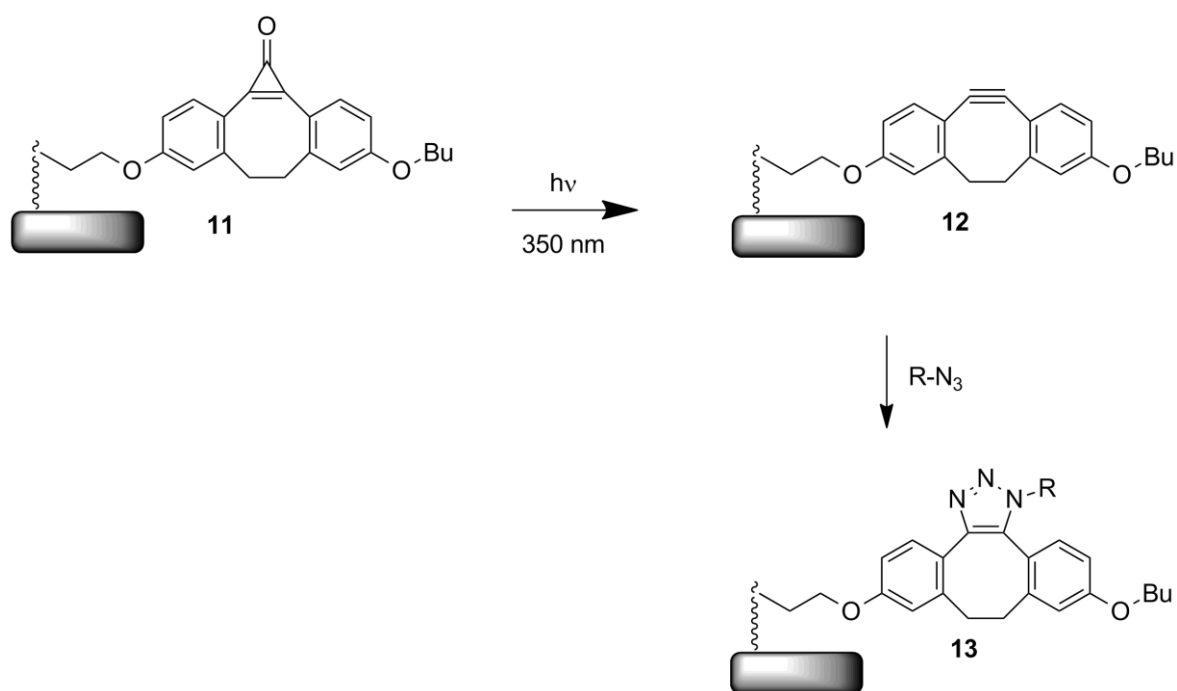


Figure 7. Jablonski diagram contains possible photochemical processes of a molecule, which can absorb a photon to reach the excited state. The excited molecule can lose vibrational energy or emit light termed as fluorescence to reach again. Alternatively, the molecule undergoes intersystem crossing to reach the triplet state, followed by phosphorescence.

In 1935, Jablonski explained the photochemical phenomenon of phosphorescence employing the graphical representation of different electronic states of a molecule and the transition between them in a diagram.^[92] Upon absorption of a photon with particular wavelength, the irradiated molecule is excited from the singlet ground state (S₀) to the first excited singlet state (S₁). Following the Franck-Condon principle, the excited molecule loses vibrational energy to reach the vibrational ground state of S₁. Thereof, the molecule can undergo a further non-radiative transition to the ground state S₀ *via* internal conversion (IC) or to the first excited triplet state (T₁) *via* intersystem crossing (ISC). The energy can also be released by the emission of light, termed as photoluminescence, which is divided into fluorescence and phosphorescence. Excited molecules have also the oppor-

tunity to react with a reactant in a chemical reaction. In general, there are several possible electronic and vibrational transitions upon light excitation. To decide which photochemical process is preferred, the quantum yield (Φ) is defined as the number of times a specific event transition occurs after absorption of a photon (value between 0 and 1). Light-induced reactions are based on the absorption of photons to generate highly reactive molecules, which can undergo chemical reactions.

In the following section, different light-induced reactions are presented, with the main advantage being the temporal and spatial control over chemical reactions. For instance, cyclopropanones can undergo light-induced decarbonylation upon UV irradiation ($\lambda = 350$ nm) to generate dibenzocyclooctynes, which allow the copper-free azide-alkyne cycloaddition (Scheme 5).^[93]

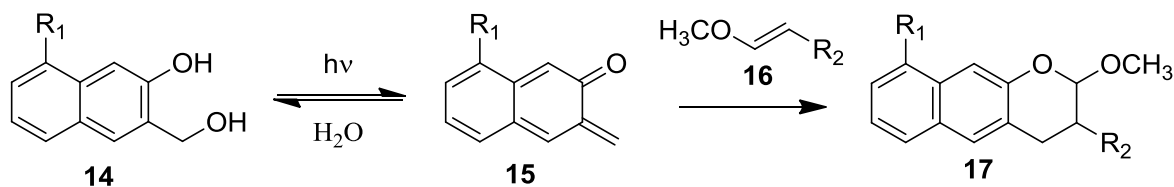


Scheme 5. Cyclopropanone moiety **11** was attached to polymer brushes and subsequently photoactivated to generate dibenzocyclooctynes **12**. In presence of azide-derived fluorescent dyes, dibenzocyclooctynes could undergo copper-free azide-alkyne cycloaddition to obtain **13**. Adapted with permission from [93]. Copyright 2010 American Chemical Society.

After attachment of cyclopropanones **11** on poly(*n*-hydroxysuccinimide 4-vinyl benzoate) brushes using amide coupling, a shadow mask was employed to generate the light-induced decarbonylation of cyclopropanone in spatially resolved fashion on a glass platform. Subsequent copper-free azide-alkyne cycloaddition of

the resulting dibenzocyclooctyne moiety **12** with azide functionalized dyes was restricted to the irradiated areas. The decarbonylation of cyclopropanones to yield dibenzocyclooctynes occurs quickly and quantitatively within 90 s using a low power UV lamp (3.5 mW/cm²). The subsequent reaction with azides was completed after 20 min. The drawback of the cyclopropanone photoactivation is the irreversibility of the process, therefore unreacted dibenzocyclooctynes retain reactive after UV irradiation.

In addition, Popik and coworker demonstrated the use of the light-induced hetero-Diels-Alder reaction of naphthoquinone methides with electron-rich alkene as efficient ligation strategy for small molecules (Scheme 6).^[94]

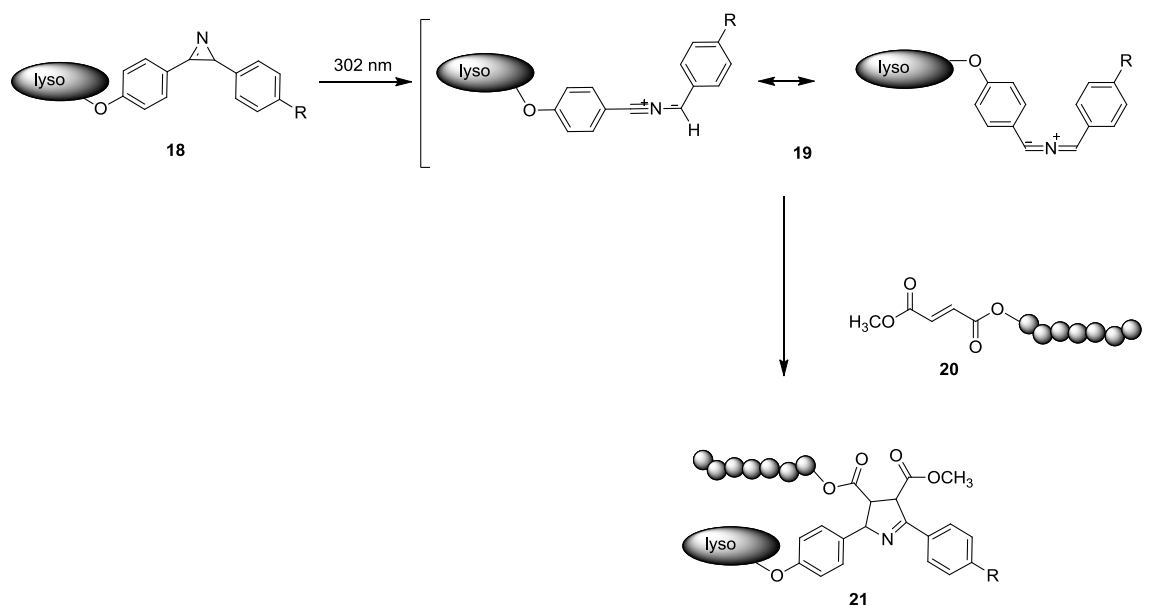


Scheme 6. 3-(Hydroxymethyl)-2-naphthol **14** dehydrogenated to the highly reactive naphthoquinone methide **15** upon irradiation with UV light ($\lambda = 300$ nm). Naphthoquinone methide could undergo Diels-Alder reaction with vinyl ethers **16** leading to **17**. Adapted with permission from [94]. Copyright 2011 American Chemical Society.

Upon UV irradiation ($\lambda = 300$ nm), 3-(hydroxymethyl)-2-naphthol **14** dehydrogenated to the highly reactive naphthoquinone methides **15**, which acted as the diene in the hetero-Diels-Alder reaction with vinyl ethers. Unreacted naphthoquinone methides regenerated to the starting diol in aqueous solution. Due to the competition between hydration and cycloaddition of naphthoquinone methides, the naphthoquinone methide moieties were very selective and reacted only with vinyl ethers **16** or enamines in aqueous solutions. The short lifetime ($\tau \sim 7$ ms) of the active form allowed for spatial control over the reaction due to less migration, however 16 UV lamps ($\lambda = 300$ nm; each 4 W) were necessary for the complete conversion after 20 min to **17**.

Lim and Lin have developed another light-induced azirine-alkene cycloaddition upon irradiation with 302 nm for the rapid (~ 2 min) and selective protein conjugation (Scheme 7).^[95]

Introduction

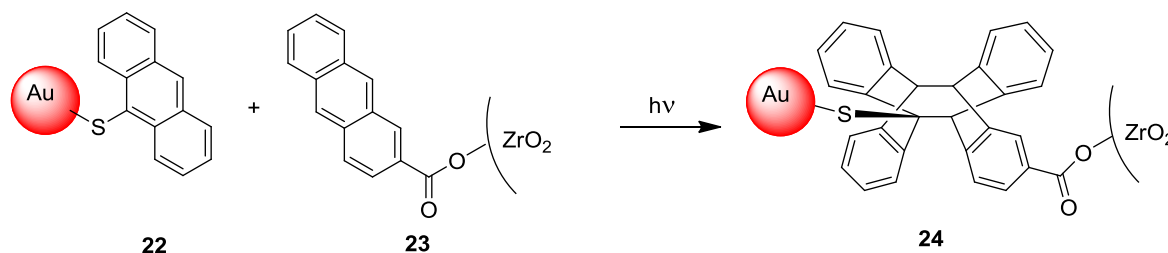


Scheme 7. Light-induced azirine-alkene cycloaddition between azirine-containing lysozyme **18** and dimethylfumarate-linked poly(ethylene glycol) **20** to generate the lysozyme-PEG conjugate **21**. Adapted from [95] with permission from The Royal Society of Chemistry.

The UV irradiation of azirine **18** led to highly reactive nitrile ylide intermediate **19**, which can undergo a 1,3 dipolar cycloaddition with activated alkenes to yield a pyrroline product **21**. The azirine ligation was successfully utilized to couple azirine-containing lysozyme **18** to dimethylfumarate-linked poly(ethylene glycol) **20** in aqueous media. Thus, the azirine-alkene cycloaddition is a rapid and efficient ligation for bioconjugation and the nitrile ylide intermediate **19** showed even higher reactivity than nitrile imine moieties, which are formed as intermediates in tetrazole-ene cycloaddition. However, the synthesis of the azirine compounds is demanding and the generated pyrroline product **21** showed no fluorescence in comparison to the pyrazoline product of the tetrazole-ene cycloaddition.

Despite the great success of light-induced reactions for the surface modification of 2D surfaces, there is a lack of light induced reactions for NP modification.

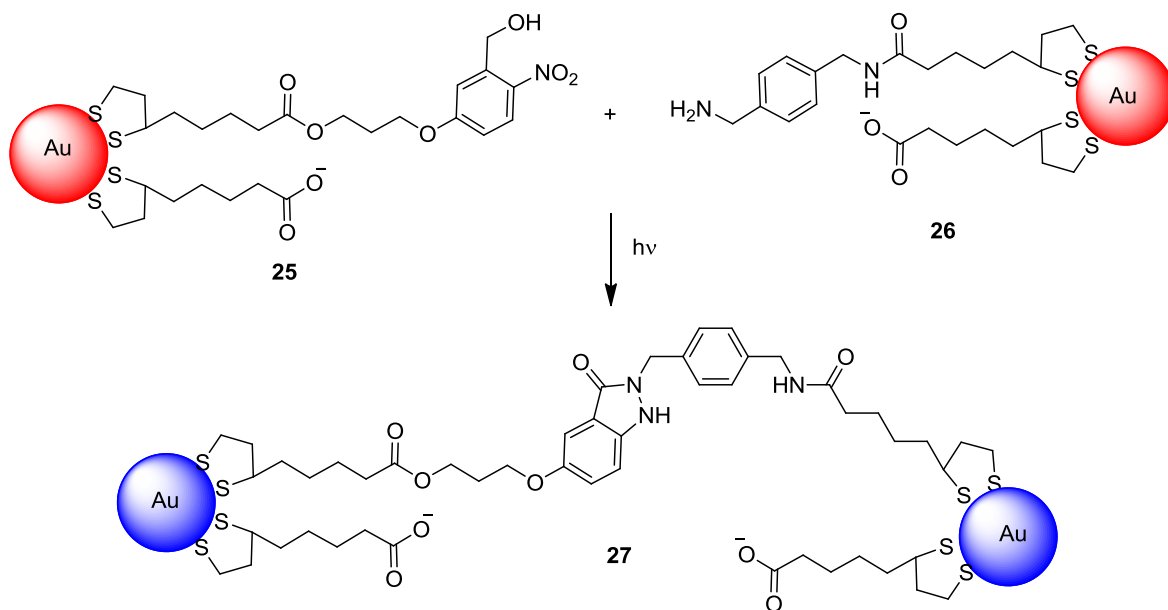
There are limited examples for the light-induced covalent assembly of NPs. For instance, Smith and Watson employed anthracene-modified nanomaterials for light-induced agglomeration (Scheme 8).^[96] First, 9-anthracenethiolate-capped Au NPs **22** with average diameters of 15 nm were prepared following the method of Brust.^[14a] Upon irradiation with 385 nm for up to 45 h, anthracene moieties underwent interfacial, light-induced [4+4] cycloaddition between the Au NPs to form Au NP assemblies.



Scheme 8. Light-induced [4+4] cycloaddition between anthracene-capped Au NPs **22** and anthracene-coated ZrO₂ films **23** upon irradiation with 355 nm to obtain Au NP-patterns onto ZrO₂ films **24**. Adapted with permission from [96]. Copyright 2010 American Chemical Society.

Subsequently, the anthracene-capped Au NPs **22** were coupled to anthracene-coated ZrO₂ films **23** upon irradiation with 355 nm for 90 min (Scheme 8). Using a mask, the Au NPs could finally be patterned onto ZrO₂ films. The ToF-SIMS images showed a poor resolution of irradiated and non-irradiated regions of several micrometers. Although Smith and Watson demonstrated the successful use of light-induced cycloaddition for the assembly of nanomaterials by UV/Vis spectroscopy, TEM images and ToF-SIMS images, the approach with the anthracene moiety as photoreactive group had many drawbacks, such as the long irradiation of several hours and toluene as solvent. The main drawback was the intramonolayer photodimerization of the anthracene groups onto one NP, which decreased the number of photoreactive groups on the NP surface. As control experiments, tetra-*n*-octylammonium bromide (TOAB)-capped Au NPs were irradiated and showed no agglomerations, but the stability of TOAB-capped Au NPs was different from anthracene-capped Au NPs. To proof that the covalent binding was the reason for the NP assembly, the reversibility of the anthracene dimers upon irradiation with 250-290 nm should lead again to Au NP dispersion without any agglomeration, however this experiment was not performed.

Lai *et al.* functionalized the surface of Au NPs with *o*-nitrobenzyl alcohol **25** and benzylamine **26** to assemble Au NPs into 1D arrays by light-induced indazolone linkage **27** in aqueous solution (Scheme 9).^[97]



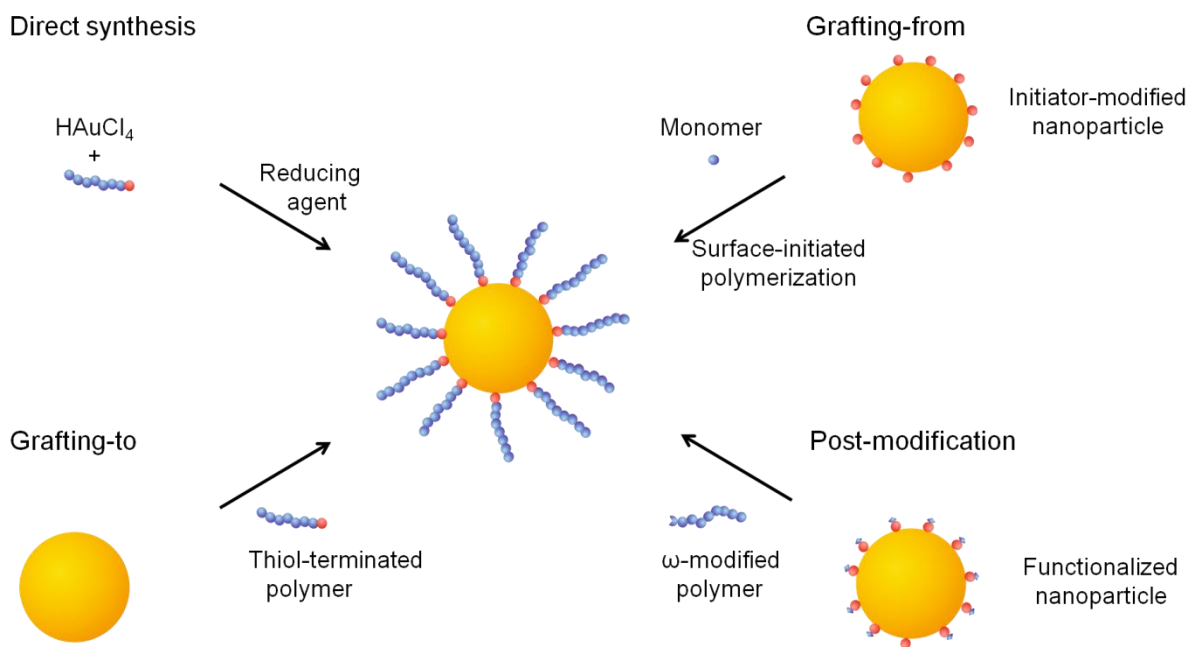
Scheme 9. Light-induced reaction of *o*-nitrobenzyl alcohol-capped Au NPs **25** and benzylamine-capped Au NPs **26** to assemble the Au NPs in 1D arrays **27**. Adapted from [97] with permission from The Royal Society of Chemistry.

Thioctic acid was used as inert linker in the ratio of 100:1 to the photoreactive group to stabilize the Au NPs. Upon irradiation with $\lambda > 310$ nm, different 1D nanochains were formed depending on the concentration and irradiation time of 0 min to 30 min. Lai *et al.* demonstrated the use of light-induced indazolone linkage **27** for the assembly of Au NPs with short irradiation time in aqueous solution. However, the reaction between *o*-nitrobenzyl alcohol **25** and benzylamine **26** was not orthogonal to functional groups such as amine or carboxyl acid groups and was therefore not applicable for the reaction with biomolecules. Additionally, *o*-nitrobenzyl alcohol **25** and benzylamine moieties **26** were coated on Au NPs with the same diameter and the reaction of both counterparts could not be proven by TEM. However, the NP assembly based on light-induced reactions is complicated in comparison to the ease of triggered NP assembly caused by salt, pH or temperature.^[98]

In the presented work, photoenol chemistry and tetrazole-ene chemistry are employed for the light-induced modification of NP surfaces. The main benefits of both reactions are the orthogonality, high efficiencies, and fast reaction kinetics which will be discussed in detail in the following chapters. Photoenol chemistry is discussed in detail in the introduction of chapter 3 (p. 41-46) and tetrazole-ene chemistry in the introduction of chapter 5 (p. 85-87).

1.3.2 Polymer Nanocomposites

Polymer nanocomposites consist of polymer or copolymer and nanoparticles and have attracted significant interest in recent years due to their unique properties and broad range of potential applications.^[99] The embedment of NPs in various polymer matrices or polymer coatings of NPs in core/shell structure for the stabilization of NPs are typical examples for polymer nanocomposites.^[100] The following section focuses on core/shell structures as they are particularly sought-after due to the combination of optical and catalytic properties of NPs and the chemical nature of polymers, which makes them attractive for the incorporation of drugs and other biomedical/biosensing applications in hydrophilic milieus.^[101] When considering the biomedical applications, it is necessary to prepare stable and biocompatible NPs with well-defined surface coatings.^[102] The methods for the preparation of core/shell nanocomposites are classified in four main approaches: the direct-synthesis method, grafting-from strategy, grafting-to strategy and post-modification technique (Scheme 10).^[103]



Scheme 10. Main approaches for the preparation of polymer nanocomposites based on covalent linkages can be classified in the direct-synthesis method, grafting from strategy, grafting-to strategy and post-modification technique. Adapted from [103]. Copyright 2009, with permission from Elsevier.

The direct-synthesis method is based on the reduction of metal salt in presence of the polymer. For the synthesis of Au NPs, Corbierre *et al.* stabilized Au NPs with thiolated poly(styrene) and thiolated poly(ethylene glycol) with different molecular weights.^[104] Thermogravimetric analysis revealed the lower grafting density in case of polymers with higher molecular weight. In general, a one-step procedure is preferred due to the simplicity of one step. However, the direct-synthesis method in presence of the polymer results in NP cores with a broad size distribution.^[105] With the advances in living/controlled radical polymerization, the grafting-from approach has extensively been utilized to induce polymerization on the surface of initiator-modified NPs. In such a manner, Raula *et al.* esterified an initiator to mercaptoundecanol-capped Au NPs to polymerize poly(*N*-isopropylacrylamide) *via* reversible addition-fragmentation chain-transfer (RAFT) polymerization.^[106] The thermally responsive poly(*N*-isopropylacrylamide) collapsed at higher temperature in aqueous solution leading to an increase of the hydrodynamic radius and a blue shift in the SPR signal due to less stabilization of the polymer shell and aggregations. The polymerization on the NP surface leads to a higher grafting density in comparison to the grafting-to approach, where the anchored polymer brushes imposes steric hindrance. However, the polymerization typically requires temperatures exceeding 60 °C leading to agglomerations of the thermally unstable NPs.^[107] In addition, the assessment of the length and dispersity of the grafted polymer is often challenging. Recently, such problems have been circumvented by the use of functionalized polymers containing e.g. thiols or amines, which can be used for direct ligand exchange on the NP surface in a grafting-to approach. Electrostatically stabilized NPs such as citrate-capped Au NPs can be used for ligand exchange reaction with sulfur containing RAFT polymers.^[108] For instance, the dithioester group at the ω -terminus of the RAFT polymer poly(oligo(ethylene glycol)methacrylate) allowed the direct immobilization to pre-formed citrate-capped Au NPs through the covalent sulfur-Au bond.^[109] The drawback of ligand exchange reaction is the need of a specific binding group for each type of NP.^[110] With the development of *click* chemistry and living/controlled radical polymerization, pre-formed NPs can be post-modified in a modular and defined way. Zhang *et al.* substituted tetraoctylammonium-capped Au NPs with lipoic acid functionalized azide poly(ethylene glycol).^[79b] The azide moiety can undergo azide-alkyne 1,3-cycloaddition with alkyne-terminated poly(*N*-

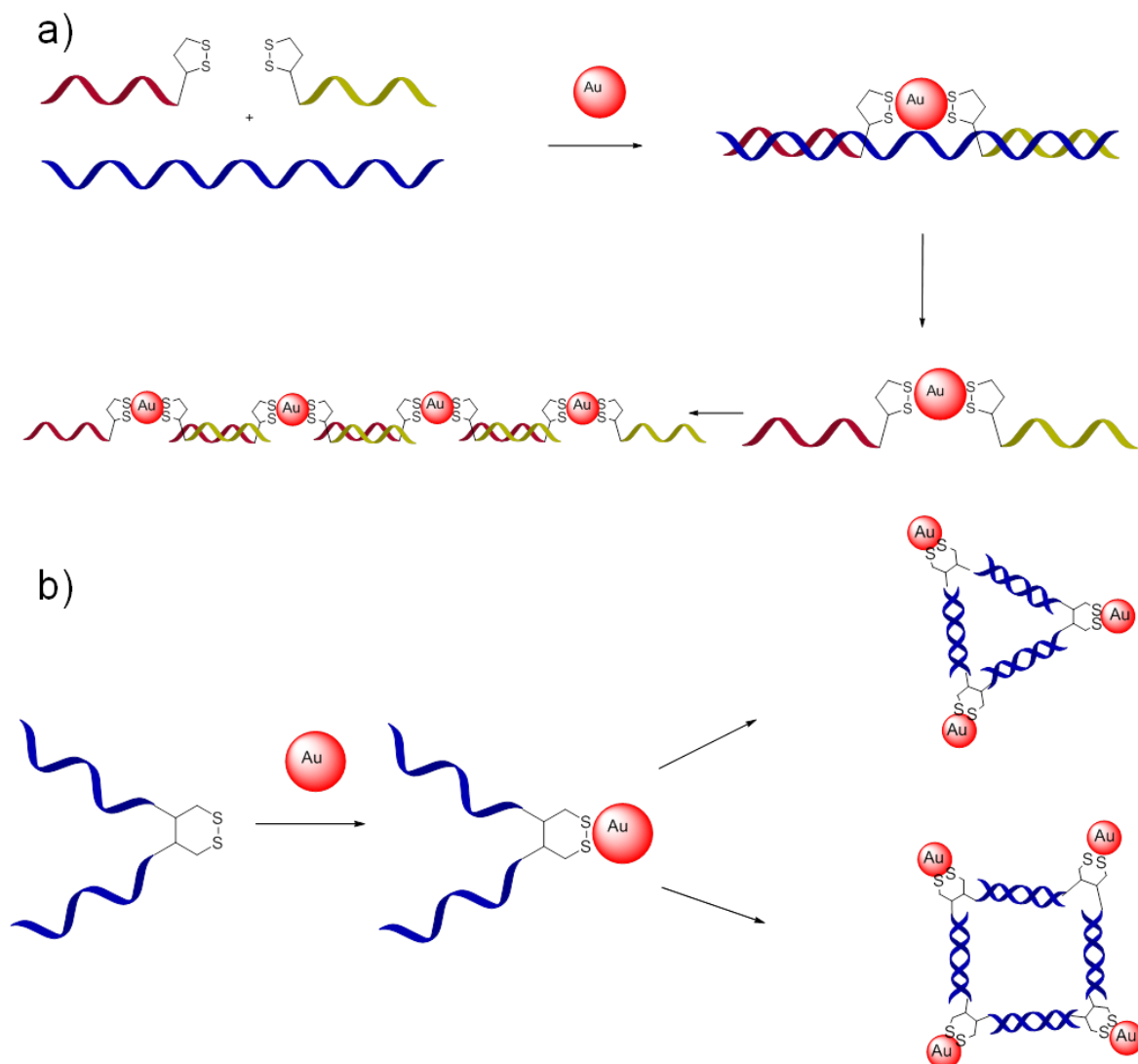
isopropylacrylamide), which was synthesized in a RAFT polymerization process. In addition to azide-alkyne cycloaddition, the Diels-Alder reaction is applied more and more for the functionalization of NPs. Particularly, the reversibility of the Diels-Alder reaction offers the possibility to trigger the properties of the polymeric nanocomposite such as solubility several times. Constanzo *et al.* prepared a thiol-terminated poly(styrene)-*b*-PEG diblock copolymer *via* Diels-Alder linkage.^[111] After functionalization of Au NP with the block copolymer and dispersion in the PEG matrix, thermal treatment led to the cleavage of PEG and hydrophobic poly(styrene)-modified Au NPs, which resulted in a migration of the Au NPs to the film surface.

To prepare polymer nanoparticle core/shell structures, the grafting-from and the direct synthesis method have the benefit of less steric hindrance, which results theoretically in a higher grafting density. However, the direct synthesis method leads to a broad size distribution of the NPs. The grafting-to and the post-modification approach allow for a thorough characterization of the tethered molecules as well as the NPs prior to the grafting.

1.3.3 DNA-Nanoparticle Conjugates

One of the first biomolecules of interest, which was immobilized on NPs, was DNA. In 1996, Mirkin *et al.* attached for the first time thiolated DNA to Au NPs and induced aggregation using complementary DNA.^[112] In the meanwhile, the stability in saline solutions of DNA-NP conjugates was improved for example by the use of cyclic disulfides^[113] or even tetra-thiol groups^[114] as anchoring groups. Moreover, cyclic disulfide-containing DNA enabled stable DNA-Ag NP conjugation.^[115] When Ag NPs with complementary DNA was added, the Ag NPs assembled to form networks associated with a red shifting in SPR.

Introduction

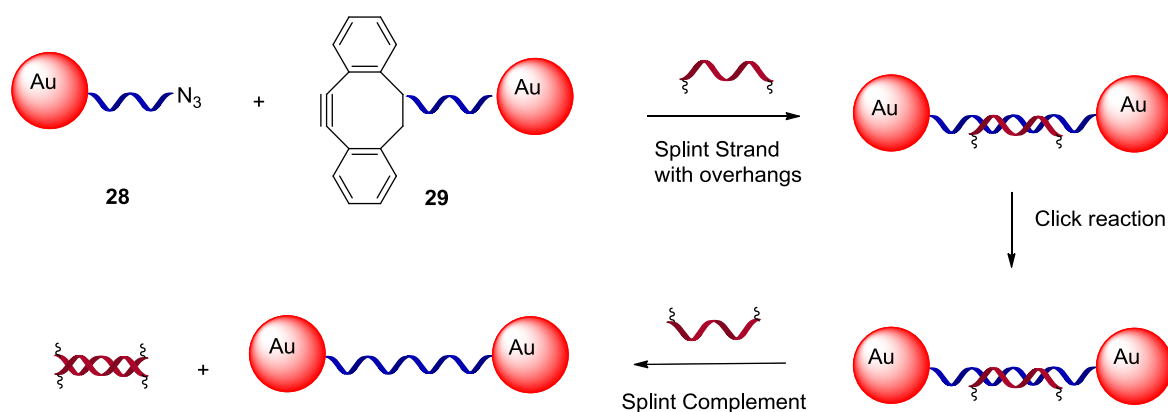


Scheme 11. a) Template DNA controlled immobilization to construct linear chains. Adapted with permission from [116]. Copyright 2012 American Chemical Society. b) Flexible DNA modification approach for the construction of DNA-Au NPs conjugates in different patterns. Adapted from [117] with permission from The Royal Society of Chemistry.

To construct more defined DNA-NP networks, Zhang *et al.* hybridized two thiolated DNA strands with a template DNA to position the thiol groups at a certain distance (Scheme 11a).^[116] Depending on the space between the thiols groups, Au NPs with 5 nm or 10 nm in size could be incorporated within the network. After removal of the template DNA, the two DNA strands are located on the opposite side of the NP and can be further used to form linear chains of NP through hybridization. The methodology using a template DNA is limited to one dimension, therefore Wen *et al.* prepared cyclic disulfides with two DNA arms (Scheme 11b).^[117] After binding to Au NPs, the DNA arms could specifically hybridize to form tetra-

hedral or triangle patterns. Besides the formation of NP networks, the functionalization of DNA with particular markers or proteins allows for the DNA directed immobilization of desired species. The methodology was used for the development of microarrays,^[118] but was then expanded to immobilize various biomolecules on Au and Ag NPs.^[119]

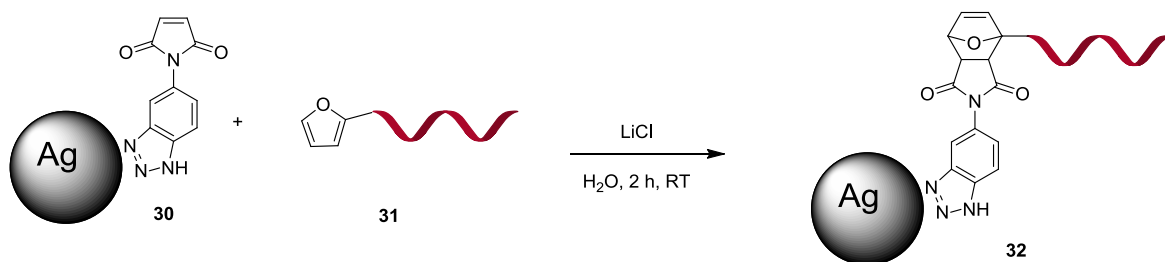
Recently, copper-free *click* chemistry was employed for the construction of NP assemblies (Scheme 12).



Scheme 12. Dimer formation of DNA-Au NP conjugates using templating splint strands and strain-promoted azide-alkyne cycloaddition between azide **28** and alkyne-modified Au NPs **29**. Adapted from [120] with permission from The Royal Society of Chemistry.

Au NPs were functionalized with discrete number of azide **28** and strained alkyne-modified ssDNA **29** and subsequently brought together with a splint strand, which is complementary to both immobilized DNA strands with non-complementary overhangs.^[120] After the successful azide-alkyne cycloaddition, the splint strands were removed and dimers or trimers of Au NPs were still observed.

In addition, Chen *et al.* prepared benzotriazole-maleimide coated Ag NPs **30**, which were able to undergo Diels-Alder reaction with cyclopentadiene-modified PEG and furan-modified ssDNA **31** (Scheme 13).^[121]



Scheme 13. Maleimide-capped Ag NPs **30** and furan-modified ssDNA **31** can undergo Diels-Alder reaction to generate ssDNA-Ag NP conjugate **32**. Adapted from [121] with permission from The Royal Society of Chemistry.

Moreover, ssDNA-Ag NP conjugates **32** were further functionalized with the protein myoglobin using DNA-directed immobilization of myoglobin-modified complementary DNA strand.

In general, DNA-nanoparticle conjugates can be designed in various networks using complementary DNA strands attached to the NP surface. In addition, DNA directed immobilization is a powerful tool for the incorporation of various biomolecules on the NPs.

1.4 Surface Immobilization of Nanoparticles

In the past decade, the modification and application of engineered nanomaterials, in particular variable types of functional metallic nanoparticles, have attracted growing interest. The high expectations for their use for the preparation of novel plasmonic and electronic devices have not yet been fulfilled. This is mainly due to stability issues posed by NP assembly and patterning, such as the preparation of the micron and submicron NP arrays essential for electronic, optical and sensor applications.^[122] Both top-down approaches such as lithography as well as bottom-up approaches based on chemical ligation strategies have been employed to pattern NPs. In recent years, the research focused on the combination of both methodologies often using van der Waals and electrostatic interactions or covalent bonding jointly with lithography based techniques to fabricate functional structures in well-defined patterns. For instance, Rotello and co-workers prepared photoactivatable Au NPs containing UV cleavable protecting groups. The fabrication of patterns was achieved by photolithography and electrostatic assem-

bly based on surface charge after a protecting group cleavage.^[123] A different approach based on chemical electron beam lithography was reported by Mendes *et al.* After immobilization of nitro groups onto silica wafers, electrostatic binding of citrate-capped Au NPs was achieved after the reduction of nitro to amine groups and additional protonation.^[124] However, despite the initial success of the electrostatically driven assembly, the chemically directed assembly using covalent ligation strategies is preferred due to stronger and specific binding, which is crucial for electronic applications involving high electric fields.^[125] Such a covalent approach based on Huisgen 1,3-dipolar cycloadditions and microcontact printing (μ CP) was previously employed to design patterns of dyes,^[126] yet also biomolecules such as proteins^[127] and DNA.^[128] Recently, the strategy was expanded to immobilize azide functionalized Au NPs to alkyne coated Au surfaces.^[129] However, μ CP has limitations as it is based on the use of pre-patterned stamps and their deformation as well as the spreading of ink lead to blurring of the desired pattern.^[130] In addition, μ CP is only applicable to flat surfaces and generally does not allow for a temporal control.

1.5 Applications of Nanoparticles

NPs can be designed in various composites, sizes, and shapes with different surface chemistry to enable specific interaction with biomolecules and cells in biomedical applications including biosensors, imaging, and drug delivery. Due to their unique optical properties, noble metallic NPs such as Au and Ag have been extensively studied for detection and sensing of biomolecules. A key step for the stabilization of NPs is the functionalization with small molecules, polymers or biomolecules to prevent NPs from agglomeration and tailor them for targeting.

Biosensing

The sensing of biomolecules and toxic substances is of particular interest in biomedical applications. In general, the biosensors imparts two functions: on one side the binding of the target species and on the other side the transduction of the binding event.^[131] Due to their small sizes and their unique optical and electrical

properties including LSPR, fluorescence and SERS, Au and Ag NPs are suitable as biosensors in combination with attached biomolecules.

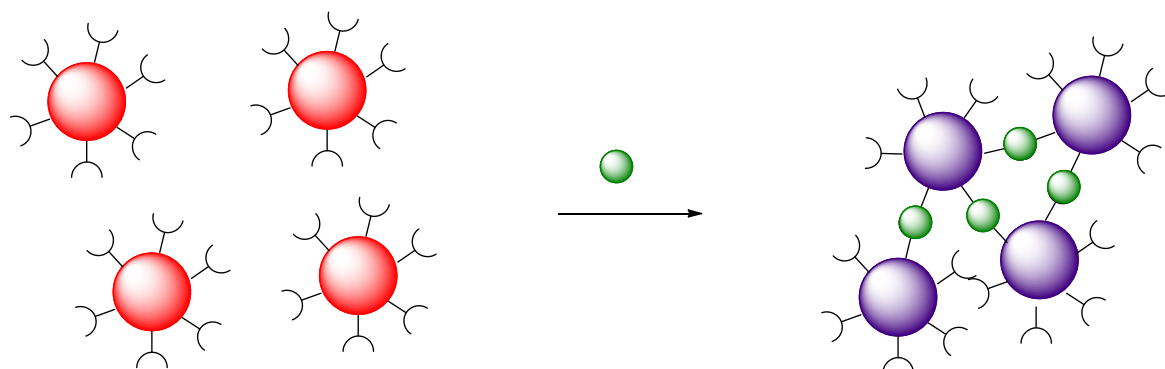


Figure 8. Principle of nanoparticle based immunoassay, which detects spectroscopically the aggregation of Au or Ag NPs after treatment with specific proteins or DNA strands (green). Adapted by permission from Macmillan Publishers Ltd: Nature [112], copyright 1996.

The seminal work of Leuvering *et al.* in 1980 presented a new NP based immunoassay for proteins,^[132] which was later expanded by Mirkin *et al.* for the colorimetric detection of DNA.^[112] Both immunoassays were based on the aggregation of Au or Ag NPs after treatment with specific proteins or DNA (Figure 8), which resulted in a color change from red to purple or gray in the case of Au NPs. Moreover, Medley *et al.* demonstrated the use of Au NPs functionalized with aptamers, which are DNA strands with specific targeting ability, for the colorimetric detection of cancer cells.^[133] The binding to the diseased cells led to a color change due to the closer distance between the Au NPs, which could be observed by naked eye or by absorbance measurement. Interestingly, DNA-Au NP conjugates enable the cellular uptake despite the negative surface charge.^[7] So called nano-flares are DNA functionalized Au NP allowing cellular uptake and coupling to RNA in living cells.^[134] Upon the hybridization, complementary Cy5 labeled DNA strands were released and the RNA could be quantified through fluorescence measurements. Moreover, bioconjugates of Au NPs and antibodies against epidermal growth factor receptors, which were overexpressed in precancers, allowed the optical imaging of precancer.^[135] Beyond cancer cells, every bacteria, virus or pathogen have their unique nucleic acids sequences, which can be employed for the targeting and detection of diseases.^[136]

Besides Au NPs, Ag NPs with their 100× higher molar extinction coefficient exhibits much higher sensitivity.^[137] Graham *et al.* demonstrated the opportunity of DNA-Ag NP conjugates for the detection of DNA relating to disease.^[138] In their approach, they functionalized Ag NPs with a mixed monolayer of Raman dye and specific DNA strand to detect the target DNA via SERS measurements.

NP arrays of Au or Ag NPs attracted much attention for the sensing of biomolecules due to the well-studied methods including lithography, microcontact printing, and physical engineering. The unique properties such as LSPR and SERS allowed the detection of a wide range of analytes.^[139]

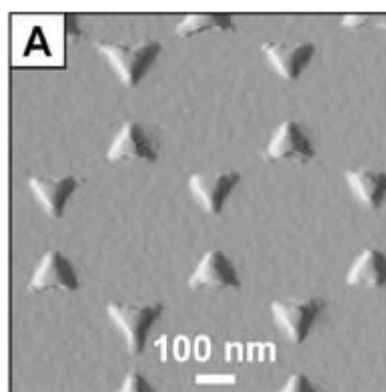


Figure 9. Atomic force microscopy image of triangular Ag NPs on a glass substrate. Reprinted with permission from [140]. Copyright 2002 American Chemical Society.

For instance, Haes *et al.* fabricated triangular Ag NPs by nanospheres lithography and functionalized the Ag NPs with thiol-containing self-assembled monolayers (Figure 9).^[140] After covalent attachment of biotin by amide coupling, the biotin-coated Ag NP array enabled the detection of streptavidin evidenced by the LSPR red shift of 27 nm after incubation of 100 nM streptavidin. NP bioassays are extraordinary sensitive and selective and can be reused after washing procedures. Additionally, several research groups are interested in the detection of pathogens such as virus and bacteria. Therefore, Ag nanorods arrays are highly sensitive SERS substrate to distinguish various viruses including adenovirus, rhinovirus or human immunodeficiency viruses due to the different nucleic acids and proteins.^[141]

Drug Delivery

The development of biofunctionalized NPs for the targeting delivery of therapeutics has emerged a new field for the medical treatment.^[142] Liposomes,^[143] dendrimers,^[144] polymeric NPs^[145] were extensively studied as pharmaceutical carriers, but also metallic NPs serve as platform for drug delivery. Mirkin's group demonstrated increased drug solubility and efficacy through attachment to DNA-Au NP conjugates.^[146] The hydrophobic drug Paclitaxel was covalently bonded *via* amide bond formation to fluorescein-labeled DNA-Au NPs conjugates, which were subsequently used for the visualization of the Paclitaxel-DNA-Au NP conjugates in the cell (Figure 10).

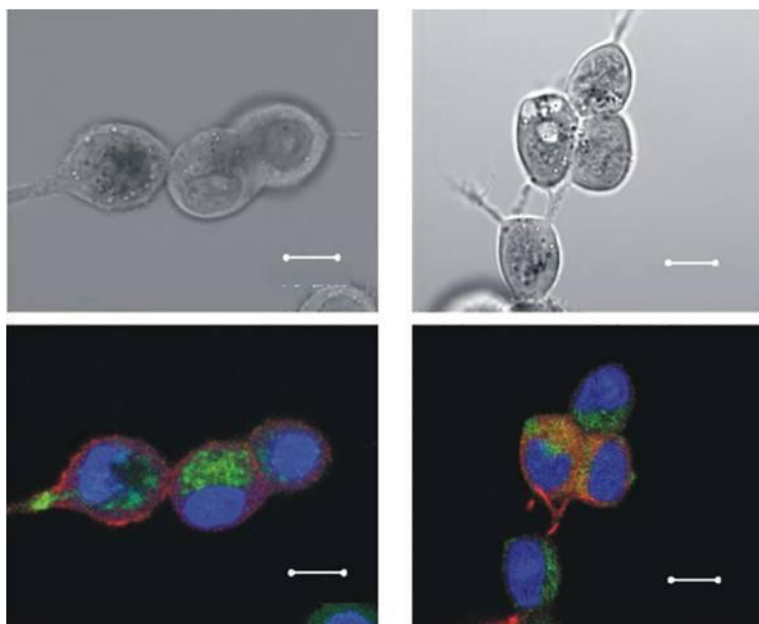


Figure 10. Bright-field (top) and overlaid fluorescence (bottom) image of human breast cancer cells showing the cellular uptake of fluorescein-labeled DNA-Au NPs conjugates. Scale bar is 10 μm . Adapted with permission from [146]. Copyright 2011 American Chemical Society.

In addition, Au NPs alone can lead to cell death *via* photothermal treatment. Particularly, Au nanorods have an absorption maximum in the near-IR region and irradiation with corresponding light generates heat, which can cause cell damage.^[147] Tailoring the surface of Au NR with specific recognition units, Au NR were able to distinguish between malignant and non malignant cells and caused cell death with higher affinity to cancer cells.^[148]

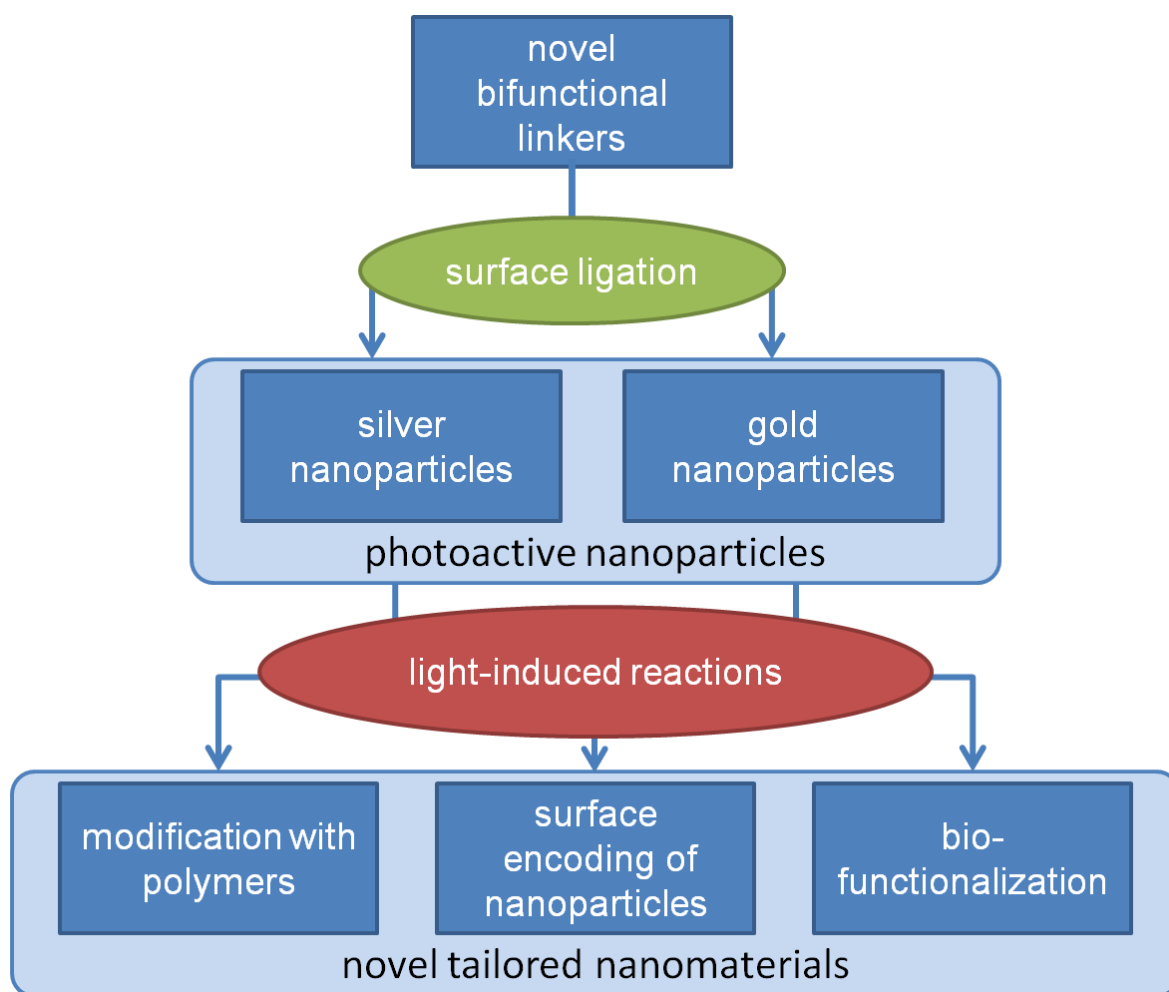
Food Packaging

The antimicrobial and antibacterial activity of Ag NPs is well known in literature.^[149] Therefore, polymeric Ag nanocomposites are the most sought-after nanomaterials due to the good stabilization of the long polymeric chains.^[101] Particularly, the food packaging industry is interested in Ag NPs as additives for plastics to inhibit bacteria growth and increase the shelf-life of the food.^[150] The incorporation of Ag NPs in polymer matrixes such as PEG or poly(lactic acid) allows the stabilization of Ag NPs to obtain antimicrobial material. Moreover, Damm *et al.* reported the higher antimicrobial efficacy of Ag NPs in polyamide 6 in comparison to Ag microparticles.^[151] Both nanocomposites were treated with *Escherichia coli* bacteria revealing the better silver ion release of Ag NPs although the filler content was lower (0.06 wt.%) than of Ag microparticles (1.9 wt.%).

In summary, NPs have great potential for the application in biomedicine, biosensing and food packaging. Although nanotechnology is often called a cross-sectional technology, further efforts have to be made in nanomaterials to become economically profitable for the translation of nanotechnology research into commercialization.

2 Research Outline

The aim of this thesis is to establish light-induced chemical reactions for the functionalization of metallic NPs with polymers and biomolecules. Several general requirements should be fulfilled for the ligation strategy of NPs, in particular concerning biofunctionalization: first, the reaction conditions should be mild, catalyst-free, orthogonal, and high yielding in aqueous solutions. Second, functionalization of NPs should be evidenced unambiguously and comprehensively with various characterization techniques. In Scheme 14, the preparation of novel tailored nanomaterials is depicted based on novel bifunctional linkers, which are attached to the surface of NPs to generate photoreactive NPs for light-induced reactions.



Scheme 14. Schematic illustration of the preparation of novel tailored nanomaterials using light-induced reactions.

For this purpose, we focus on the light-induced photoenol chemistry and nitrile imine mediated tetrazole-ene chemistry (NITEC) due to their appealing properties of high yields, (bio)orthogonality and spatiotemporal control. Metallic NPs, Au and Ag NPs, should be employed due to their unique optical properties and the number of applications in the field of biosensing and drug delivery. In order to tether NPs with photoenol or tetrazole moieties, novel bifunctional linkers have to be synthesized which should contain both the NP anchoring group (thiols for Au NPs and benzotriazoles for Ag NPs) and the photoreactive groups for further modification. Photoreactive NPs are envisaged for the light-induced modification with functional polymers or biomolecules, which need to contain the respective dienophile or dipolarophile to be able to undergo Diels-Alder reaction (photoenol-modified NPs) or NITEC reaction (tetrazole-modified NPs).

Subsequently, prepared NP conjugates should be characterized with various techniques such as UV/Vis spectroscopy, zeta potential measurements, transmission electron microscopy, fluorescence spectroscopy, and gel electrophoresis.

In addition, photoreactive Au NPs should be encoded in a spatially resolved fashion using direct laser writing (DLW) techniques into variable patterns employing a rapid Diels–Alder cycloaddition with surface anchored enes to design Au NP covered surfaces.

3 Light-Induced (Bio)Functionalization of Gold and Silver Nanoparticles¹

Introduction

Bifunctional linkers receive growing importance for the covalent binding of biomolecules to NP surfaces. In general, bifunctional linkers consist of three building blocks, namely the anchoring group, the spacer and the functional group for further functionalization.^[152] Benzotriazoles are known to bind strongly through the 1 or 3 nitrogen position of the triazole ring^[153] and enable the corrosion inhibition on Cu^[154] or Ag.^[155] It is assumed that benzotriazoles form polymeric species with metal ions on the NP surface and thereby benzotriazoles are able to replace citrate groups due to the higher binding affinity.^[156] Graham and coworkers synthesized a library of benzotriazole containing compounds for the stabilization of Ag NP surfaces and additional SERS measurements.^[157] Moreover, the benzotriazole maleimide linker has been successfully employed for the immobilization of furan-modified DNA onto Ag NPs, subsequent SERS detection of the DNA was achieved.^[158]

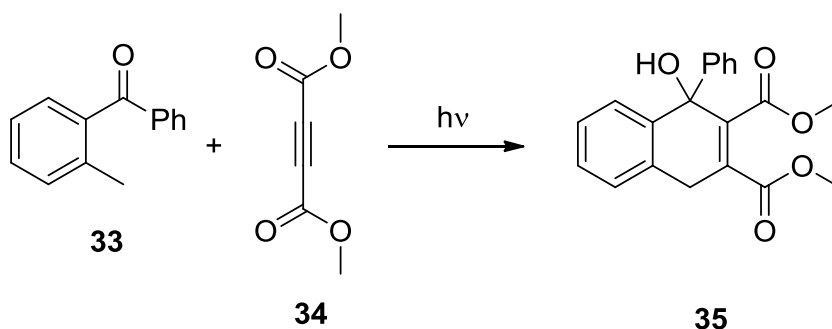
On one hand side, the spacer between the anchoring group and the functional group has the purpose to increase the availability of the functional group for further reactions and minimize the steric hindrance. On the other side, the spacer also influences the solubility of the NPs. For instance, the group of Mattoussi improved the water solubility of Au NPs and quantum dots employing ethylene glycol units.^[159]

Various functional groups have already been added to the NP surface through the anchoring of bifunctional linkers.^[160] However, there are only few reports on the use of photoactivatable groups on the NP surface for orthogonal *click* reactions, although light-induced reactions represent a powerful tool for the tailoring of (nano) materials.^[161] The spatial and temporal control over the reactions implies the opportunity to immobilize NPs on surfaces in a spatially resolved fashion or to engineer complex materials such as Janus particles.^[162] Smith *et al.* attached

¹ Parts of this chapter have been adapted from Stolzer, L.; Ahmed, I.; Rodriguez-Emmenegger, C.; Trouillet, V.; Bockstaller, P.; Barner-Kowollik, C.; Fruk, L. *Chem. Commun.* **2014**, 50, 4430 with permission from The Royal Society of Chemistry.

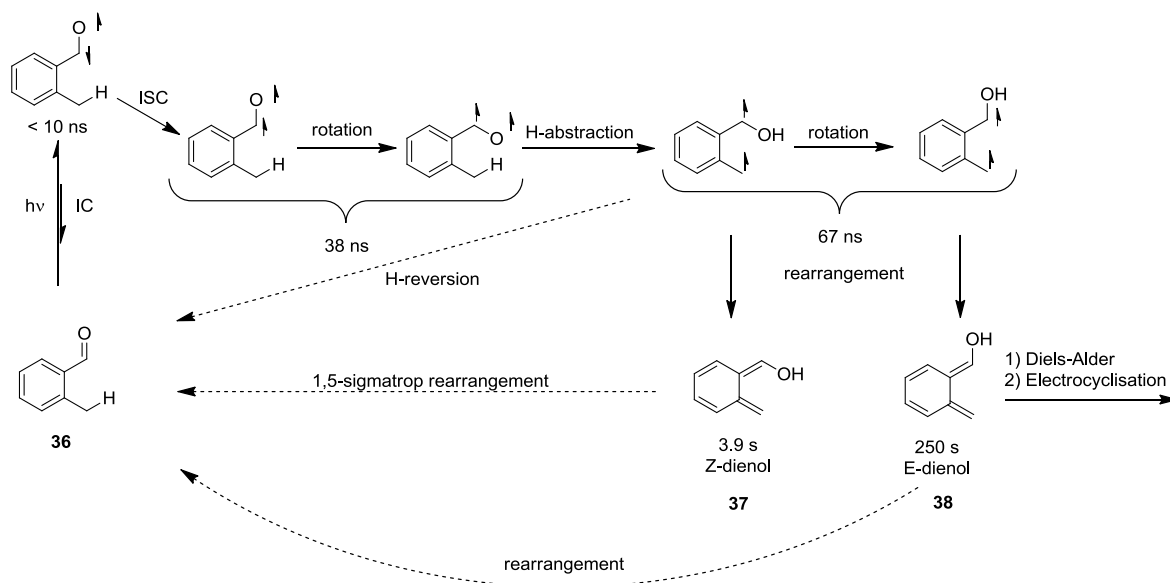
anthracene moieties to Au and ZrO₂ NP surfaces and generated a NP assembly under UV irradiation.^[96] The aggregation was attributed to the [4+4] light-induced cycloaddition of the anthracene groups, although intramonolayer photodimerization could occur and resulted in reduced reactivity. Therefore, a more sophisticated approach using two different counterparts for the light-induced reaction imparts a higher reactivity and a higher selectivity.

As already mentioned in section 1.3.1 (p. 22-27), many light-induced reactions are known in organic synthesis for the coupling of small molecules and find recently application in polymer and material science. Among them, photoenol based Diels-Alder cycloaddition is a well-known light-induced reaction, which is based on the tautomerization to dienes under UV irradiation allowing the trapping of dienophiles.



Scheme 15. Light-induced Diels-Alder reaction of *o*-substituted benzophenone **33** and dienophile **34** to proof the tautomerization and long lifetime *via* Diels-Alder trapping.^[163]

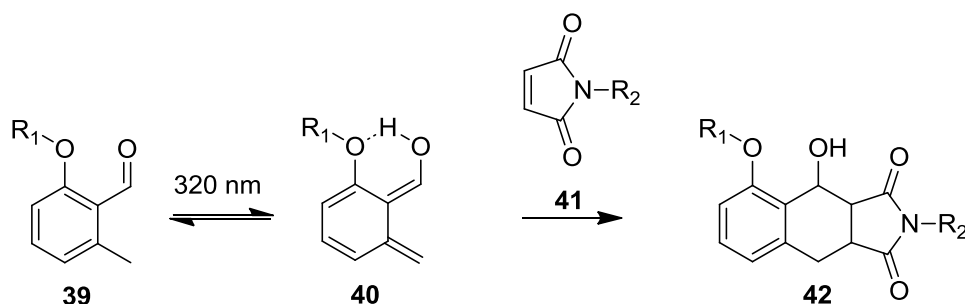
Already in 1961, Yang *et al.* recognized the ability of *o*-substituted benzophenones **33** to trap dienophiles **34** *via* Diels-Alder reactions (Scheme 15).^[163] Photoexcitation of benzophenones generates intermolecular hydrogen abstraction leading to bond reorganization to hydroxy-*o*-quinodimethane or photoenol intermediate, which enables the rapid Diels-Alder cycloaddition with dienophiles.



Scheme 16. Overview of the rearrangement of **36** to the formation of Z-dienol **37** and E-dienol **38**: ortho-alkyl substituted benzaldehyde **36** can absorb a photon to achieve the excited singlet state. A followed intersystem crossing leads to the triplet state, subsequent rotation and H-abstraction generates after rearrangement Z-dienol **37** and E-dienol **38**, which can undergo Diels-Alder cycloaddition.

Tchir and Porter determined the exact lifetimes of the E and Z-photoenol *via* flash photolysis experiments and explained the detailed reaction mechanism (Scheme 16).^[164] The ortho-alkyl substituted benzaldehyde **36** can absorb a photon to reach the excited singlet state, followed by an intersystem crossing to the triplet state. After rotation and H-abstraction, the molecule can rearrange to the Z-dienol **37** or E-dienol **38**, which has a longer lifetime as measured in degassed cyclohexane. The E-dienol **38** is able to undergo Diels-Alder cycloaddition or electrocyclicization or rearranges back to the ortho-alkyl substituted benzaldehyde.

In addition, photoenol chemistry was successfully used for the light-induced cycloaddition of polymeric building blocks.^[165] Photoenol precursors were coupled to poly(ϵ -caprolactone) and reacted efficiently with maleimide-modified poly(methyl methacrylate) under UV irradiation ($\lambda_{\text{max}} = 320\text{ nm}$). The strategy was expanded for the hetero-Diels-Alder reaction of photoenol-functionalized poly(ϵ -caprolactone) to RAFT polymers with non-activated dithioester groups.^[166]



Scheme 17. 2-Formyl-3-methylphenoxy group **39** tautomerizes under UV irradiation to photoenol intermediate **40**, which is stabilized by hydrogen bonding. Reaction with electron-deficient dienophile such as maleimide **41** leads to photoadduct **42**.

The group of Barner-Kowollik found that 2-formyl-3-methylphenoxy groups **39** exhibits higher reactivity due to an internal hydrogen bond which stabilized the photoenol intermediate **40** (Scheme 17). With the choice of different dienophiles, Winkler *et al.* were able to selectively form ABC triblock copolymers using both photoenol precursor 2,5-dimethylbenzophenone and 2-formyl-3-methylphenoxy for highly orthogonal light-induced Diels-Alder reactions.^[167] The photoenol moiety was further utilized for the formation of single-chain polymeric nanoparticles *via* intramolecular cross-linking of single polymer chains^[168] and the formation of macrocyclic aliphatic polyesters *via* intramolecular light-induced Diels-Alder reaction of α,ω -functionalized polymer.^[169] Due to the high efficiency and the orthogonality of the light-induced Diels-Alder reaction with photoenol moieties, Zydziaik *et al.* presented the generation of sequential defined macromolecules employing two photoreactive heterofunctional synthons based on photoenol **13** and thioaldehyde chemistry.^[170] Additionally, the great benefit of light-induced reaction is the ability to functionalize surfaces in a spatially resolved fashion, which was demonstrated by Pauloehrl *et al.*^[171] By the use of a shadow mask, the photoenol-coated surface was patterned with maleimido-peptides. In another demonstration of surface modification, the photoenol moiety was also modified with dopamine **46**, which is able to bind to various surfaces (Figure 11).^[172]

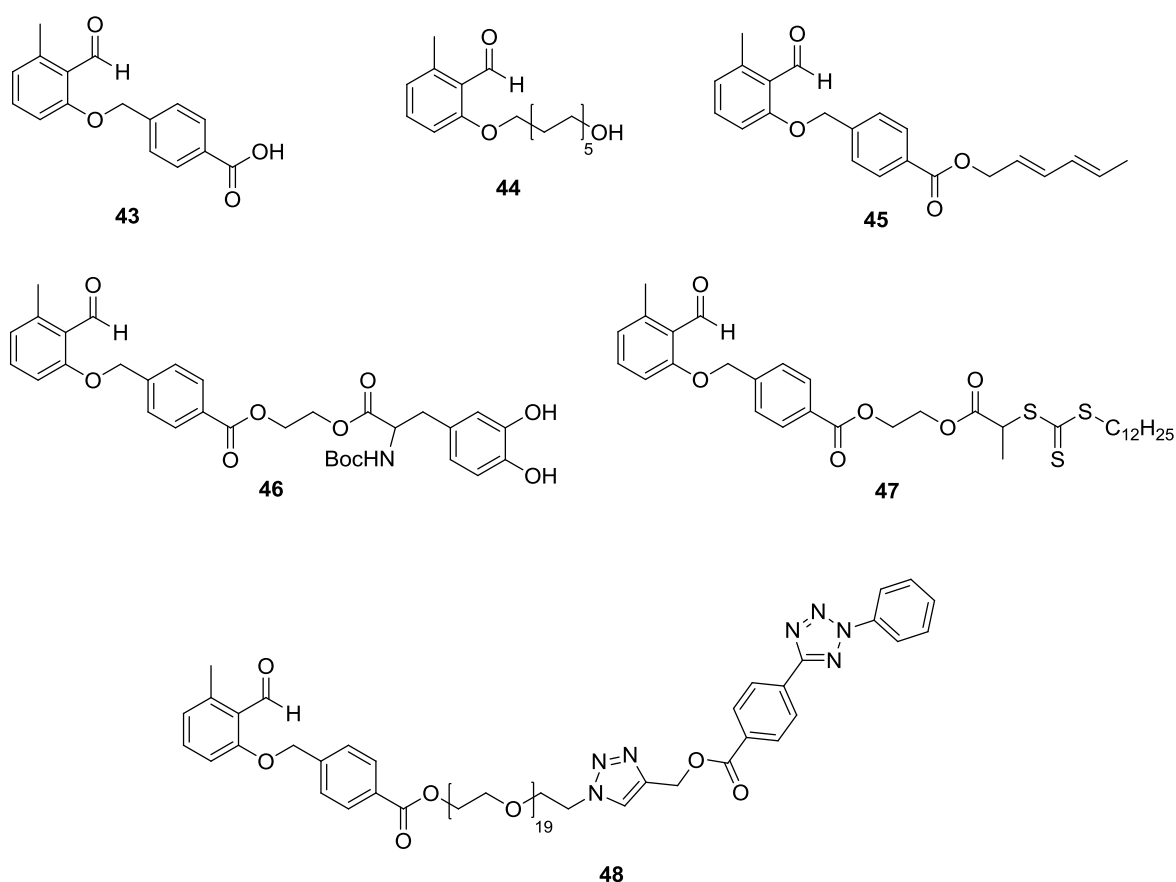


Figure 11. Overview of bifunctional linkers containing the photoenol moiety: **43**,^[171] **44**,^[166] **45**,^[170] **46**,^[172] **47**,^[162] and **48**^[173] were published by the Barner-Kowollik group.

The surface patterning with maleimide-carrying polymers and peptide through light-induced cycloaddition was evidenced by time-of-flight secondary ion mass spectrometry (ToF-SIMS) measurements. The photoenol chemistry has also expanded the use of biosurfaces such as hyaluronic acid films or cellulose. In addition, biosurfaces were functionalized in a spatially controlled manner with poly(trifluoroethyl methacrylate) and a model peptide.^[174] Furthermore, photoenol-containing DNA was synthesized and utilized for the light-induced DNA-protein conjugation with maleimide-modified protein.^[175] Moreover, a bifunctional PEG linker containing tetrazole and photoenol moiety **48** was prepared and orthogonal addition of maleimide was achieved using two different, reaction specific wavelengths.^[173]

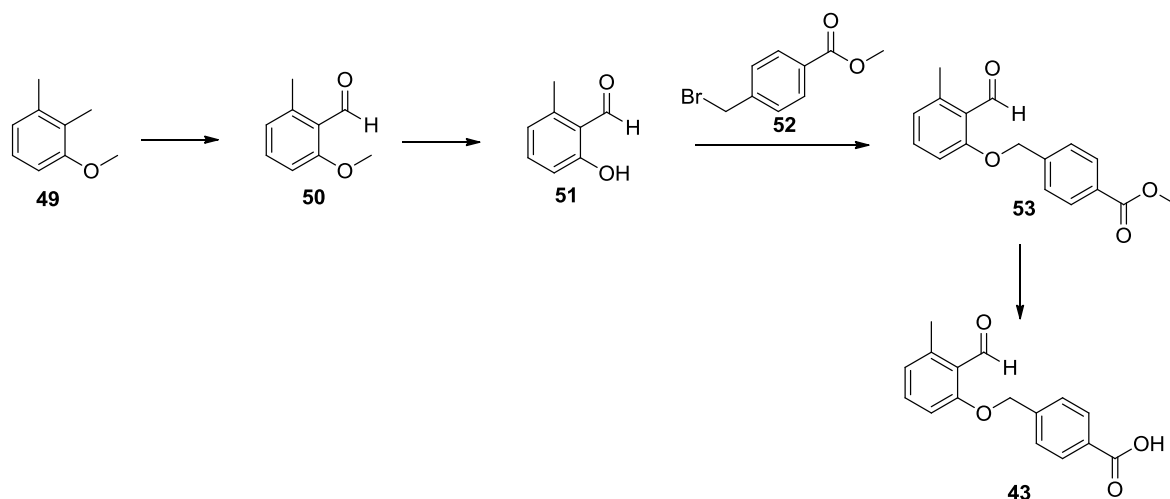
Besides application of photoenol chemistry in solutions and 2D surfaces, Kaupp *et al.* demonstrated the three dimensional functionalization of microparticle employing photoenol chemistry.^[162] The novel photoenol RAFT agent **47** was used

for polymerization and resulting RAFT polymers were immobilized on microparticle to create Janus spheres.

Within this chapter, the synthesis of novel benzotriazole-photoenol linkers will be presented and employed for the surface modification of Ag NPs. The photoenol-modified Ag NPs undergo light-induced reactions with functional polymers.

Results and Discussion

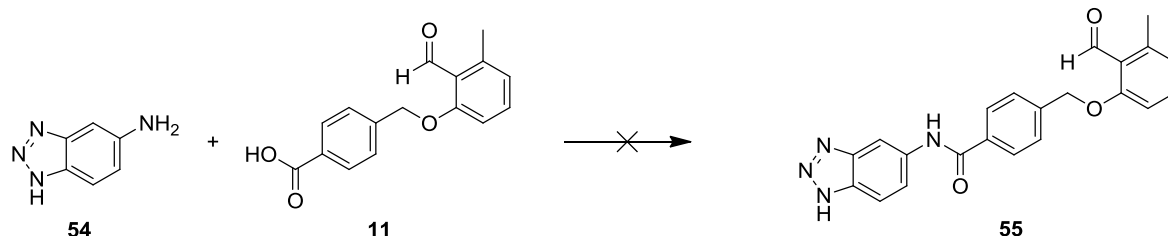
The great versatility and high orthogonality of the photoenol group (Figure 11) motivated us to functionalize Ag NP with photoenol moieties for light-induced modification with polymers. Ag NPs are of particular interest due to their antimicrobial activity and higher excitation coefficient in comparison to Au NPs. Therefore, a new bifunctional linker had to be synthesized containing benzotriazole as the anchoring group for Ag NP and a photoreactive photoenol precursor. The inclusion of ethylene glycol units for the connection of both groups should allow the application of this linker in aqueous solution for reactions with biomolecules.



Scheme 18. Synthesis of 4-((2-formyl-3-methylphenoxy)methyl)benzoic acid **43**.

First, the carboxyl acid functionalized photoenol precursor **43** was synthesized according to literature procedures in four steps (Scheme 18).^[171] To prepare a bifunctional linker containing both an photoenol and a benzotriazole moiety, the amide coupling strategy was chosen due to the stable amide bond. The commercial available 5-aminobenzotriazole **54** was utilized as an amine-terminated

benzotriazole molecule for amide coupling with 4-((2-formyl-3-methylphenoxy)methyl)benzoic acid **11** using various amide coupling reagents (Scheme 19).



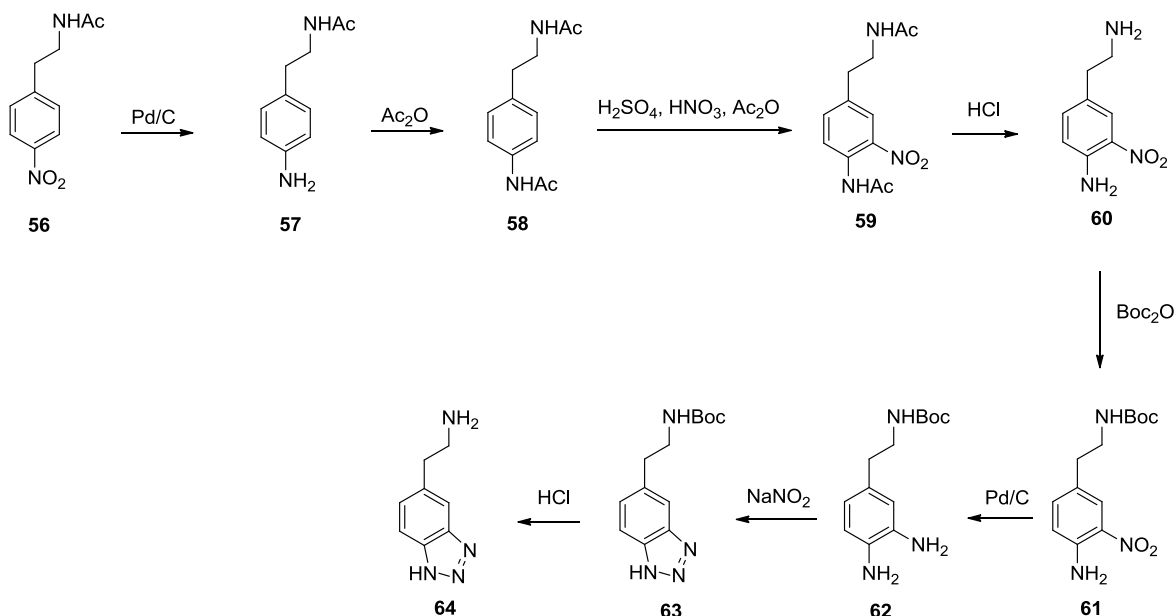
Scheme 19. Synthesis route for the amide coupling of 5-aminobenzotriazole **54** 4-((2-formyl-3-methylphenoxy)methyl)benzoic acid **43** (reaction conditions see Table 2).

However, the desired product **54**, although analyzed using fast atom bombardment mass spectrometry, could not be isolated after purification of the reaction mixture by column chromatography.

Table 2. Overview of different reaction conditions for the amide coupling between 5-aminobenzotriazole **54** and 4-((2-formyl-3-methylphenoxy)methyl)benzoic acid **43**.

Reagents	Solvent	Reference
ethyl chloroformate, triethylamine	THF	[171]
EDC, HOBt	DMF	-
EDC, HOBt, <i>N</i> -methylmorpholine	DMF	-
triethylamine, Mukaiyama reagent	DMF	[176]
DCC, NHS	DMF	[177]

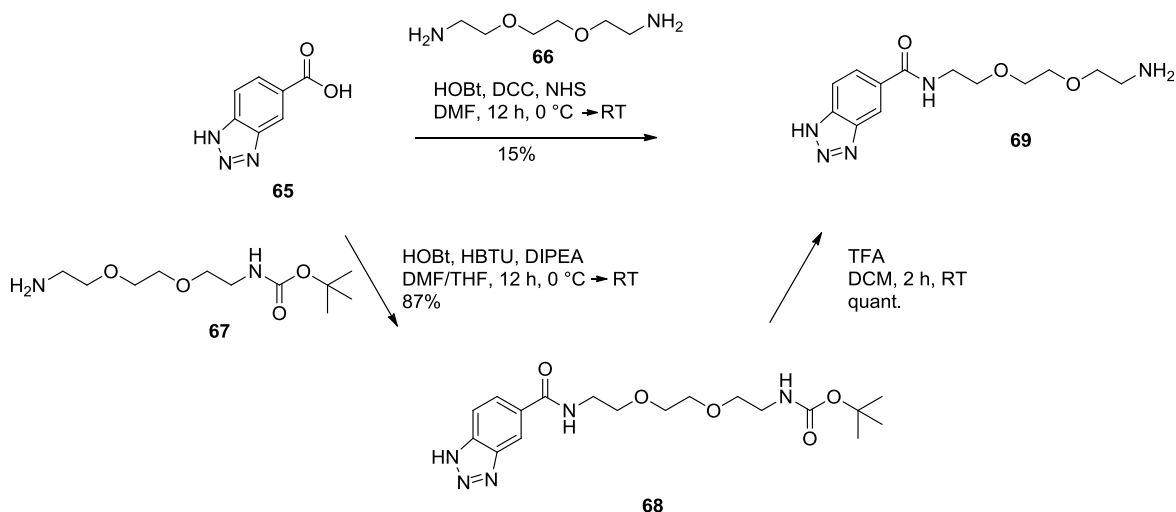
To increase the nucleophilicity of the amine moiety, another amino-terminated benzotriazole linker with an ethyl group between the phenyl group and the amine moiety was synthesized as alkylamines exhibit higher nucleophilicity in comparison to aniline derivatives.^[178]



Scheme 20. Synthesis of 2-(1*H*-benzo[*d*][1,2,3]riazol-5-yl)ethanamine **64**.

According to the literature,^[179] *N*-(4-nitrophenethyl)acetamide **56** was converted in eight steps to the desired 2-(1*H*-benzo[*d*][1,2,3]riazol-5-yl)ethanamine **64** (Scheme 20). Nevertheless, the amide coupling of **64** to 4-((2-formyl-3-methylphenoxy)methyl)benzoic acid **43** was also inefficient, which may be attributed to triazole amine acting as leaving group when amino-terminated benzotriazole is used as nucleophile and therefore a protection group is necessary.^[180] To circumvent the protection and deprotection step, we chose benzotriazole-5-carboxylic acid **65** as starting material, which enabled the reaction with amine-functionalized molecules.

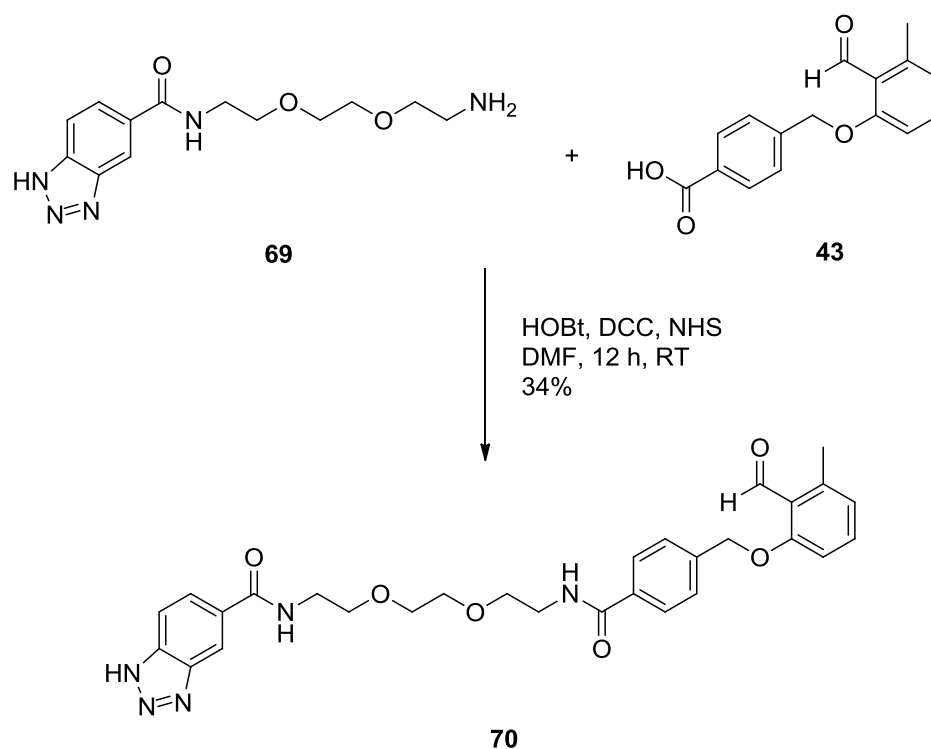
Light-Induced (Bio)Functionalization of Gold and Silver Nanoparticles



Scheme 21. Benzotriazole-5-carboxylic acid **65** can react directly with 2,2'-(ethane-1,2-diylbis(oxy))diethanamine **66** in one step to the desired product **69** or by the use of the one side Boc-protected derivative **67** followed by a deprotection step.

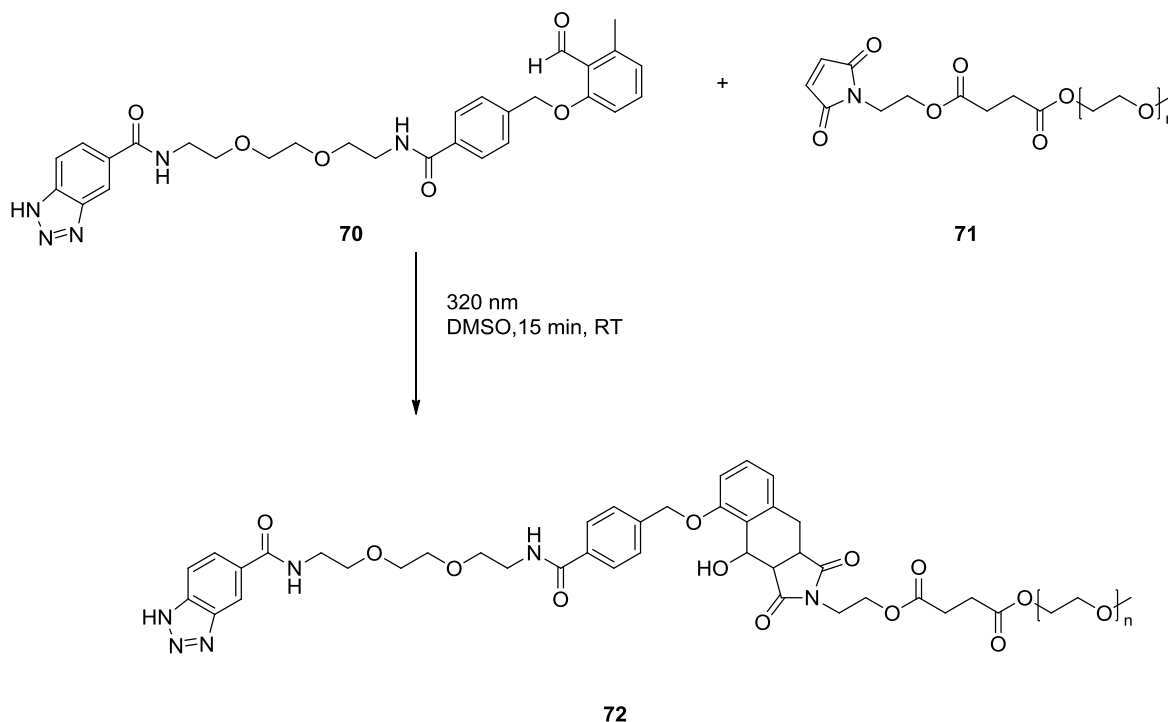
The amide coupling of benzotriazole-5-carboxylic acid **65** with 2,2'-(ethane-1,2-diylbis(oxy))diethanamine **66** was performed with 1-hydroxybenzotriazol (HOBt), *N,N'*-dicyclohexylcarbodiimide (DCC) and *N*-hydroxysuccinimide (NHS) in one step to obtain the desired product **69** with a yield of 15%. To increase the yield, the diamino-linker was first protected with *tert*-butyloxycarbonyl (Boc) protecting group on one side. After the coupling to **65**, the Boc group in **68** was deprotected using TFA to obtain **69** with a yield of 87% (Scheme 21).

The desired amine-terminated product **69** enabled further amide coupling with carboxylic acid-functionalized photoenol **43** (Scheme 22).



Scheme 22. Synthesis of *N*-(2-(2-(2-(4-((2-formyl-3-methylphenoxy)methyl)benzamido)ethoxy)ethoxy)ethyl)-1*H*-benzo[*d*][1,2,3]triazole-5-carboxamide **70** (BTPE).

Using the amide coupling reagents HOBT, DCC and NHS, benzotriazole-photoenol **70** (BTPE) was obtained after column chromatography (chloroform/methanol 19:1) with a yield of 34% (Scheme 22). To assess the reactivity of the novel photoenol linker **70**, a model reaction between BTPE **70** and maleimide-functionalized PEG **71** ($M_n \sim 1300 \text{ g mol}^{-1}$) was performed (Scheme 23). Low molecular weight maleimide-PEG was chosen due to its excellent dienophile reactivity and the ease of precise ESI-MS characterization of the adduct **72**.



Scheme 23. Model reaction of benzotriazole-photoenol **70** (BTPE) and maleimide-modified poly(ethylene glycol) **71** generate the photo-adduct **72**.

A reaction mixture of BTPE **70** and PEG-Mal **71** was irradiated using a 320 nm light source for 15 min in DMSO. Subsequent analysis by ESI-MS evidenced that a new set of peaks is formed, which was assigned to the product of the light-induced Diels–Alder reaction indicating the complete conversion to photo-adduct **72** (Figure 12).

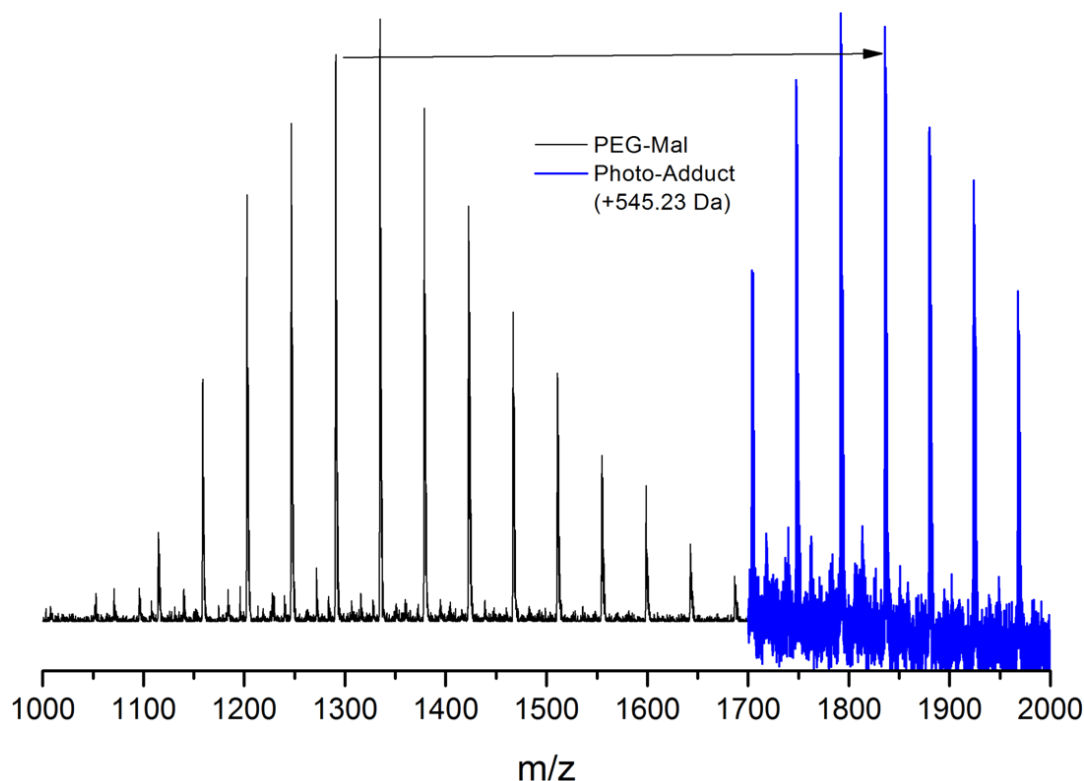
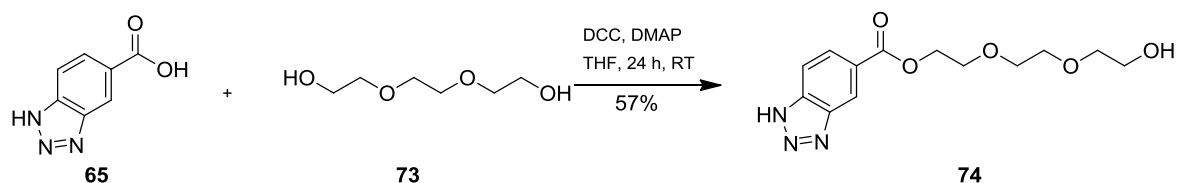


Figure 12. Zoom into the single charged region of the ESI-MS spectrum of the model reaction between BTPE **70** and PEG-Mal **71**. The blue spectrum shows the photo-adduct after 15 min irradiation. The shift of the peaks matches the mass of BTPE **70**. No other signals are observed, underlining full conversion and stability of the photo-adduct **72**.

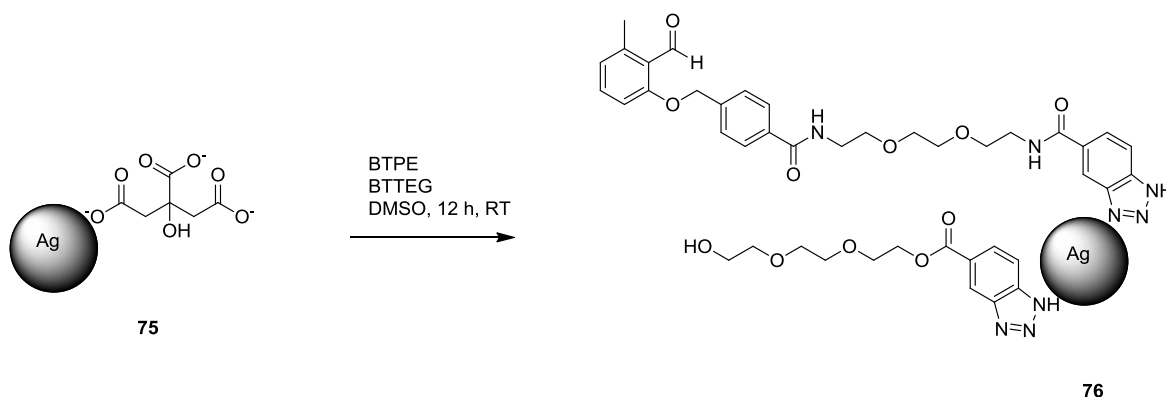
The photoenol group of **70** with two phenyl groups possesses poor water solubility, therefore a second benzotriazole linker (BTTEG **74**) was synthesized (Scheme 24) which should exhibit better water solubility.



Scheme 24. Synthesis of 2-(2-(2-hydroxyethoxy)ethyl 1H-benzotriazole-5-carboxylate **74** (BTTEG).

The incorporation of triethylene glycol to the benzotriazole allowed better water solubility. In addition, the hydroxyl group is not reactive against dienophiles. Once both benzotriazole linkers were prepared, the linkers BTPE **70** and BTTEG **74** needed to be attached to the Ag NP surface. First, we explored the one-pot

synthesis in which AgNO_3 is reduced using sodium borohydride or ascorbic acid in the presence of linker **70** to prepare photoenol decorated Ag NPs. However, the use of such reducing agents led to the reduction of the aldehyde group to the hydroxyl group in **70**, which resulted in the loss of reactivity. To circumvent this drawback, a milder ligand exchange methodology was employed in which the linker was added to the citrate-capped Ag NPs. The synthesis of citrate-capped Ag NPs was carried out following different synthesis procedure.^[181] However, the resulting Ag NPs possessed a broad size distribution. Therefore, we utilized commercially available, monodisperse Ag NPs with 20 nm in size. The ligand exchange procedure was first carried out in water with an excess of BTPE **70** and BTTEG **74** linker (10 000 eq), but led only to agglomerated Ag NPs. The colloidal stability of citrate-capped Ag NPs **75** was improved by the change of the solvent from water to DMSO and the subsequent ligand exchange with BTPE **70** and BTTEG **74** linker was efficient also due to the better solubility of both linkers in DMSO (Scheme 25).



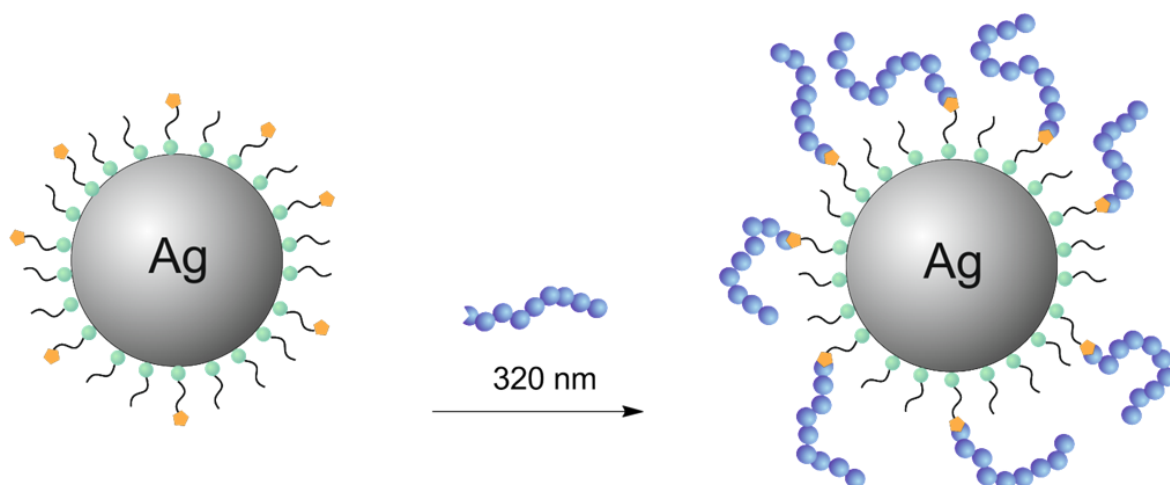
Scheme 25. Ligand exchange of citrate-capped Ag NPs **75** with BTPE **70** and BTTEG **74** linker in DMSO.

To minimize the surface crowding effect, the inert linker BTTEG **74**, which does not contain the photoenol moiety, was used in a 1 : 10 ratio (BTPE linker **70** to BTPE linker **74**). The combination of the reactive and inert linkers improved the colloidal stability of the Ag NPs-**76** and enabled control over the density (and availability) of reactive groups. After incubation in DMSO over night at ambient temperature, unbound ligands were removed by centrifugation. The concentration of modified Ag NPs-**76** was determined by UV/Vis spectroscopy and was usually in the range of nM.

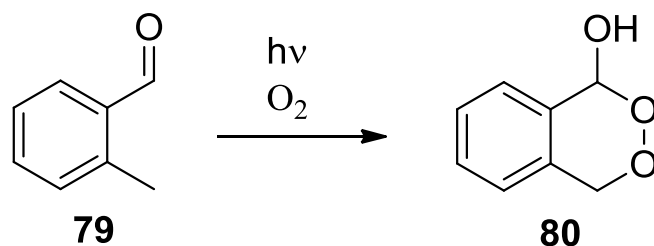
Table 3. Zeta potential measurement of citrate-capped Ag NPs-**75**, BTPE/BTTEG modified Ag NPs-**76**, PEG coated Ag NPs-**77**, and pCBMA coated Ag NPs-**78**.

Nanoparticles	Zeta Potential ^[182]	Solvent
Ag-citrate- 75	-35.0 ± 0.3	DMSO
Ag-BTPE/BTTEG- 76	-30.1 ± 0.8	DMSO
Ag-PEG 77	-29.5 ± 0.7	DMSO
Ag-pCBMA 78	37.1 ± 2.0	H ₂ O (pH = 6.40)

The efficient ligand exchange was evidenced *via* a change in the zeta potential (negative charge of the citrate-capped Ag NPs is decreased, Table 3) and X-ray photoelectron spectroscopy (XPS) measurements (Figure 17). The C 1s XP spectrum of the modified Ag NPs-**76** shows a strong decrease of the peak intensity assigned to O=C–O bonds at 288.5 eV, stemming from the replaced citrate groups.

**Scheme 26.** BTPE/BTTEG-modified Ag NPs-**76** were functionalized with PEG-Mal **39** employing light-induced Diels-Reaction.

Once the ligand exchange was confirmed, maleimide modified PEG **71** was added to the dispersion of modified Ag NPs-**75** (Scheme 26). The solution was deoxygenated by purging with nitrogen for 10 min to avoid side-reactions such as the formation of cyclic peroxide after reaction of photoenol intermediate with oxygen (Scheme 27).^[183]



Scheme 27. Possible side reaction of photoenol moiety **79** with oxygen under UV irradiation to cyclic peroxide **80**.

The flask was subsequently irradiated for 15 min by revolving around a compact low-pressure fluorescent lamp emitting at 320 nm in a custom-built photoreactor.

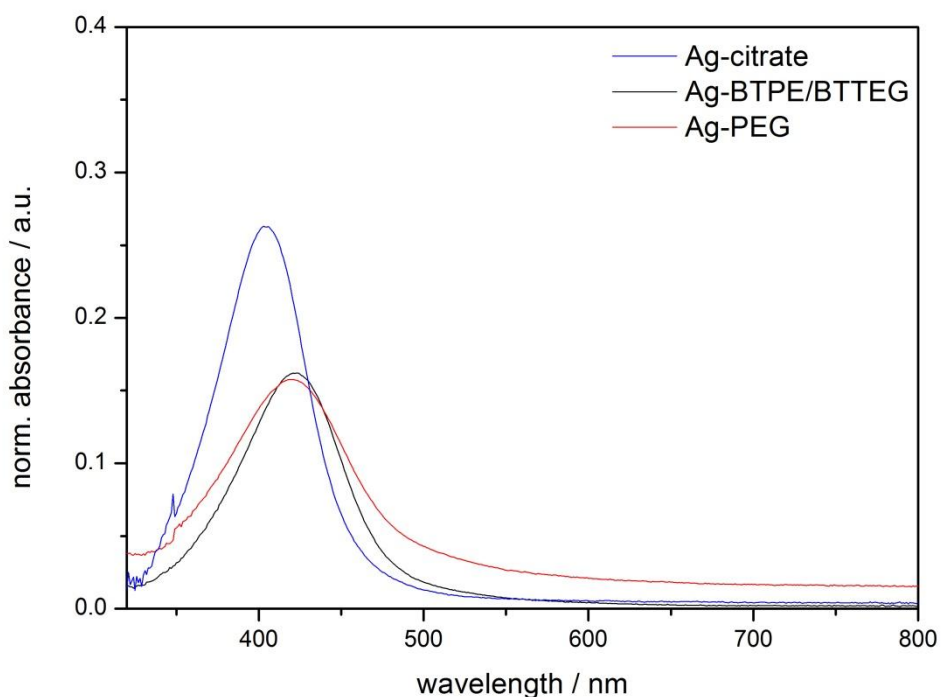


Figure 13. UV/Vis measurement of citrate-capped Ag NPs-**75**, BTPE/BTTEG modified Ag NPs-**76** and PEG-coated Ag NPs-**77**.

After performing washing steps with DMSO, UV/Vis spectroscopy was employed to evidence that the NPs remain stable and no aggregation occurs as indicated by the unchanged characteristic plasmonic resonance of Ag NPs at 420 nm (Figure 13). A first attempt to analyze the Ag core polymer shell structure was performed using dynamic light scattering (DLS). Several DLS measurements of BTPE/BTTEG modified Ag NPs-**76** and PEG-coated Ag NPs-**77** showed large de-

viations and were not reproducible, possibly due to the different scattering of the hard core and the soft shell. However, XPS analysis of PEG-coated Ag NPs shows a strong increase of the peak intensity at 286.6 eV in the C 1s spectrum, which is assigned to C–O bonds, stemming from the ethylene glycol unit (Figure 16). The formation of a corona of PEG was also evidenced by HRTEM. As depicted in Figure 14a, a 1–2 nm PEG shell can be observed around the 20 nm Ag core.

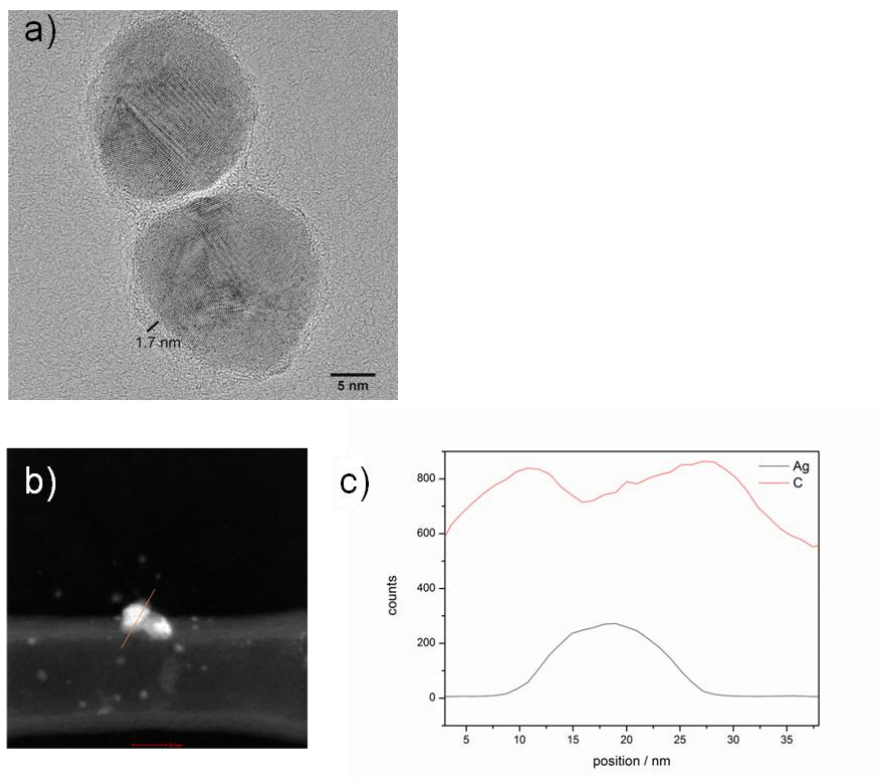


Figure 14. a) HRTEM image shows the Ag NPs-77 with poly(ethylene glycol). b) HRTEM image of Ag NPs with poly(ethylene glycol). The EDXS line scan follows the orange line. c) Carbon and silver peak intensities along the EDXS line scan showing the Ag-PEG core-shell structure. The counts of carbon and silver are plotted against the position. The core is around 20 nm and the shell around 2 nm. The overall slope of the carbon curve was background-corrected to account for slight thickness variation of the carbon support film.

To further prove the formation of the corona and the composition of Ag NPs-77, EDXS measurements were carried out. An EDXS line scan along the core-shell structure recorded a high C content in the shell resulting from the attached PEG layer and a high Ag content at the core resulting from Ag NPs (Figure 14b and c).

Once the successful light-induced modification of Ag NPs with PEG was demonstrated, the more challenging zwitterionic, non-fouling poly(carboxybetaine

methacrylate) (pCBMA) ($M_n \sim 21\,700\text{ g mol}^{-1}$) was also grafted onto the Ag NPs. First Jiang and then Barner-Kowollik group have extensively studied poly(carboxybetaine) brushes and have shown that they are able to reach high levels of antifouling towards blood plasma and other bodily fluids.^[184] In addition, these brushes have prevented bacterial and marine biofilm formation^[185] and could be used as a switchable antibacterial system.^[185a, 186] Due to the higher molecular weight of pCBMA, a longer irradiation time was used for the coupling of pCBMA (1 h vs. 15 min for PEG) to compensate for the steric hindrance effects of the longer, highly swollen polymer chain.

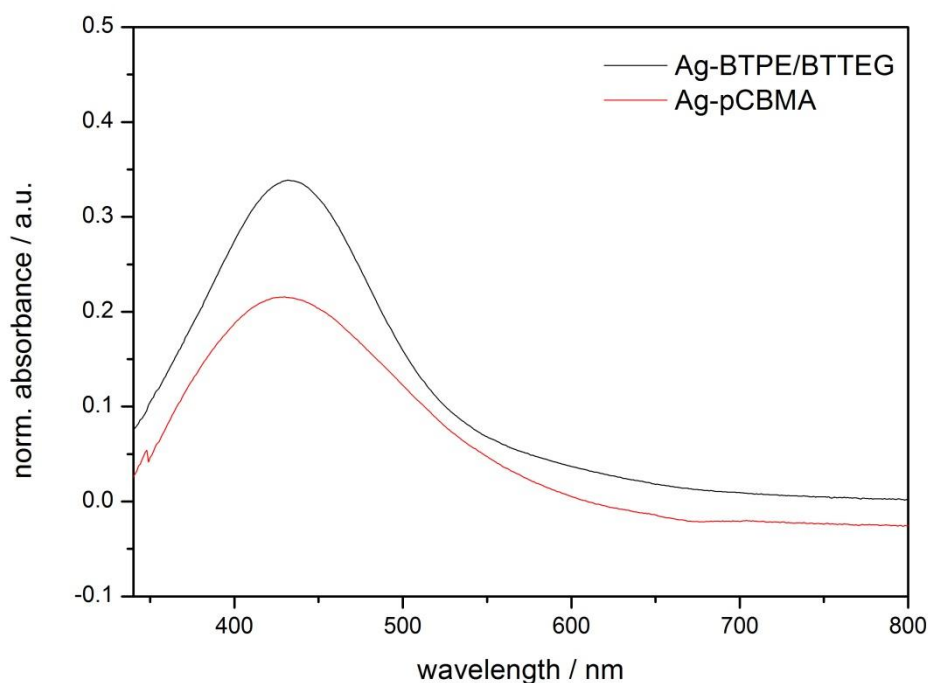


Figure 15. UV/Vis measurement of BTPE/BTTEG modified Ag NPs-76 and pCBMA-coated Ag NPs-78.

After performing washing steps with DMSO, the characteristic plasmonic resonance of Ag NPs at 420 nm in the UV/Vis spectrum evidenced the colloidal stability of Ag NPs (Figure 15). The successful photografting was unambiguously confirmed by XPS (Figure 16 and 17), EDXS analyzes (Figure 18b and c) and HRTEM measurements (Figure 18a).

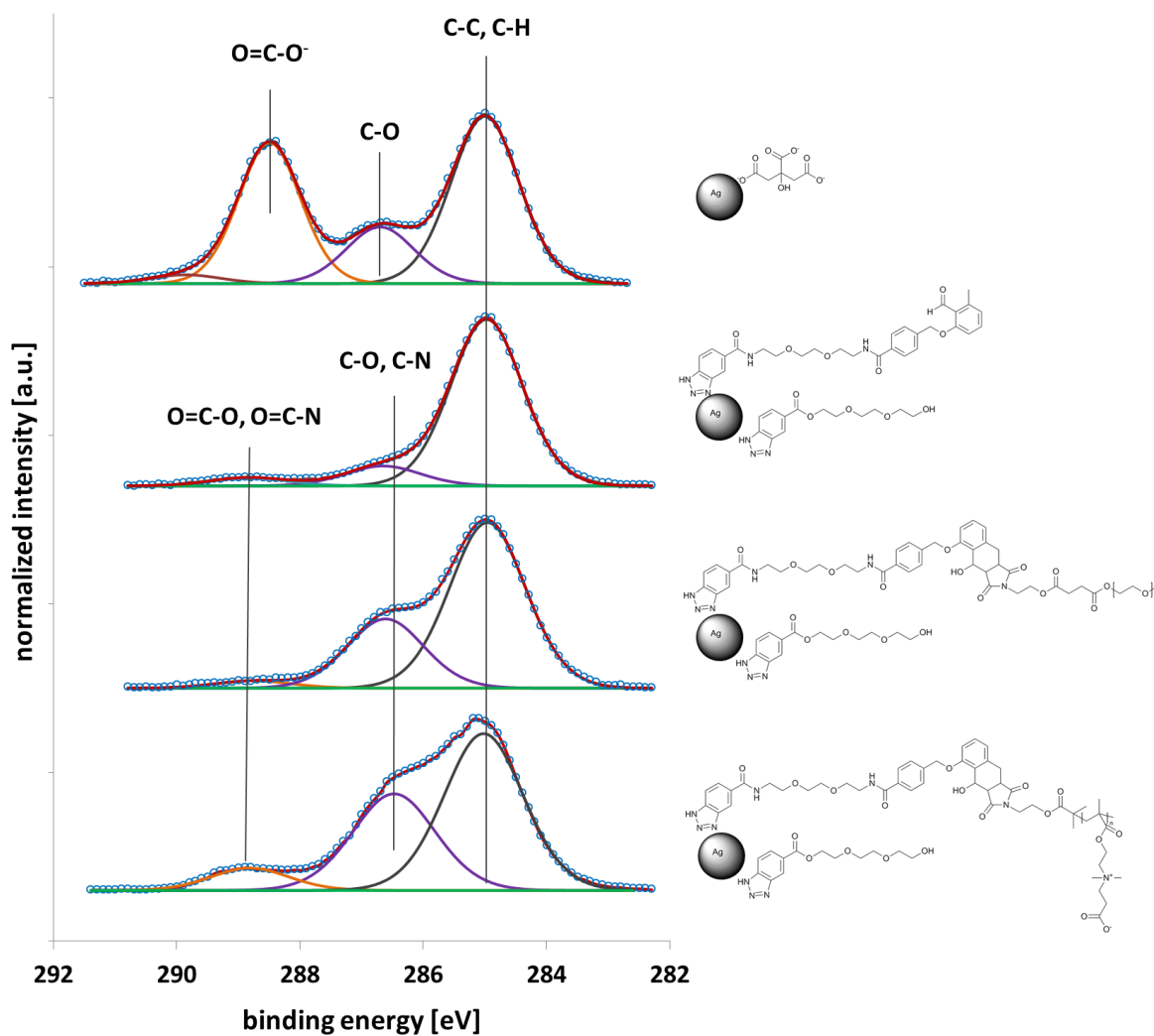


Figure 16. C 1s XPS spectra of untreated citrate-capped Ag NPs-**75** (top), modified Ag NPs-**76** (2nd row), PEG-functionalized Ag NPs-**77** (3rd row) and pCBMA-functionalized Ag NPs-**78** (bottom) evidenced successful ligand exchange and photoreactions.

Namely, the C 1s XPS spectrum of Ag NPs-**76** shows a strong increase of the peak intensity at 288.5 eV assigned to the O=C–O bonds, stemming from the carboxylic acid and ester groups of pCBMA (Figure 16).

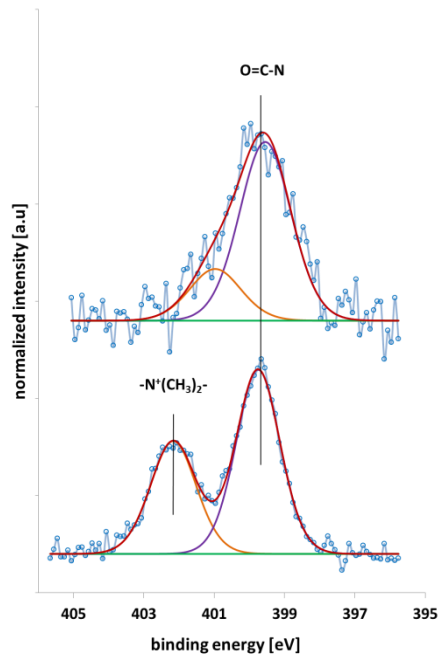


Figure 17. XPS analysis of the BTPE/BTTEG modified Ag NPs-76 (top) and pCBMA coated Ag NPs-78 shows a new peak at 402.2 eV in N 1s XP spectrum which is assigned to N⁺R₄ bonds, stemming from the quaternary ammonium of the CBMA unit.

In addition, the N 1s XPS spectrum shows a new peak at 402.2 eV assigned to the high-energy quaternary ammonium groups (Figure 17).

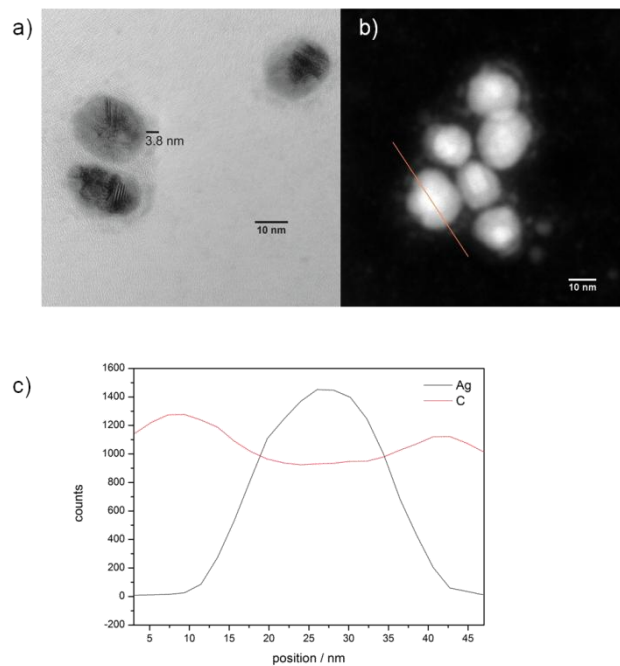


Figure 18. a) HRTEM image of pCBMA-coated Ag NPs-78. b) An EDXS line scan (orange) of pCBMA-coated Ag NPs. c) C and Ag peak intensities along the EDXS line scan showing the Ag-pCBMA core-shell structure. The counts of C and Ag are plotted against the position. The core is close to 20 nm and the shell approx. 4 nm in size.

HRTEM measurements also demonstrated the formation of the core–shell structure consisting of a 20 nm Ag core and a 4 nm pCBMA shell (Figure 18a), which was additionally ascertained by an EDXS line scan indicating the corresponding Ag and C contents (Figure 18b and c).

To exclude that non-covalent interactions between polymers and Ag NPs cause the polymer attachment, control samples – into which both polymers were added to the Ag NPs without irradiation – were carried out (Figure 19).

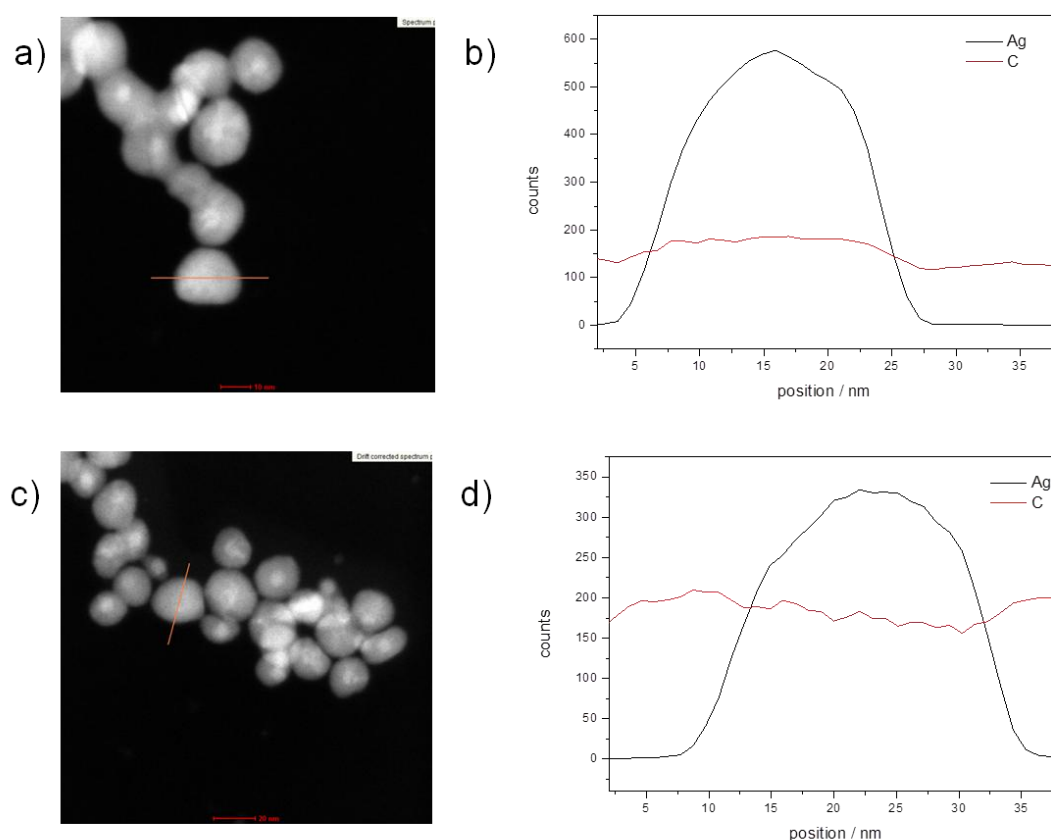
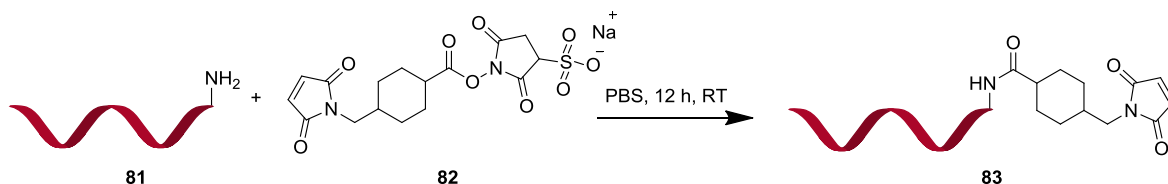


Figure 19. HRTEM image of control sample without irradiation of Ag NPs and a) Mal-PEG c) Mal-pCBMA. EDXS line scan follows the orange line and counts of carbon and silver are plotted against the position with no observable shell in the control sample of Ag NPs and b) Mal-PEG d) Mal-pCBMA.

It should be noted that control samples did not show any increase in the C content *via* EDXS line scans. Control sample of BTPE/BTTEG modified Ag NPs-76 and Mal-PEG and Mal-pCBMA without irradiation after one washing step were analyzed *via* HRTEM and only Ag NP cores were observed. The EDXS line scan follows the orange line. The counts of carbon and silver are plotted against the

position. Carbon and silver peak intensities along the EDXS line scan are not showing a higher amount of carbon on the surface of the Ag NP in both control samples. The core is around 20 nm and no shell is observable. The counts of carbon are caused by the carbon support film.

Once the successful modification of Ag NPs with functional polymers was demonstrated, the biofunctionalization of Ag NPs was attempted. For this purpose ssDNA was modified with one maleimide moiety using amino terminated ssDNA **81** (5'-GTGGAAAGTGGCAATCGTGAAG) and sulfosuccinimidyl-4-(*N*-maleimidomethyl)cyclohexane-1-carboxylate (sSMCC) crosslinker **82** (Scheme 28). An aqueous solution of commercially available DNA (10 nmol) was incubated with 2.00 mg sSMCC crosslinker **82** for 12 h at ambient temperature.



Scheme 28. Synthesis of maleimide-modified ssDNA **83**.

After high-performance liquid chromatography (HPLC) purification using a gradient of 0.1 M ammonium acetate and acetonitrile, an additional peak with a retention time of 19.0 min was observed corresponding to maleimide modified ssDNA (Figure 20).

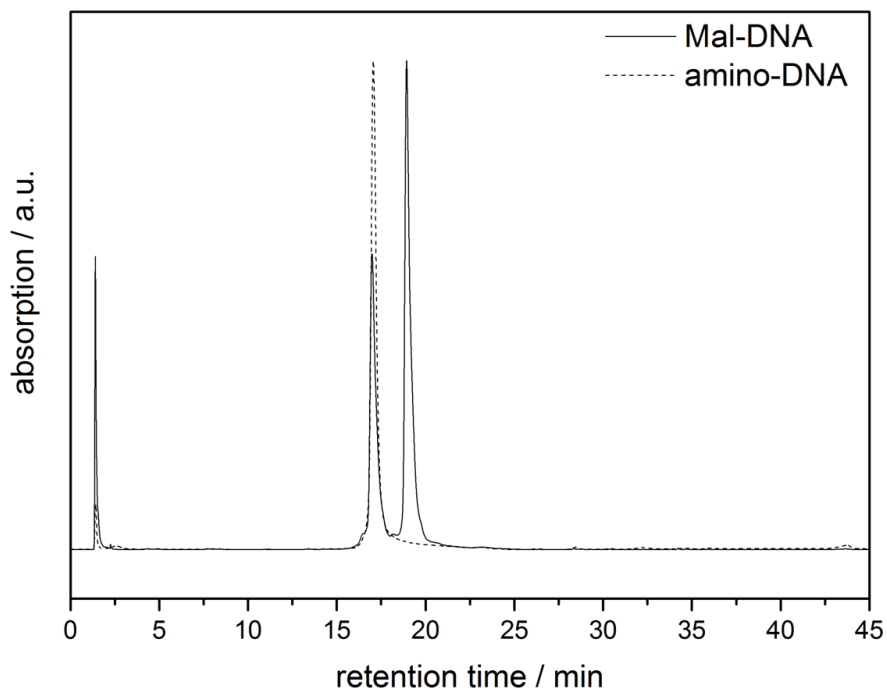
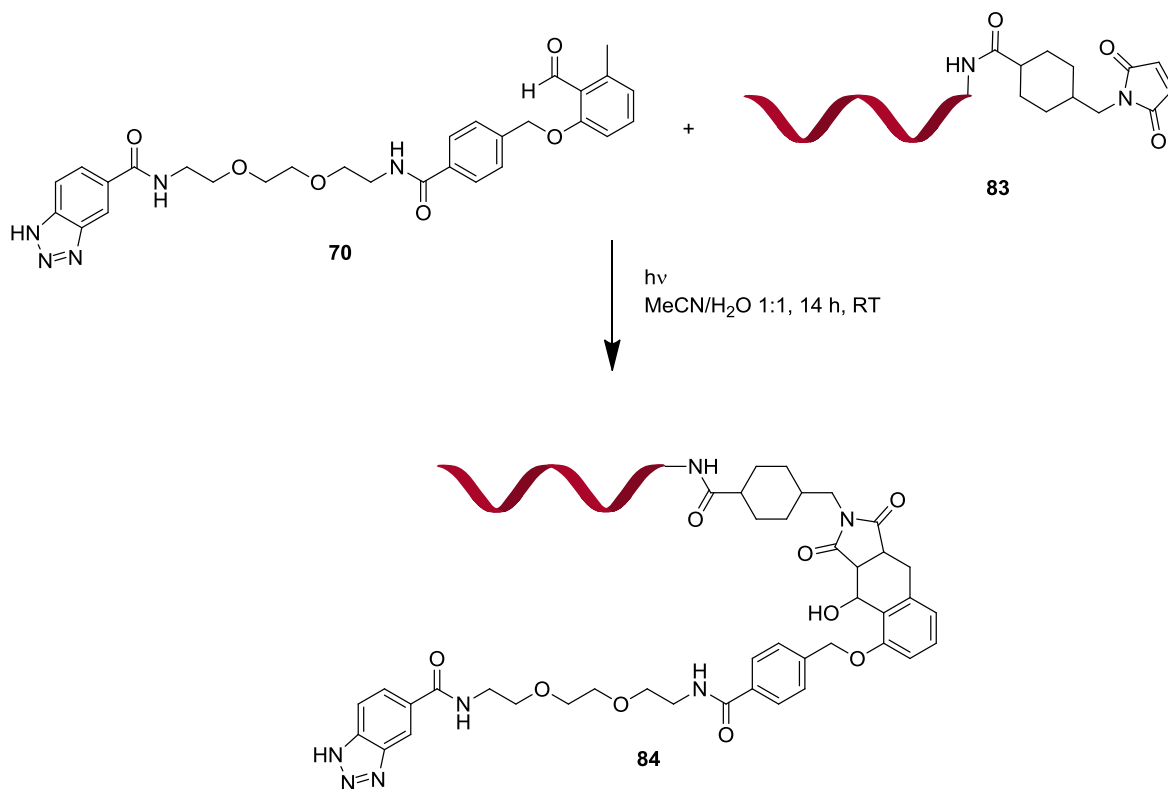


Figure 20. HPLC traces of amino-DNA **81** and maleimide-modified ssDNA **83**.

The efficient maleimide modification of amino-DNA was evidenced by MALDI mass spectrometry ($[M+H^+]$ theoretical: 7288; found: 7287.7). To assess the reactivity of Mal-DNA, a model reaction between Mal-DNA **83** and the photoenol-benzotriazole (BTPE) linker **70** was performed (Scheme 29).

Light-Induced (Bio)Functionalization of Gold and Silver Nanoparticles



Scheme 29. Photoreaction between BTPE linker **70** and maleimide-modified ssDNA **83**.

To an aqueous solution of Mal-DNA **83** (5 nmol, 1 eq), BTPE **70** (20 nmol, 4 eq) was added. The reaction mixture was aliquoted in acetonitrile/ water 1:1 in two vials, purged with nitrogen for 15 min and irradiated for 6h and 14 h. The reaction mixture was purified with NAP-5 and NAP-10 size exclusion columns, and HPLC using a gradient of 0.1 M ammonium acetate and acetonitrile (Figure 21).

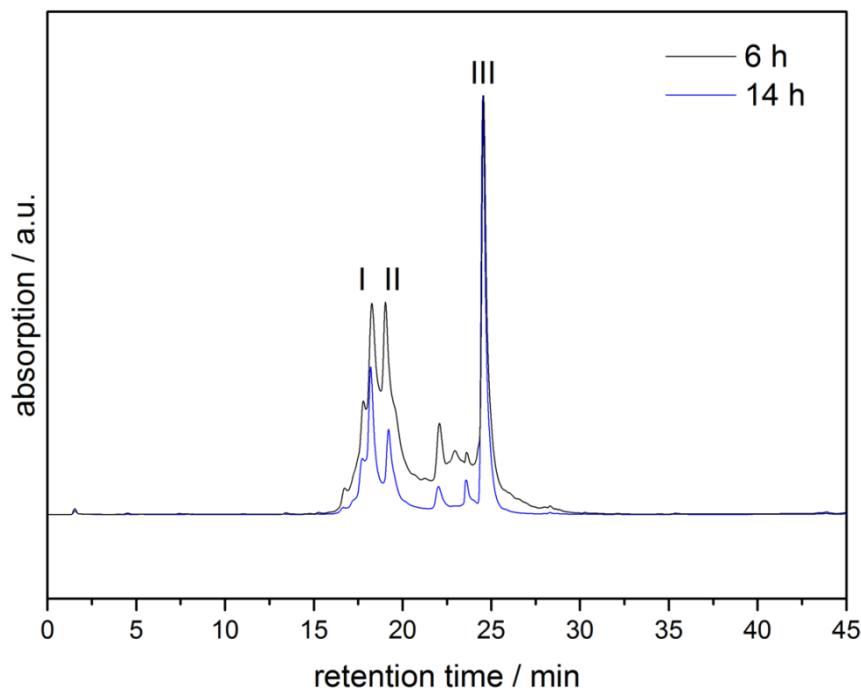


Figure 21. HPLC trace of BTPE **70** and maleimide modified ssDNA **83** after 6 h and 14 h irradiation. I: Mal-DNA+ H₂O, II: Mal-DNA **83**, III: BTPE+Mal-DNA **84**.

A new peak arose at a retention time of 24.6 min (III in Figure 23), which was assigned to the photoadduct **84** by MALDI mass spectrometry ($[M+H^+]$ theoretical: 7834; found: 7832.4).

Table 4. Different fractions I-III of HPLC trace of BTPE **70** and Mal-DNA **83**.

Peak number	Retention time / min	$[M+H^+]$ / g mol ⁻¹
I	18.3	7303.1
II	19.0	7287.7
III	24.6	7832.4

Residues of Mal-DNA **83** were detected with a retention time of 19.0 min. Peak I was assigned to a side product of maleimide-modified DNA in aqueous solution due to ring opening or addition of maleimide moiety in water across the double bond (Table 4).^[187] In addition, fraction III was analyzed by gel electrophoresis (Figure 22).



Figure 22. 21% TBE gel electrophoresis of I: 10 base pair marker, II: amino-DNA **81**, III: Mal-DNA **83** and BTPE+Mal-DNA **84** after 2 h 15 min at a voltage of 100 V using SYBR Gold staining.

After SYBR Gold staining, amino-DNA showed the highest mobility due to the lowest molecular weight (lane I). The Mal-DNA with higher molecular weight showed lower mobility in lane III. After the photoreaction, the photoadduct in lane IV possessed the highest molecular weight and the lowest mobility. In lane III and IV were also second additional bands observable, which could be attributed to the dimer formation of the DNA, already detected with the commercially available amino-DNA **81** in some gels.^[175]

The obtained benzotriazole-terminated DNA was subsequently attached to Ag NPs in a ligand exchange procedure. To achieve that, citrate-capped Ag NPs were incubated with benzotriazole-terminated DNA while sodium chloride was added stepwise using the so-called salt aging method.^[188]

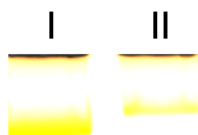


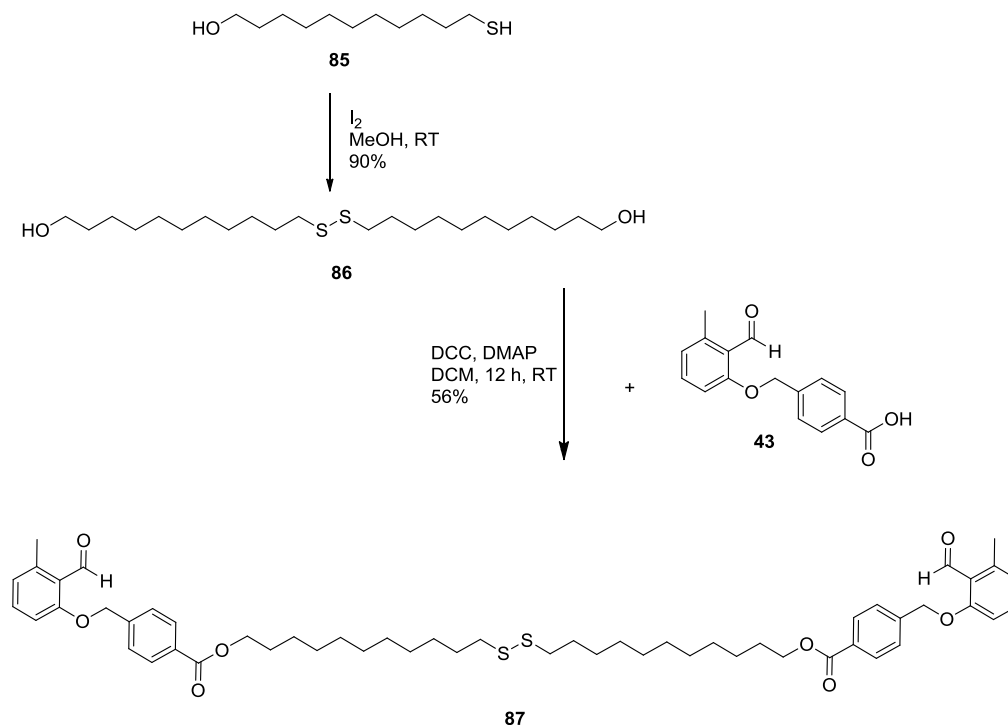
Figure 23. 2% Agarose gel of I: citrate-capped Ag NPs and II: DNA-Ag NP conjugates after 12 min at 100 V.

The successful DNA attachment on the Ag NPs was confirmed by a 2% agarose gel showing one distinct band for each Ag NP species. Comparison of DNA-Ag NP conjugate in lane II and citrate-capped Ag NPs in lane I showed a

lower mobility of the DNA-Ag NP conjugates due to the bigger size and change in charge (Figure 23).

However, we also wanted to achieve the light-induced coupling of DNA directly to the BTPE-modified Ag NPs **76**. As both components exhibited different solubility (BTPE-Ag NPs **76** in DMSO, DNA in aqueous solutions), the attachment of DNA could not be achieved as BTPE/BTTEG-modified Ag NPs **44** showed agglomeration after incubation in aqueous solutions.

Although Ag NPs exhibit a 100 × higher molar extinction coefficient than Au NPs resulting in much higher sensitivity particular useful for biosensing, the colloidal stability and reproducibility of uniform NPs is higher in the case of Au NPs.^[137] Due to the high binding affinity of thiols to Au NPs,^[13] we prepared a bifunctional linker containing a thiol moiety and a photoenol moiety (Scheme 30) for light-induced Diels-Alder reaction with polymers and biomolecules.



Scheme 30. Synthesis of photoenol disulphide linker **87** for modification of Au NPs.

First, mercaptoundecanol **85** was oxidized to the disulphur compound **86** to protect the thiol moiety, which possessed similar reactivity than the alcohol group. Carboxylic modified photoenol was coupled to the alcohol group *via* esterification using DCC and DMAP. Subsequent reduction to obtain the free thiol was carried

out with different mild reducing agents such as dithiothreitol or tris(2-carboxyethyl)phosphine leading also to the reduction of the aldehyde group to the alcohol and its loss of reactivity. However, unreduced disulphide compounds were shown to enable the stabilization of Au NPs.^[189] Following a procedure of Baranov *et al.*,^[64] citrate-capped Au NPs were incubated with photoenol-disulphide linker **87**. Au NPs were incubated with large excess of **87** in DMF/water mixture under sonication for 10 min, but the Au NPs agglomerated and could not be redispersed. Therefore, cetyltrimethylammonium chloride (CTAC)-capped Au NPs **88** were prepared and ligand exchange with photoenol-disulphide **87** was achieved after heating at 80 °C for 4 h.

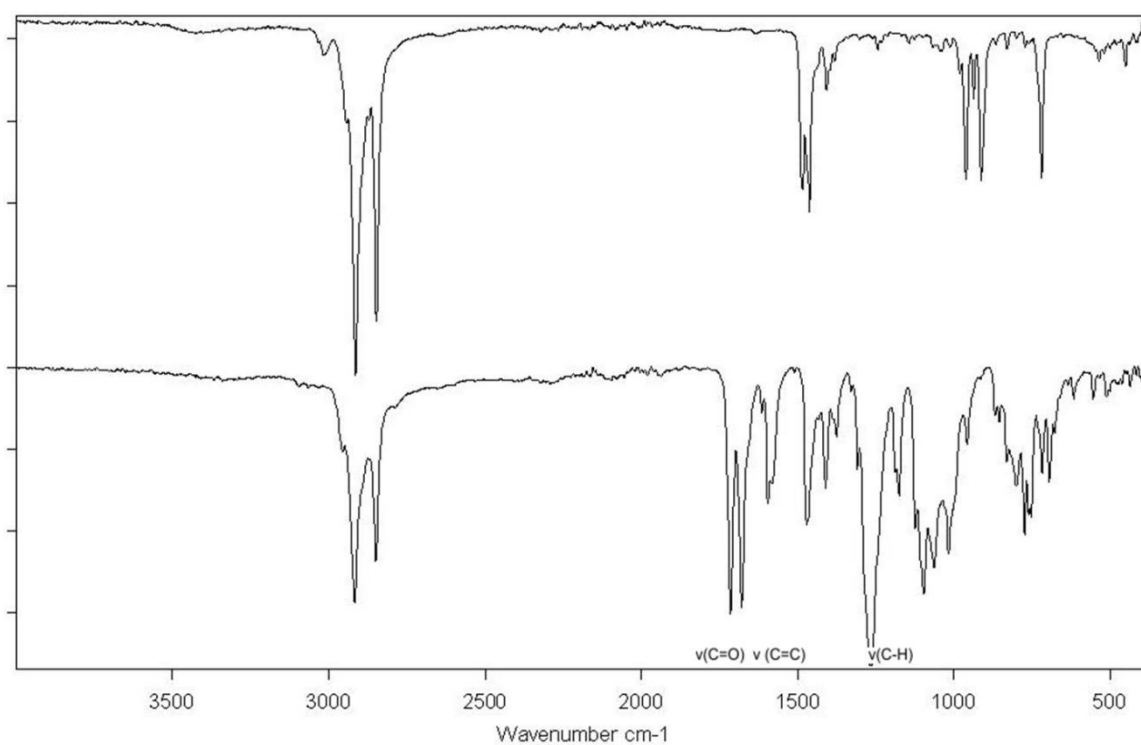


Figure 24. FT-IR spectra of cetyltrimethylammonium chloride-capped Au NPs **88** (top) and of photoenol-modified Au NPs (bottom).

After dialysis overnight, the successful modification of stable Au NPs with photoenol groups was confirmed by UV-Vis and IR spectroscopy. The new signals in FTIR spectrum of photoenol-modified Au NPs (Figure 24) at 1715 cm⁻¹ could be assigned to vibrations of C=O bonds, and aromatic C=C at 1595 cm⁻¹ and aromatic C-H bonds at 1268 cm⁻¹, all of which are only present in the photoenol group but not in the capping agent.

Once water soluble Au NPs were prepared, the photoreaction with maleimide-modified DNA **83** was carried out in acetonitrile/water mixtures under irradiation for 14 h. After washings steps with acetonitrile/water (1:1), the reaction mixture was analyzed with gel electrophoresis, but showed no shift of DNA-Au NP reaction mixture. The inefficient DNA attachment might have been caused by residual positively charged CTAC molecules in the Au NP dispersion, which interacted with the negatively charged DNA and prevented the covalent binding of the DNA to the Au NP surface. Therefore, a better washing procedure of the CTAC-capped Au NPs **88** can be attempted using for example dialysis over days.

Conclusions

In conclusion, we introduce a novel light-induced route for the covalent functionalization of photoenol-modified Ag NPs with poly(ethylene glycol) and poly(carboxybetaine methacrylate). The novel bifunctional linker containing benzotriazole as the Ag anchoring group and a caged diene (photoenol) moiety enabled photo-grafting of maleimide containing polymers to Ag NPs as demonstrated by XPS, HRTEM and EDXS. In addition, Au NPs were modified with a novel photoenol-disulfide linker *via* ligand exchange procedure. However, the attachment of maleimide-modified DNA could not be achieved with neither photoenol-capped Ag NPs nor photoenol-capped Au NPs. The inefficient DNA-NP photoconjugation could be caused by the poor water solubility of the photoenol moiety. The aromatic character of the photoenol moiety possibly restricted the availability of the photoenol moiety on the NP surface.

Although the attachment of DNA has not been successful and further optimization is needed, the success of this approach for the modification of Ag NPs with functional polymers expands the synthetic toolbox for the tailoring of nanomaterials and can be transferred to other molecular species in the future especially in organic solvent. To increase the compatibility to aqueous solutions, novel water soluble linkers bearing the photoenol moiety need to be synthesized. In particular, PEG based linker showed good water solubility and the ability to stabilize NPs in aqueous solutions.^[131] In addition, benzotriazole tends to aggregate in water with increasing concentrations (~ 16-20 mM) due to the self-assembly behavior of the benzotriazole molecule in water,^[190] therefore a more suitable anchoring group such as thiol group could be chosen.

4 Photo-Induced Surface Encoding of Gold Nanoparticles²

Introduction

The incorporation of the photoenol moiety to the surfaces of Ag NPs and Au NPs allows spatial control of the light-induced Diels-Alder reaction and the immobilization of the NPs. As aforementioned, the spatially resolved patterning of a broad range of (bio)polymers on various surfaces using photoenol chemistry in combination with a shadow mask has already been demonstrated.^[171-172, 174] Another approach to obtain spatially resolved patterning is based on the use of the direct laser writing (DLW) methodology. DLW is a powerful tool for the fabrication of complex structures. Both continuous wave and a pulsed laser can be employed.^[191] By moving the laser beam and the substrate relative to each other through a photoresist, multiphoton absorption can lead to a photoreaction at specific positions. In such a manner, the DLW setup is widely used for the preparation of polymeric microstructures based on the photopolymerization.^[192] In general, two basic components are necessary for the writing process: a photoresist, which enables polymerization to solid polymeric structure, and a photoinitiator, which absorbs light and induces the polymerization. The photoresists are classified in positive-tone photoresists^[193] focusing the laser light into solid structures to dissolve the exposed regions and negative-tone photoresists using laser light to fabricate solid, insoluble structures from a solution.^[194] The negative-tone photoresists consists commonly of acrylate monomers or blends of acrylates bearing 3 to 5 functional groups per monomer molecule.^[195] To initiate the free radical polymerization, a variety of photoinitiators was employed such as benzylidene ketone-based initiators^[196] or commercial available Irgacure 369.^[197] In addition to radical polymerization, cationic polymerization of epoxide-containing resins such as SU-8 was utilized for DLW.^[198]

Recently, it was demonstrated that light-induced reactions such as thiol-ene chemistry in combination with DLW can be used for the fabrication of three dimen-

² Parts of this chapter have been adapted from Stolzer, L.; Quick, A. S.; Abt, D.; Welle, A.; Naumenko, D.; Lazzarino, M.; Wegener, M.; Barner-Kowollik, C.; Fruk, L. *Chem. Commun.* **2015**, 51, 3363 with permission from The Royal Society of Chemistry.

sional microstructures.^[199] Residual thiols could be employed for Michael addition with a maleimide-containing molecule. Another non-radical step polymerization alternative for the preparation of three dimensional microstructures is the light-induced Diels-Alder reaction of *o*-quinodimethanes (caged photoenols) and maleimides.^[200] Residual photoenol moieties of the tetrafunctional photoenol linker in the microstructure have been addressed for further Diels-Alder reaction with small maleimide molecules to demonstrate the retained reactivity. Photoenol chemistry was also employed for the spatially resolved immobilization of specific peptides on microscaffolds, which enables cell attachment in three dimensions onto the microscaffold.^[201] In addition, Kaupp *et al.* prepared a novel RAFT agent containing a phenacylsulphide, which forms a thioaldehyde under UV irradiation.^[202] Subsequent polymerizations were performed and DLW setup allowed the spatially resolved grafting of a vast range of polymers on poly(dopamine)-coated surfaces employing thioaldehyde ligation.

Due to the preliminary results of photoenol chemistry and direct laser writing, we envisaged to pattern photoenol-modified Au NPs using direct laser writing techniques in combination with light-induced Diels-Alder cycloaddition, which is explained in the following sections.

Results and Discussion

To employ DLW as powerful tool for the immobilization of NPs, photoreactive groups such as photoenol moieties need to be attached to the NP surface. We chose Au NPs due to their higher stability in comparison to Ag NPs to avoid NP aggregation as consequence of high-energy laser pulses.^[203] The direct one-pot synthesis of photoenol functional Au NPs using an Au salt precursor and a variety of different reducing agents was not possible as the photoenol moiety is not compatible with reducing agents due to the reduction of aldehydes to hydroxyl functions, resulting in the loss of reactivity. In addition, the use of water-soluble photoenol-modified Au NPs was not desired due to the long reaction time in the protic solvent and the unsuitable boiling point of water. Namely, the DLW process causes heating of the solution, therefore high boiling solvents as DMF or DMSO are preferred.

To circumvent the issue of reduction of the aldehyde group, first, stable mercaptoundecanol (MUD)-capped Au NPs (Au–MUD) **56** were synthesized ac-

according to a literature procedure.^[106] The photoenol moiety was subsequently introduced *via* the esterification of the MUD ligands (Figure 25a).

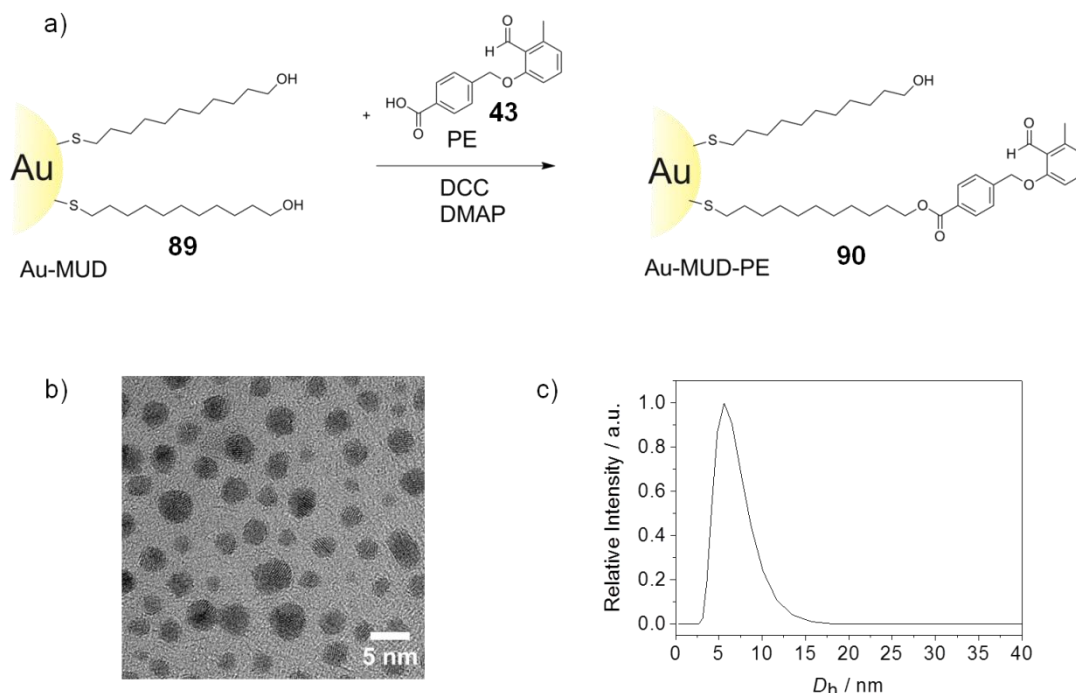


Figure 25. a) Preparation of photoenol (PE) **43** containing Au NPs (Au-MUD-PE) **90** *via* esterification. b) HRTEM image of Au-MUD-PE **90**. c) Volume average size distribution obtained *via* DLS of Au-MUD-PE **90**.

The obtained photoenol modified Au NPs (Au-MUD-PE) **90** were characterized by HRTEM (Figure 25b), dynamic light scattering (DLS, Figure 25c), FT-IR and $^1\text{H-NMR}$ spectroscopy, indicating that NPs with 3.02 ± 0.74 nm in size were coated with – on average – 209 MUD ligands, which was determined by the following estimation. Au NPs were prepared using the synthesis procedure of Raula *et al.*^[106] These authors also determined the amount of MUD ligands by thermogravimetric analysis, resulting in 235 ligands/Au NP (diameter = 3.20 nm). As we observed slightly smaller Au NPs in the range of 3.02 nm, one can estimate the ratio of ligand/Au NP by considering the smaller surface area:

$$\frac{\pi d^2}{\pi d^2} = \frac{\pi 3.02^2}{\pi 3.20^2} \approx 0.89$$

Multiplication of the number of ligands results in the number of ligands for the Au NPs with 3.02 ± 0.74 nm in diameter:

$$0.89 \cdot 235 = 209$$

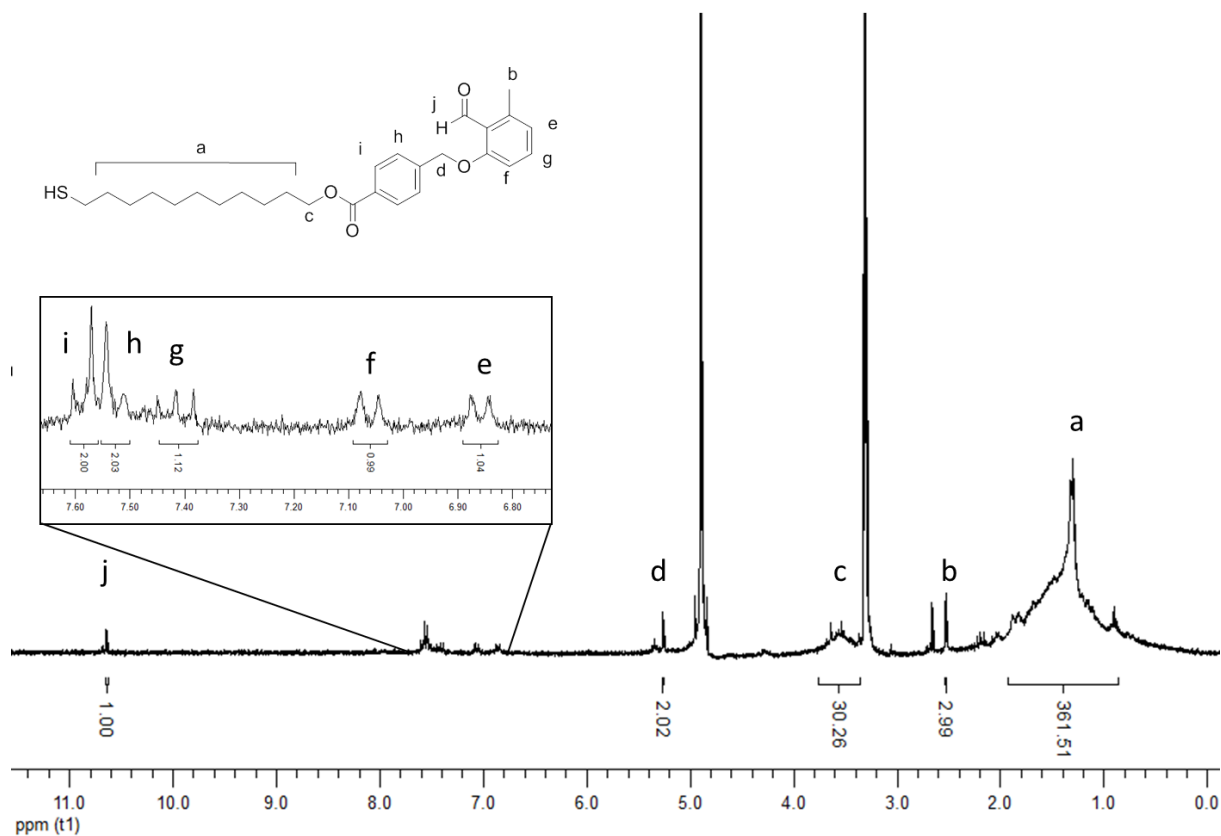
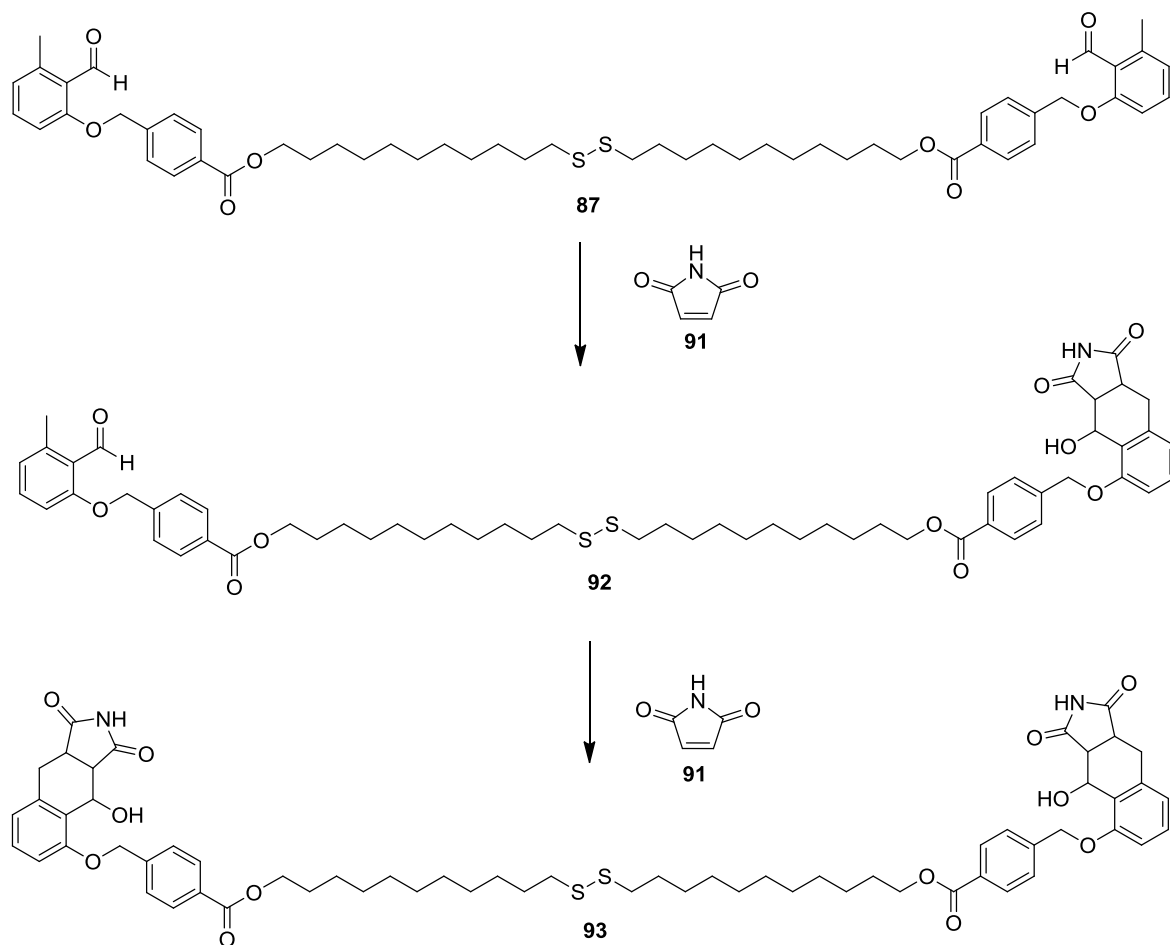


Figure 26. $^1\text{H-NMR}$ spectrum of photoenol precursor modified Au-MUD-PE **90** in CD_3OD at 250 MHz.

Furthermore, the NMR analysis of Au-MUD-PE **90** (Figure 26) was used to estimate the number of photoenol groups per Au NP. Using the integration area, we assigned that H^a corresponded to 18 H with an integration area of approximately 360, implying 1 of 20 MUD linkers or 5% yield of the esterification with photoenol moiety per MUD ligand affording approximately 10 photoenol linkers per Au NP.

In order to obtain precisely encoded patterns *via* DLW, a covalent strategy compatible with both multiphoton process and Au NPs (to avoid aggregation or destruction of crystalline core) was employed. We first assessed the potential of the photoenol based Diels–Alder reaction by employing the MUD–PE linker **87** for a test reaction with maleimide **91** (Scheme 31).

Photo-Induced Surface Encoding of Gold Nanoparticles



Scheme 31. Model reaction between photoenol disulphide linker **87** and maleimide **91** was carried out employing photoreactor and Arimed B6 UV lamp. The photoreaction initially generates mono-functionalized intermediate **92** and subsequently the di-functionalized product **93**.

A reaction mixture was irradiated in DMF and subsequent analysis by ESI-MS evidenced a new peak series, which was assigned to the product of the light-induced Diels–Alder reaction, indicating the complete conversion to the photoadduct without any by-product formation (Figure 27).

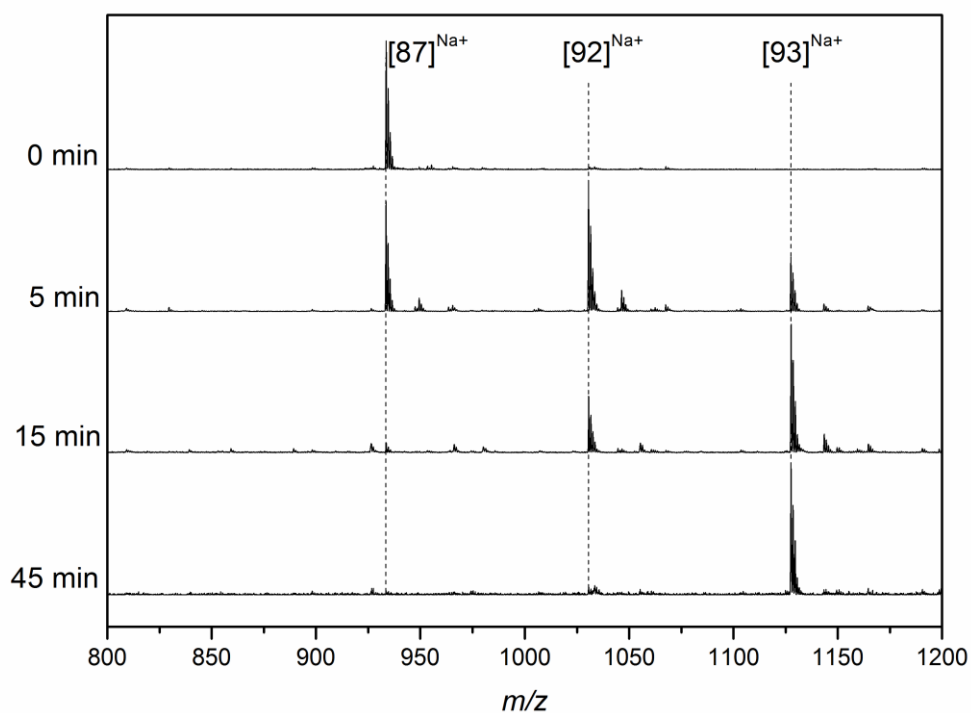
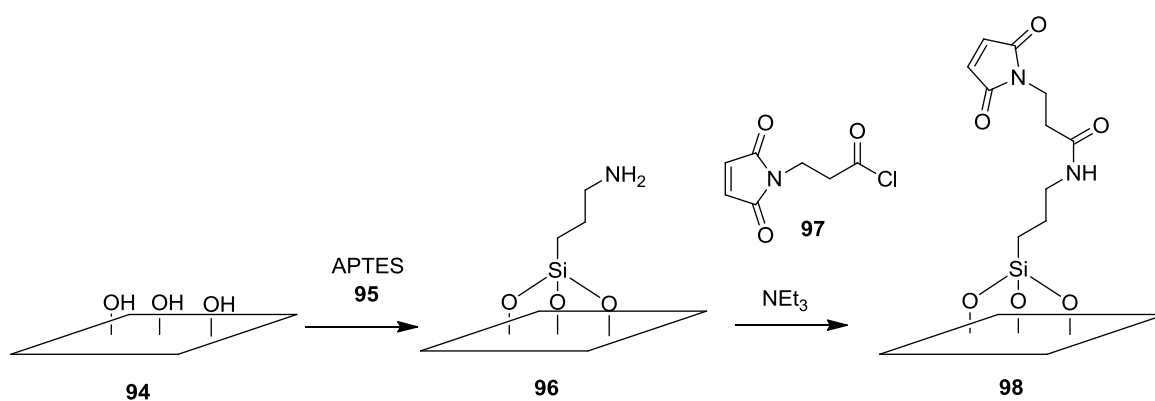


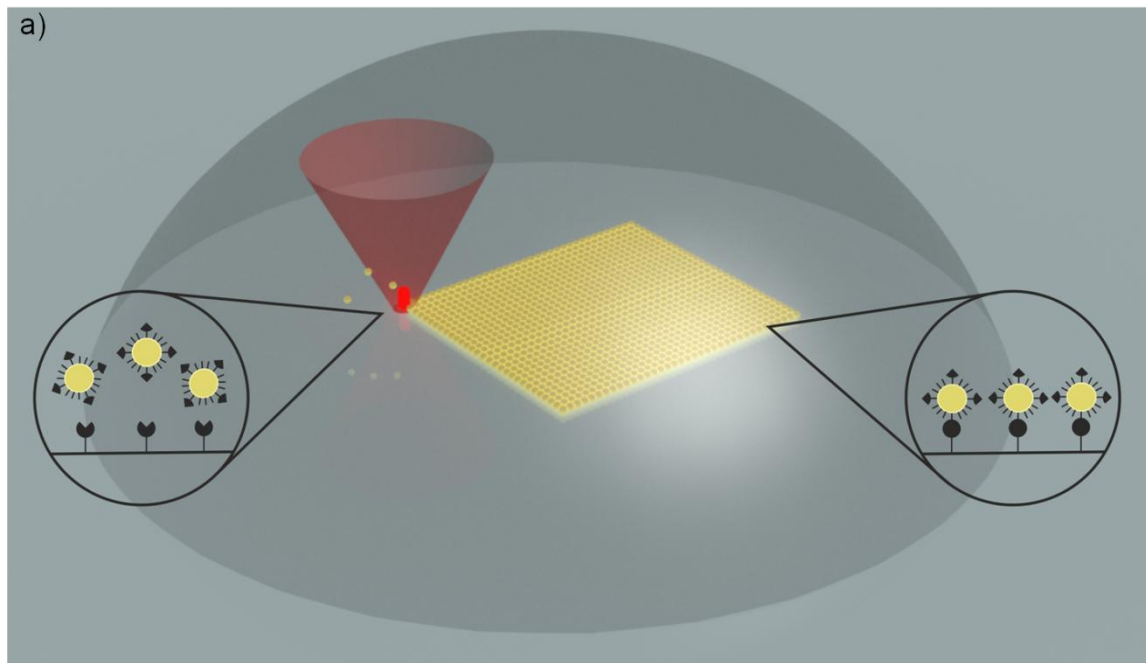
Figure 27. ESI-MS spectrum of the photoreaction between photoenol disulphide linker **87** and maleimide **91** after 0, 5, 15, and 45 min, respectively.

After confirming that the light induced Diels–Alder cycloaddition is a fast and efficient covalent strategy for Au NP modification, patterns of Au NPs on glass surfaces were designed *via* direct DLW encoding.



Scheme 32. Modification of the glass surface with maleimide groups **98** in a two step approach employing (3-aminopropyl)triethoxysilane (APTES) **95** and 4-maleimidopropanoyl chloride **97**.

First, a glass surface was modified with maleimide groups in a two step approach employing (3-aminopropyl)triethoxysilane (APTES) **95** and 4-maleimidopropanoyl chloride **98** as previously reported.^[204]



b)

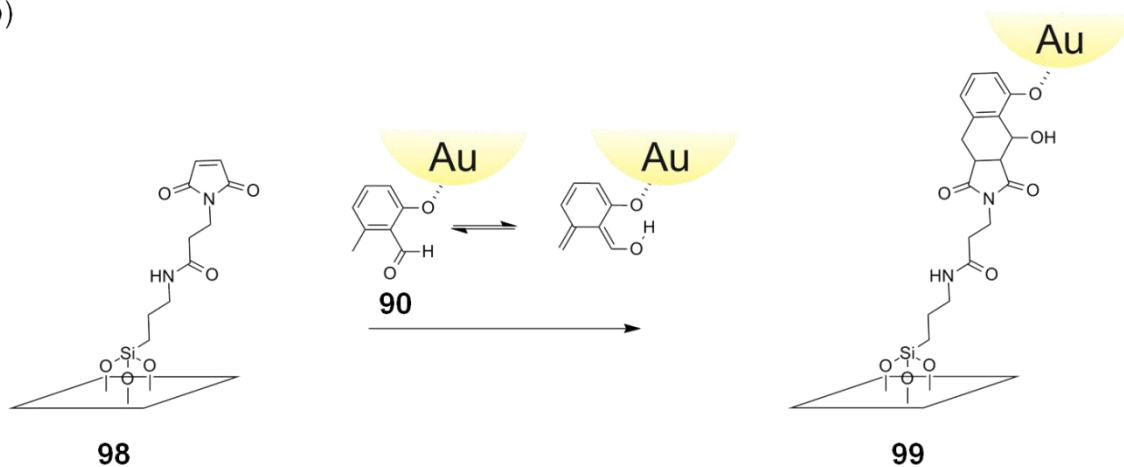


Figure 28. a) Scheme of the photo-induced surface assembly of Au NPs employing DLW. b) Light triggered Diels Alder reaction of the photo-generated *o*-quinodimethane located on the Au NPs **90** with surface anchored maleimides **98**.

Subsequently, photoenol Au NPs were patterned in square patterns ($20\ \mu\text{m} \times 20\ \mu\text{m}$) using DLW to photo-generate the *o*-quinodimethanes located on the Au NPs **90**, which underwent Diels-Alder reaction with surface anchored maleimides **98** (Figure 28).

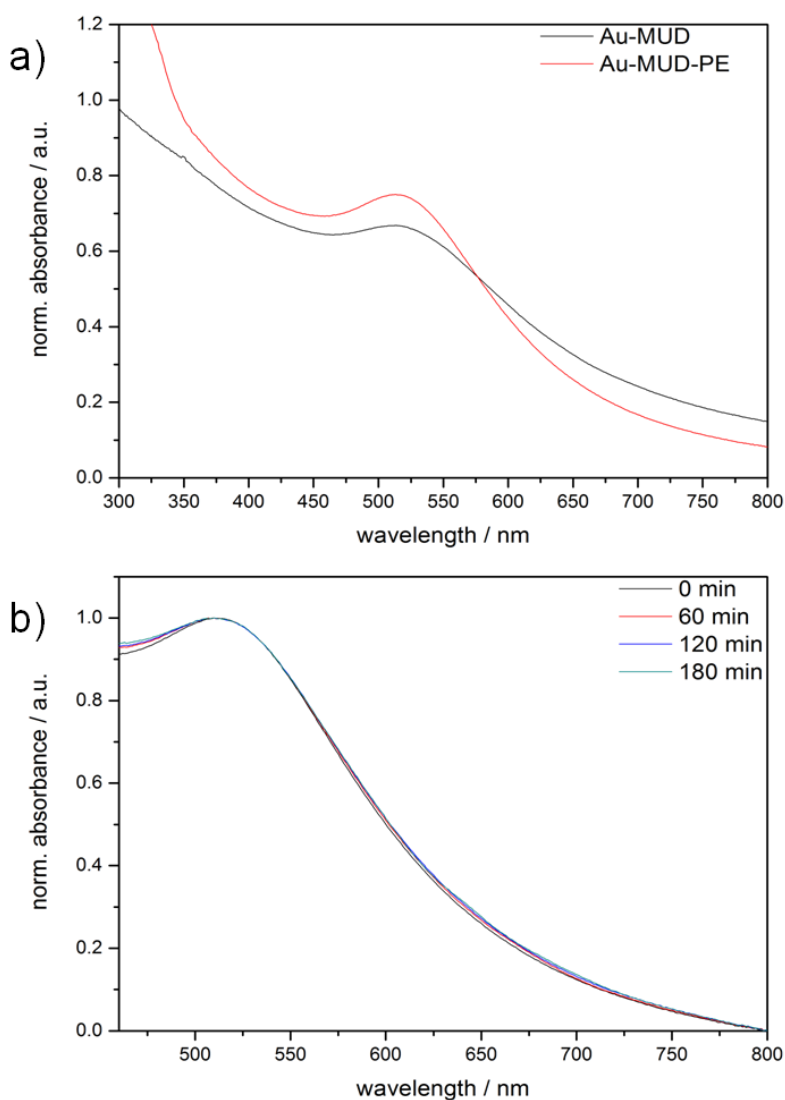


Figure 29. a) UV/Vis spectrum of mercaptoundecanol-capped Au NPs (Au-MUD) **89** and photoenol precursor modified Au-MUD NPs (Au-MUD-PE) **90**. b) UV/Vis measurement of Au-MUD-PE **90** after irradiation for 0, 60, 120, and 180 min employing an Arimed B6 UV lamp.

It should be noted that for the test reaction of MUD–PE linker and maleimide UV-A light (315–400 nm) was used to phototrigger the reaction ($\lambda_{\text{max}} = 320$ nm). Control studies indicated that Au NPs are stable under these conditions for several hours (no agglomeration was observed by UV/Vis spectroscopy, Figure 29). Nevertheless, it has been shown that laser irradiation of thiol-passivated Au NPs with UV-A wavelengths may lead to agglomerated Au NPs.^[203] Thus, we employed a multiphoton process to activate the photoenol moiety with a 700 nm pulsed laser. To ensure that there is no undesired aggregation of Au NPs, which can occur due to heating effects of the NPs and to the radical formation leading to the removal of

the monolayer on the NP surface,^[205] DLW was carried out with a range of different laser powers (0.2 mW to 4 mW) and the setup was optimized to allow for a fast and efficient activation of the photoenol moieties to minimize the aggregation.

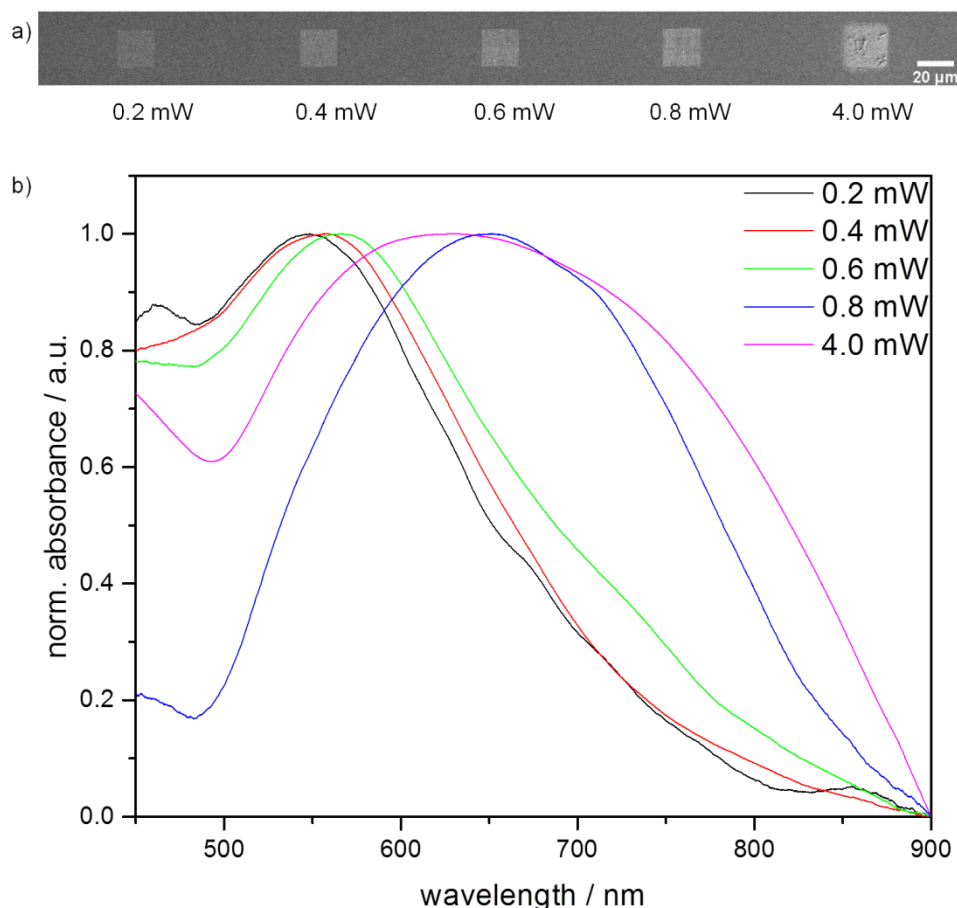


Figure 30. a) SEM image of square patterns, which were produced with different laser powers, from 0.2 mW to 4 mW. (b) UV-Vis spectra of the square patterns generated at the indicated laser powers showing aggregation of Au NPs at elevated laser powers (from 0.6 mW).

The optimum conditions were found at low laser powers (0.2–0.4 mW) (Figure 30b). Scanning electron microscopy (SEM) images of the patterns indicate that precise immobilization of NPs was achieved in the irradiated regions (Figure 30a). In addition, UV/Vis spectra of the prepared square patterns based on different laser powers were recorded, indicating that Au NP aggregation increases with laser power (localized particle plasmon resonances shift from 542 nm to more than 600 nm, Figure 30a). UV-Vis spectra further indicate that at low laser power conditions Au NPs were immobilized without significant aggregation. Thus, the NP properties remained unaltered during this mild immobilization technique.

To evidence that the assembly of Au NPs is driven by covalent Diels–Alder binding, control experiments were performed utilizing non-activated components.

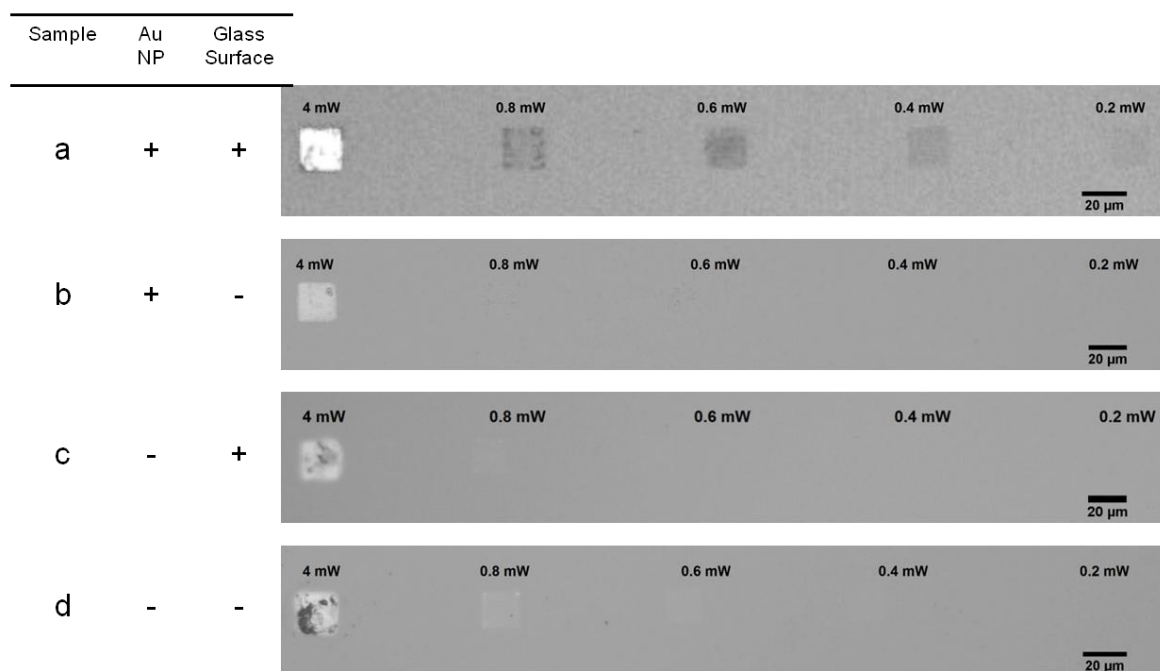


Figure 31. Microscopic images of square patterns ($20\ \mu\text{m} \times 20\ \mu\text{m}$). Different laser powers were employed for the DLW process with a) Au-MUD-PE **90** (functional) on maleimide coated glass surface **98** (functional) b) Au-MUD-PE **90** (functional) on bare glass surface (non-functional) c) Au-MUD **89** (non-functional) on maleimide coated glass surface **98** (functional) d) Au-MUD **89** (non-functional) on bare glass surface (non-functional). b) – d) are control experiments.

It was shown that no patterns are obtained when either Au–MUD NPs or bare glass surfaces were used (Figure 31, samples b and c). NP assembly is achieved only upon low laser power treatment (0.2–0.4 mW) of Au–MUD–PE **90** and maleimide coated glass surfaces (Figure 31, sample a). At a slightly increased laser power (0.6–0.8 mW), minimal immobilization is also observed in the control experiments. Furthermore, as observed from the red shift in the UV spectra (Figure 30b), the use of increased laser power (0.6–4 mW) leads to NP agglomeration due to light absorption accompanied by Au NP induced heat generation and subsequent Au NP precipitation. This results in undesired aggregation of Au NPs, leading to a decreased pattern quality due to alteration of the immobilized Au NPs and is also an explanation for the immobilization observed in the control experiments. In contrast to other Au NP immobilization techniques on this scale such as in situ formation by photoreduction of gold,^[205a] the here presented technique ena-

bles the precise tailoring and thorough characterization of the NP before immobilization. As the mild fixation step does not alter the NP properties, this approach allows for a precise immobilization of tailored Au NPs.

A significant advantage of DLW driven spatially resolved surface encoding in contrast to the stamp based μ CP is its ability to generate complex patterns not limited by the properties of the stamp. The DLW setup can be employed to produce virtually any desired pattern of Au NPs as shown in Figure 32 and Figure 33, where the Karlsruhe Institute of Technology (KIT) logo was written in two different sizes (approx. $60\ \mu\text{m} \times 30\ \mu\text{m}$ in Figure 32 and approx. $30\ \mu\text{m} \times 15\ \mu\text{m}$ in Figure 33).

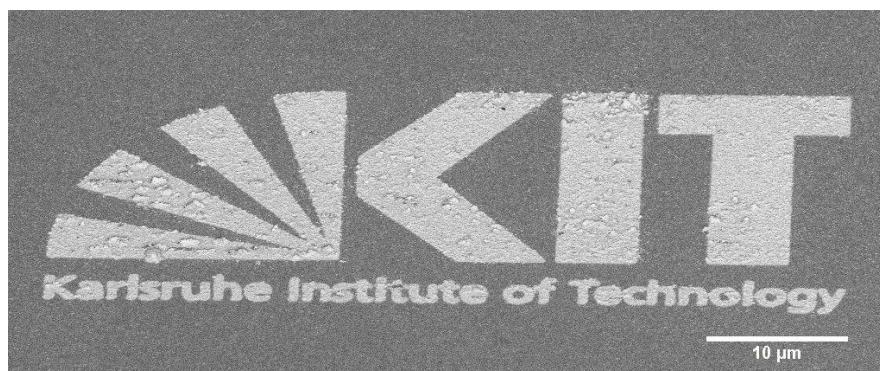


Figure 32. SEM image of KIT logo by DLW of Au-MUD-PE **90** with a total footprint of approximately $60\ \mu\text{m} \times 30\ \mu\text{m}$ (sample was tilted by 54°). Small amount of aggregation is observable.

The KIT logo in Figure 32 was a first trial to produce different patterns using a higher laser power (3.2 mW) and a smaller distance between each scanning line (100 nm), which led to aggregation in some regions. After the UV/Vis analysis of the square patterns ($20\ \mu\text{m} \times 20\ \mu\text{m}$), the laser power was lowered to 1.6 mW to enable patterning (approx. $30\ \mu\text{m} \times 15\ \mu\text{m}$) with no visible aggregation (Figure 33a).

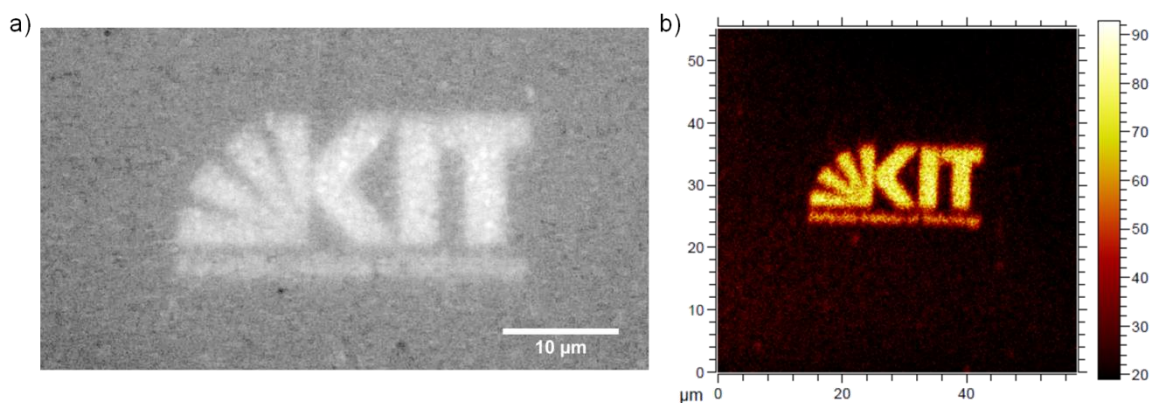


Figure 33. Direct laser writing with Au-MUD-PE **90** onto maleimide coated glass surface **98** to fabricate the KIT logo with a total footprint of approximately $30\ \mu\text{m} \times 15\ \mu\text{m}$. a) Bright field image of the fabricated KIT logo. b) ToF-SIMS image of AuS^- , Au_2S^- , and Au_4S_2^- . The KIT logo scanned with the DLW setup is clearly visible as it contains a high amount on thiolated Au.

The presence of Au NPs within the patterns was confirmed both by SEM (Figure 32) and time-of-flight secondary ion mass spectrometry (ToF-SIMS) (Figure 33b). Following the immobilization of thiolated Au NPs, a set of prominent Au_xS_y peaks dominates the high mass range of the negative polarity secondary ion mass spectrum (Figure 34a).

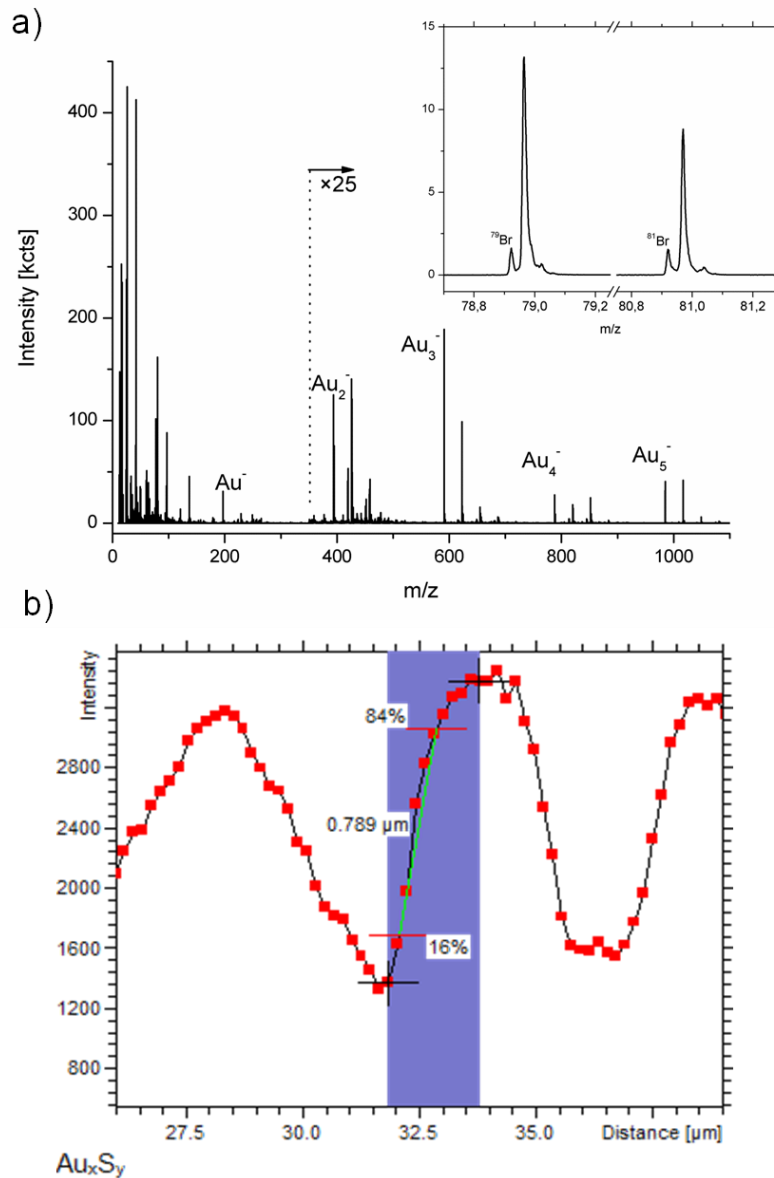


Figure 34. a) Negative polarity Secondary Ion Mass Spectrum (SIMS), high mass resolution, of immobilized thiolated Au NPs reacted with brominated maleimide according to Figure 38a obtained from a 1000x500 μm scan area with 16 individual DLW pattern as shown in Figure 33 sample a. Insert: Zoom in on bromine peaks. b) Intensity profile of Au_xS_y^- signals across the DLW patterned KIT logo shown in Figure 36b demonstrates defined boundaries between immobilized and non-immobilized areas of 0.8 μm based on the (84/16) definition.

Since many of these peaks are not accompanied by other peaks at the same nominal mass, SIMS imaging with high lateral resolution is straightforward (Figure 34b). The Au_xS_y^- intensity profile across the KIT logo obtained from the analysis shown in Figure 34b demonstrates defined boundaries between immobilized and non-immobilized areas of 0.8 μm based on the (84/16) definition. Under the as-

sumption that neighboring areas of these boundaries are not affected by exposure, the minimum distance of two patterns and thus the resolution of this technique under these precise parameters can be estimated to be 1.6 μm . Limiting factors of the resolution are the diffraction limit and the diffusion of activated Au NPs during the patterning process. Depending on the solvent, the lifetime of the o-quinodimethane varies from microseconds to seconds in solution. It can therefore be assumed that activated particles may exit the confined excitation volume and be covalently immobilized onto the substrate outside of exposed substrate areas. A precise impact of this influence is difficult to estimate since the lifetime of the o-quinodimethane on the particles is not known. Finally, only the photoenol moieties located in the contact area between the Au NP and the glass surface are expected to contribute to covalent NP immobilization.

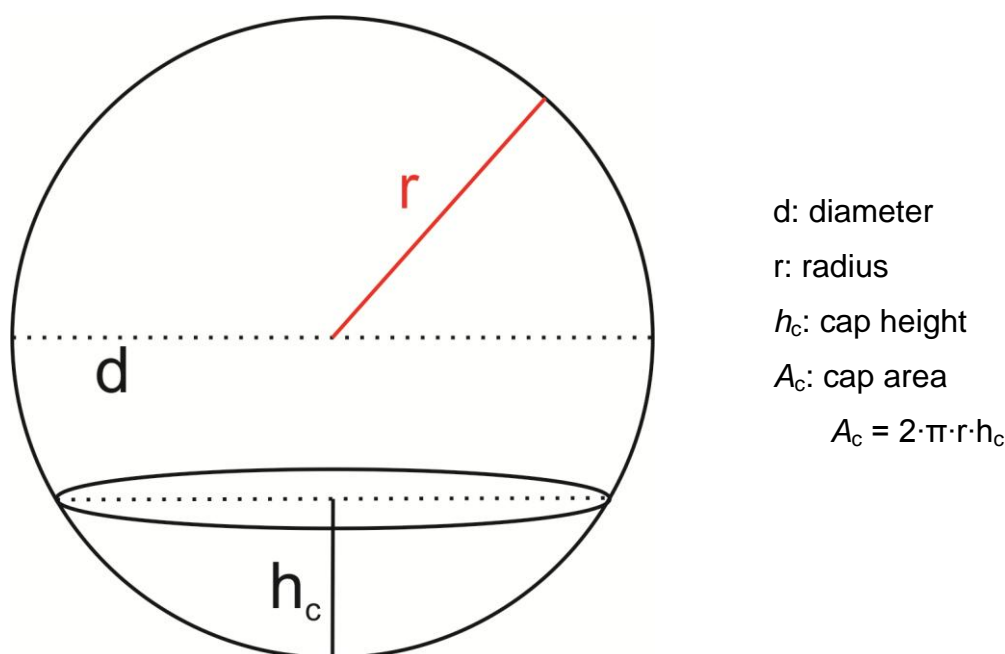


Figure 35. Schematic drawing of spherical Au NPs.

$$A_c = 2 \cdot \pi \cdot 1.51 \text{ nm} \cdot 0.28 \text{ nm} = 2.66 \text{ nm}^2$$

$$\frac{\text{contact area}}{\text{total area}} = \frac{2.66 \text{ nm}^2}{28.65 \text{ nm}^2} = 0.093$$

$$10 \text{ ligands} \cdot 0.093 = 0.93$$

Only 9.3% of the photoenol ligands on the Au NP are located on the contact area, therefore 0.93 photoenol molecules are placed on the contact area and enable the photoreaction with the maleimide onto the glass surface. According to literature,^[129] the ligands contributing to the light-induced Diels-Alder reaction are those located at the contact area. As we consider spherical Au NPs, the contact area is defined as the hemispherical cap area A_c (Figure 35). The hemispherical area A_c can be calculated with the above mentioned formula with the cap height h_c , which is similar to the diameter of a gold atom (0.28 nm), resulting in $A_c = 2.66 \text{ nm}^2$. Assuming that the 10 photoenol ligands are evenly distributed, we expect by division by the total NP area that 0.93 ligands are located at the contact area indicating that only a single covalent bond between the Au NP and the glass surface is formed during encoding, therefore a subset of residual photoreactive moieties remains available for further modifications. To confirm this hypothesis, the patterned surface was immersed in a solution of maleimide containing compounds under UV irradiation ($\lambda_{\text{max}} = 320 \text{ nm}$) to allow for the light-induced Diels-Alder reaction.

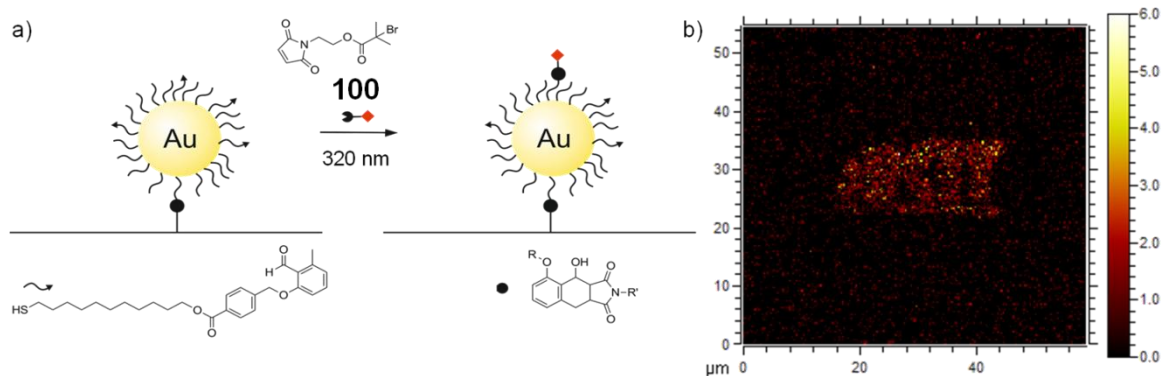


Figure 36. a) Light-induced Diels-Alder reaction between residual photoenol groups attached on Au NP and bromine containing maleimide **100**. b) ToF-SIMS image of the sum of ^{79}Br and ^{81}Br , indicating an increased amount of bromine within the KIT pattern.

To demonstrate the spatially resolved surface modification, a bromine containing maleimide, **100**, was chosen as it allows an easy and distinct determination *via* ToF-SIMS (Figure 36a). After irradiation, bromine (^{79}Br and ^{81}Br) is detected within the KIT logo pattern by ToF-SIMS and showed an increased signal in comparison with the non-modified background (Figure 36b). Since other peaks overlap with the bromine peaks at the same nominal masses (Figure 34a) SIMS imaging of bromine with high lateral resolution requires the liquid metal ion gun burst mode.

This, in combination with the low amounts of bromine, limits the obtained image quality in Figure 36b. However, as virtually any maleimide containing molecule can be used for postmodification of Au NP patterns an additional layer can be deposited onto the Au NPs *via* this approach.

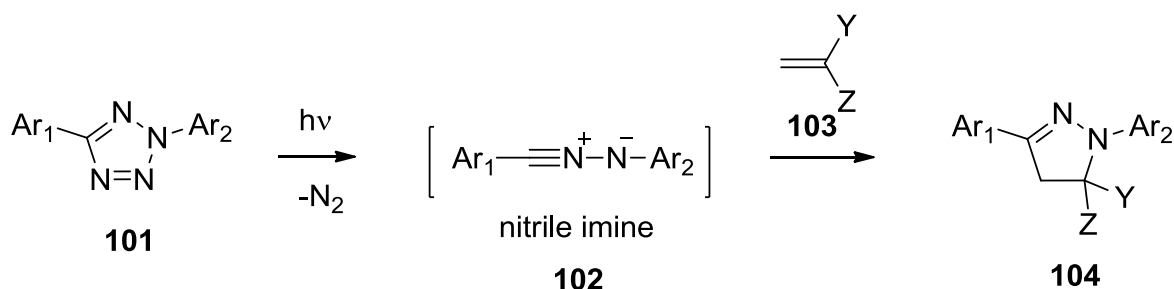
Conclusions

In conclusion, the successful fabrication of 2D micropatterns using Au NPs was demonstrated by combining DLW with multiphoton induced Diels–Alder chemistry. Au NPs were, for the first time, functionalized with photoenol precursor molecules and subsequently used for covalent, light induced surface encoding onto maleimide-coated glass substrates without aggregation of the Au NPs during the process. Residual, unreacted photoenol groups were used for further modification allowing the bottom up modification of the patterned surfaces. The combination of DLW and light-induced Diels–Alder chemistry allows for the design of virtually any desired pattern at the micron and submicron scale, which can be further modified with maleimide containing biomolecules, thus opening new avenues to design Au NP covered surfaces. Au NP arrays are also interesting as substrate for biosensing based on SERS measurements. Moreover, conductive 2D or 3D Au NP patterns can be employed in electronics.

5 Tetrazole Modified Gold Nanorods for Biofunctionalization³

Introduction

As described before, photoenol chemistry represents a powerful tool for the tailoring and the immobilization of NPs in aprotic, organic solvents. Although Pauloehrl *et al.* immobilized maleimide modified peptide in 2 h to photoenol-coated surfaces using acetonitrile/PBS 3:1,^[171] rather long reaction times in protic solvents make photoenol chemistry not the best choice for biofunctionalization of NPs in aqueous solutions. However, much faster reaction kinetics are achieved by the light-induced nitrile imine mediated tetrazole-ene chemistry (NITEC). Already in the late 1960s, Huisgen and coworkers reported the first light-induced cycloaddition between 2,5-diphenyltetrazole and methyl crotonate under UV irradiation.^[206] 2,5-Diphenyltetrazole underwent a facile cycloreversion reaction upon UV irradiation to release nitrogen and to generate the highly reactive nitrile imine dipole, which could react with dipolarophiles such as methyl crotonate to afford fluorescent pyrazoline product.



Scheme 33. Photoactivated 1,3-dipolar cycloaddition reaction between a 2,5-diaryl tetrazole **101** and a substituted alkene dipolarophile **103**.

Inspired by the work of Huisgen, Lin and coworkers demonstrated in 2008 an extremely fast NITEC reaction (≤ 1 min) for labeling of tetrazole-modified proteins with alkenes which results in a fluorescent pyrazoline product (Scheme 33).^[207] Therefore, an alkene moiety was genetically encoded in proteins inside bacteria

³ Parts of this chapter have been adapted from Stolzer, L.; Vigovskaya, A.; Barner-Kowollik, C.; Fruk, L. *Chem. Eur. J.* **2015**, DOI: 10.1002/chem.201502070 with permission from WILEY-VCH.

cells, the monitoring was enabled *in vivo* by fluorescence measurements of the NITEC product.^[208] However, UV light with 302 nm was employed to induce the reactions, which may cause damage of various biomolecules within cells upon prolonged irradiation. Therefore a range of new tetrazole linkers were synthesized, some of them enable activation with visible light (Figure 37).

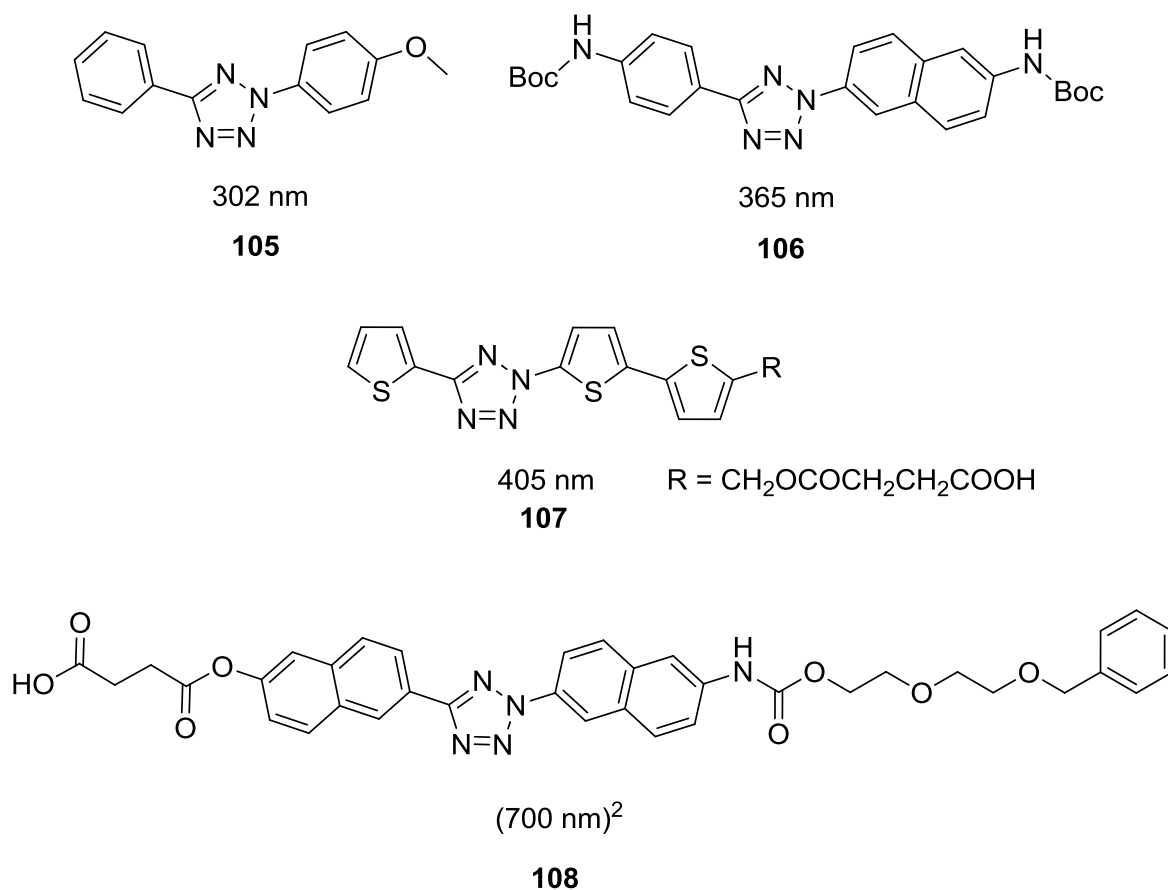


Figure 37. Design of tetrazoles with different photoactivation wavelengths: **105**,^[209] **106**,^[210] **107**,^[211] and **108**^[212] were published by the group of Lin.

Some of the diaryltetrazoles such as **106** and **107** could be activated by 365 nm, but with slower reaction kinetics due to the filtering effect of pyrazoline products, which absorbs light in the same region ($\lambda_{\text{max}} \approx 370 \text{ nm}$).^[213] However, amino and amide groups in the *para* position such as Boc-protected **106** allowed the 1,3-dipolar cycloaddition of the tetrazole moiety with excellent yields using longer wavelengths for irradiation.^[210] The design of oligothiophene-based tetrazole **107** allowed the spatiotemporally controlled imaging of microtubules *via* light-induced NITEC under visible light ($\lambda = 405 \text{ nm}$) irradiation in live mammalian cells.^[211] Moreover, naphthalene-based tetrazoles **108** have been activated by

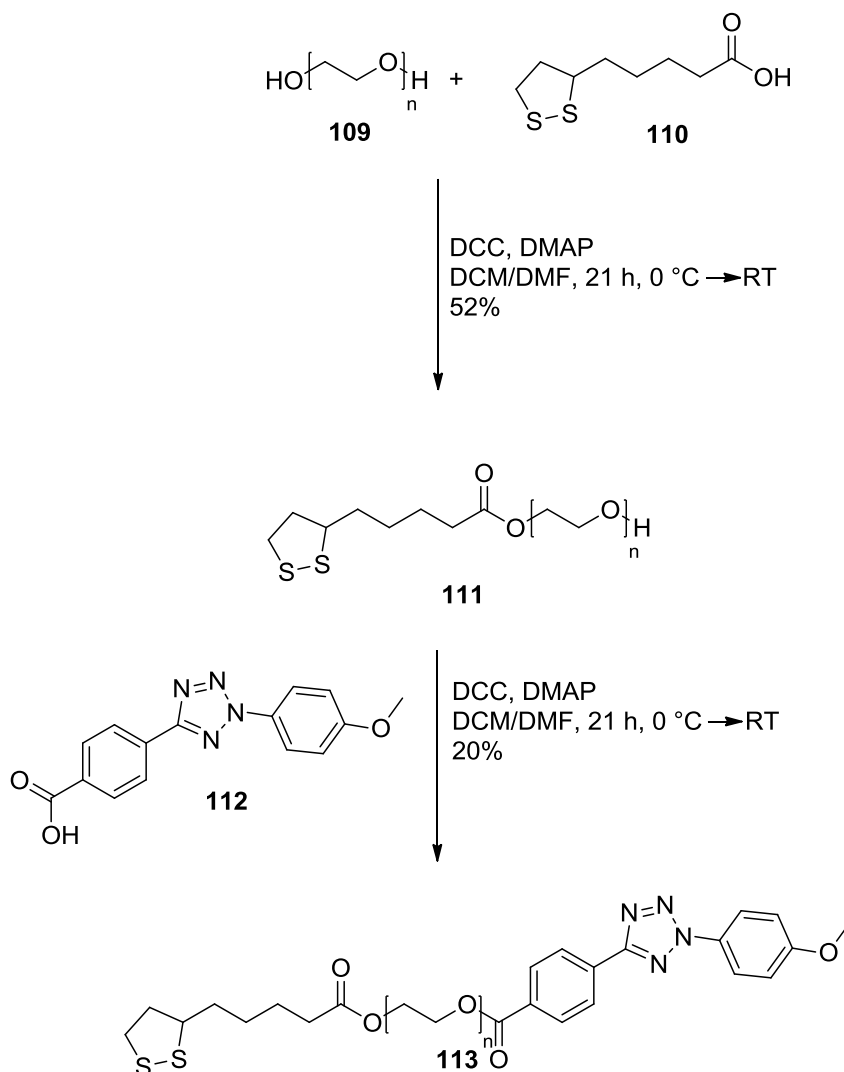
two-photon excitation with a 700 nm femtosecond pulsed laser and allowed for labeling alkene-encoded proteins in cultured cells.^[212]

The insertion of alkene and tetrazole moiety in a taxoid core, which is an anti-cancer agent; enabled the intramolecular photoclick reaction.^[214] The treatment of cells with tetrazole-taxoids allowed the imaging of fluorescent pyrazoline after UV irradiation. It should be noted, that the rapid, profluorescent NITEC reaction exhibits side reactions in water. The highly reactive nitrile imine forms after addition of water hydrazides.^[215] Additional dimerization products^[216] can also be produced. Nevertheless, NITEC reactions were already successfully used by the Barner-Kowollik group for the generation of fluorescent polymers from non-fluorescent monomers,^[217] the spatially resolved surface modification of various 2D substrates^[218] and the generation of fluorescent single-chain polymeric nanoparticles.^[219] Recently, the tetrazole moiety attached to DNA was used for the coupling of a dye and small molecules.^[220]

To summarize, the NITEC concept represents a powerful technique for the spatially and temporally controlled modification of surfaces and polymers. In particular, the profluorescent, bioorthogonal cycloaddition allows the visualization of proteins in living cells.^[221] However, it has not yet been used for the NP modification and the following section will demonstrate its applicability to design NP-biomolecule hybrids. Therefore, novel bifunctional tetrazole linker will be synthesized to enable the attachment to the NP surface. Moreover, Au NRs with their photothermal properties will be functionalized with biomolecules *via* light-induced reactions to generate fluorescent bionanoconjugates, which have potential for biosensing and drug delivery applications.

Results and Discussion

To achieve the biofunctionalization of nanorods using NITEC chemistry, we first designed a novel α,ω -bifunctional PEG linker **113**, containing tetrazole and thioctic acid anchoring groups for stabilization of Au NR surfaces. Bidentate thioctic acid is known to provide a better colloidal stability to Au NPs than monodentate thiols and has been widely used for the attachment of various species to Au surfaces.^[222] PEG **109** was esterified with thioctic acid **110** according to literature procedure^[159] and purified by column chromatography.



Scheme 34. Synthesis of thioctic acid-PEG-tetrazole **113**.

The tetrazole moiety was coupled to the thioctic acid-modified PEG **111** with esterification using DCC and DMAP to obtain the bifunctional TA-PEG-TZ linker **113** (Scheme 34). In general, PEG is the most widely used water soluble, biocompatible polymer, which has been shown to enhance the stability of Au NR in water and cell media.^[223] Furthermore, PEG can be considered a chemical separator, which creates a distance between the fluorophore moiety (reaction product) and the NP surface. It is important to avoid fluorescence quenching by the Au NR core^[224] and enable the fluorescence measurements of the pyrazoline product therefore leading to a self-reporting system. This ‘turn-on’ fluorescence ability of NITEC reaction has already been exploited for bioimaging^[221c] and in combination with reported fluorescence enhancement of Au NR surfaces,^[224] it has a great potential to increase the sensitivity of the whole system. The fluorescence enhancement of Au NR is attributed to a range of processes including better absorption of

the fluorophore molecule or enhanced coupling of the fluorescence emission to the far field.^[225]

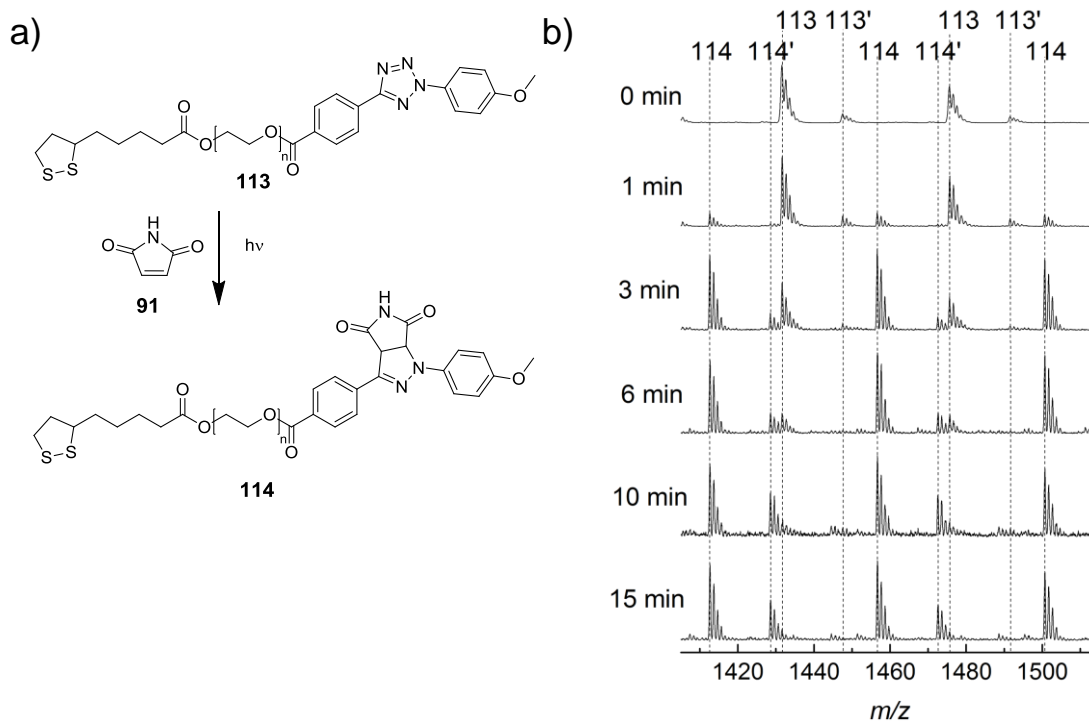


Figure 38. a) Model reaction between TA-PEG-TZ **113** and maleimide **91**. b) ESI-MS spectra recorded after 0, 1, 3, 6, 10, 15 min depicts sodium adducts (Na^+) of **113** and **114**. **113'** and **114'** may be attributed to oxidation during the ionization process.

First, the reactivity of the linker **113** was assessed by irradiation ($\lambda_{\text{max}} = 320 \text{ nm}$) of **113** and maleimide **91** (Figure 38a) in water/acetonitrile 9:1 and analyzed in detail by ESI-MS showing the complete conversion of TA-PEG-TZ **113** (Figure 38b).

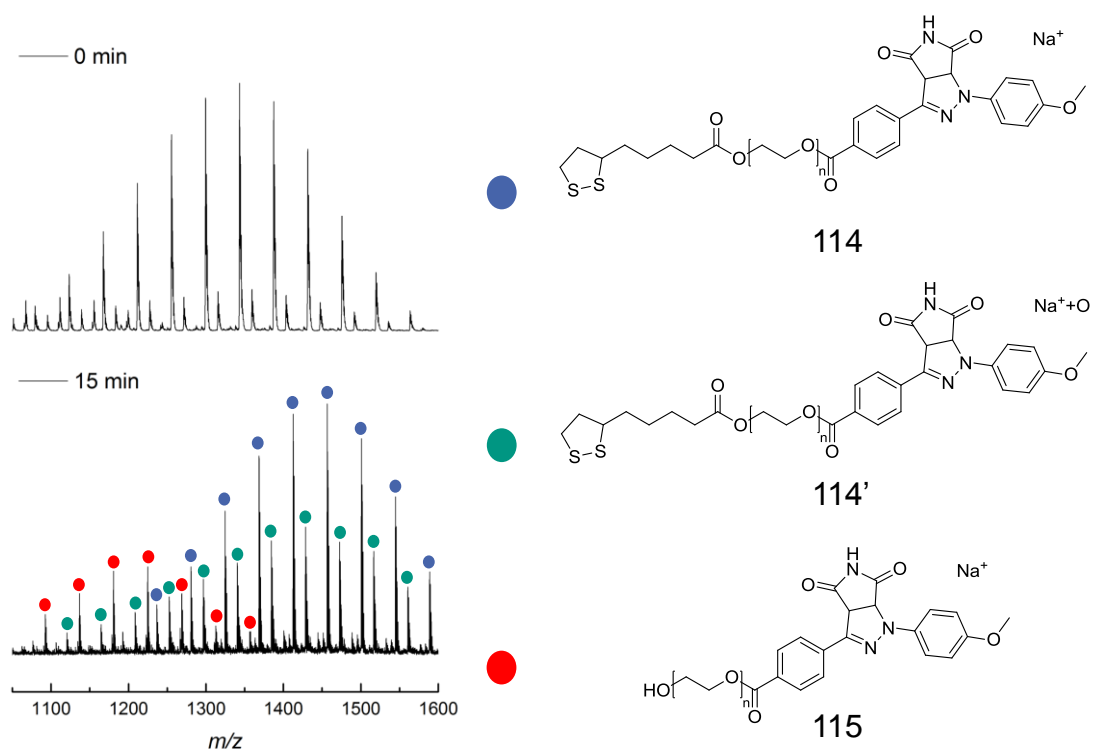


Figure 39. ESI-MS spectrum of TA-PEG-TZ **113** and TA-PEG-TZ **113** after irradiation with maleimide **91** for 15 min showing besides the product **114** (blue) and the oxidized product **114'** (green) (probably during ionization process), a by-product **115** (red) due to ester bond cleavage.

It should be noted, that besides the main product **114**, an oxidized product **114'**, which was possibly caused by oxidation during the ionization process and another by-product **115** due to the cleavage of the ester bond, were observed (Figure 39). To circumvent the by-product formation, amide linkage instead of ester bond should be used for the introduction of the functional groups due to its higher stability.^[226]

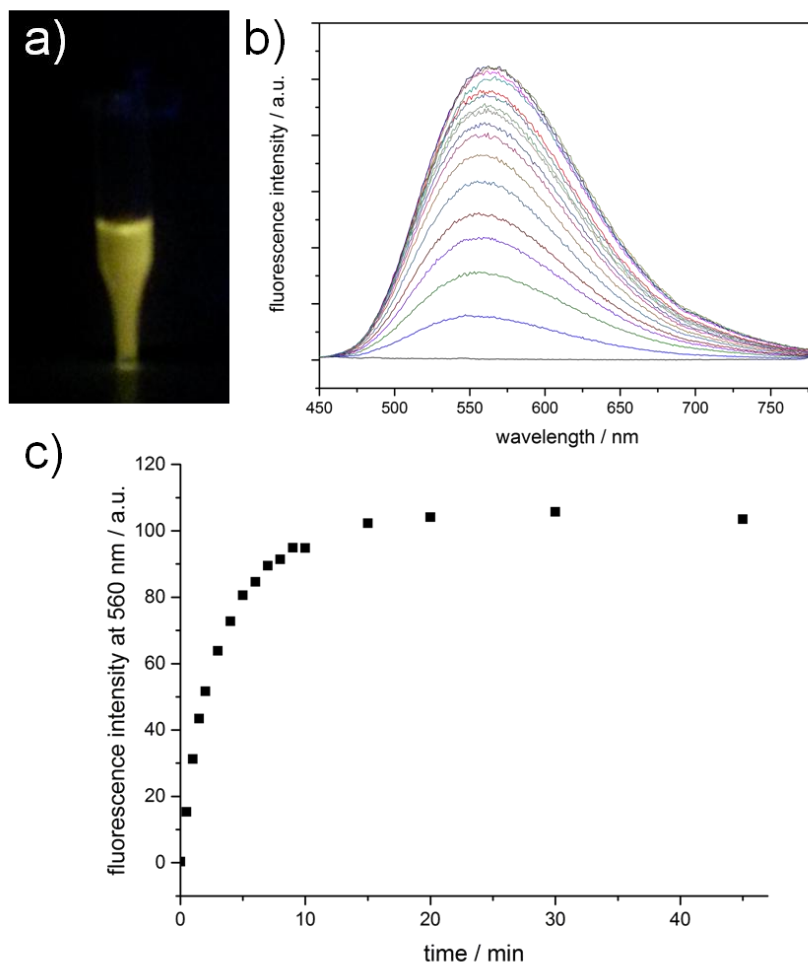


Figure 40. a) Image of a vial containing fluorescent solution of **114** excited under UV-irradiation (365 nm) by a hand-held TLC lamp. b) Fluorescence spectra of reaction mixture at extinction wavelength $\lambda_{\text{ex}} = 400$ nm. c) Evolution of fluorescence signal at $\lambda_{\text{em}} = 560$ nm derived from fluorescence spectra.

Despite the presence of the by-product **115**, the reaction can be monitored by fluorescence measurements of the main pyrazoline product **114** (Figure 40a). The fluorescence spectra exhibited the typical broad, pyrazoline emission at $\lambda_{\text{em, max}} = 560$ nm when excitation wavelength of $\lambda_{\text{ex}} = 400$ nm was used (Figure 40b). The reaction proceeds rapidly in the first few minutes when the nitrile imine concentration is high and then plateaus after about 15 min (Figure 40c). Additionally, the quantum yield of the pyrazoline product **114** was determined $\Phi_{\text{fl}} = 0.045$, which is a slightly higher value than that of literature reported diphenyltetrazoles.^[213]

After the successful assessment of the model NITEC reaction and confirmed presence of the fluorescent pyrazoline product **114**, tetrazole modified Au NR were

prepared to enable the subsequent biofunctionalization. Au NRs were synthesized according to a literature procedure using CTAB as a stabilizer.^[24]

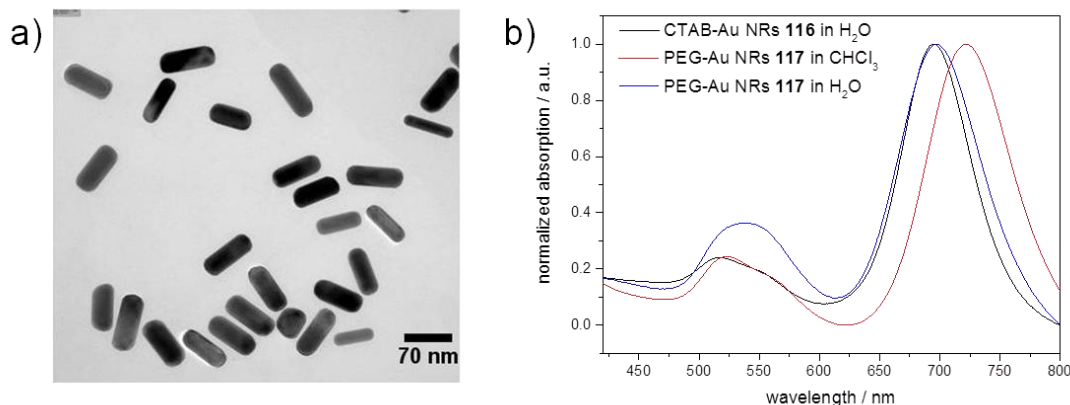


Figure 41. a) TEM image of CTAB-capped Au NRs **116**. b) UV/Vis spectra of CTAB-Au NRs **116**, pegylated Au NR **117** in chloroform and water.

The CTAB stabilized Au NRs **116** were analyzed by TEM (Figure 41a) and UV/Vis spectroscopy (Figure 41b). Au NRs of approx. 70 nm × 23 nm (aspect ratio 3) with plasmon peak at 697 nm were obtained. To attach the bifunctional linker **113** to the CTAB-coated Au NRs, the ligand exchange methodology was employed. Recently, a number of researchers have focused their efforts in the development of an efficient strategy to fully replace the toxic CTAB with thiolated species such as thiolated PEG due to the variety of diagnostic and therapeutic applications such as photothermal therapy, in which Au NR have shown significant promise.^[148] However, the removal of CTAB surface stabilizers is not straightforward. We have followed several protocols dealing with the ligand exchange of CTAB-capped Au NRs with thiolated PEG in aqueous or ethanoic solution,^[227] which either resulted in low stability or agglomeration of Au NR indicating the low efficiency of the ligand exchange. In general the efficiency of the ligand exchange can be assessed by the stability of the Au NRs after dilution below the critical micelle concentration of CTAB^[227a] and in presence of salts.

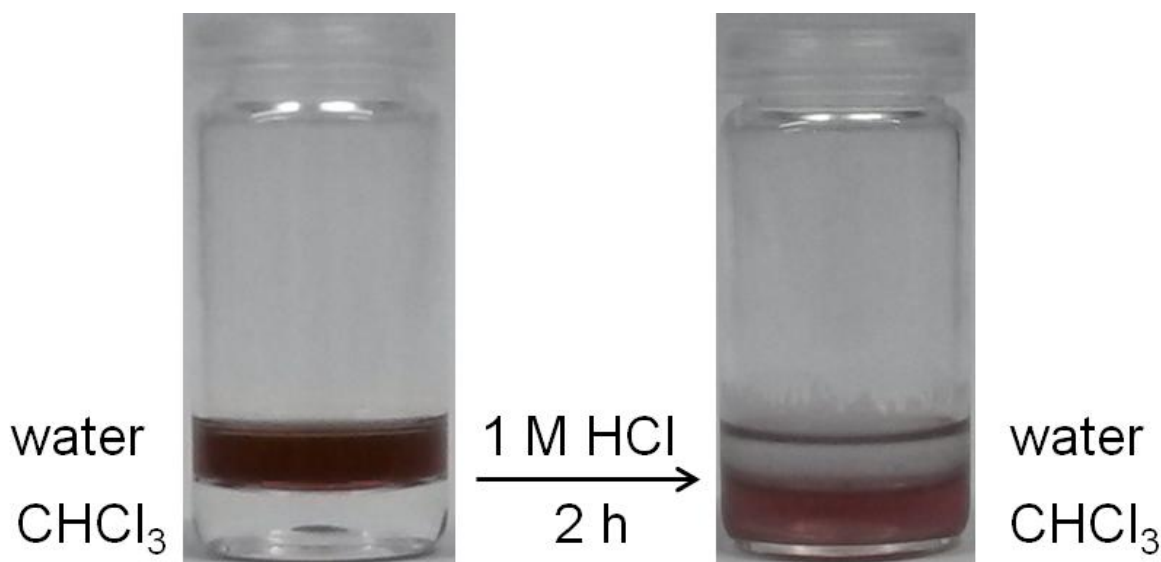


Figure 42. Two-phase system of CTAB-Au NRs **116** and PEG linkers **111** and **113** in chloroform (left). Phase transfer of Au NRs after addition of 1 M HCl and vigorously stirring for 2 h.

After several attempts to find a suitable ligand exchange procedure for our bifunctional linker **113**, we had success employing the phase transfer procedure adapted from Lista *et al.*^[228] and a mixture of reactive linker **113** and thioctic acid-PEG **111** (in 1 : 10 ratio) in order to minimize surface crowding effects. The two phase system of Au NR in aqueous solution and PEG linkers **111** and **113** in chloroform were vigorously stirred for 2 h after addition of 1M HCl solution, which led to the destabilization of the CTAB bilayer (Figure 42). After successful phase transfer, the pegylated Au NRs **84** containing tetrazole moiety are dispersed in chloroform, centrifuged and redispersed in water.

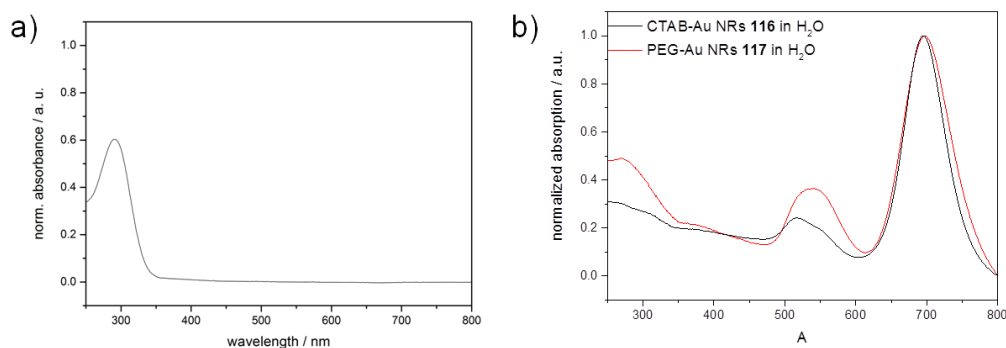


Figure 43. a) UV/Vis spectrum of TA-PEG-TZ **113** with $\lambda_{\max} = 290$ nm. b) UV/Vis spectra of CTAB-capped Au NRs **116** and pegylated Au NRs **117**.

The efficient ligand exchange was confirmed by UV/Vis spectroscopy indicating no shift of the absorption maximum at 697 nm and an increased absorption at 290 nm of the tetrazole moiety (Figure 43). The shift of the absorption maximum to 722 nm of pegylated Au NRs **117** in chloroform was attributed to the higher refractive index of chloroform than of water.^[46]

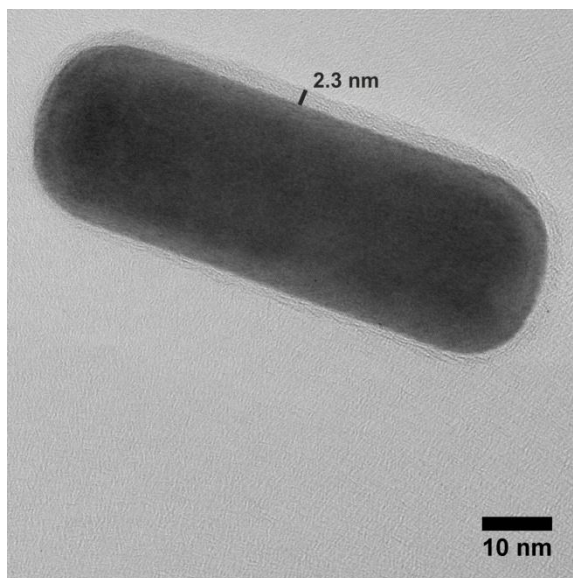


Figure 44. HRTEM image of PEG-modified Au NRs **117**.

HRTEM image of pegylated Au NR **117** (Figure 44) evidenced the Au NR core polymer shell formation after the ligand exchange – thin layer of approx. 2 nm could be observed corresponding to the polymer shell. The replacement of the positively charged CTAB could also be observed in zeta potential measurements, which showed slightly negatively charged Au NR after pegylation (Table 5).

Next, tetrazole modified Au NR **117** were biofunctionalized with maleimide containing DNA under irradiation **83** ($\lambda_{\max} = 320$ nm). 5'-maleimide DNA **83** (22 mer) was prepared using amino terminated ssDNA **81** and sSMCC crosslinker **82**. The reactivity of the maleimide modified ssDNA **83** towards tetrazole was first assessed in solution by irradiation of **83** with tetrazole containing PEG linker **113**.

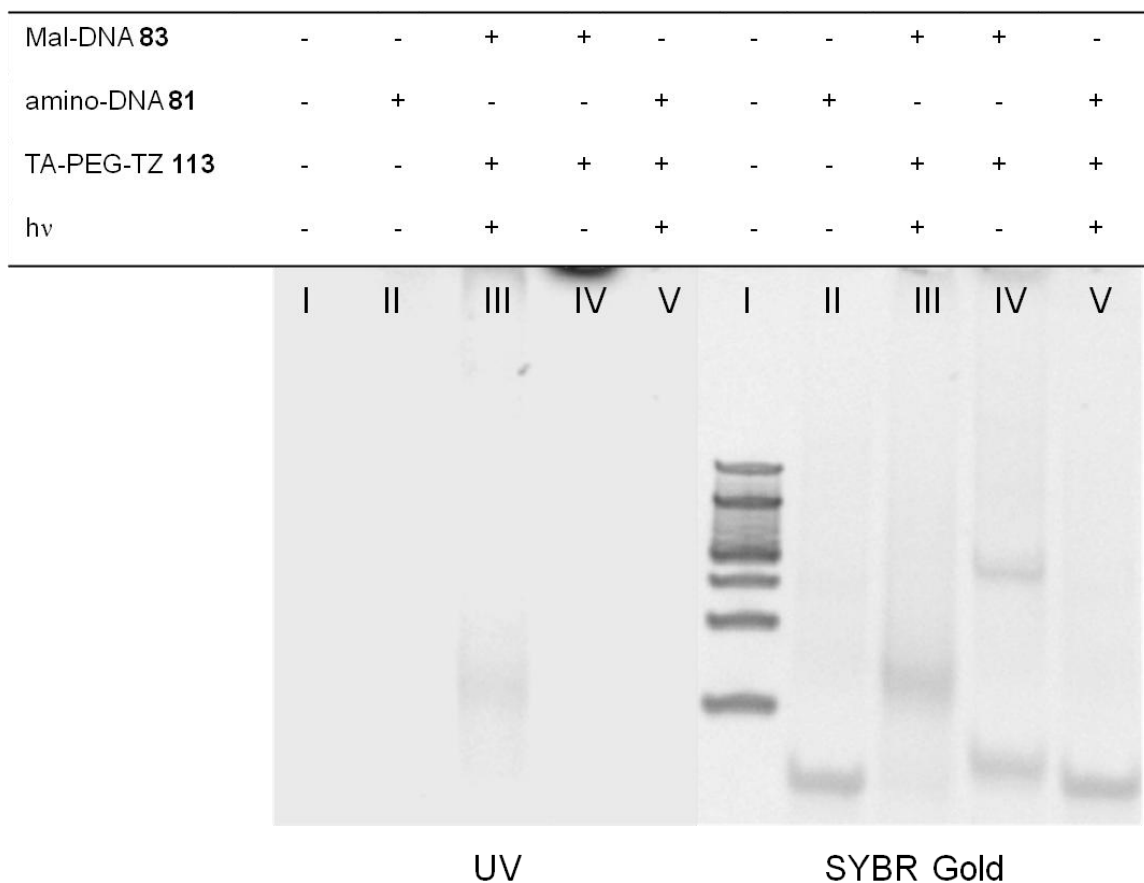
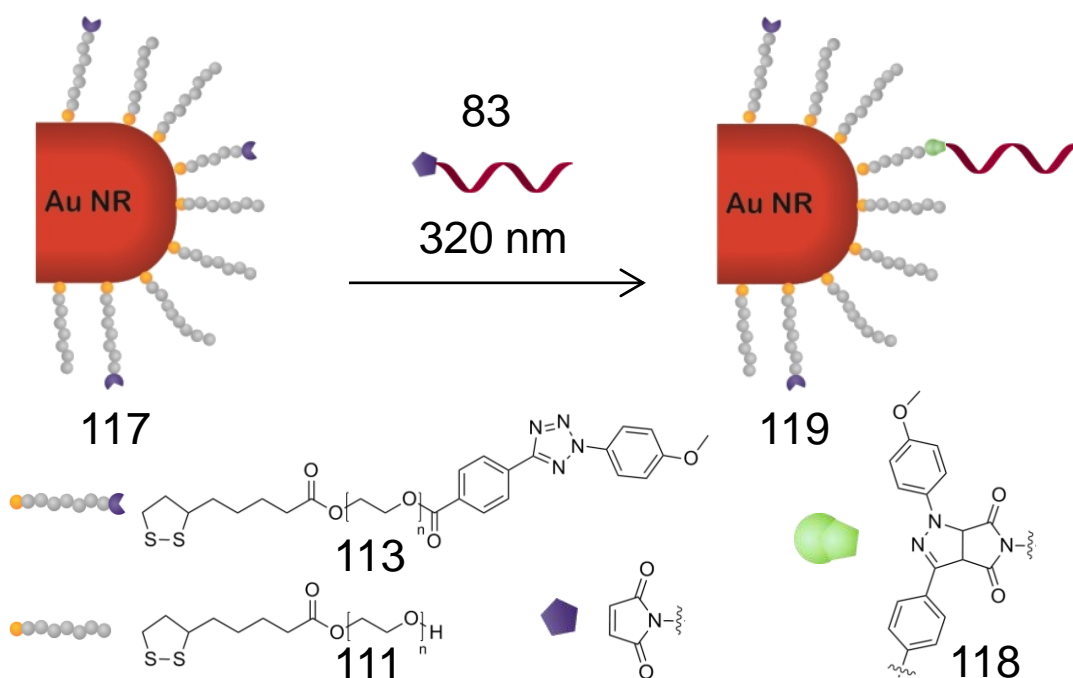


Figure 45. 21% TBE gel of model reaction between TA-PEG-TZ **113** and maleimide-modified DNA **83** before staining (left) and after staining (right). Fluorescent pyrazoline could only be observed of TA-PEG-TZ **113** with functional Mal-DNA **83** after irradiation (lane III).

Gel electrophoresis analysis showed only successful DNA-polymer conjugation when both, polymer and DNA, were functional and irradiated (Figure 45, lane III). Besides the lower mobility of the DNA-polymer conjugate due to the higher molecular weight, the fluorescence visualized the polymer-DNA conjugate by UV irradiation without any staining. Control experiments of TA-PEG-TZ **113** and Mal-DNA **83** without irradiation showed neither fluorescence nor a shift in the gel (lane IV; small shifts in comparison to amino-DNA **81** in lane II and lane V is attributed to the sSMCC modification; second higher band is attributed to DNA dimer). The highly reactive TA-PEG-TZ **113** underwent no NITEC reaction with amino-DNA **81** under irradiation demonstrating the orthogonality of tetrazole moiety to alkenes such as maleimides (lane V).



Scheme 35. Schematic illustration of the light-induced NITEC reaction of maleimide-modified DNA **83** and with TA-PEG-TZ/TA-PEG-coated Au NRs **117**.

Once the successful DNA-polymer conjugation was evidenced in solution, the tetrazole modified, pegylated Au NRs **117** and Mal-DNA **83** were irradiated for 1 h to perform the DNA functionalization of Au NRs (Scheme 35). Au NRs were centrifuged and thoroughly washed after which the analysis was performed.

Table 5. Zeta potential measurement of CTAB-Au NRs **116**, PEG-Au NRs **117** and DNA-PEG-Au NRs **119** in ddH₂O.

Nanorods	Zeta Potential in mV
CTAB-Au NRs 116	+46.2 ± 0.6
PEG-Au NRs 117	-15.6 ± 0.6
DNA-PEG-Au NRs 119	-37.5 ± 2.3

Successful DNA immobilization on the Au NR **117** was confirmed by a change in zeta potential (negative charge of DNA, Table 5), which led also to a higher mobility in gel electrophoresis compared to pegylated Au NRs **117** (Figure 46b).

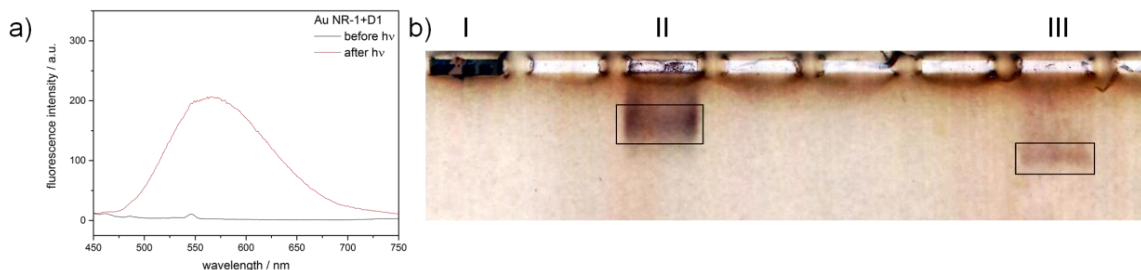


Figure 46. a) Fluorescence spectra of DNA-PEG-Au NRs **119** before and after UV irradiation. b) 0.5% agarose gel after 60 min at 80 V of CTAB-Au NRs **116** (lane I), PEG-Au NR **117** (lane II) and DNA-PEG-Au NRs **119** (lane III) showing the higher mobility of DNA-PEG-Au NRs **119** due to the additional negative charge of Mal-DNA **83**.

Additionally, fluorescence measurement at an excitation wavelength of $\lambda_{\text{ex}} = 400 \text{ nm}$ unambiguously evidenced the resulting fluorescent pyrazoline product **118** with a fluorescence emission at $\lambda_{\text{em, max}} = 565 \text{ nm}$ after irradiation (Figure 46a).

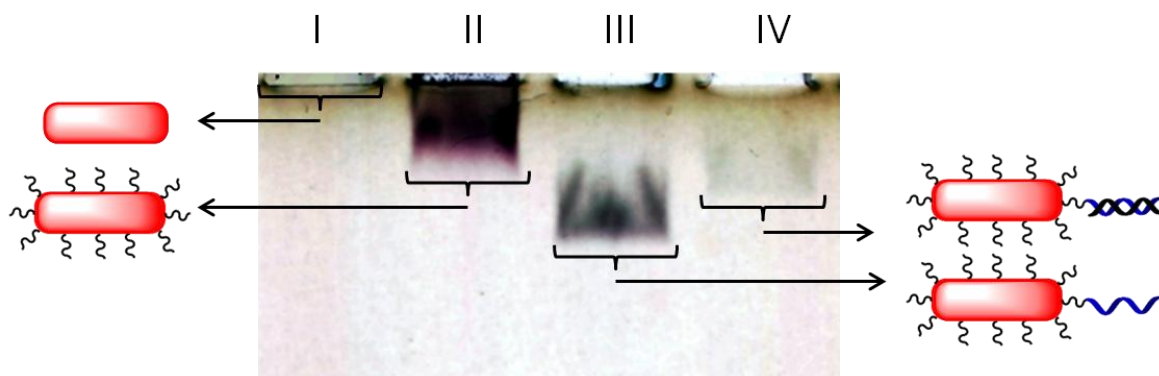


Figure 47. 0.5% agarose gel after 40 min at 80 V of CTAB-Au NRs **116** (lane I), PEG-Au NRs **117** (lane II), DNA-PEG-Au NRs **119** (lane III) and cDNA-DNA-PEG-Au NRs **120** (lane IV) showing the lower mobility of cDNA-DNA-PEG-Au NRs **120** in comparison to DNA-PEG-Au NRs **119** due to the bigger size after hybridization.

Finally, to confirm that attached DNA remains fully functional after the immobilization, DNA-PEG-Au NRs **119** was hybridized with cDNA **121** and the gel electrophoresis analysis showed that hybridization was successful (Figure 47). The Au NRs **119** can further be used for i.e. origami decoration of attachment of various species through DNA directed immobilization.^[229]

Conclusions

In conclusion, we demonstrated the use of light-induced tetrazole based NITEC reaction for biofunctionalization of Au NRs. Therefore, the novel bifunctional PEG linker containing thioctic acid as an Au anchoring group and a tetrazole moiety for light-induced reaction was synthesized. The tetrazole moiety enabled the formation of fluorescent pyrazoline compounds within 15 min in aqueous solution. In particular, the fluorescent pyrazoline product can be employed to assess the success of surface functionalization representing an excellent self-reporting system, particularly useful for monitoring of NP surface modification. We have shown that tetrazole Au NR can be modified with DNA which can further be employed in hybridization protocols by DNA directed immobilization. The biofunctionalization of Au NR was achieved, for the first time, by the use of NITEC reactions, which is a powerful ligation technique for the attachment of other sensitive biomolecules, such as antibodies under mild conditions and with the possibility of direct assessment of the reaction through formation of fluorescent product.

6 Conclusions and Outlook

In conclusion, novel light-induced reactions based on photoenol and NITEC chemistry were introduced for the covalent functionalization of Ag NPs, Au NPs and Au NRs. For Ag NPs, photoenol chemistry was employed for the light-induced modification of Ag NPs with functional polymers such as poly(ethylene glycol) and poly(carboxybetaine methacrylate) in DMSO. For Ag NPs as well as for Au NPs, novel bifunctional linkers **70** and **113** were synthesized containing either benzotriazole or thiol as NP anchoring group and photoenol for subsequent cycloaddition. Polymer-Ag NPs were successfully prepared, but direct coupling of DNA to photoenol modified NPs has not been achieved, which could be caused by the different solubility of Ag NPs (in DMSO) and DNA (aqueous solution).

Due to the stabilization of the photoenol intermediate by hydrogen bonding, the complete conversion of the photoenol occurs within minutes in aprotic solvents, yet it takes often more than 2 h in water containing mixtures.^[171] To avoid prolonged irradiation, which can be damaging for biomolecules but could also lead to agglomeration of NPs, nitrile-imine tetrazole-ene chemistry (NITEC) was employed for the biofunctionalization of Au NRs in aqueous solutions. DNA was successfully conjugated to Au NRs within 1 h. In addition, NITEC reaction results in a fluorescent pyrazoline product, which allows the monitoring of NP modification by fluorescence spectroscopy. One could envisaged that by employing calibration curves, the quantification of the surface modification using fluorescence could be possible, proving simple and straightforward way of surface characterization, which is one of the most important issues to be overcome in NP modification.

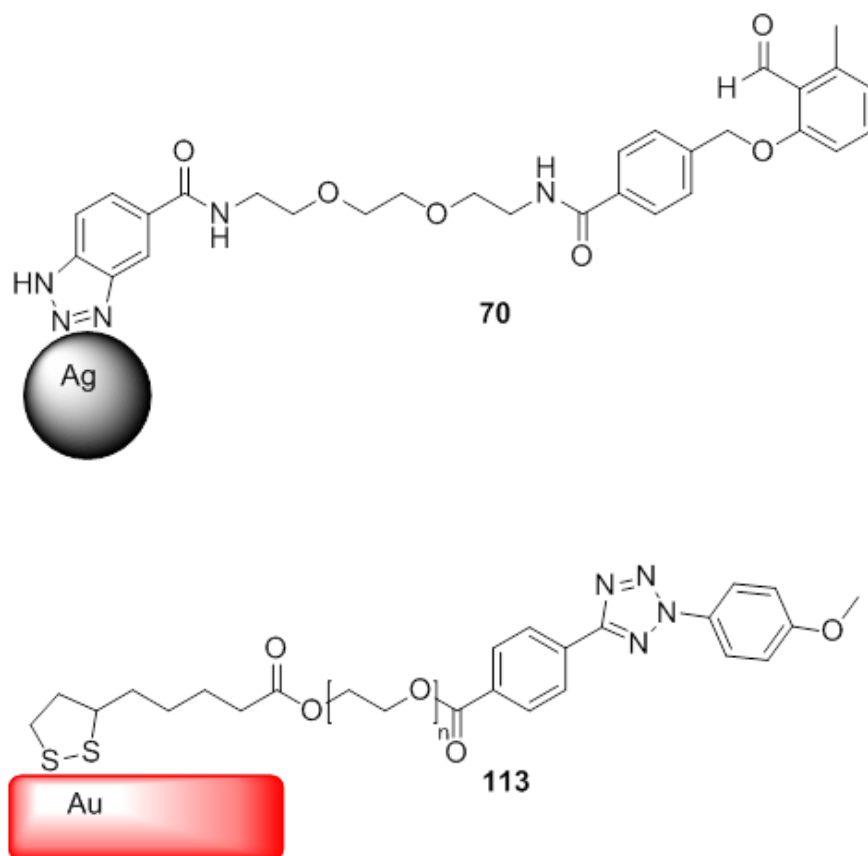
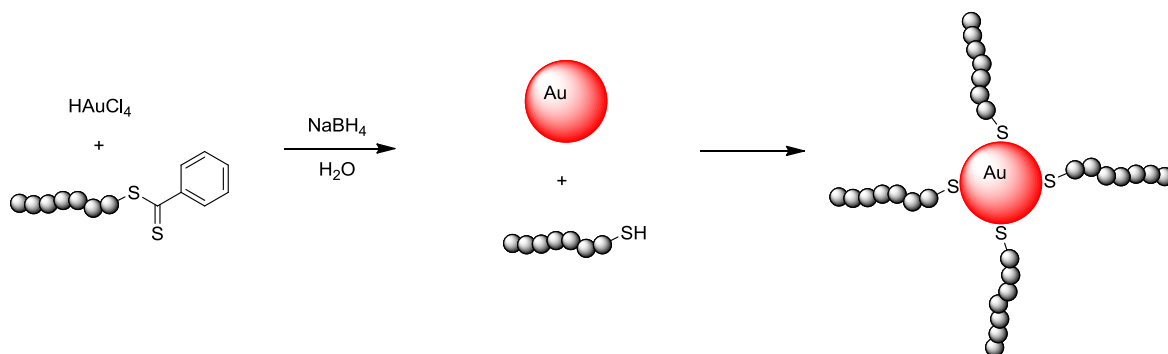


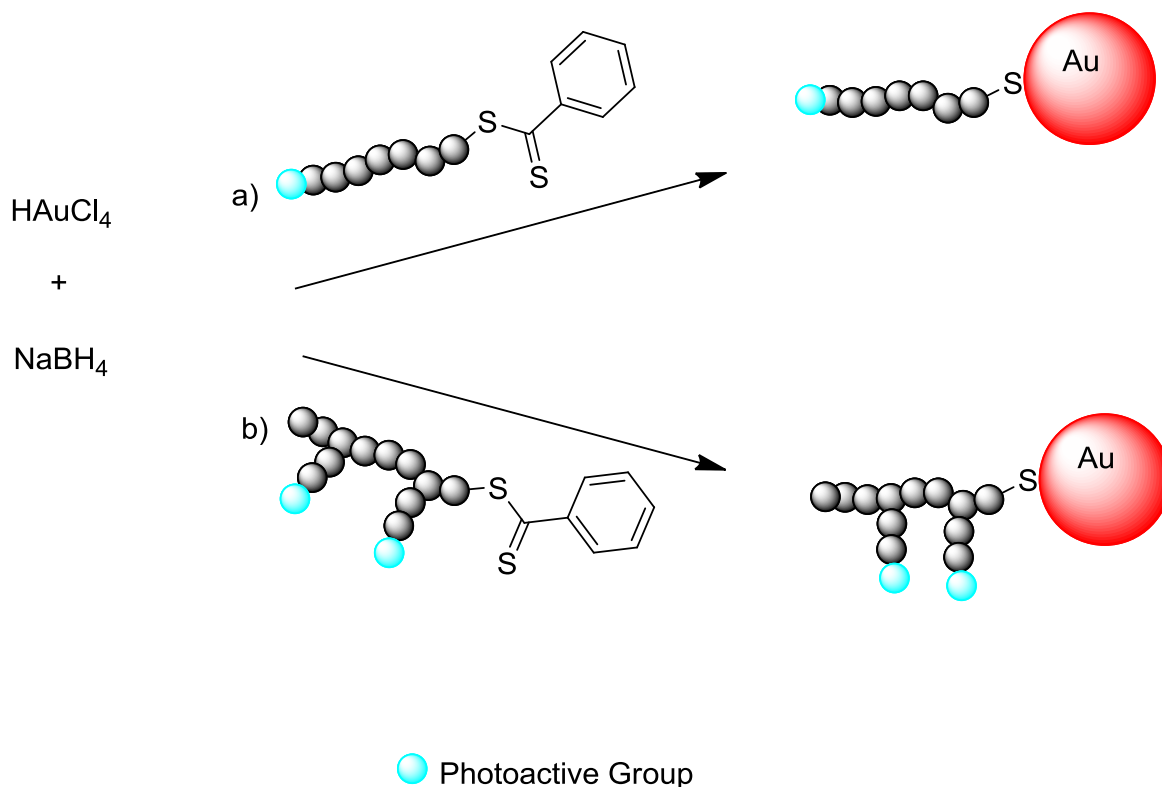
Figure 48. Novel photoactive, bifunctional linkers **70** and **113**.

Comparison of linker **70** and **113** shows triethylene glycol unit as spacer between the benzotriazole and photoenol group in **70**, in comparison to linker **113** ($M_n \sim 1500 \text{ g mol}^{-1}$), which contains a long PEG chain to increase the water solubility and separate the resulting fluorophore from the Au NR to avoid quenching (Figure 48). However, the amide bonds of linker **70** are more stable than the ester bonds of linker **113**, which were partially cleaved in aqueous solution after the reaction with maleimide (Figure 39). Therefore, the tetrazole moiety and thioctic acid should be connected to the PEG chains by amide coupling to avoid by-products and increase the stability of the PEG linker. Therefore, typically three components are required: a metal salt precursor, a reducing agent and a stabilization agent. Both linkers **70** and **113** enable NP stabilization, but the presence of reducing agents and linker **70** lead to the reduction of the aldehyde group to the hydroxyl group in **70**, which results in the loss of reactivity.^[230] Therefore, linker **70** is not applicable for one-pot synthesis of NPs using chemical reduction method. However, the tetrazole moiety should be stable in presence of reducing agents and can be employed for the one-pot procedure of NPs.



Scheme 36. Preparation of RAFT polymer-stabilized Au NPs in a one-pot synthesis using sodium borohydride as reducing agent.

An alternative possible way to circumvent the problems of introduction of functional groups to NP, in particular to Au NPs could be the use of RAFT polymers. Lowe *et al.* already demonstrated the facile preparation of metal NPs, in particular Au NPs, by the simultaneously reduction of dithioester end-capped polymers and metal salts (Scheme 36).^[231] In general, the RAFT polymerization allows the synthesis of (co)polymers in aqueous solutions with controlled architectures, predetermined molecular weights, and narrow molecular weight distributions.^[232] To prepare NPs coated with photoactive group, it can be added either to the backbone or side chain of the RAFT polymers, for example as a part of the monomer (Scheme 37).



Scheme 37. One-pot synthesis of Au NPs with the photoactive group a) in the backbone or b) in the side chain of the RAFT polymer.

In such a way, the preparation of active NP can be achieved in one-pot and the stability and solubility of NPs would be increased. This is particularly interesting when subsequent immobilization of biomolecules or the use of NP within cells is needed.

Besides allowing for mild and orthogonal (bio)functionalization of NPs, the light-induced photoenol based reaction was successfully used for the fabrication of 2D micropatterns by combining DLW with multiphoton induced Diels–Alder chemistry. Au NPs were functionalized with photoenol precursor molecules and subsequently used for covalent, light induced surface encoding onto maleimide-coated glass substrates without aggregation of the Au NPs during the process. In addition, remaining unreacted photoenol groups would be used for the attachment of additional maleimide containing molecules, once the NPs are immobilized on the surface. The minimum distance of two patterns and thus the resolution of this technique under these precise parameters was close to 1.6 μm . Limiting factors of the resolution are the diffraction limit and the diffusion of activated Au NPs during the patterning process. Depending on the solvent, the lifetime of the o-quinodimethane varies from microseconds to seconds in solution. It can therefore

be assumed that activated particles may exit the confined excitation volume and be covalently immobilized onto the substrate outside of exposed substrate areas. A precise impact of this influence is hard to estimate since the lifetime of the o-quinodimethane on the particles is not known.

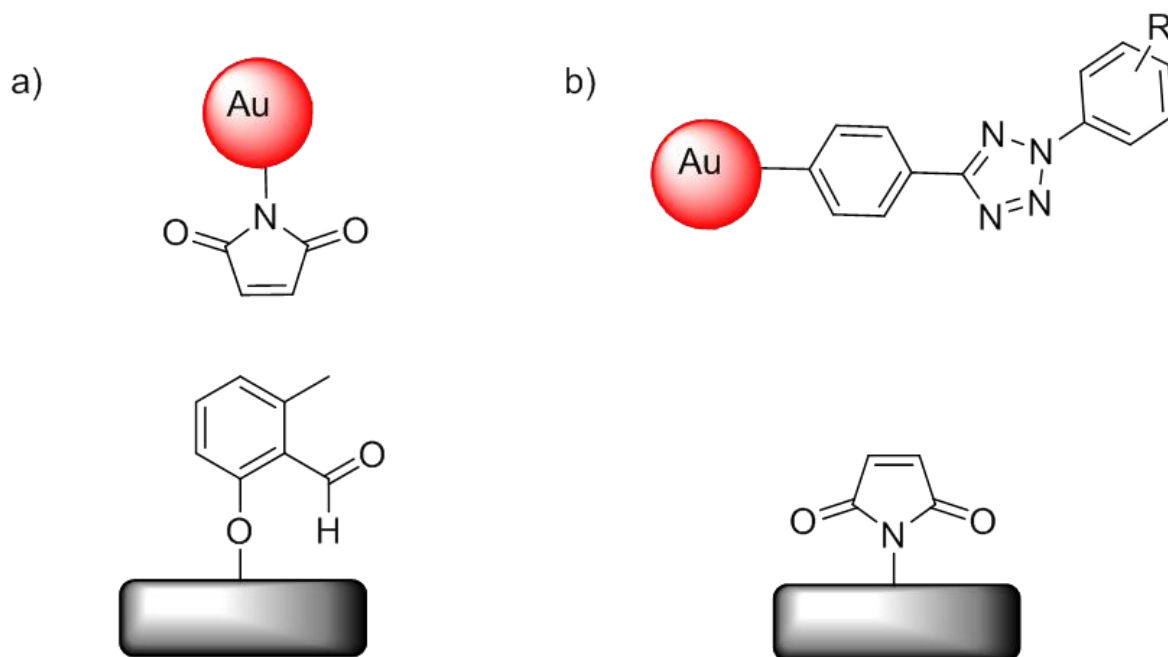


Figure 49. a) Pathway to immobilize maleimide-capped Au NPs to photoenol-coated glass surface or b) to use tetrazole-functionalized Au NPs and maleimide-coated glass surface.

To provide a better resolution of the NP micropattern, two synthetic pathways are envisaged (Figure 49): a) to prevent the diffusion of photoactivated photoenols on the Au NP surface, the photoenol moiety could be coated onto the glass surface and the Au NPs are modified with maleimide functionality; b) instead of the photoenol moiety, another highly reactive photoactive moiety with shorter lifetimes such as tetrazole could be attached to the Au NPs.

In summary, within this thesis, light-induced reactions were, for the first time, utilized for the (bio)functionalization of NPs and expanded the toolbox for the tailoring of nanomaterials. Photoenol chemistry and particularly nitrile-imine mediated tetrazole-ene chemistry feature a mild, effective, and orthogonal way for the surface modification of NPs in aprotic solvents and aqueous solutions.

7 Experimental Part

7.1 Materials and Methods

Chemicals

Di-*tert*-butyl dicarbonate (97%, Sigma-Aldrich), 2,2'-(ethylenedioxy)bis(ethylamine) (98%, Sigma-Aldrich), benzotriazole-5-carboxylic acid (99%, Sigma-Aldrich), triethylene glycol ($\geq 99\%$, Sigma-Aldrich), silver dispersion (20 nm particle size, $0.02 \text{ mg}\cdot\text{mL}^{-1}$ in aqueous buffer, contains sodium citrate as stabilizer, Sigma-Aldrich), 1-hydroxybenzotriazole hydrate (HOBt, $\geq 97\%$, Sigma Aldrich), *N,N'*-dicyclohexylcarbodiimide (DCC, 99%, Sigma-Aldrich), *N*-hydroxysuccinimide (NHS, 98%, Sigma-Aldrich), trifluoroacetic acid (TFA, $\geq 99.9\%$, Roth), 4-(dimethylamino)pyridine (DMAP, 99%, Sigma-Aldrich) O-(benzotriazol-1-yl)-*N,N,N',N'*-tetramethyluronium hexafluorophosphate (HBTU, $\geq 98.0\%$, Sigma-Aldrich), *N,N*-diisopropylethylamine (DIPEA, 99.5%, Sigma-Aldrich), copper(I) bromide (99,999%, Sigma-Aldrich), 2,2'-bipyridyl (BiPy, $\geq 99\%$, Sigma-Aldrich), 2-(dimethylamino)ethyl methacrylate (98%, Sigma-Aldrich), hydrogen tetrachloroaurate (III) hydrate ($\text{HAuCl}_4\cdot x\text{H}_2\text{O}$, 99.999%, Sigma-Aldrich), 11-mercapto-1-undecanol (MUD, 97%, Sigma-Aldrich), lithium triethylborohydride 1.0 M solution in THF (Super-Hydride, Sigma-Aldrich), iodine ($\geq 99.5\%$, Roth), maleimide (99%, Sigma-Aldrich), β -propiolactone ($\geq 90\%$, Sigma-Aldrich), hydrogen tetrachloroaurate (III) hydrate ($\text{HAuCl}_4\cdot x\text{H}_2\text{O}$, 99.999%, Sigma-Aldrich), silver nitrate (AgNO_3 , $>99\%$, Sigma-Aldrich), sodium borohydride (NaBH_4 , $\geq 99\%$, Sigma-Aldrich), 5-bromosalicylic acid (90%, Sigma-Aldrich), ascorbic acid ($\geq 99\%$, Sigma-Aldrich), poly(ethylene glycol) solution (50% in water, Sigma-Aldrich), (\pm)- α -lipoic acid ($\geq 98\%$, Sigma-Aldrich), 4-formylbenzoic acid (96%, Acros Organics), p-toluenesulfonylhydrazide (98%, Alfa Aesar), pyridine (99%, ABCR), p-anisidine (99%, ABCR), , HCl (37%, Roth), acetonitrile ($\geq 99.95\%$, Roth), ethanol (EtOH, Lachner), sodium nitrite (NaNO_2 , 98%, Alfa Aesar), dimethyl sulfoxide (DMSO, $\geq 99\%$, Sigma-Aldrich), tetrahydrofuran (THF, $\geq 99.70\%$, VWR), dimethylformamide (DMF, $\geq 99.9\%$, VWR), methanol ($\geq 99.8\%$, VWR), chloroform ($\geq 99\%$, Sigma-Aldrich), and dichloromethane (DCM, $\geq 99.80\%$, Sigma-Aldrich) were used as re-

ceived. Gel filtration NAP5 and NAP 10 columns were purchased from GE Healthcare (Germany). Ultrapure water produced with a Milli-Q Advantage A10 system was used in all experiments. All glassware for the Au NP and Au NR syntheses were cleaned with aqua regia, rinsed extensively with water, and dried before use. Syntheses of ω -maleimido-polyethylene glycol (PEG-Mal)^[233], tetrazole-acid,^[234] and ω -thioctic acid-poly(ethylene glycol) ($M_n \sim 1200 \text{ g mol}^{-1}$)^[235] were performed according to literature procedures. The glass surface was coated with maleimide groups in a two step approach employing (3-aminopropyl)triethoxysilane (APTES) and 4-maleimidopropanoyl chloride as previously reported.^[236]

DNA Oligonucleotides

Table 6. DNA oligonucleotides used in the current thesis (purchased from Sigma-Aldrich).

Name	Internal name	Sequence (5'→3')	modification
DNA	aF9	GTG GAA AGT GGC AAT CGT GAA G	5'-NH ₂ -C ₆
cDNA	cF9	CTT CAC GAT TGC CAC TTT CCA C	-

Buffers

Table 7. Buffers and the corresponding recipes.

Buffer	Composition
TBE (5x)	450 mM Tris, 450 mM boric acid, 10 mM EDTA, pH = 8 - 8.3
PBS buffer (10x)	137 mM NaCl, 2.7 mM KCl, 10 mM Na ₂ HPO ₄ ·7 H ₂ O
HPLC elution buffer	0.1 M NH ₄ OAc
Loading buffer (6x) for DNA	10 mM Tris, 60 mM EDTA, 0.03% bromophenol blue, 0.03% xylene cyanol, 60% glycerin, pH = 7.6
NP-loading buffer (6x)	10 mM Tris, 60 mM EDTA, 60% glycerin, pH = 7.6

Instruments and Methods

¹H NMR Spectroscopy

¹H NMR spectroscopy was performed using a Bruker AM 250, a Bruker AM 300 or a Bruker AM 400 spectrometer at 250 MHz, 300 MHz or 400 MHz, respectively. Samples were dissolved in CDCl₃, DMSO-d₆ or in methanol-d₄. The δ-scale is referenced to tetramethylsilane as the internal standard.

UV/Vis Spectroscopy

UV/Vis spectra were obtained using VARY 300 Scan UV-Visible Spectrometer (Varian Inc., Germany).

Fluorescence Spectroscopy

Fluorescence emission spectra were recorded in quartz cuvettes loaded with a sample volume of 160 μL on a Varian Cary Eclipse Fluorescence Spectrometer.

X-ray Photoelectron Spectroscopy⁴

X-ray photoelectron spectroscopy (XPS) measurements were performed using a K-Alpha XPS spectrometer (ThermoFisher Scientific, East Grinstead, UK). All the samples were analyzed using a microfocused, monochromated Al Kα X-ray source (400 μm spot size). The kinetic energy of the electrons was measured by a 180° hemispherical energy analyzer operated in the constant analyzer energy mode (CAE) at 50 eV pass energy for elemental spectra. Data acquisition and processing using the Thermo Avantage software is described elsewhere.^[237] The spectra were fitted with one or more Voigt profiles (BE uncertainty: + 0.2 eV). The analyzer transmission function, Scofield sensitivity factors,^[238] and effective attenuation lengths (EALs) for photoelectrons were applied for quantification. EALs were calculated using the standard TPP-2M formalism.^[239] All spectra were referenced to the C1s peak of hydrocarbon at 285.0 eV binding energy, controlled by means of the well-known photoelectron peaks of metallic Cu, Ag, and Au, respectively.

⁴ XPS was conducted by Vanessa Trouillet, Institute for Applied Materials (IAM-ESS) and Karlsruhe Nano Micro Facility (KNMF), Karlsruhe Institute of Technology (KIT).

Electrospray Ionization-Mass Spectrometry (ESI-MS)

Electrospray Ionization-Mass Spectrometry (ESI-MS) spectra were recorded on an LXQ Scientific spectrometer (ThermoFisher Scientific, East Grinstead, UK) equipped with an atmospheric pressure ionization source operating in the nebulizer assisted electrospray mode. The instrument was calibrated in the m/z range 195–1822 using a standard containing caffeine, Met-Arg-Phe-Ala acetate (MRFA) and a mixture of fluorinated phosphazenes (Ultramark 1621) (all from Aldrich). A constant spray voltage of 6 kV was used and nitrogen at a dimensionless sweep gas flow rate of 2 (approximately 3 L·min⁻¹) and a dimensionless sheath gas flow rate of 5 (approximately 0.5 L·min⁻¹) were applied. The capillary voltage, the tube lens offset voltage and the capillary temperature was set to 10 V, 70 V, and 300 °C respectively. The samples were dissolved with a concentration of 0.1 mg·mL⁻¹ in a mixture of THF and MeOH (3:2) containing 100 μmol of sodium triflate and infused with a flow of 10 μL·min⁻¹.

Transmission Electron Microscopy (TEM)⁵

Transmission Electron Microscopy (TEM) images were obtained using a CM200-FEG microscope (Philips) operating at 200 kV. Further TEM imaging, HAADF-STEM and energy dispersive X-ray spectroscopy (EDXS) were done on the Titan³ 80-300 TEM microscope (FEI) operating at 80 kV.

Fourier Transform Infrared Spectroscopy (FT-IR)

FTIR spectra were recorded by the DRIFT mode using a Bruker IFS-88 Fourier transform infrared spectrometer. Solid samples were analyzed using potassium bromide (KBr) as matrix. The absorption bands of functional groups in IR spectra are expressed in wavenumbers (cm⁻¹).

Zeta Potential

Zeta potential measurements were obtained using Nano Zeta-Sizer (ZS Nano, Malvern).

⁵ TEM was conducted by Pascal Bockstaller and Heike Störmer, Center for Functional Nanostructures (CFN), Karlsruhe Institute of Technology (KIT).

Fast Atom Bombardment Mass Spectrometry

Fast Atom Bombardment Mass Spectrometry (FAB-MS): the mass spectra were measured using Finnigan MAT90 mass spectrometer.

Matrix Assisted Laser Desorption/Ionization Time-of-Flight (MALDI-ToF)

MALDI-ToF analysis was performed on a Bruker Biflex III spectrometer using 3-hydroxypicolinic acid in aqueous ammonium citrate as the matrix.

Quantum Yield Determination

Quantum yields were determined with Quantaaurus QY C11347 of Hamatsu with excitation wavelength of 400 nm.

Size Exclusion Chromatography

Size exclusion chromatography measurements were performed using a Polymer Laboratories PL-GPC 50 Plus system, comprised of an auto injector, a guard column (PLgel Mixed C, 50 × 75 mm) followed by three linear columns (PLger Mixed C, 300 × 7.5 mm, 5 μm bead size) and a differential refractive index detector, was employed. THF at 40°C at a flow rate of 1 mL min⁻¹ was used as the eluent. The GPC system was calibrated using narrow poly(styrene) standards ranging from 476 to 2.5·10⁶ g mol⁻¹ (Polymer Standards Service (PSS), Mainz, Germany). The resulting molar mass distributions were determined by universal calibration using Mark-Houwink parameters for poly(styrene) ($K = 14.1 \cdot 10^{-5} \text{ dLg}^{-1}$, $\alpha = 0.7$). All M_n values were calculated using a poly(styrene) calibration curve and the Mark-Houwink correction parameters, K and α .

Scanning Electron Microscopy (SEM)

Scanning electron microscopy images were recorded using a Zeiss Supra 40VP. All samples were coated with a 10 nm gold layer prior to measurements.

High Performance Liquid Chromatography (HPLC)

Analytical, reverse phase HPLC was performed on Agilent 1200 instrument with Nucleodur (Macherey-Nagel) C-18 gravity column (5 μm) and UV-Vis detection at two wavelengths, 210 and 260 nm.

Flow rate: 1 mL/min

Following eluents were used:

eluent A: 0.1 M ammonium acetate

eluent B: acetonitrile

Table 8. Standard gradient for the purification of DNA oligonucleotides by HPLC. The solvents A: 0.1 M ammonium acetate, and B: acetonitrile were used.

t / min	0	10	15	20	25	32	40	45
B / %	0	5	10	15	30	80	100	0

Polyacrylamide Gel Electrophoresis (PAGE)

Native PAGE was used for the separation of DNA according to their size. 10 mL of 21% PAGE gel solution was prepared following the recipe (Table 9). After polymerization of the gel solution, the glass plates were put into an electrophoresis system (Bio-Rad). Subsequently 1 μ L of loading buffer (6 \times) was added to 5 μ L of DNA sample and loaded into the wells. Gels were run in 1 \times TBE buffer at 100 V.

Table 9. Recipe for 21% PAGE gel.

Gel component	Volume
5 \times TBE	2 mL
30% acrylamide and bis-acrylamide solution, 37.5:1.	8.4 mL
water	1.6 mL
ammonium persulfate (APS) solution (10%)	100 μ L
tetramethylethylenediamine (TEMED)	4 μ L

When the gel running was completed, the gel was transferred into a staining chamber. To prepare the staining solution for ssDNA, 3 μ L SYBR gold was added to 30 mL 1 \times TBE buffer. After shaking for 15 min, the images of the stained gels were taken under UV irradiation using Bio-Rad Gel DocTM XR imaging system.

Agarose Gel Electrophoresis

Agarose gel (1%) was prepared by dissolving 0.30 g agarose in 30 mL 0.5 \times TBE buffer in a microwave oven. After cooling down the solution slightly, the solution was casted in an electrophoresis system. After gel formation, 0.5 \times TBE

buffer was added to the chamber. Then 3 μL of loading buffer (6 \times) was added to 15 μL NP dispersion and loaded into the wells. Gels were run at 80 V.

Setup for Light-Induced Reactions

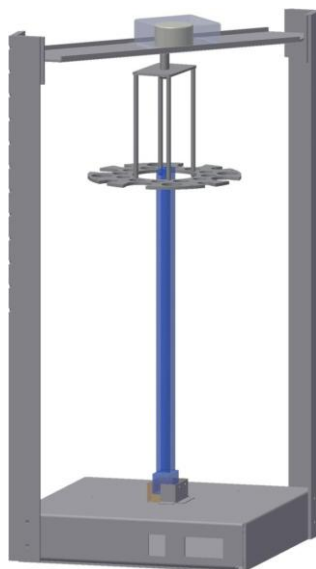


Figure 50. Drawing of the custom-built photoreactor employed in the current study.

The samples to be irradiated were crimped air-tight in headspace vials (20 mm, VWR, Germany) using SBR seals (VWR, Germany) with PTFE inner liner. The photoreactions were performed in a custom-built photoreactor (Figure 50) consisting of a metal disk which revolves at a distance of 40-50 mm around a compact low-pressure fluorescent lamp with $\lambda_{\text{max}} = 320 \text{ nm} \pm 30 \text{ nm}$ (36 W, Arimed B6, Cosmedico GmbH, Germany) (Figure 51).

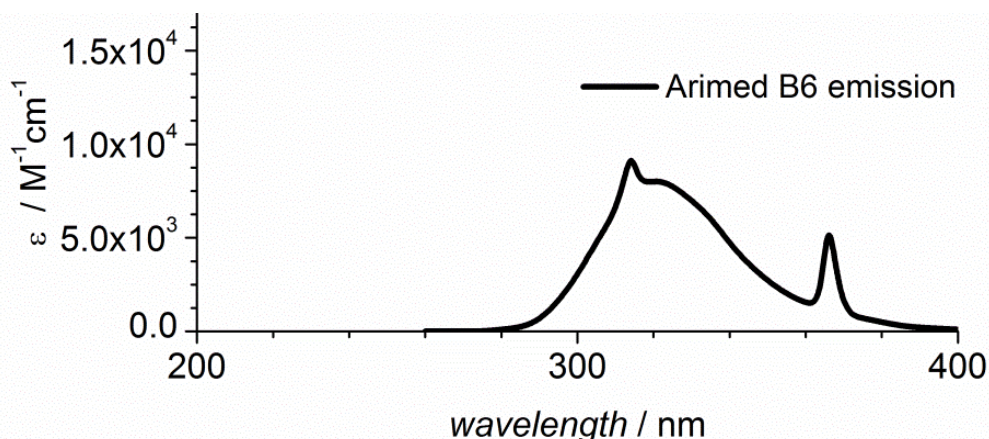


Figure 51. Emission spectrum of the employed compact low-pressure fluorescent lamp (36 W, Arimed B6, $\lambda_{\max} = 320$ nm).

Direct Laser Writing (DLW)⁶

The home-built DLW setup consisted of a laser, a device for intensive tuning during writing process, an objective, a device for the movement between the substrate and the focus, a computer, and a possibility for online observation of the writing process. As light source a Titanium Sapphire laser was employed with tunable wavelength of between 700-900 nm in a femtosecond pulsed mode or continuous wave mode. The movement of the laser focus in the substrate was achieved by employing a set of galvanometric mirrors enabled a deflection of the laser focus on both lateral axes.

Spatially Resolved Immobilization of Au NP

A droplet of suspension containing Au-MUD-PE in DMF (approximately 40 μM) was placed onto the surface of a maleimide containing glass substrate. The reaction sample was subsequently positioned into the DLW setup. All samples were produced using a scanning speed of 100 $\mu\text{m/s}$.

For squares: each pattern was scanned five times in succession at the corresponding laser power (dimension: 20 $\mu\text{m} \times 20 \mu\text{m}$). The distance of each scanning line was 200 nm. Five squares were patterned for each sample. Each square was patterned using a different laser power (0.2 mW, 0.4 mW, 0.6 mW, 0.8 mW and 4 mW). This exact procedure was also used for all control experiments. For the control experiments, either the Au NPs, the glass substrate or both the Au NPs

⁶ DLW was conducted by Alexander Quick, Institute for Technical Chemistry and Polymer Chemistry, Karlsruhe Institute of Technology (KIT).

and the glass substrate were not functional (meaning Au NPs did not contain photoenol units and/or glass substrates did not contain maleimides).

For the KIT logo: The pattern was scanned once, the distance of each scanning line was 200 nm (dimension: approximately 30 μm \times 15 μm). The corresponding laser power was 1.6 mW.

After patterning, each sample was immersed into DMF for 20 min. Then, the sample was shortly immersed into acetone and water, subsequently and dried under flow of nitrogen.

Time-of Flight Secondary Ion Mass Spectrometry (ToF-SIMS)⁷

Time-of flight secondary ion mass spectrometry was performed on a TOF.SIMS5 instrument (ION-TOF GmbH, Münster, Germany). This spectrometer is equipped with a Bi cluster primary ion source and a reflectron type time-of-flight analyzer. UHV base pressure was $< 5 \times 10^{-9}$ mbar. For high mass resolution the Bi source was operated in the “high current bunched” mode providing short Bi_1^+ or Bi_3^+ primary ion pulses at 25 keV energy and a lateral resolution of approx. 4 μm . The short pulse length of 1.1 to 1.3 ns allowed for high mass resolution. The primary ion beam was raster across a 500 \times 500 μm field of view on the sample, and 128 \times 128 data points were recorded. Primary ion doses were kept below 10^{11} ions/ cm^2 (static SIMS limit). For charge compensation an electron flood gun providing electrons of 21 eV was applied and the secondary ion reflectron tuned accordingly. Spectra were calibrated on the omnipresent C^- , C_2^- , C_3^- , or on the C^+ , CH^+ , CH_2^+ , and CH_3^+ peaks. Based on these datasets the chemical assignments for characteristic fragments were determined. For high lateral resolution imaging the primary ion source was operated in “burst alignment” mode. Here, only nominal mass resolution is obtained but the lateral resolution of the instrument is in the range of 150nm. Therefore, Au_xS_y^- peaks ($x = 1 - 5$, $y = 0 - 2$) were used for imaging since these peaks do not show adjacent signals at the same nominal mass (m/z). In case of bromine imaging this prerequisite was not given (see Fig. 34a, insert). Therefore, bromine imaging (Fig. 36b) was performed using “bunched” mode operation of the primary ion gun, providing high lateral and high mass resolution. Based on this instrument setting and the very low amount of bromine as

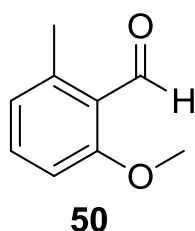
⁷ ToF-SIMS measurements were conducted by Dr. Alexander Welle, Institute for Technical Chemistry and Polymer Chemistry, Karlsruhe Institute of Technology (KIT).

compared to gold, overall count rates were much lower for bromine (Fig. 36b) as compared to gold clusters (Fig. 33b).

7.2 Syntheses

Linker Syntheses

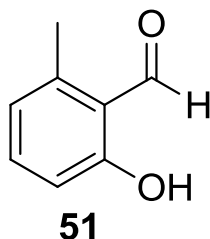
Synthesis of 2-methoxy-6-methylbenzaldehyde **50**^[240]



A vigorously stirred mixture of 4.91 g 2,3-dimethylanisole (36.0 mmol), 9.02 g copper(II) sulfate pentahydrate (110.0 mmol) in 250 mL acetonitrile/water 1:1 is heated at reflux. After 15-30 min, the mixture becomes dark green in color and TLC analysis shows that no starting material is present. The mixture is cooled to room temperature and 100 mL CH₂Cl₂ are added. The layers are separated and the aqueous phase is further extracted with additional CH₂Cl₂ (2x50 mL). The combined organic solutions are dried (NaSO₄), filtered and evaporated at reduced pressure to give the crude product **1** that is suitable for further reaction; yield: 5.20 g (96%).

¹H-NMR (250 MHz, CDCl₃) δ / ppm: 2.55 (s, 3H), 3.87 (s, 3H), 7.10 (m, 3H), 10.62 (s, 1H).

Synthesis of 2-hydroxy-6-methylbenzaldehyde **51**^[241]

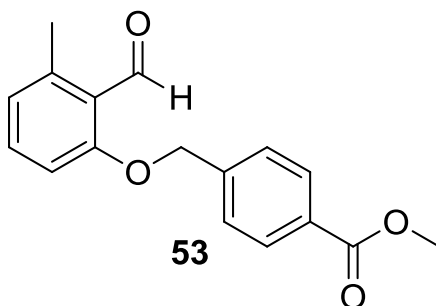


5.20 g (34.6 mmol, 1 eq.) of **50** was dissolved in 50 mL dichloromethane. 13.87 g (104.0 mmol, 3 eq.) AlCl₃ were added to the yellow solution and the mix-

ture was stirred at room temperature overnight. The color changed from yellow over red to a dark brown. Excess of aluminium chloride was cautiously quenched with water; the organic layer was extracted three times with dichloromethane and dried over sodium sulfate. The solvent was removed under reduced pressure and 3.06 g (22.5 mmol, 65 %) of dark brown oil was obtained. In order to obtain an increased overall yield for **51**, the raw product was used directly in the next step without further purification.

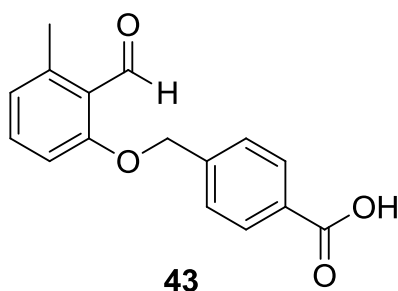
$^1\text{H-NMR}$ (250 MHz, CDCl_3) δ / ppm: 2.60 (s, 3H), 6.68-6.84 (m, 2H), 7.32-7.42 (m, 1H), 10.32 (s, 1H), 11.90 (s, 1H).

Synthesis of methyl 4-((2-formyl-3-methylphenoxy)methyl)benzoate **53**^[241]



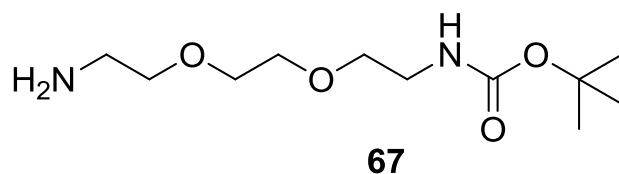
3.06 g (22.5 mmol, 1 eq.) of **51** and 5.14 g (23.7 mmol, 1.02 eq.) of methyl 4-(bromomethyl)benzoate were dissolved in 150 mL of acetone (the acetone has been pre-dried over sodium sulfate). To this solution 4.64 g (33.5 mmol, 1.5 eq.) of potassium carbonate and 91.0 mg (0.35 mmol, 0.015 eq.) of 18-crown-6 were added. The mixture was stirred at 40 °C overnight. After filtration, the solvent was removed under reduced pressure, the residue was re-dissolved in 100 mL dichloromethane/water (1:1) and acidified with aqueous HCl (3%). The aqueous layer was extracted two more times with dichloromethane (2 x 30 mL) and the combined organic layers were dried over sodium sulfate. The solvent was removed under reduced pressure, 50 mL of 7:1 v/v hexane/ethyl acetate was added and 3.71 g (13.1 mmol, 58%) pure **53** precipitated after cooling in the fridge. The pure solid was obtained after filtration and drying under reduced pressure.

$^1\text{H-NMR}$ (250 MHz, acetone- d_6) δ / ppm: 2.52 (s, 3H), 3.89 (s, 3H), 5.38 (s, 2H), 6.89 (d, $J = 7.7$ Hz, 1H), 7.13 (d, $J = 8.4$ Hz, 1H), 7.45 (t, $J = 8.2$ Hz, 1H), 7.68 (d, $J = 8.3$ Hz, 1H), 8.06 (d, $J = 8.4$ Hz, 1H), 10.73 (s, 1H).

Synthesis of 4-((2-formyl-3-methylphenoxy)methyl)benzoic acid 43^[241]

2.83 g (9.95 mmol, 1 eq.) of **53** was dissolved in 150 mL of dichloromethane and 1.20 g sodium hydroxide (29.9 mmol; 3 eq.) dissolved in 15 mL methanol were added. The reaction mixture was stirred over night at ambient temperature. The solvents were removed under reduced pressure and the residue was subsequently redissolved in 140 mL dichloromethane/water 1:1. The organic layer was extracted with water, all water layers were combined and acidified with aqueous HCl (3%) to pH 3. The aqueous layer was subsequently extracted 3 times with dichloromethane and the combined organic layers were dried over sodium sulfate. The solvent was removed under reduced pressure and 1.88 g (6.96 mmol, 70%) of a white powder was obtained.

¹H-NMR (250 MHz, acetone-d⁶) δ / ppm: 2.52 (s, 3H), 5.39 (s, 2H), 6.89 (d, J = 7.6 Hz, 1H), 7.13 (d, J = 8.4 Hz, 1H), 7.45 (t, J = 8.1 Hz, 1H), 7.68 (d, J = 8.4 Hz, 1H), 8.05 (d, J = 8.4 Hz, 1H) , 10.74 (s, 1H)

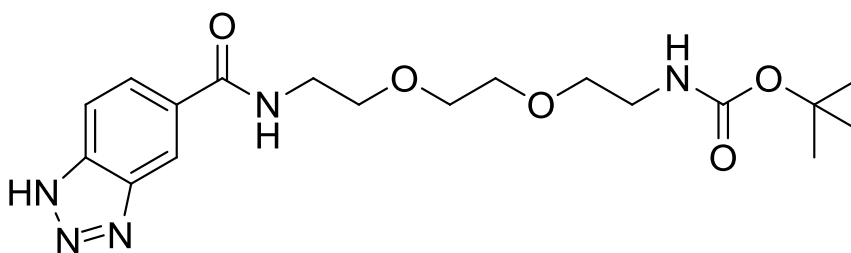
Synthesis of *N*-Boc-2,2-(ethylene-1,2-dioxy)bisethylamine 67^[242]

Compound **67** was synthesized according to a reported method^[242] with slight modification. A solution of di-*tert*-butyl dicarbonate (3.60 g, 16.8 mmol, 1 eq) in 60 mL CH₂Cl₂ was added to a solution of 2,2'-(ethylene-1,2-dioxy)bis(ethylamine) (5.00 g, 33.7 mmol, 2 eq) in 100 mL dry CH₂Cl₂ at 0 °C under argon atmosphere over a period of 6 h. The reaction mixture was stirred at 0 °C for 6 h and then at room temperature overnight. The solvent was removed under reduced pressure to afford light yellow residue which was dissolved in 50 mL of chloroform and washed twice with aqueous sodium bicarbonate solution. The combined organic layer was

dried over anhydrous MgSO_4 and concentrated to give compound **67** (5.19 g, 20.96 mmol, 62%).

^1H NMR (300 MHz, CDCl_3) δ / ppm: 1.41 (s, 9 H, CH_3), 2.61 (t, $J = 5.3$ Hz, 2 H, CH_2), 3.02 (m, 2 H, CH_2), 3.24-3.36 (m, 4 H, CH_2), 3.38-3.44 (m, 4H, CH_2), 5.41 (br, 1 H, NH).

Synthesis of *tert*-butyl (2-(2-(2-(1*H*-benzo[*d*][1,2,3]triazole-5-carboxamido)ethoxy)ethoxy)ethyl)carbamate **68**

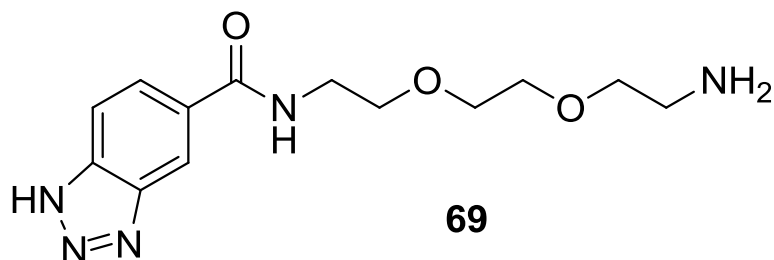


68

To a solution of benzotriazole-5-carboxylic acid (1.00 g, 6.13 mmol, 1 eq) in dry THF/DMF mixture (8:2) (20 mL), HOBt (1.00 g, 7.36 mmol, 1.2 eq), HBTU (2.80 g, 7.36 mmol, 1.2 eq) and DIPEA (4.50 g, 18.4 mmol, 3 eq) were added. The reaction mixture was cooled to 0 C and *N*-Boc-2,2'-(ethylene-1,2-dioxy)bisethylamine **1** (1.67 g, 6.74 mmol, 1.1 eq) dissolved in THF (5 mL) was then added dropwise in 30 min. The slurry obtained was purged with argon and stirred overnight at room temperature. The volatiles were then removed under reduced pressure to obtain brown residue which was purified by silica gel chromatography starting with dichloromethane to dichloromethane/ methanol (20:1) to give a brown thick oil (1.87 g, 4.78 mmol, 78%).

^1H NMR (CDCl_3 , 300 MHz) δ / ppm: 1.27 (s, 9 H, CH_3), 3.19 (t, $J = 4.7$ Hz, 2 H, CH_2), 3.45 (t, $J = 4.9$ Hz, 2 H, CH_2), 3.46-3.55 (m, 4 H, CH_2), 3.62-3.67 (m, 4 H, CH_2), 5.41 (m, 1 H, NH), 7.70 (d, $J = 8.5$ Hz, 1 H, H_{Ar}), 7.81 (d, $J = 8.5$ Hz, 1 H, H_{Ar}), 8.31 (s, 1 H, H_{Ar}); ^{13}C NMR (CDCl_3 , 75 MHz): δ 28.5 (CH_2), 40.0 (CH_2), 40.2 (CH_2), 69.5 (CH_2), 69.9 (CH_2), 70.0 (CH_2), 79.3 ($\text{C}(\text{CH}_3)_3$), 114.1 (C_{Ar}), 115.5 (C_{Ar}), 125.1 (C_{Ar}), 131.7 (C_{Ar}), 139.4 (C_{Ar}), 156.3 (NCOO), 167.7 (OCN); FT-IR (ATR) $\tilde{\nu}_{\text{max}}$: 3325, 2976, 2927, 1690, 1643, 1542, 1454, 1392, 1252, 1169 cm^{-1} ; MS (+FAB): m/z (%): 394.2 (40) $[\text{M}+\text{H}]^+$, 338 (21), 294 (100), 189 (20), 154 (27); HR-MS: (FAB) m/z calculated for $\text{C}_{18}\text{H}_{28}\text{N}_5\text{O}_5$ $[\text{M} + \text{H}^+]$: 394.2094; found: 394.2090.

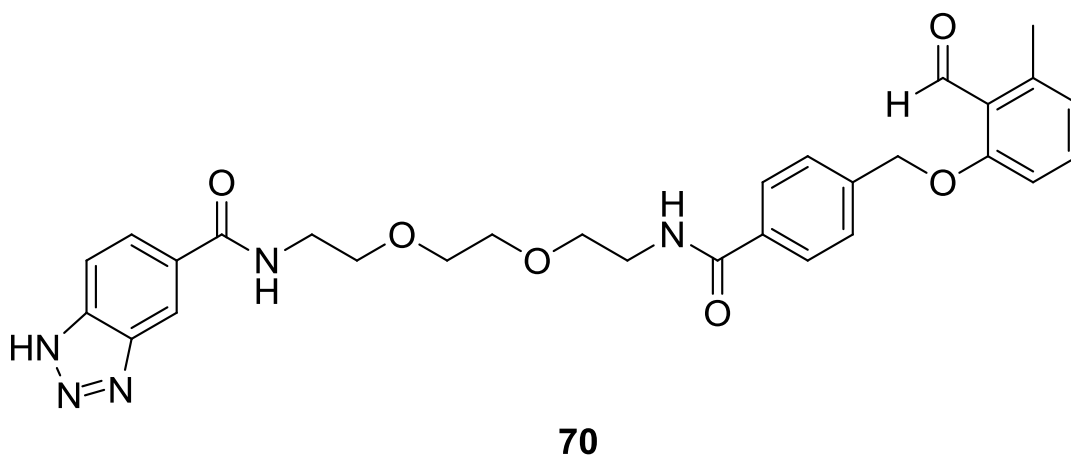
Synthesis of *N*-(2-(2-(2-aminoethoxy)ethoxy)ethyl)-1*H*-benzo[*d*][1,2,3]triazole-5-carboxamide **69**



To a stirred solution of *tert*-butyl (2-(2-(2-(1*H*-benzo[*d*][1,2,3]triazole-5-carboxamido)ethoxy)ethoxy)ethyl)carbamate (1.00 g, 2.54 mmol) in 15 mL dry CH₂Cl₂ was added TFA (6 mL). The reaction mixture was stirred at room temperature for 2 h. 15 mL CH₂Cl₂ was then added and the solvent was removed under reduced pressure. The procedure was repeated five times to remove traces of TFA to give compound **69** as brown oil in quantitative yield.

¹H-NMR (400 MHz, CD₃OD) δ / ppm: 2.99 (t, *J* = 5.1 Hz, 2 H, CH₂), 3.59-3.68 (m, 10 H, CH₂), 7.69 (d, *J* = 8.7 Hz, 1 H, H_{Ar}), 7.83 (d, *J* = 8.7 Hz, 1 H, H_{Ar}), 8.38 (s, 1H, H_{Ar}). ¹³C-NMR (100 MHz, CD₃OD) δ / ppm: 40.87 (CH₂), 40.99 (CH₂), 69.40 (CH₂), 70.69 (CH₂), 71.33 (CH₂), 116.76 (C_{Ar}), 117.37 (C_{Ar}), 122.72 (C_{Ar}), 129.94 (C_{Ar}), 144.77 (C_{Ar}), 146.36 (C_{Ar}), 171.27 (OCN). HR-MS: (FAB) *m/z* calculated for C₁₃H₂₀N₅O₃ [M + H⁺], 294.1561; found, 294.1559.

Synthesis of *N*-(2-(2-(2-(4-((2-formyl-3-methylphenoxy)methyl)benzamido)ethoxy)ethoxy)ethyl)-1*H*-benzo[*d*][1,2,3]triazole-5-carboxamide (BTPE) **70**

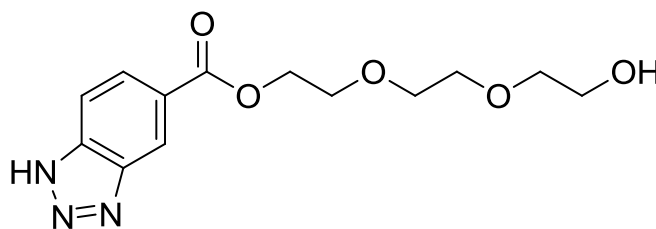


To bind 4-((2-formyl-3-methylphenoxy)methyl)benzoic acid to **43** as NHS ester, 73.0 mg (0.27 mmol, 1 eq) 4-((2-formyl-3-methylphenoxy)methyl)benzoic acid

was dissolved in 1.5 mL of dry DMF. HOBt (37.0 mg, 0.28 mmol, 1.02 eq) was added and the solution was stirred for 10 min before addition of 61.0 mg (0.30 mmol, 1.1 eq) DCC (dissolved in 1.5 mL dry DMF). After stirring for 30 minutes, 32.0 mg (0.28 mmol, 1.02 eq) NHS dissolved in 1.5 mL dry DMF was added dropwise. The reaction mixture was stirred for 2 h. Compound **69** (80.0 mg, 0.27 mmol, 1 eq) dissolved in 1.5 mL dry DMF was added dropwise and the solution was stirred overnight. After filtration, the solvent was removed under reduced pressure and purified *via* column chromatography (chloroform/methanol 19:1) to obtain a white solid (50.0 mg, 0.091 mmol, 34%).

^1H NMR (400 MHz, CDCl_3) δ / ppm: 2.45 (s, 3 H, CH_3), 3.58-3.61 (m, 12 H, CH_2), 5.00 (s, 2H, CH_2), 6.71 (t, $J = 8.0$ Hz, 2 H, CH), 7.20-7.29 (m, 3 H, CH), 7.41 (s, 1 H, CH), 7.57 (s, 1 H, CH), 7.71 (d, $J = 8.2$ Hz, 2 H, CH), 8.24 (s, 1 H, CH), 10.56 (s, 1 H, CHO). ^{13}C -NMR (100 MHz, CDCl_3) δ / ppm: 20.40 (CH_3), 38.97 (CH_2), 68.53 (CH_2), 68.66 (CH_2), 68.77 (CH_2), 69.16 (CH_2), 109.32 (C_{Ar}), 122.35 (C_{Ar}), 123.59 (C_{Ar}), 126.05 (C_{Ar}), 126.46 (C_{Ar}), 132.78 (C_{Ar}), 133.68 (C_{Ar}), 138.86 (C_{Ar}), 141.22 (C_{Ar}), 160.86 (C_{Ar}), 166.52 (OCN), 166.79 (OCN), 191.29 (CHO). HR-MS: (FAB) m/z calculated for $\text{C}_{29}\text{H}_{32}\text{N}_5\text{O}_6$ [$\text{M} + \text{H}^+$]: 546.2352; found: 546.2355.

Synthesis of 2-(2-(2-hydroxyethoxy)ethoxy)ethyl 1*H*-benzo[*d*][1,2,3]triazole-5-carboxylate (BBTEG) **74**



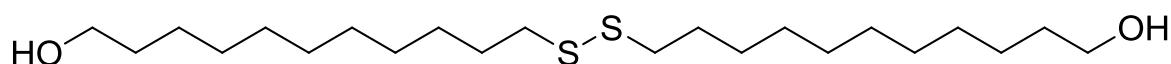
74

Benzotriazole-5-carboxylic acid (0.50 g, 3.07 mmol, 1 eq), triethylene glycol (TEG) (4.60 g, 30.7 mmol, 10 eq), DCC (0.76 g, 3.68 mmol, 1 eq), and DMAP (53.0 mg, 0.43 mmol, 0.14 eq) were dissolved in 20 mL THF and stirred under argon for 24 h at room temperature. The solvent was removed under reduced pressure and the crude product was purified by column chromatography (dichloromethane/methanol 9:1) to give **4** as yellow oil (0.52 g, 1.74 mmol, 57%).

^1H NMR (300 MHz, CDCl_3) δ / ppm: 3.68 (t, $J = 4.4$ Hz, 2 H, CH_2), 3.75-3.83 (m, 6 H, CH_2), 3.88 (t, $J = 4.4$ Hz, 2H, CH_2), 4.50 (t, $J = 4.4$ Hz, 2 H, CH_2), 7.76 (d, $J =$

8.7 Hz, 1 H, *CH*), 7.91 (d, $J = 8.7$ Hz, 1 H, *CH*), 8.53 (s, 1 H, *CH*). ^{13}C -NMR (75 MHz, CDCl_3) δ / ppm: 61.58 (CH_2), 64.23 (CH_2), 69.14 (CH_2), 70.22 (CH_2), 70.59 (CH_2), 72.52 (CH_2), 114.01 (C_{Ar}), 118.84 (C_{Ar}), 126.67 (C_{Ar}), 127.11 (C_{Ar}), 139.79 (C_{Ar}), 166.03 (OCO). HR-MS: (FAB) m/z calculated for $\text{C}_{13}\text{H}_{17}\text{N}_3\text{O}_5$ [$\text{M} + \text{H}^+$]: 295.1168; found: 295.1166.

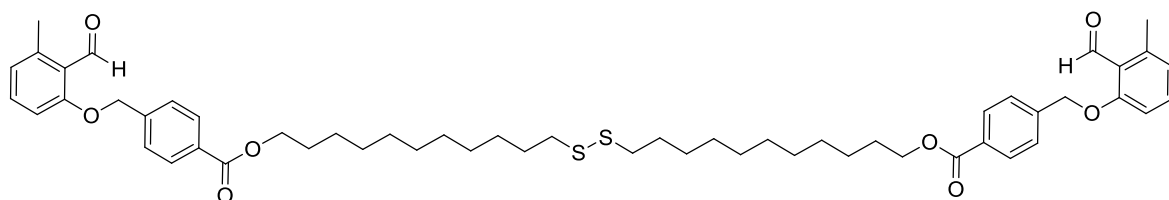
Synthesis of 11-Hydroxyundecylsulfide 86^[243]



86

11-Hydroxyundecylsulfide was prepared *via* the synthesis procedure of Friederici *et al.*^[243] A methanol solution (80 mL) containing 11-mercapto-1-undecanol (1.002 g, 4.90 mmol) was titrated by 1 M iodine methanol solution until the solution turned light yellow. Then the reaction was quenched with sodium bisulfite. The reaction mixture was evaporated to dryness under reduced pressure at ambient temperature and the product, 11-hydroxyundecylsulfide **1**, was extracted in CH_2Cl_2 as a white solid (900 mg, 90%).

Synthesis of disulfanediylbis(undecane-11,1-diyl) bis(4-((2-formyl-3-methylphenoxy) methyl)benzoate) 87



87

To a solution of 11-hydroxyundecylsulfide (0.253 g, 0.62 mmol) in 40 mL CH_2Cl_2 , 4-((2-formyl-3-methylphenoxy)methyl)benzoic acid (0.335 g, 1.23 mmol), DCC (0.277 g, 1.34 mmol) and DMAP (0.014 g, 0.11 mmol) were successively added. The resulting mixture was allowed to stir overnight at ambient temperature under argon. After the reaction was finished, the white solid was removed by filtration, solvent was removed under reduced pressure, and the residue was purified by flash chromatography on silica using a mixed eluent (cyclohexane:ethyl acetate, 5:1), obtaining **2** as a yellow solid (251 mg, 56%).

^1H -NMR (400 MHz, CDCl_3) δ / ppm: 1.18-1.38 (m, 28H, CH_2), 1.59 (qi, $J = 7.3$ Hz, 4H, CH_2), 1.69 (qi, $J = 7.3$ Hz, 4H, CH_2), 2.51 (s, 6H, CH_3), 2.60 (t, $J = 7.3$ Hz, 4H,

CH_2), 4.24 (t, $J = 6.7$ Hz, 4H, CH_2), 5.14 (s, 4H, CH_2), 6.76 (d, $J = 7.4$ Hz, 2H, CH), 6.78 (d, $J = 8.2$ Hz, 2H, CH), 7.28 (t, $J = 8.0$ Hz, 2H, CH), 7.42 (d, $J = 8.2$ Hz, 4H, CH), 7.99 (d, $J = 8.3$ Hz, 4H, CH), 10.68 (s, 2H, CHO). ^{13}C -NMR (100 MHz, $CDCl_3$) δ / ppm: 21.52 (CH_3), 26.05 (CH_2), 28.63 (CH_2), 29.27 (CH_2), 39.17 (CH_2), 65.26 (CH_2), 69.93 (CH_2), 110.31 (C_{Ar}), 123.66 (C_{Ar}), 124.69 (C_{Ar}), 127.07 (C_{Ar}), 129.68 (C_{Ar}), 134.42 (C_{Ar}), 141.22 (C_{Ar}), 142.30 (C_{Ar}), 161.92 (C_{Ar}), 166.28 (OCO), 192.00 (CHO). HR-MS: (FAB) m/z calculated for $C_{54}H_{70}S_2O_8$ [$M + H^+$]: 910.4512; found: 910.4514.

Hybridization of Au NRs-DNA 119 with cDNA

Au NR-DNA **119** dispersion (160 fmol) and cDNA-Mal (400 pmol) were incubated overnight at ambient temperature in 200 μ L 1 \times TBE. The excess cDNA was removed by washing twice with water.

Nanoparticle Syntheses

Ligand Exchange of BTPE/BTTEG

Commercially available, citrate-capped Ag nanoparticles were centrifuged (30 min \times 5000 rpm) and redispersed in the same volume of DMSO. After addition of BTPE and BTTEG in the ratio 1:10 (10 000 eq per Ag nanoparticle), the reaction mixture was incubated overnight at room temperature. Subsequent washing step (40 min \times 7000 rpm) removed the free BTPE. To determine the concentration of the resulting BTPE/BTTEG-modified Ag NPs **76** UV-Vis measurements were performed.

Synthesis of Mercaptoundecanol-capped Gold Nanoparticles (Au-MUD) **89**^[106]

Gold nanoparticles were prepared by using the synthesis procedure of Raula *et al.*^[106] $HAuCl_4$ (354 mg, $n(Au)$ 0.93 mmol) was dissolved in dry THF (10 mL) and stirred for 15 min. MUD (184 mg, 0.90 mmol) was added gradually to the mixture under constant stirring. Subsequently, the mixture was stirred for a further 30 min until the color of the mixture changed from brown to orange. Reduction was carried out at ambient temperature slowly adding Super-Hydride (6 mL) to the reaction mixture under fast stirring rate. In the beginning of the addition of the

reductant, the solution changed to a black suspension. Thereby, the temperature of the mixture slightly increased. The stirring was continued until the temperature of the mixture decreased to ambient temperature after ca. 1 h. Purification of the gold nanoparticles was conducted by centrifugation (13200 rpm) in an ethanol/THF mixture.

Synthesis of Photoenol-modified Gold Nanoparticles (Au-MUD-PE) 90

Au-MUD **89** (155 mg), which contained 28.4 μmol of ligands, DCC (3.53 mg, 17.1 μmol), and 4-DMAP (0.17 mg, 1.39 μmol) were dissolved in 1.3 mL of DMF and flushed with dry nitrogen for 15 min. 4-((2-Formyl-3-methylphenoxy)methyl)benzoic acid (1.58 mg, 5.85 μmol) dissolved in 1.3 mL of DMF was added dropwise to the mixture with stirring at ambient temperature. Subsequently, the temperature of the reaction mixture was raised to 30 °C, and kept at that temperature for 48 h. The purification of the product was accomplished by using a 2000 kDa dialysis bag in water. In the course of the exchange of DMF and water in the dialysis tube, the Au NPs precipitated. The success of the purification was ascertained by $^1\text{H-NMR}$.

$^1\text{H-NMR}$ (250 MHz, CD_3OD) δ / ppm: 0.8-1.8 (m, 360H, CH_2), 2.53 (s, 3H, CH_3), 3.57 (br, 2H, CH_2), 5.26 (s, 2H, CH_2), 6.86 (d, $J = 8.1$ Hz, 1H, CH), 7.06 (d, $J = 8.2$ Hz, 1H, CH), 7.42 (t, $J = 8.1$ Hz, 1H, CH), 7.53 (d, $J = 8.1$ Hz, 2H, CH), 7.59 (d, $J = 8.4$ Hz, 2H, CH), 10.64 (s, 1H, CHO).

Synthesis of CTAC-capped Gold Nanoparticles 88

Synthesis of CTAC-capped gold nanoparticles was performed according to literature procedure.^[244] Gold nanoparticles were synthesized in three steps. In the first, seed solution was prepared by vigorously mixing of 5 mL of aqueous CTAC solution (0.2 M), 4.5 mL of nanopure water and 515 μL of HAuCl_4 (4.86 mM) with 450 μL of ice-cold NaBH_4 (0.02 M). The seed solution was aged for 1 h at 30°C in a hot bath. In the second step, the growth solution was prepared by mixing 4.5 mL of nanopure water, 5 mL of aqueous CTAC solution (0.2 M), 515 μL of HAuCl_4 (4.86 mM), and 75 μL of ascorbic acid (0.04 M). To this colorless solution, 25 μL of seed solution was added with vigorous stirring and kept undisturbed for two days to obtain highly uniform spherical nanoparticles with LSPR at 521 nm. The size of the nanoparticles obtained at this stage was 20 nm.

Synthesis of CTAB-capped Gold Nanorods 116

Synthesis of CTAB-capped gold nanorods was performed according to literature procedure.^[24] The seed solution for gold nanorods was prepared as followed. A 5 mL amount of 0.5 mM HAuCl₄ was mixed with 5 mL of 0.2 M CTAB solution. A 0.6 mL portion of fresh 0.01 M NaBH₄ was diluted to 1 mL with water and was then injected into the Au(III)-CTAB solution under vigorous stirring. The solution color changed from yellow to brownish-yellow, and the stirring was stopped after 2 min. The seed solution was aged at room temperature for 30 min before use.

To prepare the growth solution, 2.25 g of CTAB together with 0.275 g 5-bromosalicylic acid were dissolved in 62.5 mL of warm water (50-70 °C) in a flask. The solution was allowed to cool to 30 °C, when 3 mL of 4 mM AgNO₃ solution was added. The mixture was kept undisturbed at 30 °C for 15 min, after which 62.5 mL of 1 mM HAuCl₄ solution was added. After 15 min of slow stirring, 0.5 mL of 0.064 M ascorbic acid was added, and the solution was vigorously stirred for 30 s until it became colorless. The growth solution had a CTAB concentration of about 0.05 M and was used right after preparation.

Finally, 0.2 mL of seed solution was injected into the growth solution. The resultant mixture was stirred for 30 s and left undisturbed at 30 °C for 12 h for nanorod growth. The reaction products were isolated by centrifugation at 8500 rpm for 25 min followed by removal of supernatant. The precipitates were redispersed in 10 mL of water. To determine the concentration of the resulting CTAB-capped Au NRs **116** UV-Vis measurements were performed ($\epsilon = 1.9 \cdot 10^9 \text{ M}^{-1} \text{ cm}^{-1}$).

Ligand Exchange of linker 113/linker 111

The prepared CTAB-capped Au NR dispersion (1 mL, 1.33 pmol) were placed in a vial and 0.675 mg linker **113** (1 eq, 0.45 μmol) and 5.40 mg linker **111** (10 eq, 4.5 μmol) were added. The 5 mM PEG solution was stirred for 30 min at 70 °C. After addition of 1 mL chloroform, the two phases were stirred for 10 min at 50 °C. Subsequently 200 μL of 1 M HCl was added and stirred for 2 h. After successful phase transfer, the water phase was removed, chloroform was centrifuged (5 min x 5000 rpm) and redispersed in water.

Photoreactions

Photoreaction between BTPE 70 and PEG-Mal 71

1.57 mg (2.88 μmol ; 4 eq) of **70** and 0.86 mg (0.72 μmol ; 1 eq) PEG-Mal **71** were dissolved in 1.0 mL DMSO and aliquoted in a headspace vials (200 μL in each one, Pyrex, diameter 20 mm), which were crimped air-tight using SBR seals with PTFE inner liner. The solution was deoxygenated by purging with nitrogen for 10 min. The vials were subsequently irradiated for 15 min by revolving around a compact low-pressure fluorescent lamp (Arimed B6, Cosmedico GmbH, Stuttgart, Germany) emitting at 320 nm (± 30 nm, 36 W, the emission spectrum of the employed compact low-pressure fluorescent lamp is included in Figure 51) at a distance of 40-50 mm in a custom-built photoreactor (see Figure 50). The solvents were evaporated under vacuum after the reaction, THF/methanol 3:2 (0.5 mL) was added in each vial and the four solutions were analyzed *via* ESI-MS.

Photoreaction between BTPE 70 and DNA-Mal 83

Stock solution of **70** (10.9 μg , 20 nmol; 4 eq) and 5 nmol (1 eq) DNA-Mal **83** were dissolved in 200 μL H₂O/acetonitrile 1:1 and aliquoted in a different headspace vials (200 μL in each one, Pyrex, diameter 20 mm), which were crimped air-tight using SBR seals with PTFE inner liner. The solution was deoxygenated by purging with nitrogen for 10 min. The vials were subsequently irradiated for 6 h by revolving around a compact low-pressure fluorescent lamp (Arimed B6, Cosmedico GmbH, Stuttgart, Germany) emitting at 320 nm (± 30 nm, 36 W, the emission spectrum of the employed compact low-pressure fluorescent lamp is included in Figure 51) at a distance of 40-50 mm in a custom-built photoreactor (see Figure 50). The reaction mixture was purified with NAP-5 and NAP-10 size exclusion columns, and HPLC using a gradient of 0.1 M ammonium acetate and acetonitrile.

Photoreaction between Ag-BTPE/BTTEG 76 and PEG-Mal 71

To Ag-BTPE/BTTEG dispersion (210 fmol, 1 eq) in 400 μL DMSO, PEG-Mal (2.10 nmol, 10000 eq) was added and aliquoted in a headspace vial (Pyrex, diameter 20 mm), which was crimped air-tight using SBR seals with PTFE inner liner. The solution was deoxygenated by purging with nitrogen for 10 min. The flask was

subsequently irradiated for 15 min by revolving around a compact low-pressure fluorescent lamp (Arimed B6, Cosmedico GmbH, Stuttgart, Germany) emitting at 320 nm (± 30 nm, 36 W, the emission spectrum of the employed compact low-pressure fluorescent lamp is included in Figure 51) at a distance of 40–50 mm in a custom-built photoreactor (see Figure 50). The excess PEG-Mal was removed by using a 2000 kDa dialysis bag, which allows the polymer ($M_n = 1300 \text{ g}\cdot\text{mol}^{-1}$) to pass through, while retaining Ag-core PEG-shell NPs.

Photoreaction between Ag-BTPE/BTTEG and poly(CBMA)-Mal

To Ag-BTPE/BTTEG dispersion (100 fmol, 1 eq) in 400 μL DMSO, poly(CBMA-2) (5.00 nmol, 50000 eq) was added and aliquoted in a headspace vial (Pyrex, diameter 20 mm), which was crimped air-tight using SBR seals with PTFE inner liner. The solution was deoxygenated by purging with nitrogen for 10 min. The flask was subsequently irradiated for 60 min by revolving around a compact low-pressure fluorescent lamp (Arimed B6, Cosmedico GmbH, Stuttgart, Germany) emitting at 320 nm (± 30 nm, 36 W, the emission spectrum of the employed compact low-pressure fluorescent lamp is included in Figure 51) at a distance of 40–50 mm in a custom-built photoreactor (see Figure 50). The excess p(CBMA)-Mal was removed by centrifugation (3 x).

Kinetic Study of the Light-Triggered Reaction of **87** and Maleimide **91**

0.40 mg (0.439 μmol ; 1 eq) of **87** and 0.85 mg (8.78 μmol ; 20 eq) maleimide were dissolved in 1.6 mL dry DMF and aliquoted in 4 different headspace vials (200 μL in each one, Pyrex, diameter 20 mm), which were crimped air-tight using SBR seals with PTFE inner liner. The solution was deoxygenated by purging with nitrogen for 10 min. The vials were subsequently irradiated for 0 min, 5 min, 15 min, 45 min by revolving around a compact low-pressure fluorescent lamp (Arimed B6, Cosmedico GmbH, Stuttgart, Germany) emitting at 320 nm (± 30 nm, 36 W, the emission spectrum of the employed compact low-pressure fluorescent lamp is included in Figure 51) at a distance of 40–50 mm in a custom-built photoreactor (see Figure 50). The solvents were evaporated under vacuum after the reaction, THF/methanol 3:2 (0.5 mL) was added in each vial and the four solutions were analyzed *via* ESI-MS.

Spatially Resolved Surface Encoding

Fabricated Au NP patterns were immersed into 1 mM solution of 2-(2,5-dioxo-2,5-dihydro-1H-pyrrol-1-yl)ethyl 2-bromo-2-methylpropanoate **100** in DMF ($145 \mu\text{g mL}^{-1}$). Patterning was conducted by irradiation for 15 min using a compact low-pressure fluorescent lamp (Arimed B6, Cosmedico GmbH, Stuttgart, Germany) emitting at 320 nm (± 30 nm, 36 W, the emission spectrum of the employed compact low-pressure fluorescent lamp is included in Figure 51) at a distance of 40-50 mm in a custom-built photoreactor (see Figure 50). Sample development was performed by immersing the sample into DMF (30 mL, 20 min) and subsequent rinsing with acetone (5 mL) and distilled water (5 mL).

Photoreaction between linker **113** and maleimide **91**

0.60 mg (0.40 μmol ; 1 eq.) of **113** and 0.38 mg of maleimide **91** (4.00 μmol ; 10 eq.) were dissolved in 1.2 mL H_2O /acetonitrile (9:1) and aliquoted into 6 different quartz cuvettes (200 μL in each one). The quartz cuvettes were subsequently irradiated for a) 0 min, b) 1 min, c) 3 min, d) 6 min, e) 10 min, and d) 15 min with a compact low-pressure fluorescent lamp (Arimed B6, Cosmedico GmbH, Stuttgart, Germany) emitting at 320 nm (± 30 nm, 36 W, the emission spectrum of the employed compact low-pressure fluorescent lamp is included in Figure 51) at a distance of 50 mm in a custom-built photoreactor (see Figure 50). The solvents were evaporated under vacuum after the reaction, THF (0.5 mL) was added in each vial and the six solutions were analyzed immediately *via* ESI-MS.

Photoreaction between TA-PEG-TZ **113** and DNA-Mal **83**

TA-PEG-TZ **113** (30 μg , 20 nmol, 250 eq) and DNA-Mal **83** (80 pmol, 10 eq) were dissolved in 200 μL H_2O /acetonitrile 9:1. The quartz cuvette was subsequently irradiated for 30 min with a compact low-pressure fluorescent lamp (Arimed B6, Cosmedico GmbH, Stuttgart, Germany) emitting at 320 nm (± 30 nm, 36 W, the emission spectrum of the employed compact low-pressure fluorescent lamp is included in Figure 51) at a distance of 50 mm in a custom-built photoreactor (see Figure 50). The solvents were evaporated under vacuum after the reaction, water was added and the solution was analyzed by gel electrophoresis.

Photoreaction between tetrazole modified Au NRs-117 and DNA-Mal 83

Tetrazole modified Au NRs-117 dispersion (160 fmol, 1 eq) and DNA-Mal 83 (40 pmol, 250 eq) were dissolved in 200 μL H_2O /acetonitrile 9:1. The quartz cuvette was subsequently irradiated for 30 min with a compact low-pressure fluorescent lamp (Arimed B6, Cosmedico GmbH, Stuttgart, Germany) emitting at 320 nm (± 30 nm, 36 W, the emission spectrum of the employed compact low-pressure fluorescent lamp is included in Figure 51) at a distance of 5 cm in a custom-built photoreactor (see Figure 50). The excess DNA-Mal 83 was removed by washing twice with water.

Bibliography

- [1] K. L. Kelly, E. Coronado, L. L. Zhao, G. C. Schatz, *J. Phys. Chem. B* **2003**, *107*, 668-677.
- [2] a) R. H. Prabhu, V. B. Patravale, M. D. Joshi, *Int. J. Nanomedicine* **2015**, *10*, 1001-1018; b) J. Kreuter, *Adv. Drug Deliv. Rev.* **2014**, *71*, 2-14.
- [3] A. Guerrero-Martinez, J. Perez-Juste, L. M. Liz-Marzan, *Adv. Mater.* **2010**, *22*, 1182-1195.
- [4] S. H. Wu, C. Y. Mou, H. P. Lin, *Chem. Soc. Rev.* **2013**, *42*, 3862-3875.
- [5] A. P. Alivisatos, *Science* **1996**, *271*, 933-937.
- [6] I. L. Medintz, H. T. Uyeda, E. R. Goldman, H. Mattoussi, *Nat. Mater.* **2005**, *4*, 435-446.
- [7] D. A. Giljohann, D. S. Seferos, W. L. Daniel, M. D. Massich, P. C. Patel, C. A. Mirkin, *Angew. Chem. Int. Ed.* **2010**, *49*, 3280-3294.
- [8] V. Amendola, S. Polizzi, M. Meneghetti, *Langmuir* **2007**, *23*, 6766-6770.
- [9] A. Roucoux, J. Schulz, H. Patin, *Chem. Rev.* **2002**, *102*, 3757-3778.
- [10] Y. Xia, Y. Xiong, B. Lim, S. E. Skrabalak, *Angew. Chem. Int. Ed.* **2009**, *48*, 60-103.
- [11] J. Turkevich, P. C. Stevenson, J. Hillier, *Discuss. Faraday Soc.* **1951**, 55-75.
- [12] a) J. Polte, T. T. Ahner, F. Delissen, S. Sokolov, F. Emmerling, A. F. Thunemann, R. Kraehnert, *J. Am. Chem. Soc.* **2010**, *132*, 1296-1301; b) S. Kumar, K. S. Gandhi, R. Kumar, *Ind. Eng. Chem. Res.* **2007**, *46*, 3128-3136.
- [13] C. J. Ackerson, P. D. Jadzinsky, R. D. Kornberg, *J. Am. Chem. Soc.* **2005**, *127*, 6550-6551.
- [14] a) M. Brust, M. Walker, D. Bethell, D. J. Schiffrin, R. Whyman, *Chem. Commun.* **1994**, 801-802; b) L. M. Liz-Marzan, *Chem. Commun.* **2013**, *49*, 16-18.
- [15] E. Oh, K. Susumu, R. Goswami, H. Mattoussi, *Langmuir* **2010**, *26*, 7604-7613.
- [16] M. Sakamoto, M. Fujistuka, T. Majima, *J. Photoch. Photobio. C* **2009**, *10*, 33-56.

Bibliography

- [17] K. L. McGilvray, M. R. Decan, D. Wang, J. C. Scaiano, *J. Am. Chem. Soc.* **2006**, *128*, 15980-15981.
- [18] P. X. Zhao, N. Li, D. Astruc, *Coordin. Chem. Rev.* **2013**, *257*, 638-665.
- [19] N. R. Jana, L. Gearheart, C. J. Murphy, *Adv. Mater.* **2001**, *13*, 1389-1393.
- [20] M. A. Raj, S. B. Revin, S. A. John, *Colloids Surf., B* **2011**, *87*, 353-360.
- [21] Y. Shao, Y. Jin, S. Dong, *Chem. Commun.* **2004**, 1104-1105.
- [22] S. K. Bhargava, J. M. Booth, S. Agrawal, P. Coloe, G. Kar, *Langmuir* **2005**, *21*, 5949-5956.
- [23] J. Xiao, L. Qi, *Nanoscale* **2011**, *3*, 1383-1396.
- [24] X. Ye, L. Jin, H. Caglayan, J. Chen, G. Xing, C. Zheng, V. Doan-Nguyen, Y. Kang, N. Engheta, C. R. Kagan, C. B. Murray, *ACS Nano* **2012**, *6*, 2804-2817.
- [25] P. C. Lee, D. Meisel, *J. Phys. Chem.* **1982**, *86*, 3391-3395.
- [26] X. Y. Dong, X. H. Ji, H. L. Wu, L. L. Zhao, J. Li, W. S. Yang, *J. Phys. Chem. C* **2009**, *113*, 6573-6576.
- [27] C. H. Bae, S. H. Nam, S. M. Park, *Appl. Surf. Sci.* **2002**, *197*, 628-634.
- [28] H. Li, H. Xia, D. Wang, X. Tao, *Langmuir* **2013**, *29*, 5074-5079.
- [29] C. F. Li, D. X. Li, G. Q. Wan, J. Xu, W. G. Hou, *Nanoscale Res. Lett.* **2011**, *6*.
- [30] M. Zhou, B. X. Wang, Z. Rozynek, Z. H. Xie, J. O. Fossum, X. F. Yu, S. Raaen, *Nanotechnology* **2009**, *20*.
- [31] J. A. Creighton, C. G. Blatchford, M. G. Albrecht, *J. Chem. Soc., Faraday Trans. 2* **1979**, *75*, 790-798.
- [32] K. C. Song, S. M. Lee, T. S. Park, B. S. Lee, *Korean J. Chem. Eng.* **2009**, *26*, 153-155.
- [33] F. Fievet, J. P. Lagier, B. Blin, B. Beaudoin, M. Figlarz, *Solid State Ionics* **1989**, *32-3*, 198-205.
- [34] D. Kim, S. Jeong, J. Moon, *Nanotechnology* **2006**, *17*, 4019-4024.
- [35] S. Komarneni, D. S. Li, B. Newalkar, H. Katsuki, A. S. Bhalla, *Langmuir* **2002**, *18*, 5959-5962.
- [36] B. R. Cuenya, *Thin Solid Films* **2010**, *518*, 3127-3150.
- [37] M. Haruta, N. Yamada, T. Kobayashi, S. Iijima, *J. Catal.* **1989**, *115*, 301-309.
- [38] N. Lopez, J. K. Norskov, *J. Am. Chem. Soc.* **2002**, *124*, 11262-11263.

- [39] J. P. Wilcoxon, J. E. Martin, F. Parsapour, B. Wiedenman, D. F. Kelley, *J. Chem. Phys.* **1998**, *108*, 9137-9143.
- [40] T. Huang, R. W. Murray, *J. Phys. Chem. B* **2001**, *105*, 12498-12502.
- [41] L. Shang, S. J. Dong, G. U. Nienhaus, *Nano Today* **2011**, *6*, 401-418.
- [42] J. Zheng, C. W. Zhang, R. M. Dickson, *Phys. Rev. Lett.* **2004**, *93*.
- [43] S. Link, M. A. El-Sayed, *J. Phys. Chem. B* **1999**, *103*, 4212-4217.
- [44] H. Chen, X. Kou, Z. Yang, W. Ni, J. Wang, *Langmuir* **2008**, *24*, 5233-5237.
- [45] J. J. Mock, M. Barbic, D. R. Smith, D. A. Schultz, S. Schultz, *J. Chem. Phys.* **2002**, *116*, 6755-6759.
- [46] S. K. Ghosh, S. Nath, S. Kundu, K. Esumi, T. Pal, *J. Phys. Chem. B* **2004**, *108*, 13963-13971.
- [47] Y. Sun, S. K. Gray, S. Peng, *Phys. Chem. Chem. Phys.* **2011**, *13*, 11814-11826.
- [48] A. J. Haes, R. P. Van Duyne, *Anal. Bioanal. Chem.* **2004**, *379*, 920-930.
- [49] X. Huang, P. K. Jain, I. H. El-Sayed, M. A. El-Sayed, *Lasers Med Sci* **2008**, *23*, 217-228.
- [50] Z. Zhang, J. Wang, X. Nie, T. Wen, Y. Ji, X. Wu, Y. Zhao, C. Chen, *J. Am. Chem. Soc.* **2014**, *136*, 7317-7326.
- [51] K. A. Willets, R. P. Van Duyne, *Annu. Rev. Phys. Chem.* **2007**, *58*, 267-297.
- [52] I. A. Larmour, D. Graham, *Analyst* **2011**, *136*, 3831-3853.
- [53] J. Wrzesien, D. Graham, *Tetrahedron* **2012**, *68*, 1230-1240.
- [54] N. T. K. Thanh, L. A. W. Green, *Nano Today* **2010**, *5*, 213-230.
- [55] S. H. Brewer, W. R. Glomm, M. C. Johnson, M. K. Knag, S. Franzen, *Langmuir* **2005**, *21*, 9303-9307.
- [56] W. Shenton, S. A. Davis, S. Mann, *Adv. Mater.* **1999**, *11*, 449-+.
- [57] D. van Lierop, Z. Krpetic, L. Guerrini, I. A. Larmour, J. A. Dougan, K. Faulds, D. Graham, *Chem. Commun.* **2012**, *48*, 8192-8194.
- [58] N. Shamim, L. Hong, K. Hidajat, M. S. Uddin, *J. Colloid Interf Sci.* **2006**, *304*, 1-8.
- [59] M. Giersig, P. Mulvaney, *Langmuir* **1993**, *9*, 3408-3413.
- [60] H. Hiramatsu, F. E. Osterloh, *Chem. Mater.* **2004**, *16*, 2509-2511.
- [61] M. Lin, Y. Liu, X. Chen, S. Fei, C. Ni, Y. Fang, C. Liu, Q. Cai, *Biosens. Bioelectron.* **2013**, *45*, 82-88.

- [62] M. J. Hostetler, S. J. Green, J. J. Stokes, R. W. Murray, *J. Am. Chem. Soc.* **1996**, *118*, 4212-4213.
- [63] G. H. Woehrle, L. O. Brown, J. E. Hutchison, *J. Am. Chem. Soc.* **2005**, *127*, 2172-2183.
- [64] D. Baranov, E. N. Kadnikova, *J. Mater. Chem.* **2011**, *21*, 6152-6157.
- [65] D. R. Bae, S. J. Chang, Y. S. Huh, Y. K. Han, Y. J. Lee, G. R. Yi, S. Kim, G. Lee, *J. Nanosci. Nanotechnol.* **2013**, *13*, 5840-5843.
- [66] M. A. Neouze, U. Schubert, *Monatsh. Chem.* **2008**, *139*, 183-195.
- [67] N. Erathodiyil, J. Y. Ying, *Acc. Chem. Res.* **2011**, *44*, 925-935.
- [68] W. R. Algar, D. E. Prasuhn, M. H. Stewart, T. L. Jennings, J. B. Blanco-Canosa, P. E. Dawson, I. L. Medintz, *Bioconjug. Chem.* **2011**, *22*, 825-858.
- [69] D. Arosio, L. Manzoni, E. M. Araldi, C. Scolastico, *Bioconjug. Chem.* **2011**, *22*, 664-672.
- [70] J. H. Park, J. Park, U. Dembereldorj, K. Cho, K. Lee, S. I. Yang, S. Y. Lee, S. W. Joo, *Anal. Bioanal. Chem.* **2011**, *401*, 1631-1639.
- [71] M. Prabakaran, J. J. Grailer, S. Pilla, D. A. Steeber, S. Gong, *Biomaterials* **2009**, *30*, 6065-6075.
- [72] H. C. Kolb, M. G. Finn, K. B. Sharpless, *Angew. Chem. Int. Ed.* **2001**, *40*, 2004-2021.
- [73] a) N. W. Li, W. H. Binder, *J. Mater. Chem.* **2011**, *21*, 16717-16734; b) C. Barner-Kowollik, F. E. Du Prez, P. Espeel, C. J. Hawker, T. Junkers, H. Schlaad, W. Van Camp, *Angew. Chem. Int. Ed.* **2011**, *50*, 60-62.
- [74] S. P. S. Koo, M. M. Stamenovic, R. A. Prasath, A. J. Inglis, F. E. Du Prez, C. Barner-Kowollik, W. Van Camp, T. Junkers, *J. Polym. Sci. Pol. Chem.* **2010**, *48*, 1699-1713.
- [75] D. A. Fleming, C. J. Thode, M. E. Williams, *Chem. Mater.* **2006**, *18*, 2327-2334.
- [76] H. Li, Y. Yao, C. Han, J. Zhan, *Chem. Commun.* **2009**, 4812-4814.
- [77] Y. Yao, D. Tian, H. Li, *ACS Appl. Mater. Interfaces* **2010**, *2*, 684-690.
- [78] H. Li, Q. Zheng, C. Han, *Analyst* **2010**, *135*, 1360-1364.
- [79] a) J. Lim, H. Yang, K. Paek, C. H. Cho, S. Kim, J. Bang, B. J. Kim, *J. Polym. Sci. Pol. Chem.* **2011**, *49*, 3464-3474; b) T. Zhang, Z. H. Zheng, X. B. Ding, Y. X. Peng, *Macromol. Rapid Comm.* **2008**, *29*, 1716-1720.
- [80] A. Gole, C. J. Murphy, *Langmuir* **2008**, *24*, 266-272.

- [81] J. L. Brennan, N. S. Hatzakis, T. R. Tshikhudo, N. Dirvianskyte, V. Razumas, S. Patkar, J. Vind, A. Svendsen, R. J. Nolte, A. E. Rowan, M. Brust, *Bioconjug. Chem.* **2006**, *17*, 1373-1375.
- [82] D. C. Kennedy, C. S. McKay, M. C. Legault, D. C. Danielson, J. A. Blake, A. F. Pegoraro, A. Stolow, Z. Mester, J. P. Pezacki, *J. Am. Chem. Soc.* **2011**, *133*, 17993-18001.
- [83] N. J. Agard, J. A. Prescher, C. R. Bertozzi, *J. Am. Chem. Soc.* **2004**, *126*, 15046-15047.
- [84] J. M. Baskin, J. A. Prescher, S. T. Laughlin, N. J. Agard, P. V. Chang, I. A. Miller, A. Lo, J. A. Codelli, C. R. Bertozzi, *Proc. Natl. Acad. Sci. USA* **2007**, *104*, 16793-16797.
- [85] P. Gobbo, Z. Mossman, A. Nazemi, A. Niaux, M. C. Biesinger, E. R. Gillies, M. S. Workentin, *J. Mater. Chem. B* **2014**, *2*, 1764-1769.
- [86] X. X. Wang, P. Gobbo, M. Suchy, M. S. Workentin, R. H. E. Hudson, *RSC Adv.* **2014**, *4*, 43087-43091.
- [87] J. Zhu, J. Hiltz, R. B. Lennox, R. Schirmacher, *Chem. Commun.* **2013**, *49*, 10275-10277.
- [88] J. Zhu, A. J. Kell, M. S. Workentin, *Org. Lett.* **2006**, *8*, 4993-4996.
- [89] P. Derboven, D. R. D'hooge, M. M. Stamenovic, P. Espeel, G. B. Marin, F. E. Du Prez, M. F. Reyniers, *Macromolecules* **2013**, *46*, 1732-1742.
- [90] E. Oh, K. Susumu, J. B. Blanco-Canosa, I. L. Medintz, P. E. Dawson, H. Mattoussi, *Small* **2010**, *6*, 1273-1278.
- [91] I. Ahmed, L. Fruk, *Mol. Biosyst.* **2013**, *9*, 565-570.
- [92] A. Jablonski, *Z. Physik* **1935**, *94*, 38-46.
- [93] S. V. Orski, A. A. Poloukhine, S. Arumugam, L. Mao, V. V. Popik, J. Locklin, *J. Am. Chem. Soc.* **2010**, *132*, 11024-11026.
- [94] S. Arumugam, V. V. Popik, *J. Am. Chem. Soc.* **2011**, *133*, 5573-5579.
- [95] R. K. Lim, Q. Lin, *Chem. Commun.* **2010**, *46*, 7993-7995.
- [96] A. R. Smith, D. F. Watson, *Chem. Mater.* **2010**, *22*, 294-304.
- [97] J. Lai, Y. Xu, X. Mu, X. Wu, C. Li, J. Zheng, C. Wu, J. Chen, Y. Zhao, *Chem. Commun.* **2011**, *47*, 3822-3824.
- [98] M. C. Daniel, D. Astruc, *Chem. Rev.* **2004**, *104*, 293-346.
- [99] B. C. Sih, M. O. Wolf, *Chem. Commun.* **2005**, 3375-3384.
- [100] D. D. Evanoff, Jr., G. Chumanov, *ChemPhysChem* **2005**, *6*, 1221-1231.

- [101] P. Dallas, V. K. Sharma, R. Zboril, *Adv. Colloid Interface Sci.* **2011**, *166*, 119-135.
- [102] R. A. Sperling, W. J. Parak, *Philos. Trans. A. Math. Phys. Eng. Sci.* **2010**, *368*, 1333-1383.
- [103] D. Li, Q. He, J. Li, *Adv. Colloid Interface Sci.* **2009**, *149*, 28-38.
- [104] M. K. Corbierre, N. S. Cameron, R. B. Lennox, *Langmuir* **2004**, *20*, 2867-2873.
- [105] J. Shan, H. Tenhu, *Chem. Commun.* **2007**, 4580-4598.
- [106] J. Raula, J. Shan, M. Nuopponen, A. Niskanen, H. Jiang, E. I. Kauppinen, H. Tenhu, *Langmuir* **2003**, *19*, 3499-3504.
- [107] X. D. Xiao, B. Wang, C. Zhang, Z. Yang, M. M. T. Loy, *Surf. Sci.* **2001**, *472*, 41-50.
- [108] M. I. Gibson, M. Danial, H. A. Klok, *ACS Comb. Sci.* **2011**, *13*, 286-297.
- [109] N. S. leong, K. Brebis, L. E. Daniel, R. K. O'Reilly, M. I. Gibson, *Chem. Commun.* **2011**, *47*, 11627-11629.
- [110] F. Zhang, E. Lees, F. Amin, P. Rivera Gil, F. Yang, P. Mulvaney, W. J. Parak, *Small* **2011**, *7*, 3113-3127.
- [111] P. J. Costanzo, J. D. Demaree, F. L. Beyer, *Langmuir* **2006**, *22*, 10251-10257.
- [112] C. A. Mirkin, R. L. Letsinger, R. C. Mucic, J. J. Storhoff, *Nature* **1996**, *382*, 607-609.
- [113] R. L. Letsinger, R. Elghanian, G. Viswanadham, C. A. Mirkin, *Bioconjug. Chem.* **2000**, *11*, 289-291.
- [114] N. L. Rosi, D. A. Giljohann, C. S. Thaxton, A. K. Lytton-Jean, M. S. Han, C. A. Mirkin, *Science* **2006**, *312*, 1027-1030.
- [115] J. S. Lee, A. K. Lytton-Jean, S. J. Hurst, C. A. Mirkin, *Nano Lett.* **2007**, *7*, 2112-2115.
- [116] T. Zhang, Y. Dong, Y. Sun, P. Chen, Y. Yang, C. Zhou, L. Xu, Z. Yang, D. Liu, *Langmuir* **2012**, *28*, 1966-1970.
- [117] Y. Wen, L. Chen, W. Wang, L. Xu, H. Du, Z. Zhang, X. Zhang, Y. Song, *Chem. Commun.* **2012**, *48*, 3963-3965.
- [118] C. M. Niemeyer, L. Boldt, B. Ceyhan, D. Blohm, *Anal. Biochem.* **1999**, *268*, 54-63.
- [119] C. M. Niemeyer, B. Ceyhan, *Angew. Chem. Int. Ed.* **2001**, *40*, 3685-3688.

- [120] A. Heuer-Jungemann, R. Kirkwood, A. H. El-Sagheer, T. Brown, A. G. Kanaras, *Nanoscale* **2013**, *5*, 7209-7212.
- [121] C. Chen, L. Fruk, *RSC Adv.* **2013**, *3*, 1709-1713.
- [122] a) A. A. Busnaina, J. Mead, J. Isaacs, S. Somu, *J. Nanopart. Res.* **2013**, *15*;
b) B. Yu, M. Meyyappan, *Solid-State Electron.* **2006**, *50*, 536-544; c) A. N. Shipway, E. Katz, I. Willner, *ChemPhysChem* **2000**, *1*, 18-52.
- [123] C. Subramani, X. Yu, S. S. Agasti, B. Duncan, S. Eymur, M. Tonga, V. M. Rotello, *J. Mater. Chem.* **2011**, *21*, 14156-14158.
- [124] P. M. Mendes, S. Jacke, K. Critchley, J. Plaza, Y. Chen, K. Nikitin, R. E. Palmer, J. A. Preece, S. D. Evans, D. Fitzmaurice, *Langmuir* **2004**, *20*, 3766-3768.
- [125] R. J. Barsotti, F. Stellacci, *J. Mater. Chem.* **2006**, *16*, 962-965.
- [126] D. I. Rozkiewicz, D. Janczewski, W. Verboom, B. J. Ravoo, D. N. Reinhoudt, *Angew. Chem.* **2006**, *45*, 5292-5296.
- [127] D. I. Rozkiewicz, Y. Kraan, M. W. Werten, F. A. de Wolf, V. Subramaniam, B. J. Ravoo, D. N. Reinhoudt, *Chem. Eur. J.* **2006**, *12*, 6290-6297.
- [128] D. I. Rozkiewicz, J. Gierlich, G. A. Burley, K. Gutsmedl, T. Carell, B. J. Ravoo, D. N. Reinhoudt, *ChemBioChem* **2007**, *8*, 1997-2002.
- [129] I. Rianasari, M. P. de Jong, J. Huskens, W. G. van der Wiel, *Int. J. Mol. Sci.* **2013**, *14*, 3705-3717.
- [130] A. Perl, D. N. Reinhoudt, J. Huskens, *Adv. Mater.* **2009**, *21*, 2257-2268.
- [131] M. De, P. S. Ghosh, V. M. Rotello, *Adv. Mater.* **2008**, *20*, 4225-4241.
- [132] J. H. Leuvers, P. J. Thal, M. van der Waart, A. H. Schuurs, *J. Immunoassay* **1980**, *1*, 77-91.
- [133] C. D. Medley, J. E. Smith, Z. Tang, Y. Wu, S. Bamrungsap, W. Tan, *Anal. Chem.* **2008**, *80*, 1067-1072.
- [134] D. S. Seferos, D. A. Giljohann, H. D. Hill, A. E. Prigodich, C. A. Mirkin, *J. Am. Chem. Soc.* **2007**, *129*, 15477-15479.
- [135] K. Sokolov, M. Follen, J. Aaron, I. Pavlova, A. Malpica, R. Lotan, R. Richards-Kortum, *Cancer Res.* **2003**, *63*, 1999-2004.
- [136] N. L. Rosi, C. A. Mirkin, *Chem. Rev.* **2005**, *105*, 1547-1562.
- [137] D. G. Thompson, A. Enright, K. Faulds, W. E. Smith, D. Graham, *Anal. Chem.* **2008**, *80*, 2805-2810.

- [138] D. Graham, R. Stevenson, D. G. Thompson, L. Barrett, C. Dalton, K. Faulds, *Faraday Discuss.* **2011**, *149*, 291-299.
- [139] A. N. Shipway, E. Katz, I. Willner, *ChemPhysChem* **2000**, *1*, 18-52.
- [140] A. J. Haes, R. P. Van Duyne, *J. Am. Chem. Soc.* **2002**, *124*, 10596-10604.
- [141] R. A. Tripp, R. A. Dluhy, Y. P. Zhao, *Nano Today* **2008**, *3*, 31-37.
- [142] A. Z. Wang, F. Gu, L. Zhang, J. M. Chan, A. Radovic-Moreno, M. R. Shaikh, O. C. Farokhzad, *Expert Opin. Biol. Ther.* **2008**, *8*, 1063-1070.
- [143] V. P. Torchilin, *Nat. Rev. Drug Discov.* **2005**, *4*, 145-160.
- [144] H. Yang, W. J. Kao, *J. Biomater. Sci. Polym. Ed.* **2006**, *17*, 3-19.
- [145] S. Parveen, S. K. Sahoo, *J. Drug Target.* **2008**, *16*, 108-123.
- [146] X. Q. Zhang, X. Xu, R. Lam, D. Giljohann, D. Ho, C. A. Mirkin, *ACS Nano* **2011**, *5*, 6962-6970.
- [147] L. Dykman, N. Khlebtsov, *Chem. Soc. Rev.* **2012**, *41*, 2256-2282.
- [148] X. Huang, I. H. El-Sayed, W. Qian, M. A. El-Sayed, *J. Am. Chem. Soc.* **2006**, *128*, 2115-2120.
- [149] A. Panacek, L. Kvitek, R. Prucek, M. Kolar, R. Vecerova, N. Pizurova, V. K. Sharma, T. Nevecna, R. Zboril, *J. Phys. Chem. B* **2006**, *110*, 16248-16253.
- [150] J. W. Rhim, H. M. Park, C. S. Ha, *Prog. Polym. Sci.* **2013**, *38*, 1629-1652.
- [151] C. Damm, H. Munstedt, A. Rosch, *Mater. Chem. Phys.* **2008**, *108*, 61-66.
- [152] J. Moreau, J. Marchand-Brynaert, *Eur. J. Org. Chem.* **2011**, 1641-1644.
- [153] S. Naumov, S. Kapoor, S. Thomas, S. Venkateswaran, T. Mukherjee, *J. Mol. Struct. Theochem.* **2004**, *685*, 127-131.
- [154] Y. Li, M. L. Gong, K. Ramji, Y. Z. Li, *J. Phys. Chem. C* **2009**, *113*, 18003-18013.
- [155] D. Graham, R. Brown, W. E. Smith, *Chem. Commun.* **2001**, 1002-1003.
- [156] A. Grondin, D. C. Robson, W. E. Smith, D. Graham, *J. Chem. Soc. Perk Trans. 2* **2001**, 2136-2141.
- [157] A. Enright, L. Fruk, A. Grondin, C. J. McHugh, W. E. Smith, D. Graham, *Analyst* **2004**, *129*, 975-978.
- [158] L. Fruk, A. Grondin, W. E. Smith, D. Graham, *Chem. Commun.* **2002**, 2100-2101.
- [159] H. T. Uyeda, I. L. Medintz, J. K. Jaiswal, S. M. Simon, H. Mattoussi, *J. Am. Chem. Soc.* **2005**, *127*, 3870-3878.
- [160] D. M. Kendziora, I. Ahmed, L. Fruk, *RSC Adv.* **2014**, *4*, 17980-17985.

- [161] C. Cardenas-Daw, A. Kroeger, W. Schaertl, P. Froimowicz, K. Landfester, *Macromol. Chem. Phys.* **2012**, *213*, 144-156.
- [162] M. Kaupp, T. Tischer, A. F. Hirschbiel, A. P. Vogt, U. Geckle, V. Trouillet, T. Hofe, M. H. Stenzel, C. Barner-Kowollik, *Macromolecules* **2013**, *46*, 6858-6872.
- [163] N. C. Yang, C. Rivas, *J. Am. Chem. Soc.* **1961**, *83*, 2213-&.
- [164] G. Porter, M. F. Tchir, *Chem. Commun.* **1970**, 3772-3777.
- [165] T. Gruending, K. K. Oehlschlaeger, E. Frick, M. Glassner, C. Schmid, C. Barner-Kowollik, *Macromol. Rapid Comm.* **2011**, *32*, 807-812.
- [166] K. K. Oehlschlaeger, J. O. Mueller, N. B. Heine, M. Glassner, N. K. Guimard, G. Delaittre, F. G. Schmidt, C. Barner-Kowollik, *Angew. Chem. Int. Ed.* **2013**, *52*, 762-766.
- [167] M. Winkler, J. O. Mueller, K. K. Oehlschlaeger, L. M. de Espinosa, M. A. R. Meier, C. Barner-Kowollik, *Macromolecules* **2012**, *45*, 5012-5019.
- [168] O. Altintas, J. Willenbacher, K. N. R. Wuest, K. K. Oehlschlaeger, P. Krolla-Sidenstein, H. Gliemann, C. Barner-Kowollik, *Macromolecules* **2013**, *46*, 8092-8101.
- [169] T. Josse, O. Altintas, K. K. Oehlschlaeger, P. Dubois, P. Gerbaux, O. Coulembier, C. Barner-Kowollik, *Chem. Commun.* **2014**, *50*, 2024-2026.
- [170] N. Zydziak, F. Feist, B. Huber, J. O. Mueller, C. Barner-Kowollik, *Chem. Commun.* **2015**, *51*, 1799-1802.
- [171] T. Pauloehrl, G. Delaittre, V. Winkler, A. Welle, M. Bruns, H. G. Borner, A. M. Greiner, M. Bastmeyer, C. Barner-Kowollik, *Angew. Chem. Int. Ed.* **2012**, *51*, 1071-1074.
- [172] C. M. Preuss, T. Tischer, C. Rodriguez-Emmenegger, M. M. Zieger, M. Bruns, A. S. Goldmann, C. Barner-Kowollik, *J. Mater. Chem. B* **2014**, *2*, 36-40.
- [173] K. Hildebrandt, T. Pauloehrl, J. P. Blinco, K. Linkert, H. G. Borner, C. Barner-Kowollik, *Angew. Chem. Int. Ed.* **2015**, *54*, 2838-2843.
- [174] T. Tischer, T. K. Claus, M. Bruns, V. Trouillet, K. Linkert, C. Rodriguez-Emmenegger, A. S. Goldmann, S. Perrier, H. G. Borner, C. Barner-Kowollik, *Biomacromolecules* **2013**, *14*, 4340-4350.
- [175] D. M. Bauer, A. Rogge, L. Stolzer, C. Barner-Kowollik, L. Fruk, *Chem. Commun.* **2013**, *49*, 8626-8628.

- [176] A. Warnecke, F. Kratz, *Bioconjug. Chem.* **2003**, *14*, 377-387.
- [177] B. Malisova, S. Tosatti, M. Textor, K. Gademann, S. Zurcher, *Langmuir* **2010**, *26*, 4018-4026.
- [178] C. Gunanathan, Y. Ben-David, D. Milstein, *Science* **2007**, *317*, 790-792.
- [179] a) S. Kostic, V. Soskic, J. Joksimovic, *Arzneim. Forsch.* **1994**, *44*, 697-702; b) H. P. Buchstaller, L. Burgdorf, D. Finsinger, F. Stieber, C. Sirrenberg, C. Amendt, M. Grell, F. Zenke, M. Krier, *Bioorg. Med. Chem. Lett.* **2011**, *21*, 2264-2269.
- [180] D. McKeown, C. J. McHugh, A. McCabe, W. E. Smith, D. Graham, *Heterocycles* **2002**, *57*, 1227-1230.
- [181] a) Z. Z. Wu, J. L. Liang, X. H. Ji, W. S. Yang, *Colloid Surf., A* **2011**, *392*, 220-224; b) M. P. Mallin, C. J. Murphy, *Nano Lett.* **2002**, *2*, 1235-1237.
- [182] M. Poomvanicha, J. W. Wegener, A. Blaich, S. Fischer, K. Domes, S. Moosmang, F. Hofmann, *J. Biol. Chem.* **2011**, *286*, 26702-26707.
- [183] P. Yates, A. C. Mackay, F. X. Garneau, *Tetrahedron Lett.* **1968**, 5389-5392.
- [184] a) H. Vaisocherová, V. Sevcu, P. Adam, B. Spackova, K. Hegnerova, A. de Los Santos Pereira, C. Rodriguez-Emmenegger, T. Riedel, M. Houska, E. Brynda, J. Homola, *Biosens. Bioelectron.* **2013**, *51C*, 150-157; b) C. Rodriguez-Emmenegger, E. Brynda, T. Riedel, Z. Sedlakova, M. Houska, A. B. Alles, *Langmuir* **2009**, *25*, 6328-6333; c) G. Cheng, Z. Zhang, S. Chen, J. D. Bryers, S. Jiang, *Biomaterials* **2007**, *28*, 4192-4199; d) S. Chen, S. Jiang, *Adv. Mater.* **2008**, *20*, 335-338; e) H. Vaisocherova, W. Yang, Z. Zhang, Z. Cao, G. Cheng, M. Pilarik, J. Homola, S. Jiang, *Anal. Chem.* **2008**, *80*, 7894-7901.
- [185] a) L. Mi, S. Jiang, *Biomaterials* **2012**, *33*, 8928-8933; b) L. Mi, S. Jiang, *Angew. Chem. Int. Ed.* **2014**, *53*, 1746-1754.
- [186] H. S. Sundaram, J.-R. Ella-Menye, N. D. Brault, Q. Shao, S. Jiang, *Chemic. Sci.* **2014**, *5*, 200-205.
- [187] M. J. Roberts, M. D. Bentley, J. M. Harris, *Adv. Drug Deliv. Rev.* **2012**, *64*, 116-127.
- [188] D. G. Thompson, A. Enright, K. Faulds, W. E. Smith, D. Graham, *Anal. Chem.* **2008**, *80*, 2805-2810.
- [189] L. A. Porter, D. Ji, S. L. Westcott, M. Graupe, R. S. Czernuszewicz, N. J. Halas, T. R. Lee, *Langmuir* **1998**, *14*, 7378-7386.

- [190] F. Odeh, A. Al-Bawab, Y. Z. Li, *J. Disper. Sci. Technol.* **2010**, *31*, 162-168.
- [191] M. Deubel, G. Von Freymann, M. Wegener, S. Pereira, K. Busch, C. M. Soukoulis, *Nat. Mater.* **2004**, *3*, 444-447.
- [192] H. B. Sun, S. Matsuo, H. Misawa, *Appl. Phys. Lett.* **1999**, *74*, 786-788.
- [193] J. K. Gansel, M. Thiel, M. S. Rill, M. Decker, K. Bade, V. Saile, G. von Freymann, S. Linden, M. Wegener, *Science* **2009**, *325*, 1513-1515.
- [194] K. Busch, G. von Freymann, S. Linden, S. F. Mingaleev, L. Tkeshelashvili, M. Wegener, *Phys. Rep.* **2007**, *444*, 101-202.
- [195] K. Cicha, Z. Q. Li, K. Stadlmann, A. Ovsianikov, R. Markut-Kohl, R. Liska, J. Stampfl, *J. Appl. Phys.* **2011**, *110*.
- [196] N. Pucher, A. Rosspeintner, V. Satzinger, V. Schmidt, G. Gescheidt, J. Stampfl, R. Liska, *Macromolecules* **2009**, *42*, 6519-6528.
- [197] J. Fischer, M. Wegener, *Opt. Mater. Express* **2011**, *1*, 614-624.
- [198] K. K. Seet, V. Mizeikis, S. Matsuo, S. Juodkazis, H. Misawa, *Adv. Mater.* **2005**, *17*, 541-545.
- [199] A. S. Quick, J. Fischer, B. Richter, T. Pauloehrl, V. Trouillet, M. Wegener, C. Barner-Kowollik, *Macromol. Rapid Comm.* **2013**, *34*, 335-340.
- [200] A. S. Quick, H. Rothfuss, A. Welle, B. Richter, J. Fischer, M. Wegener, C. Barner-Kowollik, *Adv. Funct. Mater.* **2014**, *24*, 3571-3580.
- [201] B. Richter, T. Pauloehrl, J. Kaschke, D. Fichtner, J. Fischer, A. M. Greiner, D. Wedlich, M. Wegener, G. Delaittre, C. Barner-Kowollik, M. Bastmeyer, *Adv. Mater.* **2013**, *25*, 6117-6122.
- [202] M. Kaupp, A. S. Quick, C. Rodriguez-Emmenegger, A. Welle, V. Trouillet, O. Pop-Georgievski, M. Wegener, C. Barner-Kowollik, *Adv. Funct. Mater.* **2014**, *24*, 5649-5661.
- [203] S. Pocovi-Martinez, M. Parreno-Romero, S. Agouram, J. Perez-Prieto, *Langmuir* **2011**, *27*, 5234-5241.
- [204] B. Yameen, C. Rodriguez-Emmenegger, C. M. Preuss, O. Pop-Georgievski, E. Verveniotis, V. Trouillet, B. Rezek, C. Barner-Kowollik, *Chem. Commun.* **2013**, *49*, 8623-8625.
- [205] a) I. Izquierdo-Lorenzo, S. Jradi, P. M. Adam, *RSC Adv.* **2014**, *4*, 4128-4133; b) A. J. Kell, A. Alizadeh, L. Yang, M. S. Workentin, *Langmuir* **2005**, *21*, 9741-9746.

- [206] J. S. Clovis, A. Eckell, R. Huisgen, R. Sustmann, *Chem. Ber.* **1967**, *100*, 60-70.
- [207] W. Song, Y. Wang, J. Qu, M. M. Madden, Q. Lin, *Angew. Chem. Int. Ed.* **2008**, *47*, 2832-2835.
- [208] W. Song, Y. Wang, J. Qu, Q. Lin, *J. Am. Chem. Soc.* **2008**, *130*, 9654-9655.
- [209] Y. Wang, W. Song, W. J. Hu, Q. Lin, *Angew. Chem. Int. Ed.* **2009**, *48*, 5330-5333.
- [210] Z. Yu, L. Y. Ho, Z. Wang, Q. Lin, *Bioorg. Med. Chem. Lett.* **2011**, *21*, 5033-5036.
- [211] P. An, Z. Yu, Q. Lin, *Chem. Commun.* **2013**, *49*, 9920-9922.
- [212] Z. Yu, T. Y. Ohulchanskyy, P. An, P. N. Prasad, Q. Lin, *J. Am. Chem. Soc.* **2013**, *135*, 16766-16769.
- [213] Y. Wang, W. J. Hu, W. Song, R. K. Lim, Q. Lin, *Org. Lett.* **2008**, *10*, 3725-3728.
- [214] Z. Yu, L. Y. Ho, Q. Lin, *J. Am. Chem. Soc.* **2011**, *133*, 11912-11915.
- [215] S. L. Zheng, Y. Wang, Z. Yu, Q. Lin, P. Coppens, *J. Am. Chem. Soc.* **2009**, *131*, 18036-18037.
- [216] Y. Wang, C. I. Vera, Q. Lin, *Org. Lett.* **2007**, *9*, 4155-4158.
- [217] J. O. Mueller, D. Voll, F. G. Schmidt, G. Delaittre, C. Barner-Kowollik, *Chem. Commun.* **2014**, *50*, 15681-15684.
- [218] a) J. O. Mueller, N. K. Guimard, K. K. Oehlenschlaeger, F. G. Schmidt, C. Barner-Kowollik, *Polym. Chem.* **2014**, *5*, 1447-1456; b) C. Rodriguez-Emmenegger, C. M. Preuss, B. Yameen, O. Pop-Georgievski, M. Bachmann, J. O. Mueller, M. Bruns, A. S. Goldmann, M. Bastmeyer, C. Barner-Kowollik, *Adv. Mater.* **2013**, *25*, 6123-6127; c) T. Tischer, C. Rodriguez-Emmenegger, V. Trouillet, A. Welle, V. Schueler, J. O. Mueller, A. S. Goldmann, E. Brynda, C. Barner-Kowollik, *Adv. Mater.* **2014**, *26*, 4087-4092; d) M. Dietrich, G. Delaittre, J. P. Blinco, A. J. Inglis, M. Bruns, C. Barner-Kowollik, *Adv. Funct. Mater.* **2012**, *22*, 304-312.
- [219] J. Willenbacher, K. N. R. Wuest, J. O. Mueller, M. Kaupp, H. A. Wagenknecht, C. Barner-Kowollik, *ACS Macro Lett.* **2014**, *3*, 574-579.
- [220] S. Arndt, H. A. Wagenknecht, *Angew. Chem. Int. Ed.* **2014**, *53*, 14580-14582.

- [221] a) R. K. Lim, Q. Lin, *Chem. Commun.* **2010**, *46*, 1589-1600; b) R. K. Lim, Q. Lin, *Acc. Chem. Res.* **2011**, *44*, 828-839; c) C. P. Ramil, Q. Lin, *Curr. Opin. Chem. Biol.* **2014**, *21*, 89-95.
- [222] E. Oh, K. Susumu, A. J. Makinen, J. R. Deschamps, A. L. Huston, I. L. Medintz, *J. Phys. Chem. C* **2013**, *117*, 18947-18956.
- [223] H. Otsuka, Y. Nagasaki, K. Kataoka, *Adv. Drug Deliver. Rev.* **2012**, *64*, 246-255.
- [224] P. Anger, P. Bharadwaj, L. Novotny, *Phys. Rev. Lett.* **2006**, *96*.
- [225] R. Bardhan, N. K. Grady, J. R. Cole, A. Joshi, N. J. Halas, *ACS Nano* **2009**, *3*, 744-752.
- [226] B. C. Mei, K. Susumu, I. L. Medintz, J. B. Delehanty, T. J. Mountziaris, H. Mattoussi, *J. Mater. Chem.* **2008**, *18*, 4949-4958.
- [227] a) C. Kinnear, H. Dietsch, M. J. D. Clift, C. Endes, B. Rothen-Rutishauser, A. Petri-Fink, *Angew. Chem. Int. Ed.* **2013**, *52*, 1934-1938; b) G. Martignoni, M. Brunelli, D. Segala, S. Gobbo, I. Borze, L. Atanesyan, S. Savola, L. Barzon, G. Masi, R. Tardanico, S. Zhang, J. N. Eble, M. Chilosi, T. Bohling, L. Cheng, B. Delahunt, S. Knuutila, *Mod. Pathol.* **2014**, *27*, 765-774.
- [228] M. Lista, D. Z. Liu, P. Mulvaney, *Langmuir* **2014**, *30*, 1932-1938.
- [229] L. Fruk, C. M. Niemeyer, *Angew. Chem. Int. Ed.* **2005**, *44*, 2603-2606.
- [230] L. Stolzer, I. Ahmed, C. Rodriguez-Emmenegger, V. Trouillet, P. Bockstaller, C. Barner-Kowollik, L. Fruk, *Chem. Commun.* **2014**, *50*, 4430-4433.
- [231] A. B. Lowe, B. S. Sumerlin, M. S. Donovan, C. L. McCormick, *J. Am. Chem. Soc.* **2002**, *124*, 11562-11563.
- [232] C. Barner-Kowollik, T. P. Davis, J. P. A. Heuts, M. H. Stenzel, P. Vana, M. Whittaker, *J. Polym. Sci. Pol. Chem.* **2003**, *41*, 365-375.
- [233] M. Glassner, K. K. Oehlenschlaeger, T. Gruending, C. Barner-Kowollik, *Macromolecules* **2011**, *44*, 4681-4689.
- [234] C. Rodriguez-Emmenegger, C. M. Preuss, B. Yameen, O. Pop-Georgievski, M. Bachmann, J. O. Mueller, M. Bruns, A. S. Goldmann, M. Bastmeyer, C. Barner-Kowollik, *Adv. Mater.* **2013**, *25*, 6123-6127.
- [235] H. T. Uyeda, I. L. Medintz, J. K. Jaiswal, S. M. Simon, H. Mattoussi, *J. Am. Chem. Soc.* **2005**, *127*, 3870-3878.

- [236] B. Yameen, C. Rodriguez-Emmenegger, C. M. Preuss, O. Pop-Georgievski, E. Verveniotis, V. Trouillet, B. Rezek, C. Barner-Kowollik, *Chem. Commun.* **2013**, *49*, 8623-8625.
- [237] K. L. Parry, A. G. Shard, R. D. Short, R. G. White, J. D. Whittle, A. Wright, *Surf. Interface Anal.* **2006**, *38*, 1497-1504.
- [238] S. Tanuma, C. J. Powell, D. R. Penn, *Surf. Interface Anal.* **1994**, *21*, 165-176.
- [239] J. H. Scofield, *J. Electron Spectrosc. Relat. Phenom.* **1976**, *8*, 129-137.
- [240] F. M. Hauser, S. R. Ellenberger, *Synthesis* **1987**, 723-724.
- [241] T. Pauloehrl, G. Delaittre, M. Bruns, M. Meissler, H. G. Borner, M. Bastmeyer, C. Barner-Kowollik, *Angew. Chem. Int. Ed.* **2012**, *51*, 9181-9184.
- [242] Y. Jung, J. M. Lee, J. W. Kim, J. Yoon, H. Cho, B. H. Chung, *Anal. Chem.* **2009**, *81*, 936-942.
- [243] M. Friederici, I. Angurell, M. Seco, O. Rossell, J. Llorca, *Dalton. Trans.* **2011**, *40*, 7934-7940.
- [244] N. Gandra, S. Singamaneni, *Chem. Commun.* **2012**, *48*, 11540-11542.

List of Figures

- Figure 1.** Nanoparticles can be classified in insulating nanoparticles, semiconductor nanoparticles, and metal nanoparticles. 3
- Figure 2.** Schematic illustration for the nucleation-growth process for the formation of gold nanoparticles. Adapted with permission from [12a]. Copyright 2010 American Chemical Society. 5
- Figure 3.** Transmission electron microscopy image of gold nanorods (left) and UV/Vis spectrum of gold nanorods of various sizes prepared using CTAB growth method (right). Reprinted with permission from [24]. Copyright 2012 American Chemical Society. 8
- Figure 4.** a) Excitation (dashed) and emission (solid) spectra of different Au nanoclusters. The excitation wavelength shifted to the lower wavelength with decreasing size. b) Emission of the three shortest wavelength emitting Au nanocluster upon UV irradiation at 366 nm. Adapted with permission from [42]. Copyrighted by the American Physical Society. 10
- Figure 5.** Schematic illustration of the plasmonic oscillation of a sphere showing that the conduction electron charge cloud oscillates in resonance with the incident light. Adapted with permission from [1]. Copyright 2003 American Chemical Society. 11
- Figure 6.** Overview of selected *click* chemistry strategies for the biofunctionalization of nanoparticles. *It should be noted that the radical thiol-ene reactions do not fulfill the *click* criteria for example for polymer-polymer conjugations.^[74] 18
- Figure 7.** Jablonski diagram contains possible photochemical processes of a molecule, which can absorb a photon to reach the excited state. The excited molecule can lose vibrational energy or emit light termed as fluorescence to reach again the again. Alternatively, the molecule undergoes intersystem crossing to reach the triplet state, followed by phosphorescence. 22

- Figure 10.** Principle of nanoparticle based immunoassay, which detects spectroscopically the aggregation of Au or Ag NPs after treatment with specific proteins or DNA strands (green). Adapted by permission from Macmillan Publishers Ltd: Nature [112], copyright 1996. 35
- Figure 11.** Atomic force microscopy image of triangular Ag NPs on a glass substrate. Reprinted with permission from [140]. Copyright 2002 American Chemical Society..... 36
- Figure 12.** Bright-field (top) and overlaid fluorescence (bottom) image of human breast cancer cells showing the cellular uptake of fluorescein-labeled DNA-Au NPs conjugates. Scale bar is 10 μ m. Adapted with permission from [146]. Copyright 2011 American Chemical Society..... 37
- Figure 13.** Overview of bifunctional linkers containing the photoenol moiety: **43**,^[171] **44**,^[166] **45**,^[170] **46**,^[172] **47**,^[162] and **48**^[173] were published by the Barner-Kowollik group. 45
- Figure 14.** Zoom into the single charged region of the ESI-MS spectrum of the model reaction between BTPE **70** and PEG-Mal **71**. The blue spectrum shows the photo-adduct after 15 min irradiation. The shift of the peaks matches the mass of BTPE **70**. No other signals are observed, underlining full conversion and stability of the photo-adduct **72**..... 52
- Figure 15.** UV/Vis measurement of citrate-capped Ag NPs-**75**, BTPE/BTTEG modified Ag NPs-**76** and PEG-coated Ag NPs-**77**. 55
- Figure 16.** a) HRTEM image shows the Ag NPs-**77** with poly(ethylene glycol). b) HRTEM image of Ag NPs with poly(ethylene glycol). The EDXS line scan follows the orange line. c) Carbon and silver peak intensities along the EDXS line scan showing the Ag-PEG core-shell structure. The counts of carbon and silver are plotted against the position. The core is around 20 nm and the shell around 2 nm. The overall slope of the carbon curve was background-corrected to account for slight thickness variation of the carbon support film. 56

Figure 17. UV/Vis measurement of BTPE/BTTEG modified Ag NPs- 76 and pCBMA-coated Ag NPs- 78	57
Figure 18. C 1s XP spectra of untreated citrate-capped Ag NPs- 75 (top), modified Ag NPs- 76 (2nd row), PEG-functionalized Ag NPs- 77 (3rd row) and pCBMA-functionalized Ag NPs- 78 (bottom) evidenced successful ligand exchange and photoreactions.	58
Figure 19. XPS analysis of the BTPE/BTTEG modified Ag NPs- 76 (top) and pCBMA coated Ag NPs- 78 shows a new peak at 402.2 eV in N 1s XP spectrum which is assigned to N ⁺ R ₄ bonds, stemming from the quaternary ammonium of the CBMA unit.	59
Figure 20. a) HRTEM image of pCBMA-coated Ag NPs- 78 . b) An EDXS line scan (orange) of pCBMA-coated Ag NPs. c) C and Ag peak intensities along the EDXS line scan showing the Ag-pCBMA core-shell structure. The counts of C and Ag are plotted against the position. The core is close to 20 nm and the shell approx. 4 nm in size.	59
Figure 21. HRTEM image of control sample without irradiation of Ag NPs and a) Mal-PEG c) Mal-pCBMA. EDXS line scan follows the orange line and counts of carbon and silver are plotted against the position with no observable shell in the control sample of Ag NPs and b) Mal-PEG d) Mal-pCBMA.....	60
Figure 22. HPLC traces of amino-DNA 81 and maleimide-modified ssDNA 83	62
Figure 23. HPLC trace of BTPE 70 and maleimide modified ssDNA 83 after 6 h and 14 h irradiation. I: Mal-DNA+ H ₂ O, II: Mal-DNA 83 , III: BTPE+Mal-DNA 84	64
Figure 24. 21% TBE gel electrophoresis of I: 10 base pair marker, II: amino-DNA 81 , III: Mal-DNA 83 and BTPE+Mal-DNA 84 after 2 h 15 min at a voltage of 100 V using SYBR Gold staining.....	65
Figure 25. 2% Agarose gel of I: citrate-capped Ag NPs and II: DNA-Ag NP conjugates after 12 min at 100 V.....	65
Figure 26. FT-IR spectra of cetyltrimethylammonium chloride-capped Au NPs 88 (top) and of photoenol-modified Au NPs (bottom).....	67

Figure 27. a) Preparation of photoenol (PE) 43 containing Au NPs (Au-MUD-PE) 90 <i>via</i> esterification. b) HRTEM image of Au-MUD-PE 90 . (c) Volume average size distribution obtained <i>via</i> DLS of Au-MUD-PE 90	71
Figure 28. ¹ H-NMR spectrum of photoenol precursor modified Au-MUD-PE 90 in CD ₃ OD at 250 MHz.....	72
Figure 29. ESI-MS spectrum of the photoreaction between photoenol disulphide linker 87 and maleimide 91 after 0, 5, 15, and 45 min, respectively.....	74
Figure 30. a) Scheme of the photo-induced surface assembly of Au NPs employing DLW. b) Light triggered Diels Alder reaction of the photo-generated o-quinodimethane located on the Au NPs 90 with surface anchored maleimides 98	75
Figure 31. a) UV/Vis spectrum of mercaptoundecanol-capped Au NPs (Au-MUD) 89 and photoenol precursor modified Au-MUD NPs (Au-MUD-PE) 90 . b) UV/Vis measurement of Au-MUD-PE 90 after irradiation for 0, 60, 120, and 180 min employing an Arimed B6 UV lamp.....	76
Figure 32. a) SEM image of square patterns, which were produced with different laser powers, from 0.2 mW to 4 mW. (b) UV-Vis spectra of the square patterns generated at the indicated laser powers showing aggregation of Au NPs at elevated laser powers (from 0.6 mW).	77
Figure 33. Microscopic images of square patterns (20 μm × 20 μm). Different laser powers were employed for the DLW process with a) Au-MUD-PE 90 (functional) on maleimide coated glass surface 98 (functional) b) Au-MUD-PE 90 (functional) on bare glass surface (non-functional) c) Au-MUD 89 (non-functional) on maleimide coated glass surface 98 (functional) d) Au-MUD 89 (non-functional) on bare glass surface (non-functional). b) – d) are control experiments.	78
Figure 34. SEM image of KIT logo by DLW of Au-MUD-PE 90 with a total footprint of approximately 60 μm × 30 μm (sample was tilted by 54°). Small amount of aggregation is observable.	79

- Figure 35.** Direct laser writing with Au-MUD-PE **90** onto maleimide coated glass surface **98** to fabricate the KIT logo with a total footprint of approximately $30\ \mu\text{m} \times 15\ \mu\text{m}$. a) Bright field image of the fabricated KIT logo. b) ToF-SIMS image of AuS^- , Au_2S^- , and Au_4S_2^- . The KIT logo scanned with the DLW setup is clearly visible as it contains a high amount on thiolated Au. 80
- Figure 36.** a) Negative polarity Secondary Ion Mass Spectrum (SIMS), high mass resolution, of immobilized thiolated Au NPs reacted with brominated maleimide according to Figure 38a obtained from a $1000 \times 500\ \mu\text{m}$ scan area with 16 individual DLW pattern as shown in Figure 33 sample a. Insert: Zoom in on bromine peaks. b) Intensity profile of Au_xS_y^- signals across the DLW patterned KIT logo shown in Figure 36b demonstrates defined boundaries between immobilized and non immobilized areas of $0.8\ \mu\text{m}$ based on the (84/16) definition. 81
- Figure 37.** Schematic drawing of spherical Au NPs. 82
- Figure 38.** a) Light-induced Diels–Alder reaction between residual photoenol groups attached on Au NP and bromine containing maleimide **100**. b) ToF-SIMS image of the sum of ^{79}Br and ^{81}Br , indicating an increased amount of bromine within the KIT pattern. 83
- Figure 39.** Design of tetrazoles with different photoactivation wavelengths: **105**,^[210] **106**,^[211] **107**,^[212] and **108**^[213] were published by the group of Lin. 86
- Figure 40.** a) Model reaction between TA-PEG-TZ **113** and maleimide **91**. b) ESI-MS spectra recorded after 0, 1, 3, 6, 10, 15 min depicts sodium adducts (Na^+) of **113** and **114**. **113'** and **114'** may be attributed to oxidation during the ionization process. 89
- Figure 41.** ESI-MS spectrum of TA-PEG-TZ **113** and TA-PEG-TZ **113** after irradiation with maleimide **91** for 15 min showing besides the product **114** (blue) and the oxidized product **114'** (green) (probably during ionization process), a by-product **115** (red) due to ester bond cleavage. 90

Figure 42. a) Image of a vial containing fluorescent solution of 114 excited under UV-irradiation (365 nm) by a hand-held TLC lamp. b) Fluorescence spectra of reaction mixture at extinction wavelength $\lambda_{\text{ex}} = 400$ nm. c) Evolution of fluorescence signal at $\lambda_{\text{em}} = 560$ nm derived from fluorescence spectra.....	91
Figure 43. a) TEM image of CTAB-capped Au NRs 116 . b) UV/Vis spectra of CTAB-Au NRs 116 , pegylated Au NR 117 in chloroform and water.....	92
Figure 44. Two-phase system of CTAB-Au NRs 116 and PEG linkers 111 and 113 in chloroform (left). Phase transfer of Au NRs after addition of 1 M HCl and vigorously stirring for 2 h.	93
Figure 45. a) UV/Vis spectrum of TA-PEG-TZ 113 with $\lambda_{\text{max}} = 290$ nm. b) UV/Vis spectra of CTAB-capped Au NRs 116 and pegylated Au NRs 117	93
Figure 46. HRTEM image of PEG-modified Au NRs 117	94
Figure 47. 21% TBE gel of model reaction between TA-PEG-TZ 113 and maleimide-modified DNA 83 before staining (left) and after staining (right). Fluorescent pyrazoline could only be observed of TA-PEG-TZ 113 with functional Mal-DNA 83 after irradiation (lane III).	95
Figure 48. a) Fluorescence spectra of DNA-PEG-Au NRs 119 before and after UV irradiation. b) 0.5% agarose gel after 60 min at 80 V of CTAB-Au NRs 116 (lane I), PEG-Au NR 117 (lane II) and DNA-PEG-Au NRs 119 (lane III) showing the higher mobility of DNA-PEG-Au NRs 119 due to the additional negative charge of Mal-DNA 83	97
Figure 49. 0.5% agarose gel after 40 min at 80 V of CTAB-Au NRs 116 (lane I), PEG-Au NRs 117 (lane II), DNA-PEG-Au NRs 119 (lane III) and cDNA-DNA-PEG-Au NRs 120 (lane IV) showing the lower mobility of cDNA-DNA-PEG-Au NRs 120 in comparison to DNA-PEG-Au NRs 119 due to the bigger size after hybridization.....	97
Figure 50. Novel photoactive, bifunctional linkers 70 and 113	100

Figure 51. a) Pathway to immobilize maleimide-capped Au NPs to photoenol-coated glass surface or b) to use tetrazole-functionalized Au NPs and maleimide-coated glass surface.	103
Figure 52. Drawing of the custom-built photoreactor employed in the current study.....	110
Figure 53. Emission spectrum of the employed compact low-pressure fluorescent lamp (36 W, Arimed B6, $\lambda_{\text{max}} = 320 \text{ nm}$).....	111

List of Schemes

- Scheme 1.** Scheme of photochemical cleavage of 2-hydroxy-1-(4-(2-hydroxyethoxy)phenyl)-2-methylpropan-1-one (Irgacure-2959) **1** to generate ketyl acetone radicals **3** which are capable to reduce Au^{3+} to Au^0 . Adapted with permission from [17]. Copyright 2006 American Chemical Society. 6
- Scheme 2.** Different strategies to modify NP surface with various (bio)molecules including one-pot synthesis with metal salt and reducing agent, ligand exchange of preformed NPs, and covalent binding to functional NPs. 14
- Scheme 3.** Bromo-functionalized Au NPs **4** were functionalized with azide moiety using sodium azide. The prepared azide-substituted Au NPs **5** were modified with propyn-1-one derivated small molecules **6**. Adapted with permission from [75]. Copyright 2006 American Chemical Society..... 19
- Scheme 4.** Strain-promoted copper-free azide-alkyne cycloaddition of dibenzocyclooctyne-modified Au NPs **8** and azide-terminated polymersomes containing poly(butadiene)-*b*-poly(ethylene glycol) copolymer **9**. Adapted from [85] with permission from The Royal Society of Chemistry. 20
- Scheme 5.** Cyclopropanone moiety **11** was attached to polymer brushes and subsequently photoactivated to generate dibenzocyclooctynes **12**. In presence of azide-derived fluorescent dyes, dibenzocyclooctynes could undergo copper-free azide-alkyne cycloaddition to obtain **13**. Adapted with permission from [93]. Copyright 2010 American Chemical Society..... 23

- Scheme 6.** 3-(Hydroxymethyl)-2-naphthol **14** dehydrogenated to the highly reactive naphthoquinone methide **15** upon irradiation with UV light ($\lambda = 300$ nm). Naphthoquinone methide could undergo Diels-Alder reaction with vinyl ethers **16** leading to **17**. Adapted with permission from [94]. Copyright 2011 American Chemical Society..... 24
- Scheme 7.** Light-induced azirine-alkene cycloaddition between azirine-containing lysozyme **18** and dimethylfumarate-linked poly(ethylene glycol) **20** to generate the lysozyme-PEG conjugate **21**. Adapted from [95] with permission from The Royal Society of Chemistry. 25
- Scheme 8.** Light-induced [4+4] cycloaddition between anthracene-capped Au NPs **22** and anthracene-coated ZrO₂ films **23** upon irradiation with 355 nm to obtain Au NP-patterns onto ZrO₂ films **24**. Adapted with permission from [96]. Copyright 2010 American Chemical Society..... 26
- Scheme 9.** Light-induced reaction of *o*-nitrobenzyl alcohol-capped Au NPs **25** and benzylamine-capped Au NPs **26** to assemble the Au NPs in 1D arrays **27**. Adapted from [97] with permission from The Royal Society of Chemistry. 27
- Scheme 10.** Main approaches for the preparation of polymer nanocomposites based on covalent linkages can be classified in the direct-synthesis method, grafting from strategy, grafting-to strategy and post-modification technique. Adapted from [103]. Copyright 2009, with permission from Elsevier..... 28
- Scheme 11.** a) Template DNA controlled immobilization to construct linear chains. Adapted with permission from [116]. Copyright 2012 American Chemical Society. b) Flexible DNA modification approach for the construction of DNA-Au NPs conjugates in different patterns. Adapted from [117] with permission from The Royal Society of Chemistry. 31

- Scheme 12.** Dimer formation of DNA-Au NP conjugates using templating splint strands and strain-promoted azide-alkyne cycloaddition between azide **28** and alkyne-modified Au NPs **29**. Adapted from [120] with permission from The Royal Society of Chemistry. 32
- Scheme 13.** Maleimide-capped Ag NPs **30** and furan-modified ssDNA **31** can undergo Diels-Alder reaction to generate ssDNA-Ag NP conjugate **32**. Adapted from [121] with permission from The Royal Society of Chemistry. 33
- Scheme 14.** Schematic illustration of the preparation of novel tailored nanomaterials using light-induced reactions..... 39
- Scheme 15.** Light-induced Diels-Alder reaction of *o*-substituted benzophenone **33** and dienophile **34** to proof the tautomerization and long lifetime *via* Diels-Alder trapping.^[163] 42
- Scheme 16.** Overview of the rearrangement of **36** to the formation of Z-dienol **37** and E-dienol **38**: *ortho*-alkyl substituted benzaldehyde **36** can absorb a photon to achieve the excited singlet state. A followed intersystem crossing leads to the triplet state, subsequent rotation and H-abstraction generates after rearrangement Z-dienol **37** and E-dienol **38**, which can undergo Diels-Alder cycloaddition. 43
- Scheme 17.** 2-Formyl-3-methylphenoxy group **39** tautomerizes under UV irradiation to photoenol intermediate **40**, which is stabilized by hydrogen bonding. Reaction with electron-deficient dienophile such as maleimide **41** leads to photoadduct **42**. 44
- Scheme 18.** Synthesis of 4-((2-formyl-3-methylphenoxy)methyl)benzoic acid **43**..... 46
- Scheme 19.** Synthesis route for the amide coupling of 5-aminobenzotriazole **54** 4-((2-formyl-3-methylphenoxy)methyl)benzoic acid **43** (reaction conditions see Table 2). 47
- Scheme 20.** Synthesis of 2-(1*H*-benzo[d[1,2,3]riazol-5-yl)ethanamine **64**. 48

Scheme 21. Benzotriazole-5-carboxylic acid 65 can react directly with 2,2'-(ethane-1,2-diylbis(oxy))diethanamine 66 in one step to the desired product 69 or by the use of the one side Boc-protected derivative 67 followed by a deprotection step.....	49
Scheme 22. Synthesis of <i>N</i> -(2-(2-(2-(4-((2-formyl-3-methylphenoxy)methyl)benzamido)ethoxy)ethoxy)ethyl)-1 <i>H</i> -benzo[<i>d</i>][1,2,3]triazole-5-carboxamide 70 (BTPE).....	50
Scheme 23. Model reaction of benzotriazole-photoenol 70 (BTPE) and maleimide-modified poly(ethylene glycol) 71 generate the photo-adduct 72	51
Scheme 24. Synthesis of 2-(2-(2-hydroxyethoxy)ethoxy)ethyl 1 <i>H</i> -benzo[<i>d</i>][1,2,3]triazole-5-carboxylate 74 (BTTEG).	52
Scheme 25. Ligand exchange of citrate-capped Ag NPs 75 with BTPE 70 and BTTEG 74 linker in DMSO.	53
Scheme 26. BTPE/BTTEG-modified Ag NPs- 76 were functionalized with PEG-Mal 39 employing light-induced Diels-Reaction.	54
Scheme 27. Possible side reaction of photoenol moiety 79 with oxygen under UV irradiation to cyclic peroxide 80	55
Scheme 28. Synthesis of maleimide-modified ssDNA 83	61
Scheme 29. Photoreaction between BTPE linker 70 and maleimide-modified ssDNA 83	63
Scheme 30. Synthesis of photoenol disulphide linker 87 for modification of Au NPs.	66
Scheme 31. Model reaction between photoenol disulphide linker 87 and maleimide 91 was carried out employing photoreactor and Arimed B6 UV lamp. The photoreaction initially generates mono-functionalized intermediate 92 and subsequently the di-functionalized product 93	73
Scheme 32. Modification of the glass surface with maleimide groups 98 in a two step approach employing (3-aminopropyl)triethoxysilane (APTES) 95 and 4-maleimidopropanoyl chloride 97	74

Scheme 33. Photoactivated 1,3-dipolar cycloaddition reaction between a 2,5-diaryl tetrazole 101 and a substituted alkene dipolarophile 103	85
Scheme 34. Synthesis of thioctic acid-PEG-tetrazole 113	88
Scheme 35. Schematic illustration of the light-induced NITEC reaction of maleimide-modified DNA 83 and with TA-PEG-TZ/TA-PEG-coated Au NRs 117	96
Scheme 36. Preparation of RAFT polymer-stabilized Au NPs in a one-pot synthesis using sodium borohydride as reducing agent.	101
Scheme 37. One-pot synthesis of Au NPs with the photoactive group a) in the backbone or b) in the side chain of the RAFT polymer.	102

List of Tables

Table 1. Chemical strategies applied for the covalent modification of NPs. Adapted with permission from [67]. Copyright 2011 American Chemical Society.....	16
Table 2. Overview of different reaction conditions for the amide coupling between 5-aminobenzotriazole 54 and 4-((2-formyl-3- methylphenoxy)methyl)benzoic acid 43	47
Table 3. Zeta potential measurement of citrate-capped Ag NPs- 75 , BTPE/BTTEG modified Ag NPs- 76 , PEG coated Ag NPs- 77 , and pCBMA coated Ag NPs- 78	54
Table 4. Different fractions I-III of HPLC trace of BTPE 70 and Mal-DNA 83	64
Table 5. Zeta potential measurement of CTAB-Au NRs 116 , PEG-Au NRs 117 and DNA-PEG-Au NRs 119 in ddH ₂ O.	96
Table 6. DNA oligonucleotides used in the current thesis (purchased from Sigma-Aldrich).....	105
Table 7. Buffers and the corresponding recipes.....	105
Table 8. Standard gradient for the purification of DNA oligonucleotides by HPLC. The solvents A: 0.1 M ammonium acetate, and B: acetonitrile were used.....	109
Table 9. Recipe for 21% PAGE gel.	109

Curriculum Vitae

Personal Details

Name	Lukas Degenhard Frank Stolzer
Date of Birth	24.10.1986
Place of Birth	München
Nationality	German

Education and Research Experience

Since 10/2011 **Karlsruhe Institute for Technology (KIT)**
Institute for Chemical Technology and Polymer Chemistry/
DFG Centre for Functional Nanostructures (CFN), Germany

Doctoral candidate

Thesis title: "*Photochemical Activation of Nanoparticles with (Bio)macromolecular Structures*"

Supervision: Dr. Ljiljana Fruk/ Prof. Dr. Christopher Barner-Kowollik

- Wet chemical synthesis of metallic nanoparticles (NPs)
- Characterization von NPs *via* UV-Vis-, IR- and NMR-spectroscopy, DLS, zeta potential, AFM
- Synthesis und analysis (ESI-MS, NMR, GPC) of polymers
- Chemical modification of NPs, DNA and peptides experience in gel electrophoresis, HPLC, SEC
- Functionalization of NPs with polymers/biomolecules using light-induced reactions
- Supervision of students/trainees

10/2006 – 09/2011 **Karlsruhe Institute of Technology (KIT)**

M.Sc. in Chemistry (grade: 1.6)

Focusing on polymer chemistry

Thesis title: "*Peptide Engineering for Surface Modification*"

Supervision: Dr. Ljiljana Fruk/ Prof. Dr. Christopher Barner-Kowollik

- Organic synthesis of functional linker
- Modification und purification of peptides
- Experience in NMR, HPLC

08/1997 - 04/2006 **High school education** (grade: 1.9)

Trifels-Gymnasium, Annweiler

Publications

- 2015 **A self-reporting tetrazole-based linker for the biofunctionalization of gold nanorods**
Stolzer, L.; Vigovskaya, A.; Barner-Kowollik, C.; Fruk, L. *Chem. Eur. J.* **2015**, DOI: 10.1002/chem.201502070.
- 2015 **Photo-induced surface encoding of gold nanoparticles**
Stolzer, L.; Quick, A. S.; Abt, D.; Welle, A.; Wegener, M.; Barner-Kowollik, C.; Fruk, L. *Chem. Commun.* **2015**, 51, 3363.
- 2014 **Light-induced modification of silver nanoparticles with functional polymers**
Stolzer, L.; Ahmed, I.; Rodriguez-Emmenegger, C.; Trouillet, V.; Bockstaller, P.; Barner-Kowollik, C.; Fruk, L. *Chem. Commun.* **2014**, 50, 4430.
- 2013 **Light-induced DNA-protein conjugation**
Bauer, D. M.; Rogge, A.; Stolzer, L.; Barner-Kowollik, C.; Fruk, L. *Chem. Commun.* **2013**, 49, 8626.

Conference Contributions

- 2014 **Light-induced functionalization of silver and gold nanoparticles**
Stolzer, L.; Barner-Kowollik, C.; Fruk, L.
HeKKaSaGOn Summer School: „Nanotechnology: Potential and Challenges”, Karlsruhe, Germany, 01.-10.09.14
(poster and talk)

Danksagung

Nach 3,5 Jahren ist es Zeit Abschied zu nehmen und vielen Personen zu danken, ohne deren Beitrag die Doktorarbeit in dieser Form nicht zustande gekommen wäre:

Ein besonderer Dank gilt meiner Familie, insbesondere meinen Eltern. Ohne ihre jahrelange Unterstützung wären das Studium und diese Arbeit nicht möglich gewesen.

Prof. Dr. Christopher Barner-Kowollik und Dr. Ljiljana Fruk möchte ich das entgegengebrachte Vertrauen in meine Person, die Möglichkeit auf dem interessanten Thema zu forschen, für die stets offene Tür und die vielen gemeinsamen Meetings danken. Nur durch die hervorragende Betreuung in diesem interdisziplinären Thema waren diese Ergebnisse möglich.

Für das fleißige Korrekturlesen und die guten Anmerkungen möchte ich mich bei Dr. Ljiljana Fruk, Dr. Anja Goldmann, Dr. Bianca Geiseler, Astrid Hirschbiel und Dr. Dania Kendziora bedanken.

Zudem möchte ich mich bei dem ganzen CFN Team für die gute Atmosphäre bedanken. Ein großes Dankeschön an Dania Kendziora und Bianca Geiseler, die mir bei Fragen in der Biochemie stets weiterhelfen konnten, mit denen ich aber auch viele Gespräche über andere Themen als Chemie führen konnte. Bei Dr. Ishtiaq Ahmed, der mir mit seiner Erfahrung in der organischen Chemie immer wieder weiterhelfen konnte, Antonina Vigovskaya, die mit ihrer fleißigen Art für ein sauberes Labor gesorgt hat, Cheng Chen, Dennis Bauer und Marko Miljevic möchte ich mich für die tolle Atmosphäre im Chemielabor bedanken.

Der gesamten MacroArc-Gruppe für die freundliche Zusammenarbeit und angenehmen Atmosphäre. Insbesondere für die Hilfe mit lichtinduzierten Reaktion möchte ich mich bei Jan Müller, Johannes Willenbacher und Dr. Kim Öhlenschläger bedanken.

Danksagung

Bei Astrid Hirschbiel und Nele Bäsch, die mich während meines Studiums und meiner Doktorarbeit begleitet haben, möchte ich mich für die vielen gemeinsame Kaffeepausen mit netten Gesprächen bedanken.

Meinem Bachelorstudenten Patrick-Kurt Dannecker möchte ich für die gute Zusammenarbeit danken und wünsche viel Erfolg bei der Doktorarbeit.

Vielen Dank für die gute Zusammenarbeit richte ich an die vielen Projektmitarbeitern, u.a. Dr. Denys Naumenko, Alexander Quick und Doris Abt.

Zudem danke ich Andreas Elkeries für die Hilfe bei diversen Computerproblemen, Evelyn Stühling, Frau Mösle und Frau Bender für die Unterstützung bei administrativen Fragen.

Ein besonderer Dank an die Personen, die in meinem Auftrag unzählige Messungen durchgeführt haben: Vanessa Trouillet für XPS, Dr. Alexander Welle für ToF-SIMS, Patrice Brenner für SEM, Annette Hochgesand für MALDI und Dr. Li Shang für Fluoreszenzmessungen.